2002

# FLUORESCENCE STUDIES IN THE INDUCTIVELY COUPLED PLASMA

## YOUNG, ANITA

http://hdl.handle.net/10026.1/1686

# FLUORESCENCE STUDIES IN THE INDUCTIVELY COUPLED PLASMA

by

## ANITA YOUNG

A thesis submitted to the University of Plymouth
In partial fulfilment for the degree of

## DOCTOR OF PHILOSOPHY

School of Environmental Sciences
Faculty of Science

**September 2002**

# Fluorescence Studies in the Inductively Coupled Plasma
## ABSTRACT
### Anita Young

An Optima 3000 ICP-AES instrument was modified and the equipment necessary to carry out axial excitation atomic fluorescence was designed and constructed. Using this calibrated system, preliminary fluorescence experiments were not successful. As fluorescence is proportional to source intensity, it was considered that the excitation source, a hollow cathode lamp, may not have been sufficiently intense to produce fluorescence.

A novel excitation source-driver system was designed and built in-house to operate HCLs, BDHCLs and LEDs with variable modulation frequencies and duty cycle capabilities. Studies investigating lamp response to changes in modulation frequency and duty cycle indicated that a lamp operated with a lower modulation frequency range (167 – 542 Hz) and higher duty cycles (30 – 50 %) should provide the preferred intense excitation conditions for the production of fluorescence in the ICP. When a Thermo Elemental PQ2 instrument was used, fluorescence was obtained immediately. Univariate searches were used to optimise several plasma parameters, i.e. forward power; viewing height ALC; plasma, nebuliser and auxiliary gas flow rates. Once the optimum conditions had been determined, calibration curves were plotted for each of the elements studied (Ba, Li, Mg and Na). The calibration showed excellent linearity over five orders of magnitude ($R^2$ values ranged from 0.99995 to 1.0000) and the precision on each data point was better than 5 % RSD. Limits of detection were determined to be 27.6, 0.51, 0.43 and 0.20 µg $l^{-1}$ for Ba, Li, Mg and Na, respectively, which approached those reported in the literature for a commercial system.

Vertical profiles of the plasma, using radial excitation, were obtained for Ba, Li, Mg and Na. Using the optimum conditions for Li and Na, vertical profiles of the plasma, using axial excitation with the more intense LEDs, were obtained. Both profiles showed that there was a relatively sharp optimum, with respect to fluorescence signal, as a function of viewing height ALC. The optimum viewing heights ALC obtained, for both radial and axial excitation fluorescence, were identical, suggesting that, irrespective of the excitation arrangement employed, only particular conditions produced in the plasma give the optimum conditions for fluorescence and that these are spatially dependent.

Plasma diagnostics were performed in an attempt to explain why fluorescence was observed using the plasma produced by the Thermo Elemental but not by the Optima 3000 generator. At a viewing height of 50 mm ALC, $T_{exc}$ and $T_{rot}$ were 3080 and 2500 K for plasmas produced using the Thermo Elemental generator and 3600 and 2830 K for the Optima 3000 generator, respectively. Temperatures were calculated using the mean emission intensity at particular wavelengths. The intensities of the emitting species from the Thermo Elemental ICP were lower than those obtained from the Optima 3000 ICP for supposedly 'identical' conditions. If the number of excited species gives rise to lower emission intensities, then there must be more atoms in the lower/ground state from the plasma produced using the Thermo Elemental generator. This is of vital importance because for fluorescence to occur the fluorescence emission intensity will be dependent on the number available in the ground state for excitation (i.e. a relatively 'cool' plasma is required for fluorescence to occur). As very similar plasma operating conditions and the same concentration solutions were used in the fluorescence experiments performed using both the Optima 3000 and the Thermo Elemental ICPs, the differences observed in plasma performance may be attributed to efficiency of coupling of the generators used.

# LIST OF CONTENTS

:

# CHAPTER 1 INTRODUCTION

# LIST OF TABLES

# LIST OF FIGURES

# Chapter 4

# LIST OF PLATES

# ACKNOWLEDGEMENTS

For Paps, sorry that you are no longer with us

Do not stand at my grave and weep.

I am not there, I do not sleep.

I am a thousand winds that blow,

I am the diamond glints on the snow.

I am the sunlight on ripened grain,

I am the gentle autumn's rain.

When you awaken in the morning's hush,

I am the swift uplifting rush

Of quiet birds in circled flight.

I am the stars that shine at night.

Do not stand at my grave and cry,

I am not there, I did not die...

Anon

# AUTHOR'S DECLARATION

At no time during the registration for the degree of Doctor of Philosophy has the author been registered for any other university award.

This study was financed with the aid of a Subdivision of Analytical Chemistry Award from The Royal Society of Chemistry.

The work described in this thesis has entirely been carried out by the author. Relevant scientific seminars and conferences were regularly attended at which work was presented and a paper has been prepared for publication.

Signed...Allang.............

Dated.29.October.2002.

# LIST OF ABBREVIATIONS

| | |
|---|---|
| A | transition probability for spontaneous emission |
| AA | Atomic Absorption |
| AC | Alternating Current |
| AES | Atomic Emission Spectrometry |
| AFS | Atomic Fluorescence Spectrometry |
| $A_J$ | probability transition |
| ALC | Above Load Coil |
| Ar | argon atoms in the ground state |
| Ar* | argon atoms in the excited state |
| $Ar^+$ | argon ions |
| $Ar^m$ | argon atoms in the special case of metastable levels |
| ASIA | Atomizer, Source, Inductively Coupled Plasmas in Atomic FluorescenceSpectrometry |
| BDHCL | Boosted Discharge Hollow Cathode Lamp |
| $B_v$ | rotational constant belonging to the vibrational quantum number v |
| c | speed of light in a vacuum |
| CTE | Complete Thermodynamic Equilibrium |
| CW | Continuous Wave |
| d | groove spacing |
| $\Delta\lambda_D$ | Doppler half-width |
| DL | Detection Limits |
| E | energy |
| e | electron |
| $e^-$ | free electrons |
| EDL | Electrodeless Discharge Lamp |
| $E_{exc}$ | excitation energy |
| $E_{ion}$ | ionisation energy |
| $E_k$ | energy state (in wavenumbers) |
| $E_i$ | ionisation potential |
| $E_p$ | excitation energy of the level p |
| ETAAS | Electrothermal Atomic Absorption Spectrometry |
| $f(v)$ | Maxwellian velocity distribution |
| f | oscillator strength |
| FWHM | Full Width-Half Maximum |
| g | statistical weight |
| $g_p$ | statistical weight of the level p |
| $g_k$ | statistical weight of the excited energy level |
| GS | Ground State |
| h | Planck's constant |
| HCL | Hollow Cathode Lamp |
| $h\nu_{cont}$ | continuum photon |
| $h\nu_{line}$ | line photon |
| I | intensity of an emitting species |
| $I_a$ | emission intensity of an atom line |
| $I_i$ | emission intensity of an ion line |
| $I_0$ | incident light intensity for a given wavelength |
| $I_1$ | transmitted light intensity |
| ICP | Inductively Coupled Plasma |
| l | path length |

| | |
|---|---|
| LCD | Liquid Crystal Display |
| LEAFS | Laser-Excited Atomic Fluorescence Spectrometry |
| LED | Light Emitting Diode |
| $\Delta\lambda_{ins}$ | instrumental broadening |
| LOD | Limit of Detection |
| LTE | Local Thermodynamic Equilibrium |
| LPIRM | Line Pair Intensity Ratio Method |
| k | Boltzmann constant |
| $k_v$ | absorption coefficient |
| $\lambda$ | wavelength of the emitting radiation |
| m | mass of a particle |
| M | analyte atoms in the ground state |
| $M^+$ | singly charged analyte atoms in the ground state |
| $M_e$ | mass of an electron |
| $M_p$ | analyte atoms in the excited state |
| $M_p^+$ | singly charged analyte atoms in the excited state |
| MS | Mass Spectrometry |
| N | grating order number |
| n | total concentration of neutral atoms or ions |
| $n_a/n_i$ | numbers of neutral atoms and ions respectively |
| $n_e$ | electron number density |
| $n_p$ | number of atoms (or ions) in the excited energy state p |
| PMT | Photomultiplier Tube |
| Q | internal partition function |
| R | radius of the plasma torch |
| r | radial position along radius R |
| $\Delta\lambda_S$ | Stark broadening |
| $S_{bl}$ | standard deviation of the blank signal |
| SCD | Segmented Charge-coupled device Detector |
| $S_J$ | oscillator strength |
| T | Absolute Temperature |
| $T_D$ | Doppler temperature |
| $T_e$ | electron temperature |
| $T_{exc}$ | excitation temperature |
| $T_{ion}$ | ionisation temperature |
| X | monoatomic gas |
| v | random velocity of a particle |
| $\nu$ | wavenumber of the line |
| $X^{bl}$ | mean blank signal |
| $X^{n+}$ | ion with n charges |
| Z(T) | partition function of the atom or ion |
| $Z_a/Z_i$ | relevant partition functions for $n_a/n_i$ |

# 1.0    INTRODUCTION

## 1.1    Fundamental Properties of an Inductively Coupled Plasma

The understanding of the fundamental properties of an inductively coupled plasma (ICP) is of importance for their characterisation and for their efficient use for analytical purposes (1). The study of excitation mechanisms aims to identify the pertinent excitation, ionisation, de-excitation and recombination processes observed for analyte behaviour (2). 'Plasma diagnostic' techniques are used to measure the physical properties of the plasma discharge that will yield significant information about the excitation mechanisms. The fundamental parameters of plasmas are considered to be the plasma temperature, electron number density, number densities of analyte and argon species, and spectral line widths (1). Spectroscopic diagnostics include the measurement of single emission lines or spectra from species in the plasma. From that emission, 'temperatures' and relative or absolute number densities may be evaluated (3). An accurate knowledge of the temperature experienced by the analyte species is one of the pre-requisites leading to the definitive understanding of solute vaporisation, dissociation, atomisation and ionisation processes that are occurring in the plasma (4). The electron number density is an important indicator of the degree of ionisation, with the free electron thought to be the primary plasma particle responsible for the excitation and ionisation within the ICP (3).

## 1.2    Principles of ICP Generation

In 1961, Reed described the first use of inductively coupled plasmas for the production of crystals (5, 6). His torch consisted of a quartz tube with a brass base, having a tangential argon gas entry; the tube being placed within the coils of a high frequency generator. A plasma was formed at atmospheric pressure by using a graphite rod to

1

provide the initial ionisation of the argon and a 10 kW, high frequency heating unit at 4 MHz as a source of power (5, 6). Reed was not primarily concerned with spectroscopy so it was not until a research team at Albright & Wilson (MfG) Ltd., Oldbury, UK turned their attention to the dynamic ICP reported by Reed that the development of the annular ICP as a spectroscopic source was first realised (5, 6).

The first analytical applications of the ICP were published in between 1963 and 1965 (7 - 9). Greenfield *et al.* used a modified Reed torch to generate an annular ICP for spectrochemical analysis (10). The torch used had an internal diameter of 25 mm and had a three-tube configuration with a central direct nebuliser consisting of a capillary tube through which ran another tube of an even smaller diameter. The capillary tube terminated just below the annular plasma and had a side arm through which argon gas was passed (11). Liquid (both aqueous and organic) was drawn up the central tube by the pressure differential created around the central capillary and turned into an aerosol. Because of the fragility of the total consumption nebuliser, it was later replaced by a capillary tube with a 2 mm bore through which the aerosol from the external nebuliser flowed (11). The argon jet, from the nebuliser, punched a hole in the initial spheroidal plasma and an annular plasma resulted, thus producing a long tailflame, which was used as the spectroscopic source (10).

Some time later, Fassel and co-workers (9) generated a spheroidal ICP in a laminar flow torch. In contrast to the annular plasma, sample aerosol flowed around the plasma in the spheroidal ICP (12). Subsequently, the properties of an annular plasma were appreciated (13), which is the preferred system today. The Fassel torch was adopted by manufacturers as their role model because it had an internal diameter of 18 mm and, as a consequence of this, used lower gas flows and powers to achieve similar figures of merit to that of the Greenfield torch.

Various names were used, *e.g.* induction coupled plasma spectrometric excitation source (9), high frequency plasma source (14), induction plasma (15), induction-coupled and radio-frequency plasma torch (16), before the term inductively coupled plasma and its corresponding acronym, ICP were agreed upon (17).

A plasma is a partially ionised gas that is macroscopically neutral (18) and, if a monoatomic gas, X, is used, can be described by the following equilibrium (Equation 1.1) (19):

$$X = \sum_{n=1}^{p} X^{n+} + \sum_{n=1}^{p} ne \qquad (1.1)$$

where $X^{n+}$ is an ion with n charges and e is the electron. The gas normally used to generate the plasma is argon. Argon is a monoatomic element with a high first ionisation energy (15.76 eV) and is relatively chemically inert. The major species present in the plasma are analyte atoms (M) in the ground (M) and excited state $(M_p)$; singly charged analyte ions in the ground $(M^+)$ and excited state $(M_p^+)$; free electrons $(e^-)$; argon atoms in the ground (Ar) and excited state $(Ar^*)$ and Ar ions $(Ar^+)$. Other species that may be present in the plasma include the special case of metastable levels $(Ar^m)$; and photons, both continuum $(h\upsilon_{cont})$ and line $(h\upsilon_{line})$ (2).

### 1.2.1 Formation Mechanisms of Analyte Ions

The ultimate purpose of the diagnostic work on the ICP is to clarify the excitation mechanisms for support argon gas and the analytes introduced into the plasma (20, 21). However, a comprehensive understanding of how all of these species are formed, and how they interact with one another has still not been fully achieved. The common reactions encountered in plasma discharges are outlined in Sections 1.2.11 – 1.2.1.6.

### 1.2.1.1 Collisional Excitation and De-Excitation by Electrons

Collisional excitation and de-excitation by electrons in a plasma can be described by Equations 1.2 and 1.3 below:

Analyte atoms $\quad M + e^-$ (high energy) $\leftrightarrow M_p + e^-$ (low energy) $\quad\quad$ (1.2)

Analyte ions $\quad M^* + e^-$ (high energy) $\leftrightarrow M_p^* + e^-$ (low energy) $\quad\quad$ (1.3)
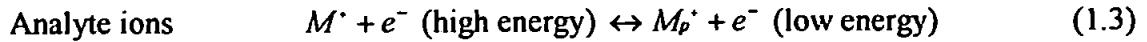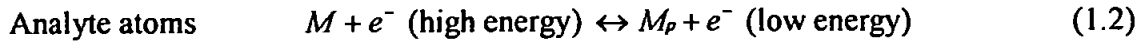
In the forward process, kinetic energy is taken from the electron by the analyte atom or ion which is left in an excited state (Equation 1.2). For this process to occur the energy of the electron must be equal to, or exceed, the transition energy of the analyte species involved. The reverse process involves the transfer of excitation energy from the excited atom or ion to the colliding electron (Equation 1.3) (2).

### 1.2.1.2 Collisional Ionisation and Three-Body Recombination

Collisional ionisation and three-body recombination within a plasma can be described by Equations 1.4 and 1.5:

$$M_p + e^- \rightarrow M^+ + e^- + e^- \quad\quad (1.4)$$

$$M^+ + e^- + e^- \rightarrow M_p + e^- \quad\quad (1.5)$$
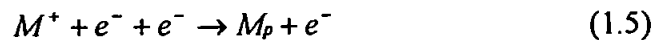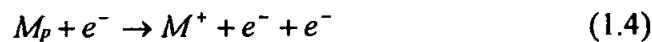
If the electron energy matches or just exceeds the ionisation energy then this process leads to the production of analyte ions, normally in the ground state (Equation 1.4). The reverse process, three-body recombination, is an ion decay mechanism whereby excited state analyte atoms may be produced (Equation 1.5) (2).

### 1.2.1.3 Radiative Recombination

Radiative recombination can be described by Equation 1.6:

$$M^+ + e^- \rightarrow M_p + h\upsilon_{cont} \qquad (1.6)$$

The products of this reaction are excited analyte atoms and a continuum photon. The reverse process, photo ionisation, is not as important in the ICP because, for the most part, the analyte lines are optically thin for re-absorption to take place (2).

### 1.2.1.4 Radiative De-Excitation

Radiative de-excitation can be described by Equations 1.7 and 1.8:

$$\text{Atoms} \qquad M_p \rightarrow M + h\upsilon_{line} \qquad (1.7)$$

$$\text{Ions} \qquad M_p^* \rightarrow M^+ + h\upsilon_{line} \qquad (1.8)$$
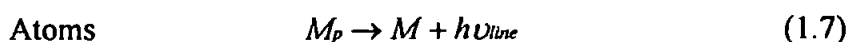
These are the most significant processes in terms of ICP spectrometry since they create the characteristic line spectra used for chemical analysis. The reverse processes are not favourable in an ICP due to its low optical density (2).

### 1.2.1.5 Penning Ionisation and Excitation

Penning ionisation and excitation can be described by Equations 1.9 – 1.11:

$$M + Ar^m \rightarrow M^+ + Ar + e^- \qquad (1.9)$$

$$M + Ar^{m*} \rightarrow M_p^+ + Ar + e^- \qquad (1.10)$$

$$M + Ar^{m*} \rightarrow M_p + Ar \qquad (1.11)$$
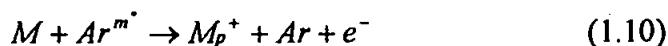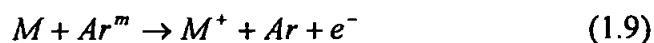
Penning ionisation reactions produce ionised and/or ionised and excited analytes depending on the energies involved, with excess energy being carried away in the form of kinetic energy of the free electrons (22). Equation 1.9 describes the production of analyte ions for any species whose ionisation energy is less than the Ar metastable energies of 11.55 and 11.71 eV and, similarly, Equation 1.10 describes the production of excited analyte ions. Equation 1.11 shows that direct excitation of atoms and ions is also possible, although, the energy restrictions are quite critical (2).

### 1.2.1.6 Charge Exchange with Argon

Charge exchange with argon is described by Equation 1.12:

$$Ar^+ + M \rightarrow Ar + M_p^+ + \Delta E \qquad (1.12)$$

Equation 1.12 shows an asymmetrical charge transfer taking place between Ar ions and analyte atoms (2). This leads to the production of excited state analyte ions. The energy difference is dissipated as kinetic energy of the colliding partners (2).

### 1.3 Local Thermal Equilibrium in an Inductively Coupled Plasma

If every energy exchange process occurring in the ICP was exactly balanced by its reverse process then the system would be in a state of complete thermodynamic equilibrium (CTE). From thermodynamic arguments, all energy distributions in CTE follow the Boltzmann, Saha and Maxwell-Boltzmann distributions and, are described by only one temperature (1).

The Boltzmann law describes the equilibrium between the populations of the various levels within the same ionisation state, including both excited and ground states, Equation 1.13.

$$n(p) = n\left[\frac{g_p}{Z(T)}\right]\exp\left(\frac{-E_p}{kT}\right) \qquad (1.13)$$

where, n(p) is the number of atoms (or ions) in the excited energy state p, n is the total

number of neutral atoms or ions, $g_p$ is the statistical weight of the level p, Z(T) is the

partition function of the atom or ion, $E_p$ is the excitation energy of the level p, k is the

Boltzmann constant and T is the absolute temperature (1).

The Saha law describes the equilibrium between two successive ionisation states,

Equation 1.14:

$$\frac{n_i n_e}{n_a} = \left(\frac{2\pi m_e kT}{h^2}\right)^{3/2}\left(\frac{2Z_i}{Z_a}\right)\exp\left(\frac{-E_i}{kT}\right) \qquad (1.14)$$

where $n_a$ and $n_i$ are the numbers of neutral atoms and ions, respectively, $Z_a$ and $Z_i$ are

the relevant partition functions, $n_e$ is the electron number density, $m_e$ is the mass of the

electron, and $E_i$ is the ionisation potential (1).

The Maxwell-Boltzmann law describes the kinetic motions of species in a high

temperature medium. The Maxwellian velocity distribution, $f(v)$, is given by Equation

1.15:

$$f(v) = 4\pi v^2\left(\frac{m}{2\pi kT}\right)^{3/2}\exp\left(\frac{-mv^2}{2kT}\right) \qquad (1.15)$$

where m and v are the mass and random velocity of the particle, respectively (1).

Since the energy exchange processes described in Equations 1.13 – 1.15 include

collisional as well as radiative processes, emitted photons must be completely absorbed

in the CTE system. In actual plasmas, the radiative processes that occur are out of

balance because the complete absorption of photons requires high optical densities for all radiative transitions. The plasma is optically thin and unexcited atoms in the outer regions cannot reabsorb emission from the centre. This lack of self absorption means that techniques such as ICP - Atomic Emission Spectrometry (AES) and – Atomic Fluorescence Spectrometry (AFS) have large, linear dynamic ranges.

When collisional processes are dominant in a system, each point of the system can be described by an individual temperature, which is governed by the various distribution laws. The temperatures governing the Boltzmann, Saha and Maxwell-Boltzmann distributions are defined as the excitation temperature, $T_{exc}$, the ionisation temperature, $T_{ion}$, and the electron temperature ($T_e$). Doppler temperatures, $T_D$, are used instead of $T_e$ for particles heavier than an electron. This state is known as local thermodynamic equilibrium (LTE) and, mathematically, the criterion for LTE is described in Equation 1.16 (1).

$$n_e \geq 1.6x10^{12} T_e^{1/2} (\Delta E)^3 \qquad (1.16)$$

where $n_e$ is in cm$^{-3}$, $T_e$ is the electron temperature (K) and $\Delta E$ is the energy difference (eV) between the states in question. The conventional ICP is generally accepted not to be in LTE because various measured 'temperatures' differ from each other.

## 1.4    Temperature Measurements in an Inductively Coupled Plasma

The species present in a plasma are distributed over many different energy states. The states of distribution are often defined by different 'temperatures' that depend on the species used for the temperature measurements. The theory and techniques used for temperature measurements in an ICP are described in detail in Chapter 4.

## 1.5    Introduction to Atomic Fluorescence Spectrometry

### 1.5.1    Types of Fluorescence

Atomic fluorescence is a radiational deactivation process that occurs after the excitation of ground state atoms by the absorption of radiation of a characteristic wavelength from an appropriate external excitation source (23). There are two basic types of atomic fluorescence, resonance fluorescence and non-resonance fluorescence. Resonance fluorescence occurs when ground state atoms absorb and re-emit radiation of the same wavelength. Non-resonance fluorescence occurs when the exciting line and the observed fluorescent line are of two different wavelengths. The different processes by which an atom can absorb and re-emit fluorescence radiation are explained in more detail and illustrated in Figure 1.1 (18, 23, 24).

When the absorption and re-emission of fluorescence radiation occurs between the same upper and lower energy level, resonance fluorescence occurs. The lower state may be the ground state or a metastable state and in these cases the processes are called resonance fluorescence and excited resonance fluorescence. Resonance systems are the most useful analytically as they generate the most intense fluorescence and hence offers the best limits of detection and sensitivity (23, 24).

Direct line fluorescence is a non-resonance fluorescence that occurs when transitions between the excited state of the resonance line and a lower intermediate level are allowed by the selection rules, these being $\Delta l = \pm 1$ (2). The upper level is common to both the radiational and de-excitation process and when the excitation energy is higher than the fluorescence energy the process is known as Stokes direct line fluorescence. If the excitation energy is lower than the fluorescence energy then the process is called anti-Stokes direct line fluorescence. The advantage of direct line fluorescence is that if

9

appropriate filters are used then scatter from the excitation radiation can be eliminated (23, 24).

When the upper levels of the exciting line and the emitted line are different, stepwise line fluorescence occurs. Normal stepwise fluorescence involves the absorption of radiation, a partial deactivation to a lower excited state, and a fluorescence transition (23, 24).

Thermally assisted fluorescence is the converse of stepwise line fluorescence and occurs as a stepwise absorption of energy by an atom to reach an excited state. It has very few analytical applications as the fluorescence is weak and occurs when the first excited state is very close to the ground state. If the de-excitation is to the ground level, the process is called thermally assisted anti-Stokes stepwise line fluorescence (23, 24).

Sensitised fluorescence occurs when an atom/molecule (donor) becomes excited by an external source and transfers its excitation energy to the sample atom (acceptor) by collision. The acceptor then undergoes radiative deactivation resulting in atomic fluorescence (23, 24).

## 1.5.2 Quenching of Fluorescence

The population of the excited state in atomic fluorescence is comparatively large in terms of thermal equilibrium. The lifetime of the excited atoms is very brief, and fluorescence results from the deactivation of these atoms. If, however, collisions occur between excited atoms and other atoms, molecules and electrons present in the atomiser, de-activation will occur without any fluorescence radiation being emitted. This process is known as quenching.

10
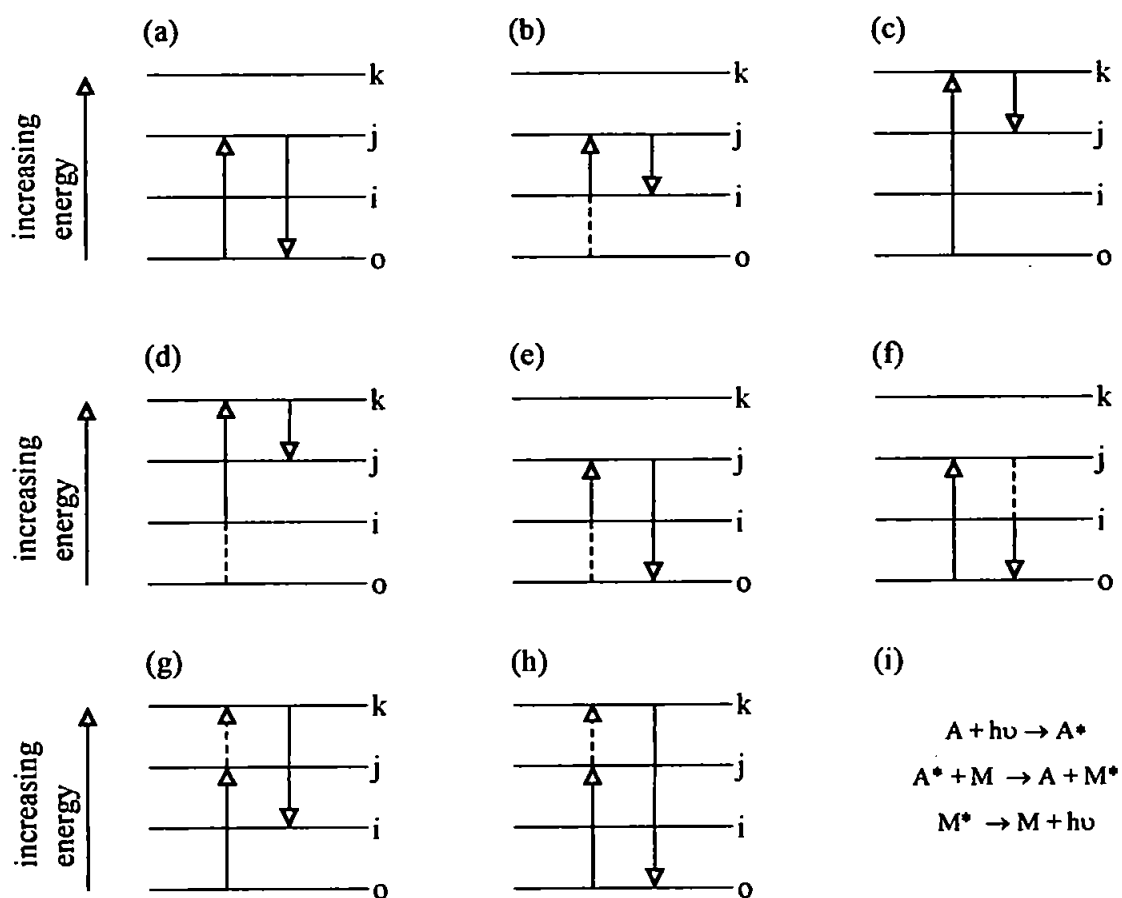
**Figure 1.1: Types of fluorescence: (a) resonance; (b) excited resonance; (c) Stokes direct line; (d) excited Stokes direct line; (e) anti-Stokes direct line; (f) Stokes stepwise; (g) thermally assisted stepwise; (h) thermally assisted anti-Stokes stepwise; and (i) sensitised (A, donor; M, acceptor) (18, 23, 24)**

### 1.5.3 Basic Instrumental Configuration Required for AFS

The basic instrumental layout for the production of fluorescence (Figure 1.2) has remained relatively unchanged for over a hundred years. Radiation from a modulated excitation source is directed through an atom cloud, part of it is absorbed and subsequently re-emitted as fluorescence radiation. The fluorescence radiation, which is collected off-axis relative to the excitation source, is resolved with either a monochromator or a filter and the intensity measured by means of a suitable detector. The output of the detector is fed to a lock-in amplifier to distinguish between the fluorescence signal and the emission signal from the atomiser.
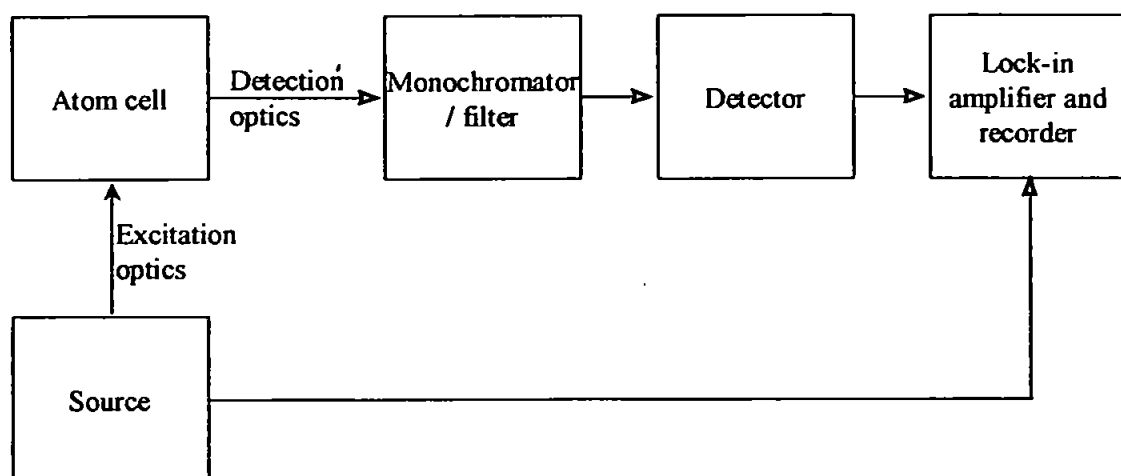
**Figure 1.2: Typical instrumental arrangement for atomic fluorescence spectroscopy**

## 1.5.4 Inductively Coupled Plasmas in Atomic Fluorescence Spectrometry

In 1969, Hussein and Nickless were the first to use an ICP as an excitation source in flame AFS (25). However, it was some seven years later before the ICP was mentioned in the scientific literature in connection with being an atom cell for AFS. Montaser and Fassel used a plasma torch with an extended outer tube as an atomiser, and electrodeless discharge lamps (EDLs) as sources. The ICP-AFS limits of detection (LOD) for Cd, Hg and Zn were found to be superior to those obtained by ICP-AES by a factor of 2 - 8 when the same experimental facilities were used for the measurements (26).

In 1979, Pollard *et al.* investigated the analytical utility of a continuous wave (CW) argon ion pumped dye laser as a source with a conventional ICP as an atomiser in AFS (27). They concluded that atomic fluorescence in the ICP using a CW laser source was possible, however, the system was not useful analytically because of the limited wavelength range of the CW laser employed, its high cost and the fact that they obtained poor (or not substantially improved) LODs compared with ICP-AES (27).

Epstein *et al.* were the first workers to use pulsed dye laser excitation in the ICP (28). The atomic and ionic fluorescences of Fe, Sn, Ba and In excited by both flashlamp and nitrogen laser pumped pulsed dye-lasers were studied. Detection limits were not superior to those obtained by ICP-AES and laser-excited atomic fluorescence spectrometry (LEAFS), however, the authors concluded that there was no reason for thinking that further improvements could not be made (28).

In 1981, Demers and Allemand published an important paper in which they described a single channel AF instrument utilising an ICP, generated in a torch with an extended outer tube, as an atomiser, and pulsed hollow cathode lamps (HCLs) as sources (29). This work established that the HCL-ICP-AFS technique was amenable to the

determination of several elements simultaneously. Specifically, it was shown that HCL-ICP-AFS provided excellent detection limits for a large number of elements, exhibited large dynamic ranges and negligible baseline drift, was virtually free from spectral interferences, and was free from the numerous background interferences that plague ICP-AES determinations. This work was the precursor to the introduction of the first commercially available AF spectrometer incorporating an ICP as an atomiser (30 - 32).

A paper by Omenetto in 1982 described an ICP-AF system in which a graphite rod was used as an atomiser (33). The LODs obtained for a number of elements were said to be better than those reported in the literature for electrothermal atomic absorption spectrometry (ETAAS). A year later, Kosinski *et al.* reported on the use of two low power ICPs, one as a source and the other as an atomiser in an AF system (34). Limits of detection for sixteen elements were compared with fluorescence detection limits using other radiation sources and were found to be within one order of magnitude for the best reported values using the ICP as an excitation source for flame AFS (35). Greenfield described a similar system in 1981 (36). He used a high power ICP as a source and a low power ICP as an atomiser in a single instrument. It was felt that this technique, atomiser, source, inductively coupled plasmas in atomic fluorescence spectrometry (ASIA), had the advantage of versatility. Although this paper discussed the instrumentation required in theory, no results were reported.

In 1984, a preliminary communication appeared in which Omenetto *et al.* described the use of an excimer (XeCl) pumped dye laser as a source and a conventional ICP torch as atomiser in an AFS system (37). The LODs reported were greatly superior to those reported by Demers and Allemand for HCL-ICP-AFS (29, 32) and by Fassel and co-workers and Boumans for ICP-AES (38, 39). Two more papers quickly followed

describing the important parameters for the analytical use of laser excited AFS and the analytical characteristics of a number of elements in atomic and ionic AFS (40, 41).

In 1985, Greenfield and Thomsen published the early results from their ASIA system (42). The LODs reported were mainly equal to, or better than, those reported previously by plasma systems other than those involving lasers as sources. In 1987, Greenfield *et al.* published what was said to be the first study of non-resonance transitions in AFS using a dual plasma system (43). It showed that ASIA demonstrated a remarkable freedom from interferences in resonance fluorescence and an even greater freedom when in non-resonance mode (44 - 53). Demers claimed improved sensitivity by the use of boosted discharge hollow cathode lamps (BDHCLs) in HCL-ICP-AFS (54). This is understandable because fluorescence is proportional to the intensity of the excitation source and it is accepted that BDHCLs may be operated at higher currents than standard HCLs. Greenfield *et al.* compared a high power ICP with BDHCL as sources in AFS (55). The LODs obtained with the plasma were at least an order of magnitude lower than those obtained with the BDHCL. An excellent review published in 1994 gives a deeper insight into the use of ICPs as both atomisers and sources in AFS (23).

### 1.5.5 General Requirements of an Atomisation Cell for AFS

For an AFS system, the atomisation cell should have a high quantum efficiency (*i.e.* cause minimal quenching of the excited atoms), efficiently dissociate the sample into ground-state atoms, and be stable with low noise characteristics (56). Suitably energetic atomic generators include flames (57), electrothermal atomisers (33) and the ICP (26 - 55).

The background signal from an AFS system consists of the background signal from the atomisation cell, and atomic or molecular emission signals resulting from the excitation of the sample matrix by the atomisation cell (56). The magnitudes of the background signals determine the noise level of the 'zero' reading baseline. In contrast, the AF signal is affected by the atomisation efficiency of the atomisation cell. For an ICP atomisation cell, these parameters are optimised by the use of a torch configuration and plasma operating conditions different from those commonly used for ICP-AES. The conditions used, which give rise to this required energetic state, are considered critical and have been the centre of debate (58).

### 1.5.5.1 Comparison of Typical Operating Conditions used for ICP-AFS and ICP-AES

Typical operating conditions used for ICP-AFS and ICP-AES are compared in Table 1.1 (56). Table 1.1 shows that similar plasma gas flows are required to operate plasmas used in ICP-AFS and ICP-AES. However, in contrast, no auxiliary gas flow is used for ICP-AFS. The most important difference in operating conditions is that the injector gas flow for ICP-AFS should be 1.5 to 2.0 L min$^{-1}$ to reduce the plasma background. For efficient sample excitation in ICP-AES the injector gas flow is generally below 1.0 L min$^{-1}$. However, it is noted that the velocity profile of the injector gas entering the plasma will be dependent upon the bore of the injector. Consequently this will affect the residence time of analyte species and hence the energy exchange processes within a given body of the plasma.

**Table 1.1: Comparison of typical operating conditions for ICP-AFS and ICP-AES systems (56)**

| Conditions | ICP-AFS | ICP-AES |
|---|---|---|
| Gas flow (L min$^{-1}$) | | |
| Plasma | 8 - 11 | 10 - 15 |
| Auxiliary | None | 1 - 2 |
| Nebuliser | 1.5 - 2.0 | 0.5 - 0.8 |
| Forward power (W, at 40 MHz) | | |
| Aqueous samples | 600 - 900 | 1000 |
| Non-aqueous samples | 500 - 700 | 1200 - 1300 |
| Solution uptake rate (ml min$^{-1}$) | | |
| Aqueous samples | 1 - 3 | 1 - 3 |
| Non-aqueous samples | 0.5 – 1.0 | 0.5 – 1.0 |
| Observation height in the ICP | Element dependent (see Figure 1.3) | 12 - 20 mm *ALC |

*ALC = above load coil

## 1.5.5.2 Torch Configuration and Observation Heights used for HCL-ICP-AFS

At conventional ICP-AES observation heights, typically 12 – 20 mm ALC, the plasmas high spectral background is sufficient to saturate the detector of an AFS system unless a spectral bandpass inappropriately small for AFS is used. However, the ICP used in AFS must produce a large population of ground-state atoms, in contrast to ICP-AES, where excitation of atoms is important. Consequently, the AF signal is more suitably measured higher in the tailflame, where both plasma background and emission from the sample are much lower. Obviously, the tailflame region should be stable and laminar to minimise signal drift and noise (56).

When lasers are used for excitation, the conventional Fassel torch used for ICP-AES is suitable for ICP-AFS systems but is inappropriate when using conventional excitation sources. An appropriate ICP torch for non-laser excitation of fluorescence is similar to the Fassel torch used for ICP-AES with two exceptions. First, the length of the outer coolant plasma tube is extended to stabilise the plasma tailflame and to delay air entrainment. This extension increases the length of the plasma tailflame to several centimetres beyond the outer tube, and increases the sample residence time. Second, in the load coil region, the nozzle of the injector has a gentle taper followed by a short straight section to obtain a laminar gas flow in the plasma tailflame and to minimise diffusion of the axial channel (56).

Optimum observation heights in the plasma, relative to the top of the load coil are shown in Figure 1.3 for various elements. For HCL-ICP-AFS, highest observation heights, 95 to 105 mm, are noted for the more easily dissociated elements (e.g., Au, Cd, Cu, Pb, Se, Zn) and easily ionised metals (all alkali metals). In this region, the baseline noise is low because of the low plasma emissions background and sample matrix emission (56).

Elements

Observation heights (mm)

All others | 85 - 105

Alkaline earths, Cr, In, certain rare earths | 75 - 85

Refractories, most rare earths | 55 - 65

40

0
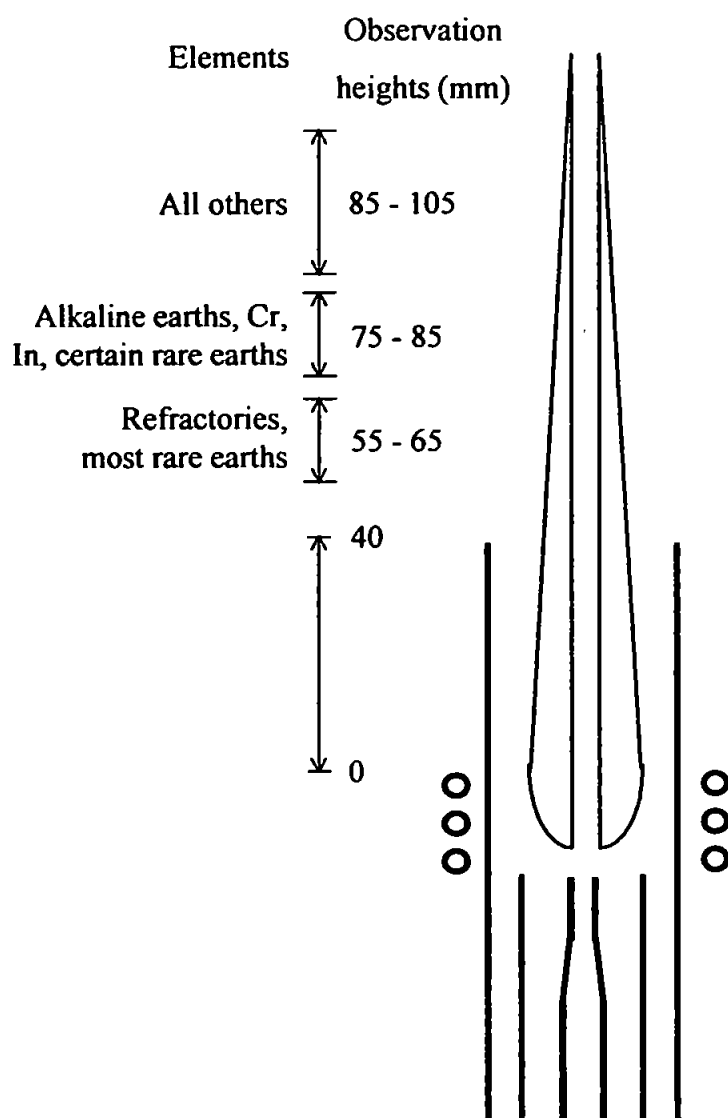
Figure 1.3: Torch and observation heights used for the determination of a range of elements in HCL-ICP-AFS (56)

The refractory elements and most lanthanides are measured at approximately 55 to 65 mm ALC. The higher plasma temperatures at lower observation heights are stated to be beneficial in effectively dissociating refractory elements into free atoms (56). However, the baseline noise is much larger in this region because of the plasma background, emission from the sample matrix, and large spectral bandpasses (one to several nanometers) typically used in AFS (56).

## 1.5.5.3 Radial Versus Axial Excitation Fluorescence Studies

To date, all fluorescence studies have 'focused' on a radial excitation arrangement (27 – 55, 59 - 74) and no in depth study using axial excitation has been published (41, 75, 76). Figure 1.4 illustrates the arrangement for both radial and axial excitation using an HCL/BDHCL as an excitation source and an ICP as an atomiser. Figure 1.4 demonstrates that, in the radial excitation mode, collection of fluorescence is restricted by the position of the source radiation. However, by irradiating axially, a larger number of atoms lie within the excitation sources' light beam and hence any fluorescence can be collected from a larger cell volume. Axial excitation fluorescence therefore offers a greater potential for increased fluorescence efficiency that that created by a normal radial excitation arrangement.
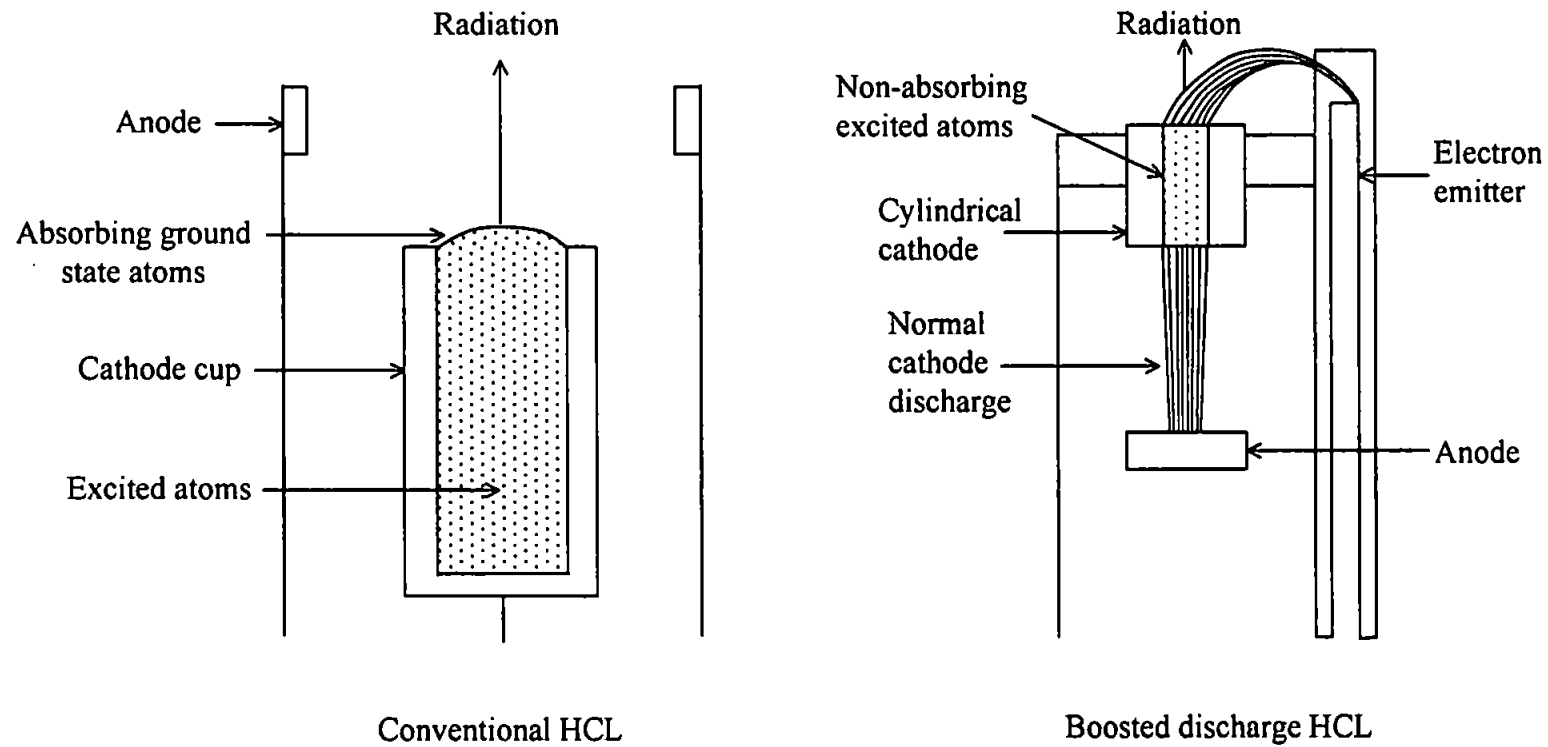
Figure 1.5: Schematic of conventional and boosted discharge hollow cathode lamps (56)

### 1.5.6 Limits of Detection

The ICP-AFS detection limits for the non-refractory and refractory elements excited by HCLs, ICPs and lasers are presented in Tables 1.2, 1.3 and 1.4, respectively. For comparison, the detection limits for both the non-refractory and refractory elements by ICP-AES and ICP-Mass Spectrometry (MS) are presented in Table 1.5.

The fluorescence signal is proportional to the intensity of the incident excitation light source falling on the atom cell. Therefore, one would expect the system with the highest source intensity to have the lowest LODs. From Tables 1.2 and 1.3 it appears that the LODs obtained by an HCL-ICP-AFS system are far superior to those obtained by both ICP-ICP-AFS and ASIA. It also suggests that the majority of the LODs obtained by ICP-ICP-AFS are equal to those obtained by ASIA. For a 'true' comparison of the LODs to be made between different systems, the instruments should be operated under their optimum conditions. Another consideration is that the efficiency of transfer of energy from the source to the atom cell depends on the optical system. For example, the efficiency of the optical system is quoted as 13 % (77) for ICP-ICP-AFS and as 1 – 2 % (53) for ASIA. If both systems had identical optics then the LODs obtained would be quite different. Overall conclusions as to the most sensitive systems are therefore hard to make.

For most commonly determined refractory elements, the HCL-ICP-AFS detection limits are comparable to, or better than those obtained by ICP-AES. However, ICP-AES can provide detection limits that are one or two orders of magnitude superior to HCL-ICP-AFS for the majority of the refractory elements. In contrast, the detection limits for all the remaining elements by HCL-ICP-AFS are fully comparable (if not superior) to those obtained using ICP-AES. In practice, limits of sensitivity (and to a certain extent LODs) will be dependent upon the atomisation and excitation efficiency derived from the

23

energy exchange processes within the same plasma. In fluorescence, as long as the plasma cell offers efficient atomisation (with reduced excitation processes, *i.e.* higher ground state population) then the intensity of the fluorescence excitation source has a contributing influence on the above analytical characteristics (assuming collection efficiency of detectors are comparable).

**Table 1.2: Detection Limits (DL) for the non-refractory elements for HCL/ICP-ICP-AFS**

| Element | Wavelength (nm) | HCL-ICP-AFS *DL (ng ml⁻¹) | Ref. | ICP-ICP-AFS *DL (ng ml⁻¹) | Ref. | ASIA *DL (ng ml⁻¹) | Ref. |
|---|---|---|---|---|---|---|---|
| Ag | 328.1 | < 0.1 | (56) | - | - | - | - |
| As | 193.7 | 25 | (56) | 15 | (60) | - | - |
| Au | 242.8 | 0.3 | (54) | - | - | - | - |
| Bi | 223.1 | 2 | (54) | - | - | - | - |
| Ca | 422.7 | < 0.1 | (56) | 0.6 | (60) | 0.2 | (53) |
| Cd | 228.8 | < 0.1 | (54) | - | - | - | - |
| Co | 240.7 | 0.4 | (54) | 30 | (61) | 9.5 | (53) |
| Cr | 357.9 | 0.4 | (54) | 6 | (61) | 3 | (53) |
| Cs | 852.1 | 3 | (56) | - | - | - | - |
| Cu | 324.8 | 0.1 | (56) | 0.6 | (60) | 0.4 | (53) |
| Fe | 248.3 | 0.3 | (54) | 7.5 | (61) | 5 | (53) |
| Ga | 417.2 | 4 | (56) | - | - | - | - |
| Hg | 253.6 | 5 | (54) | - | - | - | - |
| In | 451.1 | 2 | (54) | - | - | - | - |
| K | 766.5 | 0.6 | (54) | - | - | - | - |
| Li | 670.8 | < 0.1 | (56) | - | - | - | - |
| Mg | 285.2 | < 0.1 | (56) | 0.3 | (60) | - | - |
| Mn | 279.5 | 0.2 | (56) | 13.5 | (61) | - | - |
| Na | 589.0 | < 0.1 | (56) | 1.5 | (60) | 0.1 | (53) |
| Ni | 232.0 | 0.2 | (56) | 150 | (34) | 0.1 | (53) |
| Pb | 217.0 | 5 | (54) | - | - | 27 | (53) |
| Pd | 340.4 | 2 | (54) | - | - | - | - |
| Pt | 265.9 | 15 | (56) | - | - | - | - |
| Rb | 780.0 | 1 | (56) | - | - | - | - |
| Rh | 343.5 | 0.3 | (56) | - | - | - | - |
| Ru | 372.8 | 10 | (56) | - | - | - | - |
| Sb | 217.6 | 7 | (56) | - | - | - | - |
| Se | 196.0 | 10 | (54) | - | - | - | - |
| Sr | 460.7 | 0.3 | (56) | 0.3 | (77) | - | - |
| Te | 214.3 | 2 | (54) | - | - | - | - |
| Tl | 377.7 | 25 | (56) | - | - | - | - |
| Zn | 213.9 | < 0.1 | (54) | 3 | (77) | 2 | (53) |

* normalised to 3 standard deviations

**Table 1.3: Detection limits for the refractory elements for HCL/ICP-ICP-AFS**

| Element | Wavelength (nm) | HCL-ICP-AFS *DL (ng ml$^{-1}$) | Ref. | ICP-ICP-AFS *DL (ng ml$^{-1}$) | Ref. | ASIA *DL (ng ml$^{-1}$) | Ref. |
|---------|-----------------|------------------|------|------------------|------|------------------|------|
| Al | 396.2 | 5 | (56) | 15 | (77) | 20.5 | (53) |
| B | 249.8 | 60 | (56) | 15 | (77) | 28 | (53) |
| Ba | 553.6 | 25 | (56) | 1.35 - | (77) | 3.5 | (53) |
| Be | 234.9 | 0.5 | (56) | - | - | - | - |
| Eu | 459.4 | 20 | (56) | - | - | - | - |
| Ge | 265.1 | 25 | (56) | - | - | - | - |
| Hf | 286.6 | 400 | (56) | 45 | (77) | - | - |
| Mo | 334.9 | 8 | (56) | 150 | (78) | 63 | (53) |
| Nb | 313.3 | 600 | (56) | - | - | - | - |
| P | 178.2 | 2000 | (56) | 120 | (77) | - | - |
| Re | 346.9 | 400 | (56) | - | - | - | - |
| S | 182.0 | 2000 | (56) | - | - | - | - |
| Sc | 391.2 | 5 | (56) | - | - | - | - |
| Si | 251.6 | 40 | (56) | 10.6 | (77) | 54.5 | (53) |
| Sn | 224.6 | 25 | (56) | - | - | - | - |
| Ta | 271.5 | 1500 | (56) | - | - | - | - |
| Ti | 337.2 | 25 | (56) | - | - | - | - |
| U | 358.5 | 5000 | (56) | - | - | - | - |
| V | 318.5 | 20 | (56) | 60 | (77) | | |
| W | 255.1 | 200 | (68) | - | - | 428 | (53) |
| Y | 410.2 | 300 | (56) | 30 | (77) | - | - |
| Yb | 398.8 | 0.7 | (68) | 15 | (77) | - | - |
| Zr | 360.1 | 400 | (56) | 15 | (77) | - | - |

* normalised to 3 standard deviations

**Table 1.4: Detection limits for the non-refractory and refractory elements for LE-ICP-AFS**

| Element | Species | Laser excited line (nm) | Fluorescence line (nm) | *DL (ng ml$^{-1}$) | Ref. |
|---------|---------|------------------------|------------------------|--------------------|------|
| Al | I | 328.07 | 338.3 | 1.3 | (78) |
| Al | I | 394.4 | 396.2 | 0.4 | (31) |
| Au | I | 267.6 | 267.6 | 11 | (78) |
| B | I | 249.67 | 249.8 | 4 | (31) |
| Ca | II | 393.37 | 396.9 | 1 | (79) |
| Ce | II | 407.58 | 401.2 | 400 | (80) |
| Dy | II | 407.8 | 394.5 | 400 | (80) |
| Er | II | 404.84 | 374.3 | 260 | (80) |
| Eu | II | 305.49 | 290.7 | 72 | (80) |
| Ga | I | 287.42 | 294.42, 294.36 | 1 | (31) |
| Gd | II | 407.84 | 354.6 | 75 | (80) |
| Hf | II | 263.87 | 303.1 | 16 | (78) |
| In | I | 303.94 | 325.6 | 300 | (79) |
| Ir | I | 284.97 | 292.7 | 58 | (78) |
| La | II | 403.17 | 379.1 | 170 | (80) |
| Lu | II | 302.05 | 296.3 | 85 | (80) |
| Mo | I | 313.26 | 317.0 | 5 | (31) |
| Na | I | 589 | 589.6 | 0.1 | (79) |
| Nb | II | 292.78 | 267.7 | 11 | (78) |
| Nd | II | 406.11 | 428.5 | 470 | (80) |
| Pb | I | 283.3 | 405.8 | 1 | (31) |
| Pd | I | 324.27 | 340.5 | 6 | (78) |
| Pr | II | 406.13 | 405.7 | 240 | (80) |
| Pt | I | 265.94 | 271.9 | 34 | (78) |
| Si | I | 286.16 | 251.43, 251.61, 251.92 | 1 | (31) |
| Sr | II | 407.77 | 416.2 | 7 | (79) |
| Ta | II | 268.52 | 276.2 | 20 | (78) |
| Tb | II | 403.31 | 400.6 | 650 | (80) |
| Ti | II | 307.86 | 316.26, 316.85 | 1 | (31) |
| Tm | II | 301.53 | 313.1 | 140 | (80) |
| Tl | I | 377.57 | 352.9 | 4 | (31) |
| U | II | 409.01 | 386.0 | 20 | (31) |
| V | II | 268.9 | 290.88 | 3 | (31) |
| Y | II | 508.74 | 371.03 | 0.6 | (31) |
| Yb | II | 303.11 | 279.06 | 25 | (80) |
| Zr | II | 310.69 | 256.89, 257.14 | 3 | (31) |

* normalised to 3 standard deviations

**Table 1.5: Detection limits for the non-refractory and refractory elements for ICP-AES and ICP-MS (23)**

| Non refractory | | | Refractory | | |
|---|---|---|---|---|---|
| Element | *ICP-AES DL (ng ml⁻¹) | *ICP-MS DL (ng ml⁻¹) | Element | *ICP-AES DL (ng ml⁻¹) | *ICP-MS DL (ng ml⁻¹) |
| Ag | 1.5 | 0.003 | Al | 6 | 0.006 |
| As | 30 | 0.006 | B | 3 | 0.09 |
| Ca | 0.15 | 2 | Ba | 0.15 | 0.002 |
| Cd | 1.5 | 0.003 | Hf | - | 0.0006 |
| Co | 3 | 0.0009 | Mo | 7.5 | 0.003 |
| Cr | 3 | 0.02 | P | 45 | 0.3 |
| Cu | 1.5 | 0.003 | Si | 5 | 0.7 |
| Fe | 1.5 | 0.4 | Sn | 60 | 0.002 |
| Hg | 30 | 0.004. | V | 3 | 0.002 |
| Mg | 0.15 | 0.007 | W | 30 | 0.001 |
| Mn | 0.6 | 0.002 | Y | 0.3 | 0.0009 |
| Na | 6 | 0.05 | Yb | - | 0.001 |
| Pb | 30 | 0.001 | Zr | 1.5 | 0.004 |
| Pt | 30 | 0.002 | | | |
| Sb | 90 | 0.001 | | | |
| Zn | 1.5 | 0.004 | | | |

* normalised to 3 standard deviations

## 1.5.7 Operation of HCLs and BDHCLs

A HCL comprises a hollow cylindrical cathode lined with the element of interest contained within a glass envelope filled with an inert gas. When a potential is applied between the electrodes, at the pressures used, the discharge concentrates into the hollow cathode. The filler gas becomes charged at the anode, and the ions produced are attracted to the cathode and accelerated by the field. The bombardment of these ions on the inner surface of the cathode causes metal atoms to sputter out of the cathode cup. Further collisions excite these metal atoms and a simple, intense characteristic spectrum of the metal is produced (80).

The detection limits for HCL-ICP-AFS improved significantly when boosted discharge HCLs (Superlamps, Photron Pty Ltd., Dandenong, Australia) became commercially available. Boosted discharge HCLs (Figure 1.5) use a second discharge, between a common anode and a second, filament shaped cathode. *En-route* to the anode, the electrons emitted from the filament cathode pass through a cylindrical cathode, rather than a cup shaped anode as with conventional HCLs. The electron beam enhances excitation of the filler gas which, in turn, leads to efficient excitation of atoms sputtered from the discharge wall (56).

The output stability of BDHCLs is comparable to that of conventional HCLs, and their lifetime, when operated in the pulsed mode, is at least twofold longer. BDHCLs provide 3 to 15 fold gains in AF signal for elements that require a high energy for excitation (*i.e.* non-refractory transition metals). Elements that require a low energy for excitation show little or no gain output (*i.e.* alkali and most refractory elements) (56).

29

Radiation

Anode

Absorbing ground
state atoms

Cathode cup

Excited atoms

Conventional HCL

Radiation

Non-absorbing
excited atoms

Cylindrical
cathode

Normal
cathode
discharge

Electron
emitter

Anode

Boosted discharge HCL
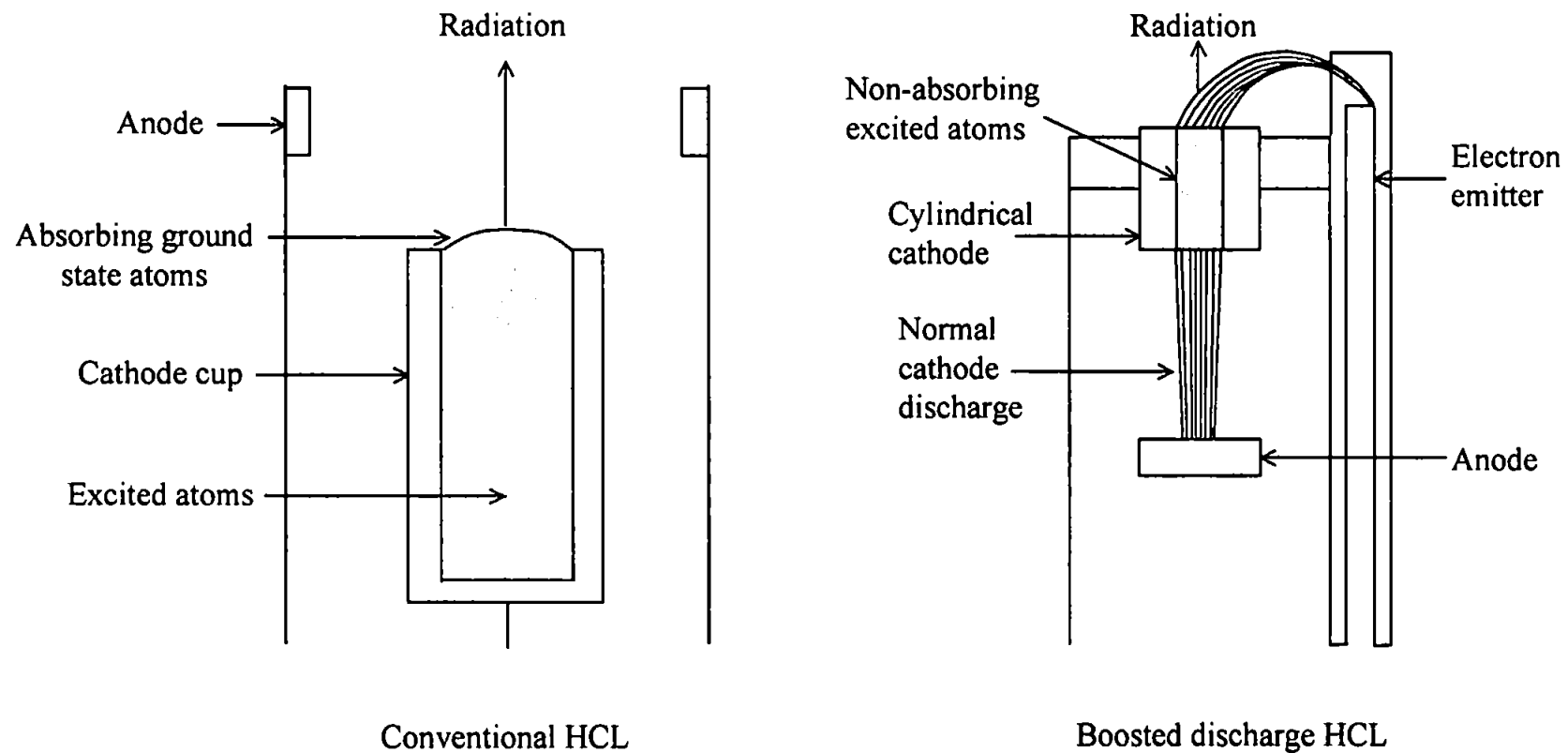
Figure 1.5: Schematic of conventional and boosted discharge hollow cathode lamps (56)

## 1.6   Aims and Objectives

All of the literature published thus far has focused on radial excitation of the plasma, *i.e.* the excitation source is focused through the side of the plasma thereby illuminating only a small cross section of the atom cell. One of the aims of the present work was to use novel 'axial excitation' which would allow the potential for both high efficiency excitation of the analyte and very high efficiency collection of fluorescence by a suitable detection system. The development and assembly of ICP-equipment hardware and novel optical trains, including axial excitation/fluorescence would involve:

(i)     construction of the source-to-atomiser optical path using conventional and boosted HCLs, modulation of source excitation and fluorescence collection using phase-locked detectors, mirror and/or condensing lens arrangement and,

(ii)    construction of the atomiser-to-detector optical path using extended ICP torches, lenses and fibre optics.

Ideally, a system would comprise a stand-alone, free-running generator with a compartment large enough to accommodate the torch and optics, a horizontal torch and quartz optics. The excitation would be by BDHCLs powered by a commercial modulated supply. Detection would be by a conventional photomultiplier tube (PMT) and amplifier system.

This programme would be expected to allow a fundamental study of the analytical benefits of AFS using an ICP as an atom cell. The majority (if not all) of the literature concerning ICP-AFS indicates that both a much lower power should be applied to the plasma and that the gas flows are somewhat different to those used in typical ICP-AES operation. Consequently, the plasma used under ICP-AFS conditions will likely possess very different properties to a plasma operated under ICP-AES conditions. Another aim

31

of this study was therefore to characterise this low power plasma in terms of its relative population states, 'temperatures' and electron number densities.

A variety of factors influence the analytical performance of ICP spectrometry. In ordinary operations, analyses under so-called compromise conditions usually provide results that exhibit good precision and accuracy. However, the selection of optimum parameters should be based on studies of the behaviour of the plasma itself. Spectrochemical characteristics of the ICP must therefore be elucidated. One principle objective of this study was to investigate the fundamental mechanisms that form in a plasma operated under fluorescence conditions (low power and high nebuliser gas flow rates).

## 2.0 THE DESIGN, CONSTRUCTION AND TESTING OF EQUIPMENT FOR USE IN PRELIMINARY FLUORESCENCE EXPERIMENTS

### 2.1 Introduction

The last few decades have seen much progress in AFS with the introduction of more intense sources such as the BDHCL, XeCl pumped dye lasers and the ICP. The driving force for this being that the intensity of the atomic fluorescence signal is proportional to the intensity of the incident light provided that saturation has not occurred (59). In addition, AFS utilises long linear dynamic ranges (like AES) and is well suited to the development of simple and low-cost instrumentation. At the same time, AF spectra are relatively simple, like atomic absorption (AA) spectra. Moreover, if the excitation source is modulated synchronously, the baseline drift will be limited to that of the electronics. Finally, if an ICP is used as an atomisation cell, the possibility arises that some inter-element effects may be reduced substantially and scattered radiation interferences may be eliminated for all practical purposes (29).

Although the characteristics of ICP-AFS are attractive, the technique has rarely been used for routine analysis, primarily because of the absence of available instrumentation. The first commercially available multi-element AF spectrometer incorporating an ICP as an atomiser was introduced by the Baird Corporation in the early 1980's (29, 32). However, this instrument was only available for a short period of time. Alternatively, a standard commercial ICP may be used as an atomizer (possibly with a change of torch) with an external HCL as a light source. Simple optics are all that is required to transfer light energy from the source to the atomizer and there is no doubt that in the case of AES instruments the existing monochromator would be more than sufficient for the task of isolating the fluorescence wavelengths produced.

33

This study, previously as stated, describes the use of a commercial ICP-AE spectrometer in the AF mode in order to investigate its potential to improve upon the sensitivity and LODs of the parent instrument in its AES mode. One means of achieving this improvement would be to use an axial excitation approach (81). To date, all studies have focused on the use of a radial excitation arrangement (59, 60 – 74), and no in-depth investigation using axial excitation has been published (41, 75, 76). Axial excitation offers a greater potential for increased fluorescence than that created by a normal radial excitation arrangement. This is because fluorescence emission is proportional to the light energy absorbed in the atomiser cell, and therefore any increase in the size of the cell would be beneficial. By irradiating axially, a larger number of atoms lie within the light beam and hence are available to fluoresce. With this arrangement in mind it was proposed that the cell size in ICP-AFS could be increased by using a plasma torch with an extended outer sleeve and suitable flow conditions for producing a plasma tailflame many centimetres long. A sufficiently intense excitation source would then be used to irradiate this tailflame in an axial manner: Excitation optics would be aligned so that the beam passes down through the central channel of the plasma. To contend with the elongated tailflame and the hot gases associated with a vertical plasma, a novel optical assembly would be necessary. Suitable fibre optic guides and 'condensing lens' arrangements would be used for both the excitation and detection systems. A coolant (argon gas) would be made to flow down through the optical train which, together with water cooling, would greatly reduce the risk of damage to the optics caused by the excessive thermal environment above the plasma. Owing to the specificity of AFS, expensive monochromators would be unnecessary. This system would employ narrow bandwidth interference filters to isolate the emitted wavelength region of interest. A modulated excitation source and an amplifier phase-locked detection system would complete the assembly.

## 2.2 Experimental: Instrumental Development for the Testing of Equipment used in Preliminary Fluorescence Experiments

The basic instrumental layout for the production of fluorescence is presented in Chapter 1 (Section 1.5.3, Figure 1.2). Radiation from a modulated excitation source (HCL, BDHCL, EDL, ICP, light emitting diode (LED) or a laser) is directed through an atom cloud, produced from an analyte that has been introduced into a relatively low temperature atomizer. This atomizer can, for example, be a flame, a heated graphite rod or a plasma.

Part of the radiation from the excitation source is absorbed and subsequently re-emitted as fluorescence radiation. The fluorescence radiation is resolved with either a monochromator or a filter and the intensity measured by means of a suitable detector. The output of the detector is fed to a lock-in amplifier to distinguish between the modulated fluorescence radiation and the continuous emission signal from the atomiser.

The aim of this section of work was to design and construct the equipment necessary to perform ICP – atomic fluorescence and to test the excitation and detection equipment before any preliminary fluorescence experiments were performed.

### 2.2.1 Instrumental Development

#### 2.2.1.1 Plasma Torch

A plasma torch with an extended coolant tube is required in ICP-AFS to stabilise the plasma tailflame and delay air entrainment (56). Figure 2.1 shows the design of the demountable plasma torch with an extended coolant tube used in the initial ICP-AFS experiments. This was specially constructed (H. Baumbach & Company Limited, Ipswich, Suffolk, UK) in order to fit directly into the Optima 3000 ICP (The Perkin-

Elmer Corporation, Norwalk, CT, USA) torch mounting and load coil assembly. Injectors (0.85 and 1.5 mm i.d.) were manufactured from alumina ceramic with the top 5.0 mm of the injector being a constant bore to reduce dispersion effects on gas flows (56).

## 2.2.1.2 Demountable X and Y-Axis Translation Plate

A demountable X and Y-axis translation plate (39 x 29 x 7cm) was designed and constructed from aluminium (Plates 2.1 and 2.2) to fit the Optima 3000 ICP (The Perkin-Elmer Corporation) torch and optics housing. This plate allowed a fibre optic to be positioned for radial emission, absorption and fluorescence scanning of the whole plasma along both the vertical (Y) and horizontal (X) axes. Reproducible positioning of the collector fibre optic was controlled by two fine screw multi-turn calibrated pots.

20 mm o.d.

18 mm o.d.

16 mm o.d.

Load coil

60 mm

159 mm

6 mm o.d.

Plasma gas flow →

6 mm o.d.

Auxiliary gas flow →

Alumina ceramic injector tube

Nebuliser gas flow
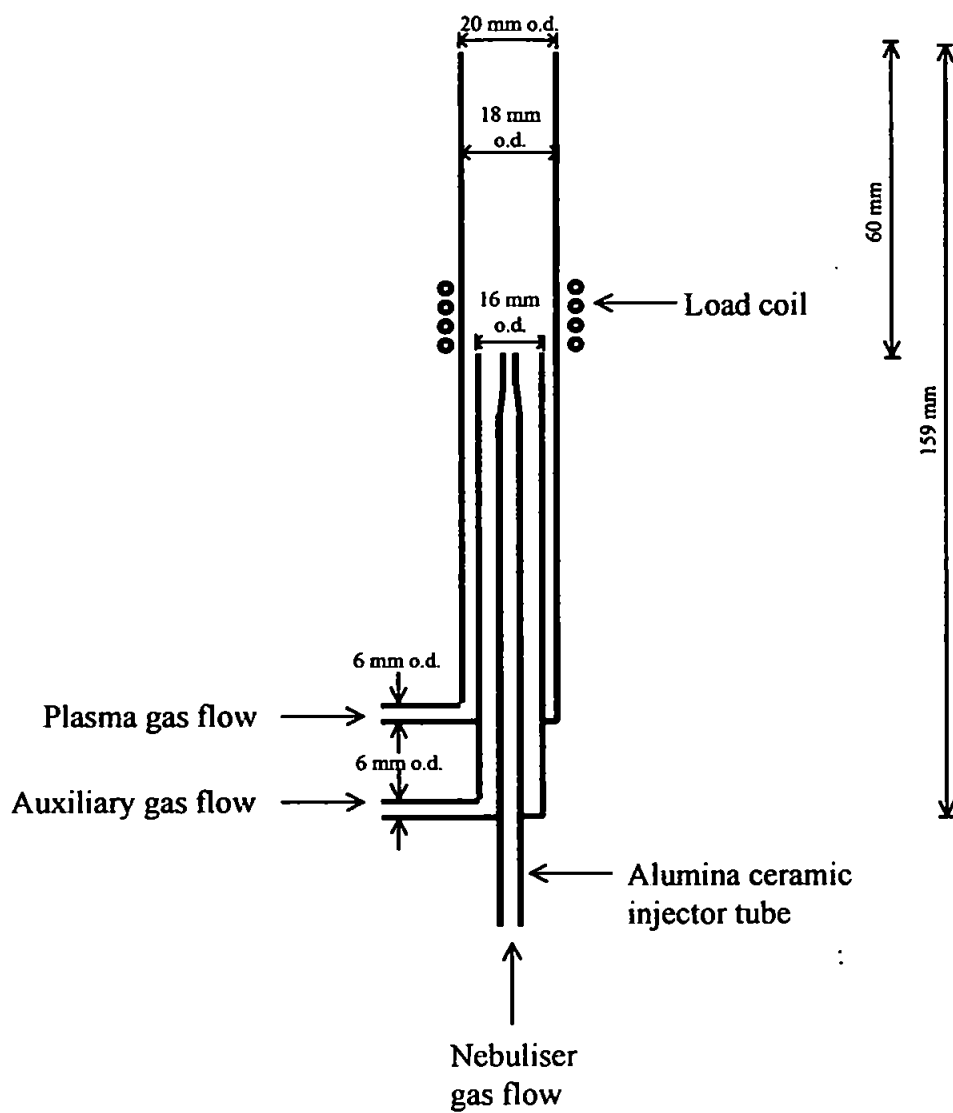
**Figure 2.1: Specially constructed demountable torch used in preliminary ICP-AFS experiments**

Plate 2.1: Front view of the demountable X and Y-axis translation plate
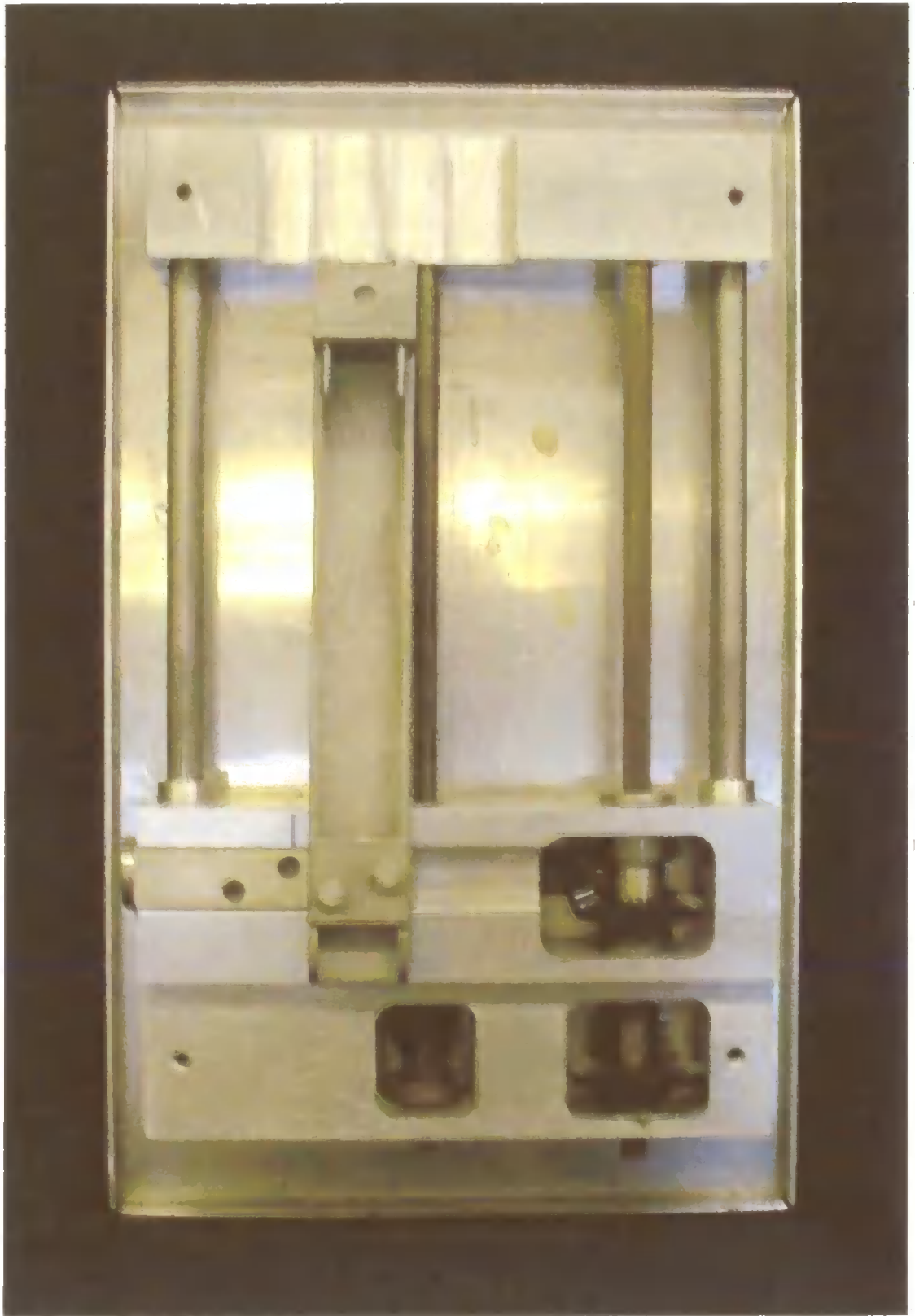
Plate 2.2: Rear view of the demountable X and Y-axis translation plate

### 2.2.2 Testing of Optical Filters and Fibre Optics

The optical filters (Model Nos. 5325 and 5370; L.O.T. Oriel, Leatherhead, Surrey, UK), used throughout this study were tested before use. This was to ensure that the filter chosen provided sufficient light throughput for the analyte of interest. A standard Tungsten table lamp was shone through each filter onto a monochromator and PMT (1700 Series; SPEX Industries INC., Metochen, N.J. 08840). Measurements were taken using a Datascan 2 (ISA Instruments S.A. (U.K.) Ltd., Middlesex, U.K.) interfaced with a Current/Phase Stepper Drive and a monochromator and PMT (1700 Series, SPEC Industries INC.). An IEEE488 communications port provided standardised electronic protocols to receive commands and send data to a host computer. All readings were automated by constructing a program within the instrument software (SpectRad Version 2 for Windows; ISA Instruments S.A. (U.K.) Ltd.).

All fibre optics were transmission tested before use. The intensity of a light source was measured using a light meter before and after transmission through a fibre optic. The difference in light throughput was calculated and expressed as a percentage.

### 2.2.2.1 Testing of the Detection System used for Preliminary Fluorescence Experiments in Emission Mode

It was necessary to test the complete detection system using a mode that was both easy to measure and reproducible. This was to ensure that both the optics and electronics were working correctly before any preliminary fluorescence experiments were performed. To this end, the emission mode was chosen using the output from the Optima 3000 ICP (The Perkin-Elmer Corporation), modulated using a light chopper. A schematic of the experimental arrangement and conditions are presented in Figure 2.2 and Table 2.1, respectively.

The detection system employed two fibre optics (3.0 and 5.0 mm i.d., 1.0 m in length; Fiberguide Industries, Stirling, New Jersey, USA), a light chopper (10 bladed chopper disc operated at 665 Hz; Model 9479; EG & G Brookdeal, Bracknell, Berkshire, UK), an optical filter ($\lambda_{max}$ 320 nm; Model No. 5325; L.O.T. Oriel), a photomultiplier tube (800 V; I.L. R 955; Hamamatsu Photonics UK Ltd., Enfield, UK) operated by a high voltage power supply (Model 456; EG & G Ortec, Oakridge, USA), and a lock-in amplifier (Model 9503; EG & G Brookdeal).

The demountable X and Y-axis translation plate position was fixed centrally at a viewing height of 30 mm ALC. Solutions of varying copper concentration (0 - 1000 mg $dm^{-3}$) were prepared and aspirated into the plasma while the signal from the lock-in amplifier (direct read, meter value) was observed and recorded.

:

.
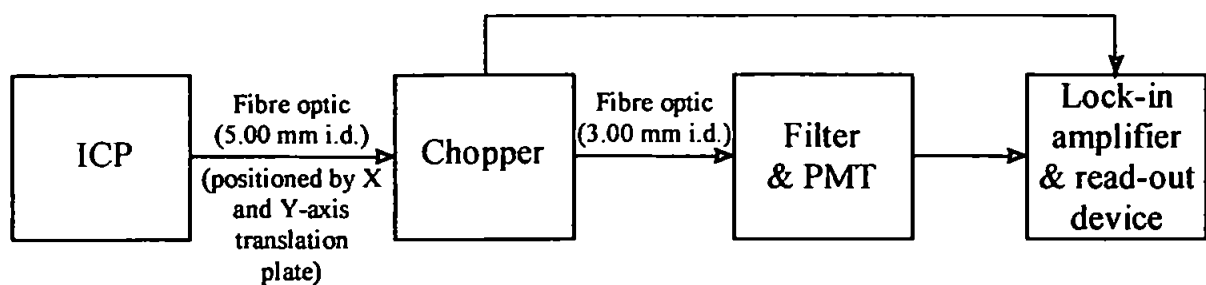
**Figure 2.2: Schematic arrangement of the external detection system used for the Optima 3000 ICP when operated in emission mode**

:

.

**Table 2.1: Instrumental parameters used for the Optima 3000 ICP and external**

**detection system when operated in emission mode**

| Instrument Type | |
|---|---|
| Perkin-Elmer (PE) Optima 3000 ICP-AES | |
| **RF Generator** | |
| Frequency | 40.68 MHz, free running |
| Power | 1000 W, adjustable in 5 W increments |
| **Sample Introduction System** | |
| Nebuliser | Ebdon V-Groove high solid |
| Torch | Demountable with 1.5 mm i.d. alumina injector |
| Spray Chamber | PE Scott Double Pass |
| Peristaltic Pump | Gilson Minipuls 3, computer controlled |
| Uptake Rate | 1.0 ml min$^{-1}$ |
| **Argon Flow Rate** | |
| Plasma | 16 L min$^{-1}$ |
| Auxiliary | 0.8 L min$^{-1}$ |
| Nebuliser | 1.0 L min$^{-1}$ |
| **External Detection System** | |
| Filter        : | $\lambda_{max}$ 320 nm (Model no. 5325) |
| PMT | 800 V |

## 2.2.3 Cold Vapour Mercury Fluorescence Experiments

A mercury HCL (primary current 5 mA; Starna, Romford, Essex, UK) operated by a lamp power supply (Vokam, Shandon Power Supply Type 2541; Thermo Shandon Inc., Pittsburg, USA) was used as the excitation source and a cold vapour mercury cell was used as the atom cell. A bi-convex quartz lens (1 x 2.9 cm diameter, 6.4 cm focal length; L.O.T. Oriel) was used in a 2f:2f arrangement (inverted, Figure 2.3) in order to focus the emission from the hollow cathode lamp through a light chopper (10 bladed chopper disc operated at 665 Hz; Model 9479; EG & G Brookdeal) onto the cold vapour mercury cell. An identical lens was used in a 2f:2f arrangement (inverted) to focus the fluorescence radiation from the cold vapour mercury cell onto the filter and detector. A schematic of the experimental arrangement used in illustrated in Figure 2.4.

As fibre optics were to be used in the preliminary fluorescence experiments, the above experiment was repeated with the addition of fibre optics. The experimental arrangement used is illustrated in Figure 2.4. The emission from the lamp was focused using a bi-convex quartz lens (1 x 2.9 cm diameter, 6.4 cm focal length; L.O.T. Oriel) in a 2f:2f arrangement (inverted) through a light chopper (10 bladed chopper disc operated at 665 Hz; Model 9479; EG & G Brookdeal) onto the end of a fibre optic (3.0 mm i.d., 1.0 m in length; Fiberguide Industries) leading to the atom cell. Similarly, an identical lens was used to focus the fluorescence radiation in a 2f:2f arrangement from the cold vapour mercury cell onto the end of another fibre optic (5.0 mm i.d., 1.0 m in length; Fiberguide Industries) leading to the detection system.

The detection system comprised an optical filter ($\lambda_{max}$ 260 nm; Model No. 5325; L.O.T. Oriel), a photomultiplier tube (800 V; I.L. R 955; Hamamatsu Photonics UK Ltd.) operated by a high voltage power supply (Model 456; EG & G Ortec), and a lock-in amplifier (Model 9503; EG & G Brookdeal).
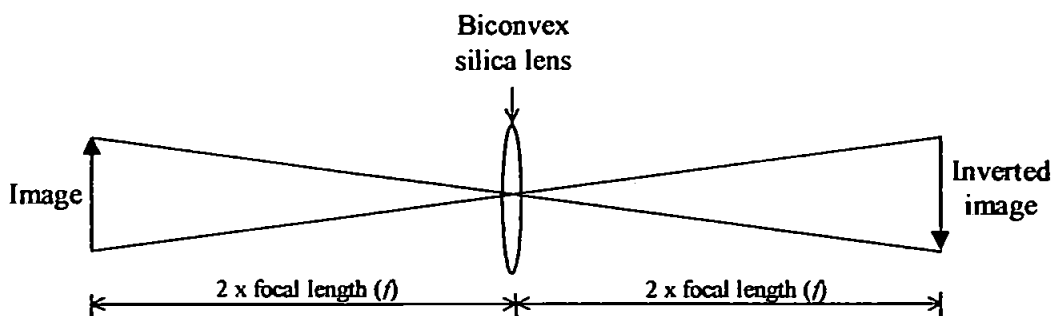
Figure 2.3: Schematic of a 2f:2f arrangement
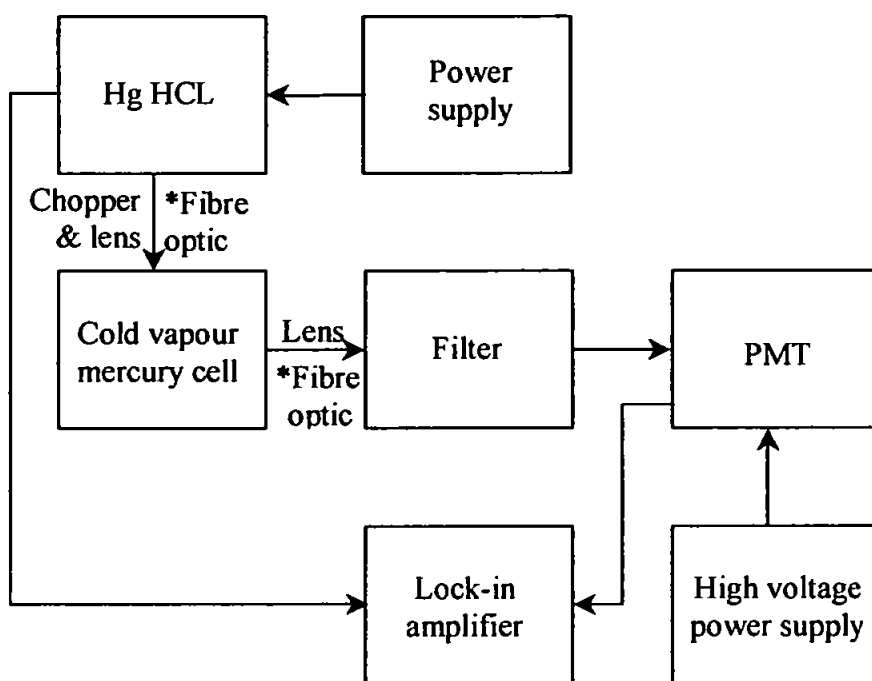


Figure 2.4: Schematic of the cold vapour mercury fluorescence arrangement using

focusing lenses with and without the use of *fibre optics

## 2.2.4 Production of the Required Plasma Conditions for Preliminary Fluorescence Experiments

### 2.2.4.1 Calibration of the ICP Forward Power Range

The Optima 3000 ICP (The Perkin-Elmer Corporation) was power calibrated between 750 – 1500 W by a Perkin-Elmer engineer.

### 2.2.4.2 Production of the Extended Tailflame

Using the Optima 3000 ICP (The Perkin-Elmer Corporation) and the range of plasma conditions given in Table 2.2 (*i.e.* low power, *ca.* 750 - 1000 W), high nebuliser gas flows (variable up to 1.5 L min$^{-1}$), very low auxiliary gas flows ($\leq$ 0.5 L min$^{-1}$) and reduced plasma (12 –17 L min$^{-1}$) gas flows, a concentrated lithium solution (1000 µg ml$^{-1}$) was aspirated into the plasma.

### 2.2.4.3 Chemicals and Reagents

All reagents used (Ba, Cu, Li & W) were of 'AnalaR' reagent grade (Merck, Poole, Dorset, UK) and all solutions were prepared using doubly deionised water (Milli-Q, Millipore, Harrow, Middlesex, UK).

Calibration standards were prepared by serial dilution of commercially available stock standard solutions (1000 and 10000 µg ml$^{-1}$).

**Table 2.2: Instrument parameters for the Optima 3000 ICP when operated in**

**fluorescence mode**

| Instrument Type | |
|---|---|
| Perkin-Elmer (PE) Optima 3000 ICP-AES | |
| **RF Generator** | |
| Frequency | 40.68 MHz, free running |
| Power | 750 – 1000 W, adjustable in 5 W increments |
| **Sample Introduction System** | |
| Nebuliser | Ebdon V-Groove high solids |
| Torch | Demountable with 0.85/1.5 mm i.d. alumina injector and 60 mm extended coolant tube (from auxiliary) |
| Spray Chamber | PE Scott Double Pass |
| Peristaltic Pump | Gilson Minipuls 3, computer controlled |
| Sample Uptake Rate | 2.0 ml min$^{-1}$ |
| **Argon Flow Rate** | |
| Plasma | 12 - 17 L min$^{-1}$ |
| Auxiliary | Variable up to 0.50 L min$^{-1}$ |
| Nebuliser | Variable up to 1.5 L min$^{-1}$ |

## 2.2.5 Results and Discussion

### 2.2.5.1 Testing the Detection System when Operated in Emission Mode

Results presented in Figure 2.5 demonstrate a linear relationship between concentration of Cu in solution and the ICP emission signal at 324.7 nm when the emitted radiation is modulated (667 Hz). The chopped intensity reaching the PMT resulted in a linear demodulated signal output (mV) from the lock-in amplifier when the optical and electronic detection system were working correctly. However, some limitations upon signal definition and sensitivity were felt to contribute to a loss in detection capability. For example, the lock-in amplifier may be able to detect a very intense modulated emission signal and produce a steady, stable signal that increases with increasing solution concentration. However, this is a different scenario to that used to detect fluorescence, where the continuum background and continuous analyte emission levels can be concomitantly high and may greatly reduce the sensitivity of the detector. A simple experiment was devised to test this theory. The emission from a modulated HCL was directed through an iris/filter assembly onto a PMT and the signal on the lock-in amplifier observed. The signal increased with increasing current applied to the lamp and also registered zero when the lamp was covered. When the light from an intense continuous source was directed onto the PMT, together with that from the modulated HCL, the lock-in amplifier did not produce a steady signal. In this experiment, the continuous light source (analogous to a plasma) was effectively 'saturating' the PMT (reducing the available sensitivity) and hence reducing the ability of the lock-in amplifier to lock-in to the modulated signal. It was therefore concluded that where background levels of emission from the plasma cannot be reduced, the ability of the amplifier to detect fluorescence will be severely hampered.

In a modulation cycle, the lock-in amplifier monitors the background emission, then the background emission plus the fluorescence signal. Both signals are then amplified and a subtraction performed to obtain the fluorescence signal. Thus, any instability in the background emission signal becomes important. This effect from instability could be rectified by the use of a differential amplifier that monitors the background emission continuously, as well as the background emission and the fluorescence signal in order to obtain the fluorescence signal. The demountable X and Y-axis translation plate, fibre optics, light chopper modulator, interference filter (Cu, $\lambda_{max}$ 320 nm), PMT and lock-in amplifier, were all employed in this successful experiment.
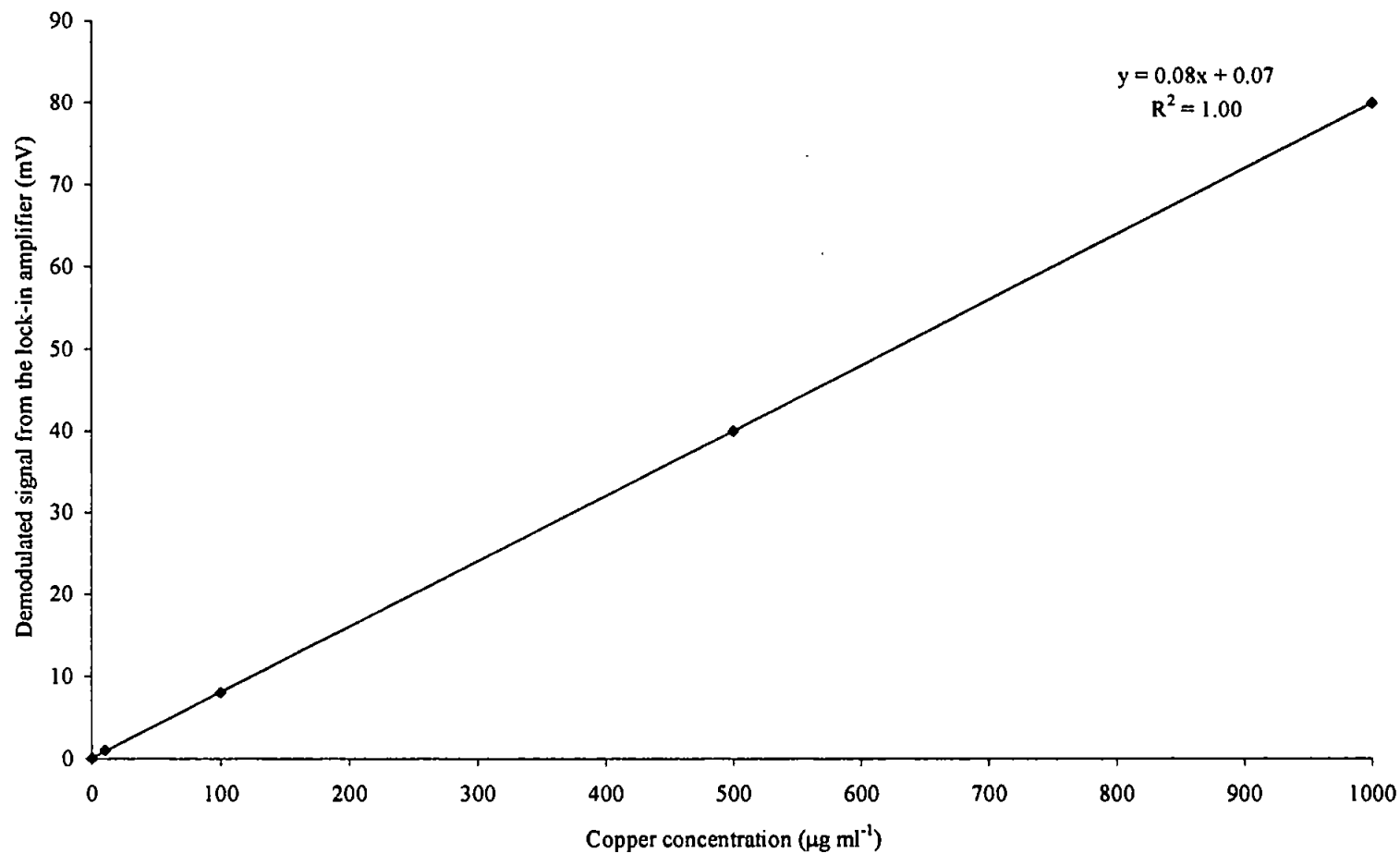
**Figure 2.5: Effect of Cu solution concentration on a modulated (667 Hz) ICP emission signal at 324.7 nm observed using the lock-in amplifier**

**(n = 3, RSDs < 2 %)**

## 2.2.5.2 Cold Vapour Mercury Fluorescence Experiments

Using the arrangement shown in Figure 2.4, without the use of fibre optics, a cold vapour mercury cell was excited by a mercury HCL and fluorescence radiation was detected at right angles to the excitation beam. A stable signal was obtained on the lock-in amplifier which increased proportionally with increasing intensity of the excitation source. When the excitation source was 'blocked off', no meter reading was observed on the lock-in amplifier. The cold vapour mercury cell was replaced with another cell that did not contain mercury vapour to ensure that the signal was not due to a scattering effect. No signal was obtained, indicating that the signal observed was due to mercury fluorescence.

The same observations were made when fibre optics were used, employing the arrangement shown in Figure 2.4. It was important to use the fibre optics in the cold vapour mercury fluorescence experiments because this arrangement would be used in the axial excitation assembly. The only differences between Figure 2.4 and the experimental assembly to be used in Figure 2.6 was that a cold vapour mercury cell was used as the atomiser instead of the ICP and that the excitation was produced in a tangential, and not axial, manner.

## 2.2.5.3 Calibration of the ICP

The ICP was calibrated between 750 – 1500 W. The plasma could not be calibrated below 750 W because the calibration was for a commercial ICP-AES instrument with a typical forward power operating range of 1000 – 1500 W.

## 2.2.5.4 Production of the Extended Tailflame

Using low forward power (*ca.* 750 W), a high nebuliser gas flow rate (1.5 L min$^{-1}$ through a 0.85 and 1.5 mm i.d. injector), low auxiliary ($\leq$ 0.2 L min$^{-1}$) and reduced plasma (14 L min$^{-1}$) gas flow rates, the required elongated tailflame plasma was produced in the extended coolant tube torch. This was visually observed and verified by the required plasma structure. The tailflame was seen to extend to approximately 18 cm above the load coil when a concentrated lithium solution (1000 mg dm$^{-3}$) was aspirated.

Both a 0.85 and a 1.5 mm i.d. alumina injector were used in producing the required extended tailflame. In the literature, nebuliser gas flow rates are typically around 1.5 – 3.0 L min$^{-1}$ (29, 32, 56, 66). However software limitations and the high back-pressure of the nebuliser meant that higher nebuliser gas flow rates (> 2.0 L min$^{-1}$) could not be reproduced. It was calculated that if a smaller bore injector was used (0.85 mm i.d.) then this covered the same velocity range as that produced by a 1.5 mm i.d. injector with a higher nebuliser gas flow rate.

Visual observations of the plasma structure using both injectors looked similar but it was decided to use a 1.5 mm i.d. injector in future experiments. This was to ensure that the conditions used in the preliminary fluorescence experiments matched those described in the literature (29, 32, 56, 66) as closely as possible.

## 2.3 Experimental: Design, Construction and Testing of a Fibre Optic Axial Excitation Assembly

### 2.3.1 Axial Alignment Frame

In order to achieve axial excitation of the plasma using the commercially available Optima 3000 ICP-AES (The Perkin-Elmer Corporation), the entrance optics had to enter the torch box from above. Use of a chimney allowed direct axial access to the plasma. A replacement chimney in the form of an axial alignment frame, designed and constructed in-house, allowed the exhaust gases to escape and served as the entry point to the torch box whilst holding a glass condenser system in alignment to 'house' the excitation optics (Plates 2.3 and 2.4, see also Figure 2.6). Frame dimensions were approximately 40 cm in length by 10 cm in diameter and the base of the axial alignment frame was bolted to the instrument. A 'fork' at the top of the frame held the condenser system in place and allowed vertical adjustment (controlled by a screw thread). Two collars were used to optically align the condenser centrally using a laser. Each collar had four sprung adjustable screw threads to allow for any expansion of the glass and frame.
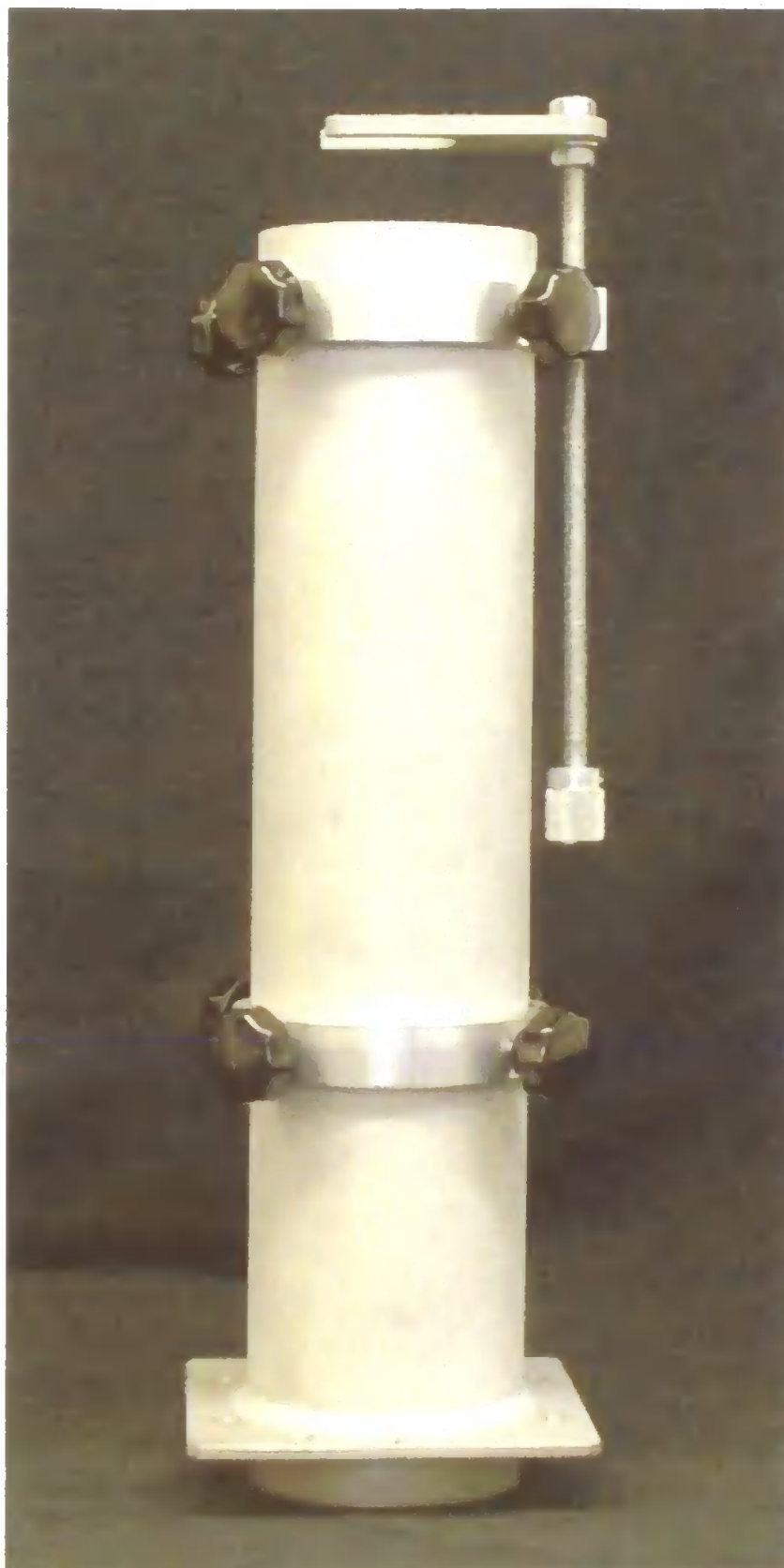
**Plate 2.3: Side view of the axial alignment frame**

Plate 2.4: Plan view of the axial alignment frame

### 2.3.1.1 Condenser System

Any optics positioned above the plasma had to withstand the high temperatures (typically 100 to 200°C) associated with the extended tailflame. Water cooling was considered essential to prevent the excitation fibre optic from the HCL/BDHCL and the optical 'beam probe' from overheating. Several different designs for the condenser system were evaluated.

The initial condenser design as a single unit, curved at the top to lead the fibre optic away from the hot exhaust gases proved to be problematic for two reasons. First, the requisite angle of curvature meant that the optical beam probe used for the entrance optics would have to be sealed into the condenser (and therefore not exchangeable). Second, the use of a single condenser assembly would not allow the use of different sizes of optical fibres. In order to overcome these problems, a design consisting of two inter-linking water cooled condensers was made from borosilicate glass (Plates 2.5 and 2.6).

The straight condenser was 50 cm long with a 3.0 cm external diameter (Plate 2.5). Both side arms, for channelling water, exit at the top for access and safety whilst the water inlet was placed as far from the plasma as possible with the two arms joined together for strength. In addition, the extended side arm was also fixed to the side of the condenser to prevent damage. The probe-end of the condenser was indented and narrowed to hold the optical beam probe in a vertical and central position. The angled condenser was approximately 27 cm long with an external diameter that varied depending on the type of fibre optic used for axial excitation (Plate 2.6). This condenser fitted into a quickfit joint at the top of the straight condenser at an angle of approximately 30° to the horizontal plane. A separate arm attached to the angled condenser allowed argon gas to flow down through the centre of the straight condenser and cool the optical beam probe.

This condenser system solved both problems in that the optical beam probe slid easily into the straight condenser and if the fibre optic required changing, only the angled condenser needed to be exchanged. An argon gas flow rate of 3.0 L min$^{-1}$ and a water flow rate of 2.0 L min$^{-1}$ ensured the necessary cooling of the assembly.

## 2.3.1.2 Optical Beam Probe

A cylindrical, optical beam probe (for focusing or collimating the axial excitation beam directed along a fibre optic) was designed and constructed from aluminium. The optical beam probe held a 5.0 mm focal length, 10 mm o.d. silica bi-convex lens (L.O.T. Oriel) and was 3.1 cm long with an external diameter of 1.5 cm. Four helical 'V-grooves' (0.05 cm deep) were engraved around the circumference of the probe (Plate 2.7) so that a tangential 'cushion' of argon gas (at the end of the lens) met hot gases from the plasma which were forced around the condenser.

## 2.3.1.3 Fibre Optic Axial Excitation Assembly

A schematic diagram of the fibre optic axial excitation assembly attached to the torch box of the Optima 3000 ICP (The Perkin-Elmer Corporation) is shown in Figure 2.6 (Plate 2.8).
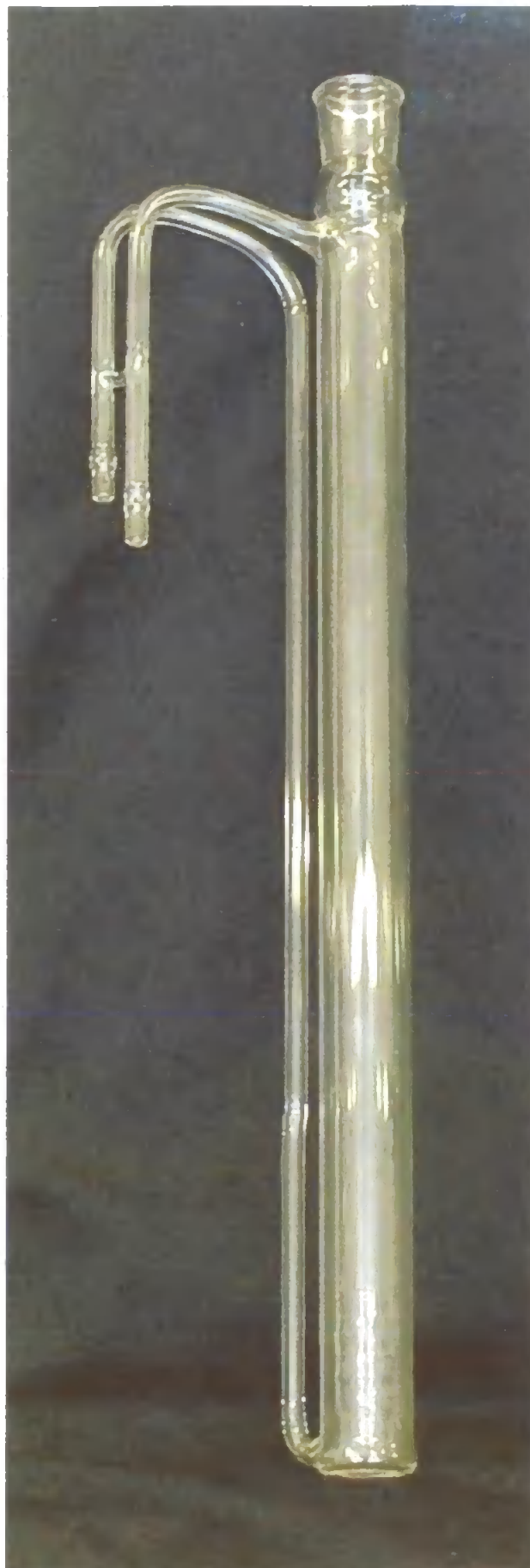
**Plate 2.5: Straight condenser (part of the inter-linking condenser system)**
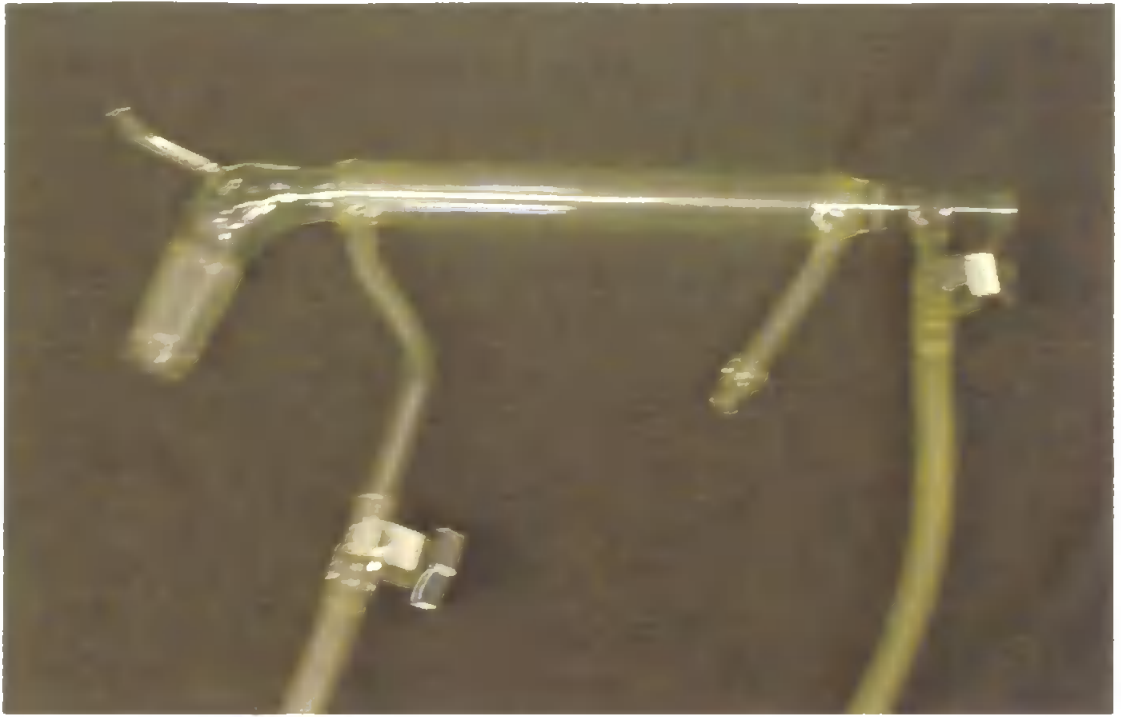
**Plate 2.6: Angled condenser (part of the inter-linking condenser system)**



**Plate 2.7: Optical beam probe**
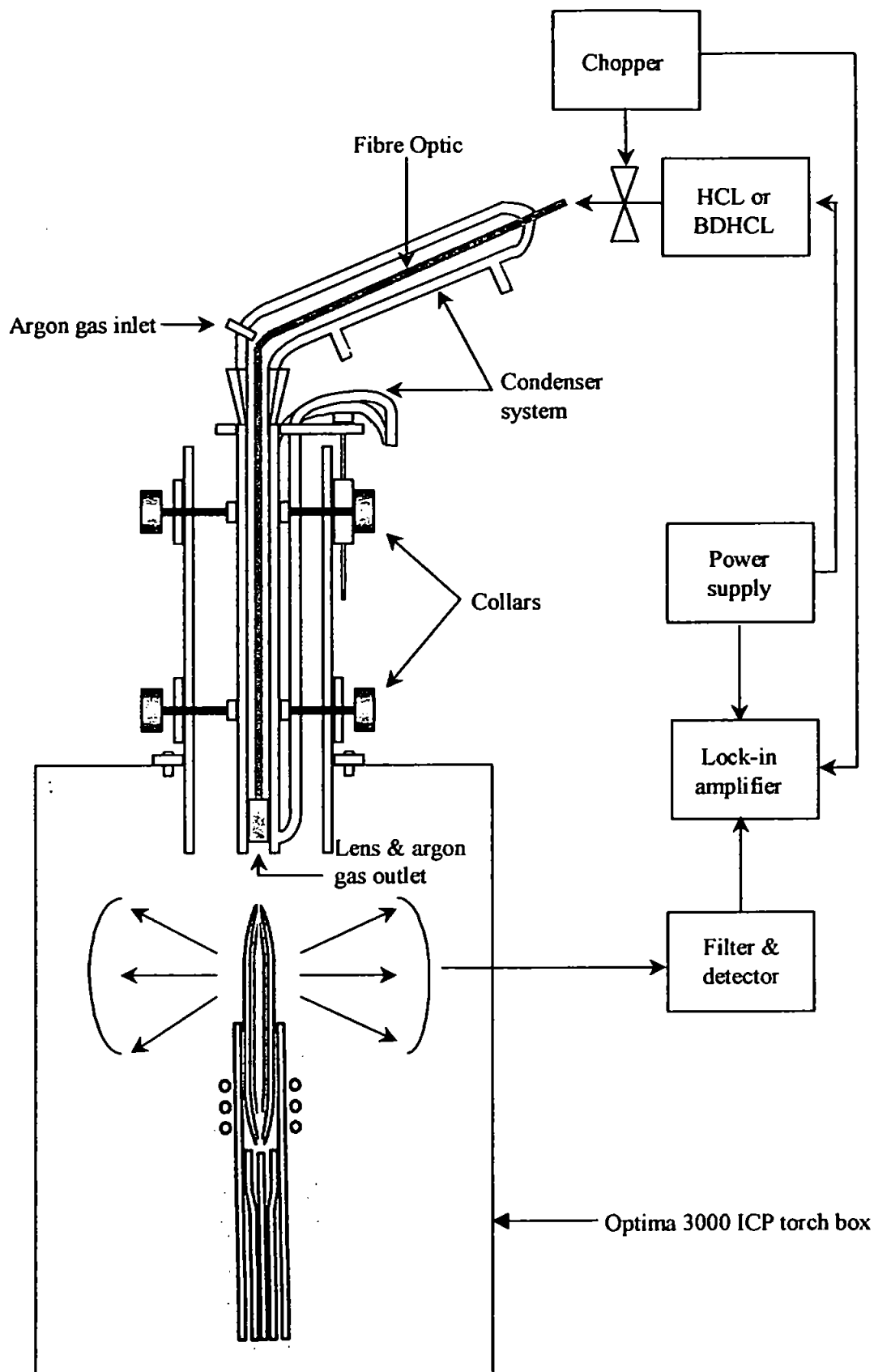
**Figure 2.6: Schematic diagram of the fibre optic axial excitation assembly attached**

**to the torch box of the Optima 3000 ICP**
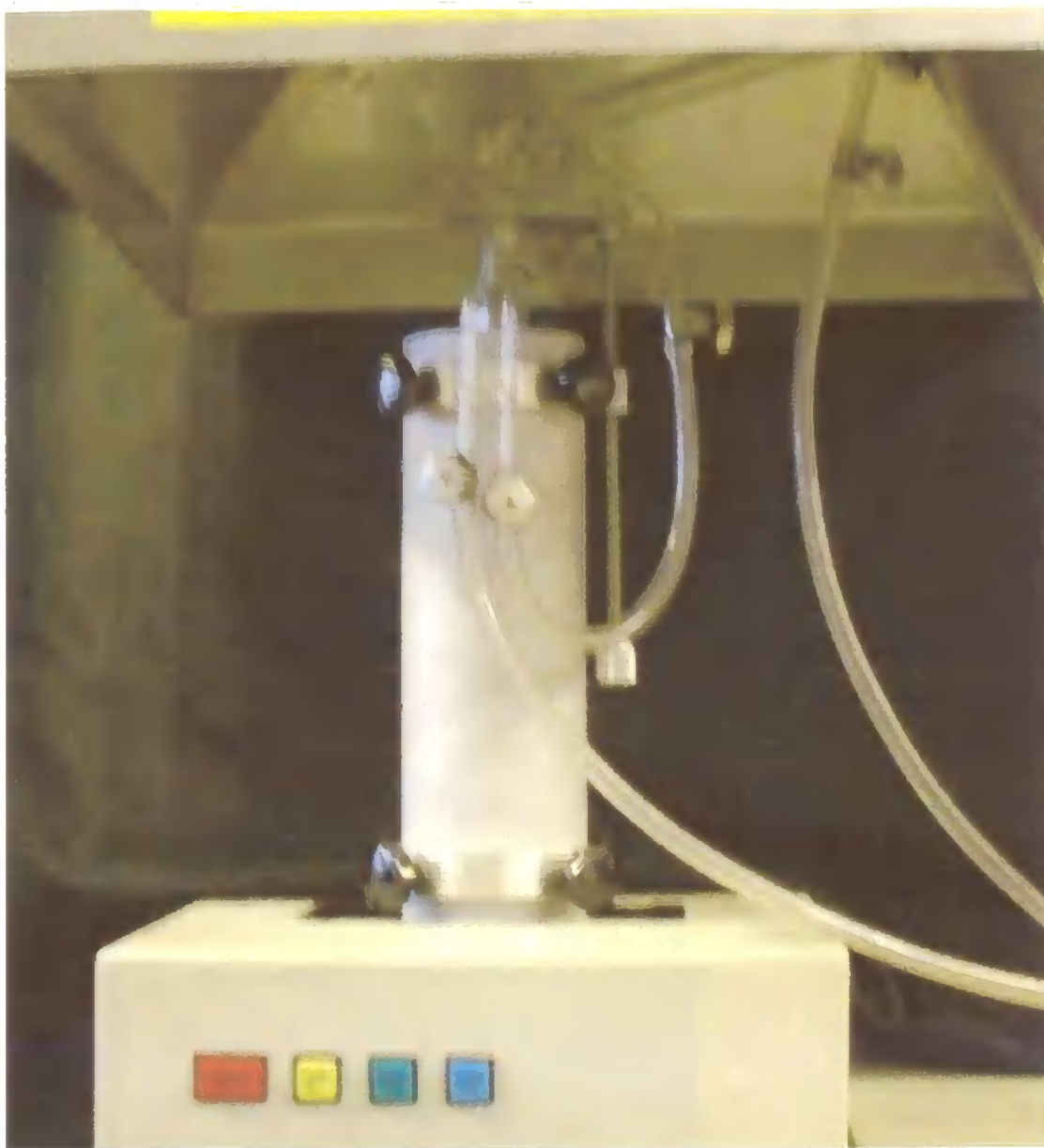
**Plate 2.8: Fibre optic axial excitation assembly attached to the torch box of the**

**Optima 3000 ICP**

### 2.3.1.4 Integrated Lens/Door Assembly for Fluorescence Detection

A door-replacement plate (240 x 400 mm; Plates 2.9 and 2.10, respectively) was designed and constructed from aluminium to fit the torch box housing of the Optima 3000 ICP (The Perkin-Elmer Corporation). The plate housed a bi-convex silica lens (50 mm diameter, 50 mm focal length; L.O.T. Oriel) allowing the lens to be positioned for radial fluorescence scanning of the plasma along both the vertical (Y) and horizontal (X) axes. The lens could also be moved closer to and further away from the plasma to produce a suitable focal point.
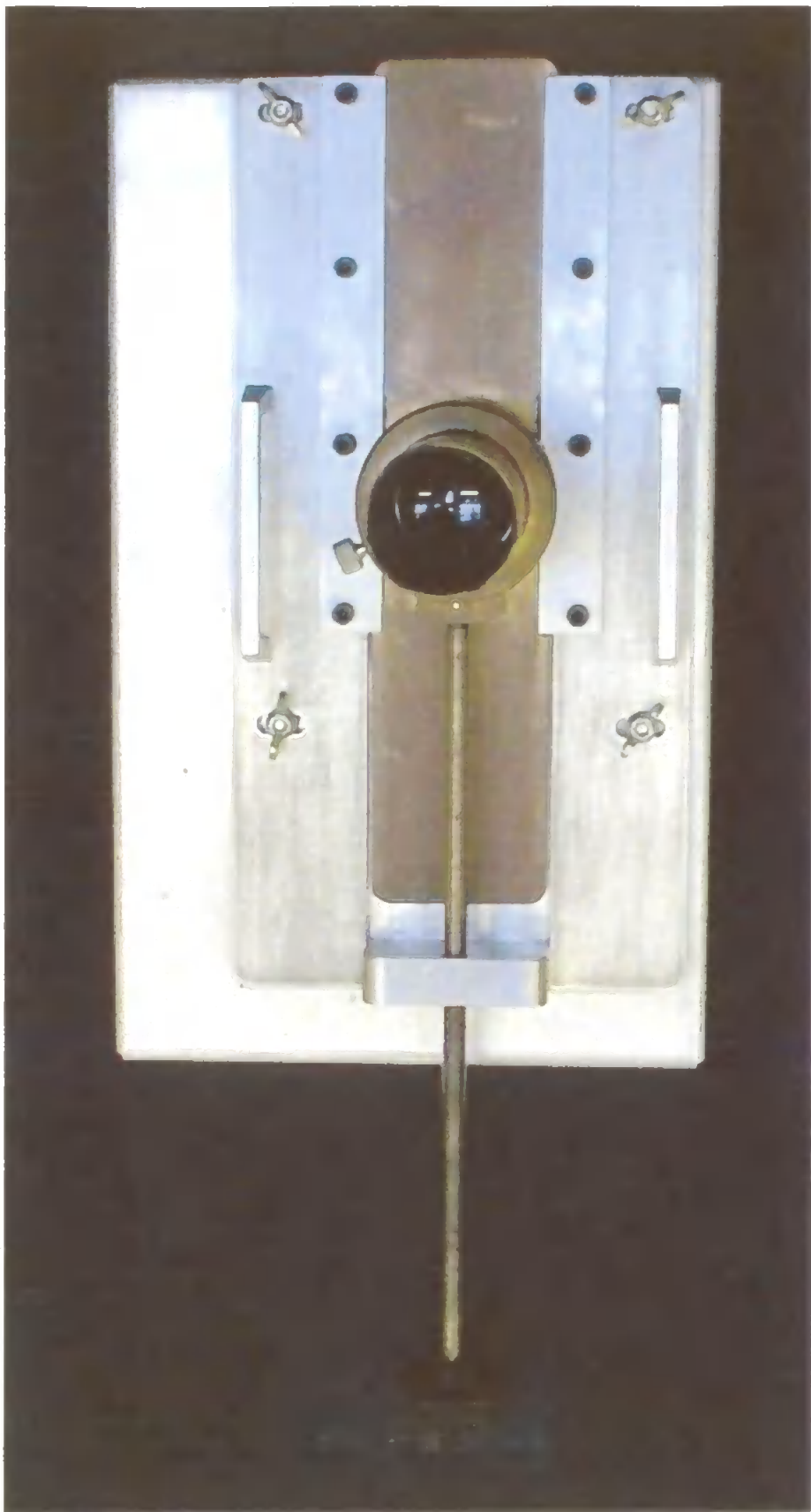
Plate 2.9: Front view of the integrated lens/door assembly for detection

Plate 2.10: Rear view of the integrated lens/door assembly for detection

### 2.3.2 Axial Alignment and Focusing Experiments

Prior to the use of either a HCL or a BDHCL for excitation, the optical beam probe, fibre optic, and condenser assembly required alignment. A He:Ne laser allowed a concentrated light source to be used for focusing and for axial alignment through the optical train. The flat top of the ceramic injector together with the torch base allowed the laser light to be visualised when centralising the axial beam. Two options were available with the optical beam probe: (i) defocused / collimated and (ii) variable depth of focus above the load coil down the extended plasma tailflame. A collimated beam was chosen to illuminate the central channel of the tailflame.

### 2.3.3 Instrumentation for Axial Fluorescence Experiments

HCLs or BDHCLs (Starna) operated by a lamp power supply (Shandon Power Supply Type 2541, Vokam) were used as excitation sources in preliminary fluorescence experiments. Lamp operating conditions are presented in Table 2.3. An Optima 3000 (radially-viewed) ICP-AE spectrometer (The Perkin-Elmer Corporation) was used as the atom cell. The instrument was equipped with a specially constructed demountable plasma torch (Section 2.2.3.1) fitted with an alumina injector (1.5 mm i.d.), a Perkin-Elmer 'Scott-type' double pass spray chamber, and an Ebdon V-groove high-solids, high flow nebuliser (P.S. Analytical Ltd., Kent, UK). Instrumental operating conditions are given in Table 2.2. The detection system comprised a fibre optic (5.0 mm i.d.; Fiberguide Industries), a light chopper (10 bladed chopper disc operated at 667 Hz, Model No. 9479, EG & G Brookdeal) to modulate the beam, optical filters (Model Nos. 5325 & 5370; L.O.T. Oriel), a photomultiplier tube (I.L. R 955/R446/IP28; Hamamatsu Photonics UK Ltd.) operated by a high voltage power supply (Model No. 456, EG & G Ortec), and a lock-in amplifier (Model No. 9503, EG & G Brookdeal). Operating

conditions are listed in Table 2.4. A schematic of the experimental arrangement used for

the Optima 3000 ICP (The Perkin-Elmer Corporation) when operated in axial excitation

fluorescence mode is shown in Figure 2.7.

**Table 2.3: Operating conditions used for excitation sources in preliminary axial excitation fluorescence experiments**

| Lamp type | |
|---|---|
| Barium HCL | Primary current 10 mA |
| Copper BDHCL | Primary current 15 mA, boost current 25 mA |
| Mercury HCL | Primary current 5 mA |
| Tungsten HCL | Primary current 15 mA |
| Light chopper | 10 bladed chopper disc operated at 665 Hz |

**Table 2.4: Instrument parameters used for the detection system in preliminary axial excitation fluorescence experiments**

| Component | |
|---|---|
| Barium filter | Oriel optical filter, Model No. 5370, 1" diameter, 20 nm bandpass, $\lambda_{max}$ 460 nm |
| Copper filter | Oriel optical filter, Model No. 5325, 1" diameter, 20 nm bandpass, $\lambda_{max}$ 320 nm |
| Mercury filter | Oriel optical filter, Model No. 5325, 1" diameter, 20 nm bandpass, $\lambda_{max}$ 260 nm |
| Tungsten filter | Oriel optical filter, Model No. 5325, 1" diameter, 20 nm bandpass, $\lambda_{max}$ 300 nm |
| PMT | 800 V |
| **Optics** | |
| Fibre optics | 3.0 and 5.0 mm diameter, 1.0 m length |
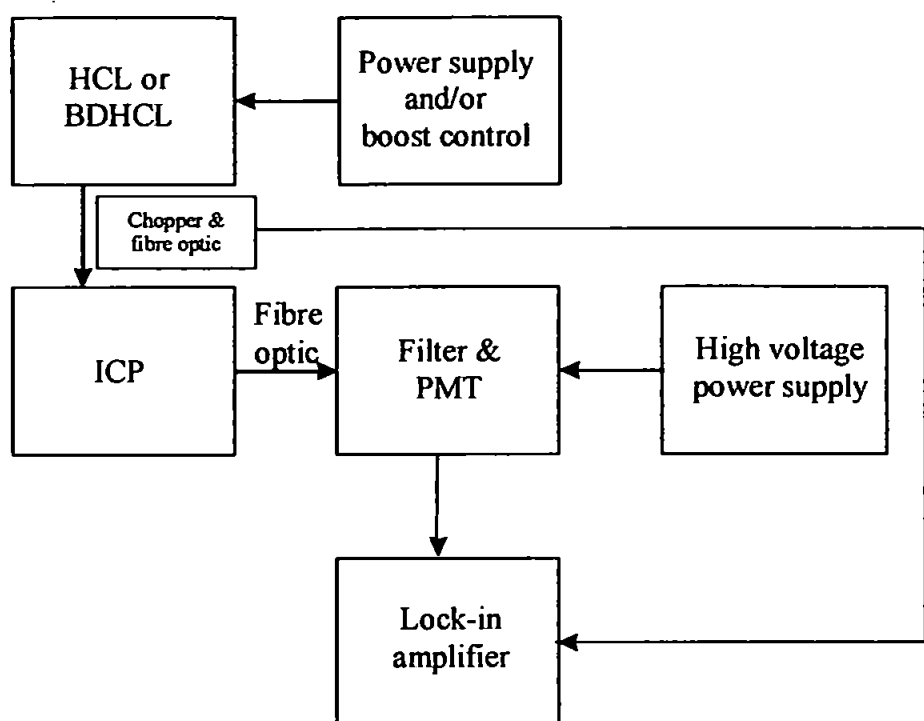
**Figure 2.7: Schematic of the experimental arrangement used for the Optima 3000**

**ICP when operated in fluorescence mode**

### 2.3.4 'Preliminary' Fibre Optic Axial Excitation Assembly Fluorescence Experiments

Using the experimental arrangement shown in Figure 2.7 and the conditions set out in Tables 2.2, 2.3 and 2.4, preliminary fluorescence experiments were performed in an attempt to observe and, if possible, optimise fluorescence conditions. The variables were plasma gas flow rate, modulation frequency, primary and boost lamp current. Ba and W HCLs and Ba and Cu BDHCLs were investigated for use as excitation sources. At the time, software limitations meant that power and nebuliser gas flow rates were restricted to a minimum and maximum of 750 W and 1.5 L min$^{-1}$, respectively. Barium was selected for further investigation because it has been shown to produce efficient atomisation and fluorescence in the plasma at 750 W (82). Solutions of varying concentration (100 µg dm$^{-3}$ – 100 mg dm$^{-3}$) were aspirated into the plasma. The position of the demountable X and Y-axis translation plate was fixed horizontally in the centre of the plasma and a vertical translation was performed from 10 - 140 mm ALC. These experiments are summarised in Tables 2.5 - 2.8.

**Table 2.5: Conditions used for preliminary axial excitation fluorescence experiments**

| Experiment No. | Lamp type | Primary lamp current (mA) | Boost lamp current (mA) | Plasma gas flow (L min$^{-1}$) |
|---|---|---|---|---|
| 1 - 4 | Barium HCL | 15 | - | 14 - 17* |
| 5 - 8 | Mercury HCL | 5 | - | 14 - 17* |
| 9 - 12 | Tungsten HCL | 15 | - | 14 - 17* |
| 13 - 16 | Barium BDHCL | 15 | 20 | 14 - 17* |
| 17 - 20 | Copper BDHCL | 15 | 25 | 14 - 17* |

*1 L min$^{-1}$ increments

**Table 2.6: Conditions to study the effect of primary lamp current in preliminary axial excitation fluorescence experiments**

| Experiment No. | Lamp type | Primary lamp current (mA) | Plasma gas flow (L min$^{-1}$) |
|---|---|---|---|
| 21 – 23 | Barium HCL | 15 - 25* | 14 |
| 24 – 26 | Barium HCL | 15 - 25* | 15 |
| 27 - 29 | Barium HCL | 15 - 25* | 16 |
| 30 - 32 | Barium HCL | 15 - 25* | 17 |

*5 mA increments

**Table 2.7: Conditions to study the effect of boost current in preliminary axial excitation fluorescence experiments**

| Experiment No. | Lamp type | Primary lamp current (mA) | Boost lamp current (mA) | Plasma gas flow (L min$^{-1}$) |
|---|---|---|---|---|
| 33 - 36 | Barium BDHCL | 15 | 20 – 50* | 14 |
| 37 - 40 | Barium BDHCL | 15 | 20 – 50* | 15 |
| 41 - 44 | Barium BDHCL | 15 | 20 – 50* | 16 |
| 45 - 48 | Barium BDHCL | 15 | 20 – 50* | 17 |

*10 mA increments

**Table 2.8: Conditions to study the effect of modulation frequency in preliminary axial excitation fluorescence experiments**

| Experiment No. | Lamp type | Primary lamp current (mA) | Plasma gas flow (L min$^{-1}$) | Modulation frequency (Hz) |
|---|---|---|---|---|
| 49 – 57 | Barium HCL | 15 | 14 | 167 – 967[*] |
| 58 – 66 | Barium HCL | 15 | 15 | 167 – 967[*] |
| 67 – 74 | Barium HCL | 15 | 16 | 167 – 967[*] |
| 75 - 83 | Barium HCL | 15 | 17 | 167 – 967[*] |

[*]100Hz increments

## 2.3.5 Results and Discussion: Fibre Optic Axial Excitation Assembly Fluorescence Experiments

No fluorescence signal was observed from experiments 1 - 83. However, from these preliminary experiments a number of modifications were made to the optical arrangement.

(i)     A 50 mm focal length bi-convex silica lens (inverted 2f:2f) was used to focus the emission from the HCL onto the end of the excitation fibre optic. This resulted in a marked increase in the intensity of the axial excitation beam.

(ii)    For scanning experiments, an optical beam probe was employed to focus the required radiation onto the collector fibre optic.

To increase the intensity of the axial excitation beam further, a modulated power supply (I.L Atomic Absorption Spectrometer Model 151, Thermo Electron Corporation, Waltham, USA) for the HCLs was used instead of a rotating chopper disc. When a rotating chopper disc was used as a means of discriminating between the fluorescence and emission signal, the intensity was averaged over the time that the signal was chopped, *i.e.* if the lamp was run at 5 mA the actual intensity was averaged at 2.5 mA when a 50:50 on:off system was employed. When a modulated power was used, this averaging effect was taken into account and the lamp was run at much higher currents during the on period. Hence, the intensity of the lamp was increased. The lamp modulation operated an 8 ms square wave on, 19 ms wave off period. Experiments 1 – 83 were repeated with the modifications to the system but again no fluorescence signals were observed.

From the experiments performed the results suggested that the coupling and collection efficiency were too poor to provide a sufficiently intense enough excitation source to

enable fluorescence to take place. In ASIA the efficiency of transfer was calculated to be approximately 1 % (82) whereas the highest ever transfer efficiency recorded was 13 % (34). The fibre optics used for both excitation and detection were employed in the successful cold vapour mercury cell experiment (Section 2.2.5.2) suggesting that there was sufficient light transmission to enable fluorescence to take place. To further ensure that the fibre optics were 'fit for the purpose', they were light tested and found to have transmissions of 97 % and 62 % for the excitation and detection fibre optics, respectively. Therefore, it was reasonable to anticipate some response from the fibre optic excitation assembly.

The minimum power attainable with the Optima 3000 WinLab Software at 750 W was a limiting factor because the LOD is inversely proportional to the viewing height and power in the plasma (83). Theoretically, this should have given good results for some elements, (e.g. Ba), but a forward power of 750 W is too high if lower limits of detection are the objective. It was considered necessary to acquire a new software package to enable the parameters of lower forward powers and higher nebuliser gas flow rates to be obtained from the Optima 3000 ICP. These important parameters being displayed in the literature (29, 32, 56, 66) for the production of fluorescence. Values below 750 W were also tried but were outside the calibration range. However, forward powers below 750 W also proved unsuccessful in the attempt to produce fluorescence.

Given these restraints, the conditions necessary for Ba fluorescence were, theoretically, still achievable. If, as known, the fluorescence emitted will be proportional to the intensity of the excitation source, one possible approach would be to improve the efficiency of the excitation optical train together with the collection efficiency of the detector system.

## 2.4 Experimental: Design, Construction and Testing of an Improved Transmission Mirror-Based Axial Excitation Assembly

### 2.4.1 Mirror-Based Axial Excitation Assembly with a Fibre Optic Detection System

The experiments described in Section 2.3.4 were repeated using a surface mirrored axial excitation assembly instead of the fibre optic axial excitation assembly (Figure 2.8 and Plate 2.11). Initially, a focusing lens was used with the mirror-based excitation assembly with the aim that the excitation emission from the lamp would be focused to a point above the load coil known to provide the 'optimum' conditions for barium fluorescence (82). The use of a collimating lens was also investigated in order that the whole central channel of the plasma could be illuminated.

### 2.4.1.1 Mirror-Based Axial Excitation Assembly with a Fishtail Fibre Optic Detection System

The experiments described in Section 2.4.1 were repeated using a glass fishtail fibre optic (0.30 x 100 mm leading to a 5.0 mm i.d. fibre optic bundle, L.O.T. Oriel) and a silica fibre optic (3.0 mm diameter, 1.0 m long; Fiberguide Industries) that led directly to the detection system instead of *via* the demountable X and Y-axis translation plate. The potential advantage from using a fishtail fibre optic was that a long section of the tailflame could be measured at once thereby increasing the collection efficiency of the detector system. The experimental arrangement was similar to that given in Figure 2.8 except for the use of the X and Y-axis translation plate. A schematic of the coupling of the fibre optics is presented in Figure 2.9.
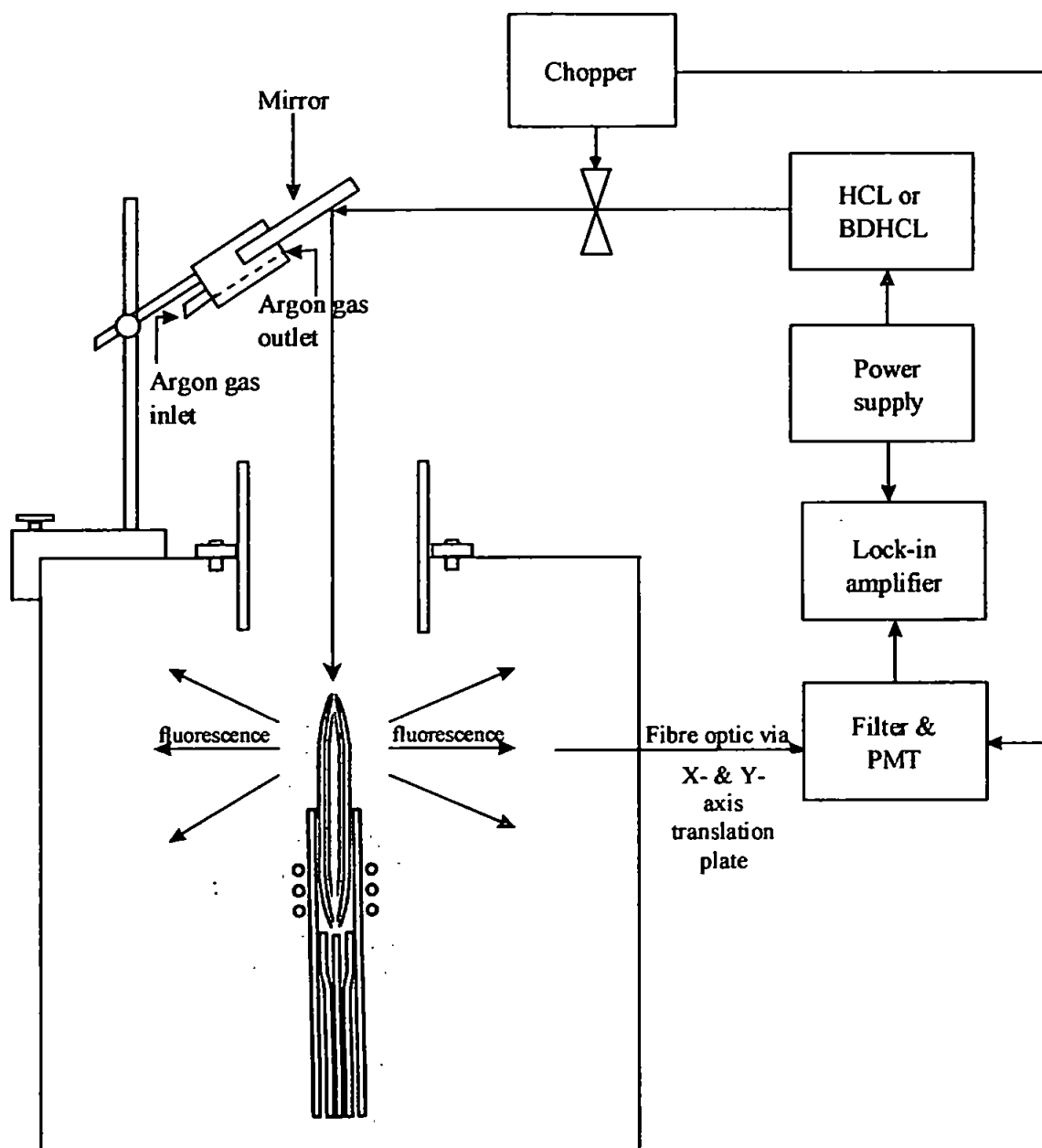
**Figure 2.8: Schematic diagram of the mirror-based axial excitation assembly attached to the torch box of the Optima 3000 ICP**
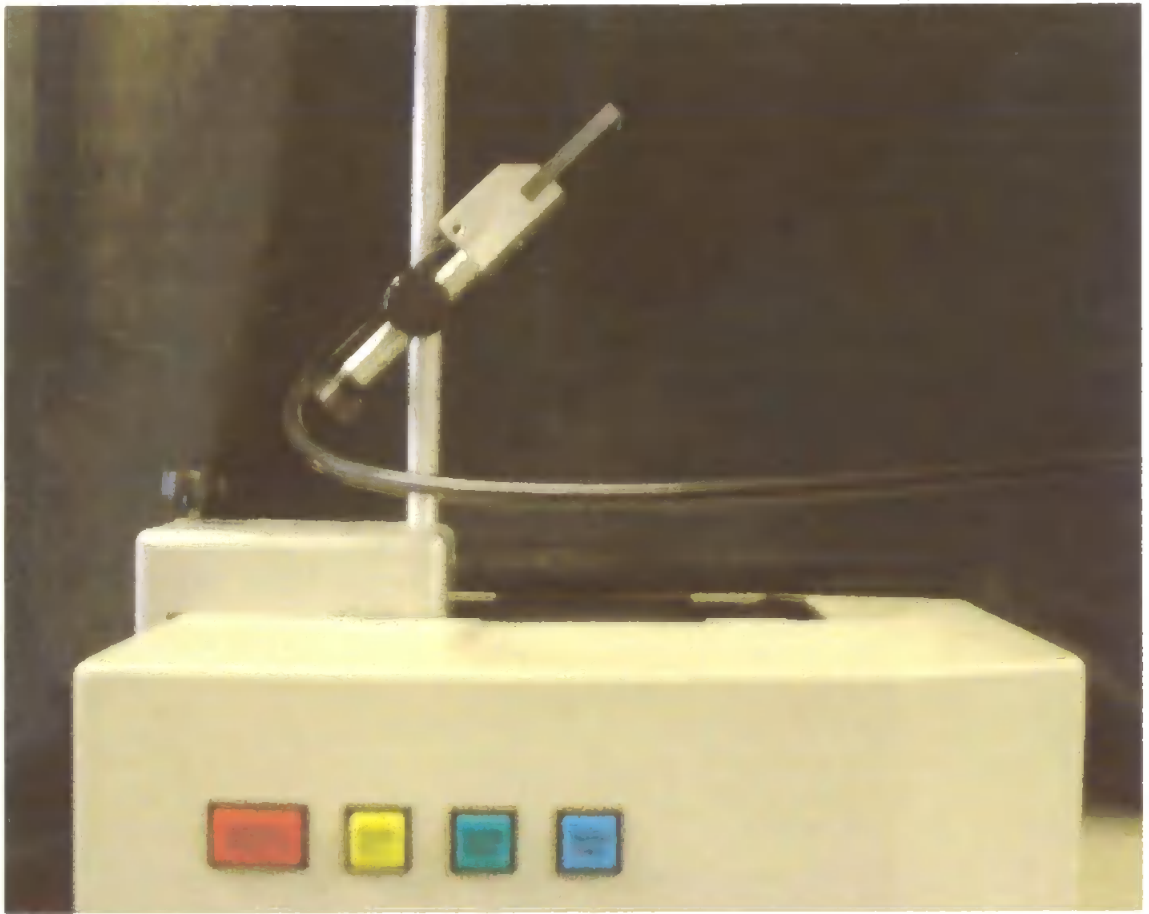
**Plate 2.11: Mirror-based axial excitation assembly attached to the torch box of the**

**Optima 3000 ICP**
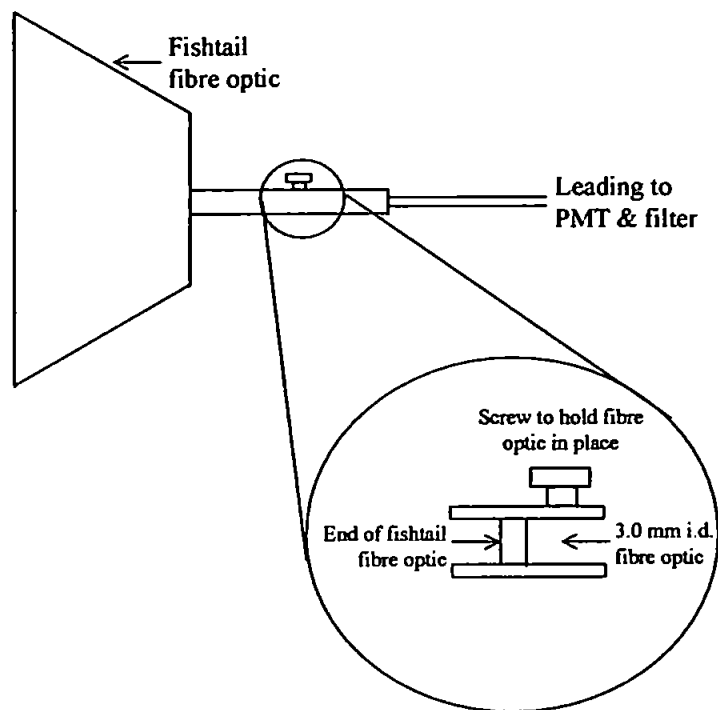
**Figure 2.9: Schematic of the coupling of the fishtail fibre optic and the fibre optic leading to the detection system**

## 2.4.1.2 Mirror-Based Axial Excitation Assembly with a Silica Lens Detection System

Experiments described in Section 2.4.1.1 were repeated using the integrated lens/door assembly. A bi-convex silica lens (50 mm diameter, 50 mm focal length; L.O.T. Oriel) arranged in a 2f:2f (inverted) manner was used to focus the emission from the plasma onto a filter prior to detection by a PMT. Both the excitation source and the silica lens were focused at a height of 70 mm ALC as this is recorded as the optimum viewing height ALC for barium fluorescence under the ICP power and gas flow rates conditions employed (82).

## 2.4.2 Results and Discussion: Mirror-Based Axial Excitation Assembly Fluorescence Experiments

A second axial excitation assembly was designed and constructed. The excitation system consisted of a mirror, adjustable both vertically and horizontally, set at a 45° angle to either a focusing or collimating lens (to allow greater light throughput, see Figure 2.8 and Plate 2.11). A stream of argon gas made to flow over the mirror's surface greatly reduced the excessive thermal environment produced above the plasma and helped prevent blooming effects. Suitable fibre optic guides (later replaced with a silica lens system) were used for the detection system. A modulated excitation source and an amplifier phase-locked detection system completed the assembly.

The use of a fishtail fibre optic enabled a long section of the tailflame to be monitored simultaneously. Fishtail fibre optic experiments were therefore performed in order to determine whether the fluorescence profile was so shallow over the whole length of the tailflame that the fluorescence signal could not be detected at any one particular viewing height. Elements to be analysed had to be selected carefully because the fishtail was

made of borosilicate. Barium was chosen because of its wavelength (455.403 nm) and lamp availability. The other BDHCL available was copper (324.735 nm) but this could not be used in this arrangement because transmission below 350 nm is severely limited. No fluorescence was observed when various barium concentrations (1 – 100 µg ml$^{-1}$) were aspirated into the plasma.

The fishtail fibre optic used for detection was replaced with a silica lens system. This allowed a much greater light throughput to reach the detection system. However, no fluorescence signal was observed, so a 'back-to-basics' approach was adopted.

## 2.5 Experimental: Preliminary Transverse Excitation Fluorescence Experiments

### 2.5.1 Fibre Optic Transverse Excitation Experiments

Since no fluorescence was observed when illuminating axially, transverse excitation experiments were performed. The experiments described in Section 2.3.4 were repeated, but instead of positioning the excitation source in an axial manner, an adaptation was made to the demountable X and Y-axis translation plate such that the excitation and detection fibre optics could be held horizontally at right angles to one another. Further modifications included the use of beam probes to focus the emission (and hence increase the intensity) from the excitation source onto the plasma and the fluorescence emission onto the filter and detection system. The fibre optics and beam probes used for both excitation and detection were focused onto the central channel of the plasma. The experiment was repeated with a collimated beam so that a comparison could be made.

## 2.5.2 Integrated Lens/Door Assembly for Excitation

A door-replacement plate (220 x 380 mm) similar to the one described in Section 2.3.1.4 was designed and constructed from aluminium. The front view of the door-replacement plate is shown in Plate 2.12 but the rear view is not shown as it is virtually identical to Plate 2.10.

The plate housed a bi-convex silica lens (50 mm diameter, 50 mm focal length; L.O.T. Oriel) within a guide tube allowing the lens to be positioned for focusing the excitation source onto the plasma along both the vertical (Y) and horizontal (X) axes in a 2f:2f arrangement. The lens could also be moved closer to and further away from the plasma to produce a suitable focal point.
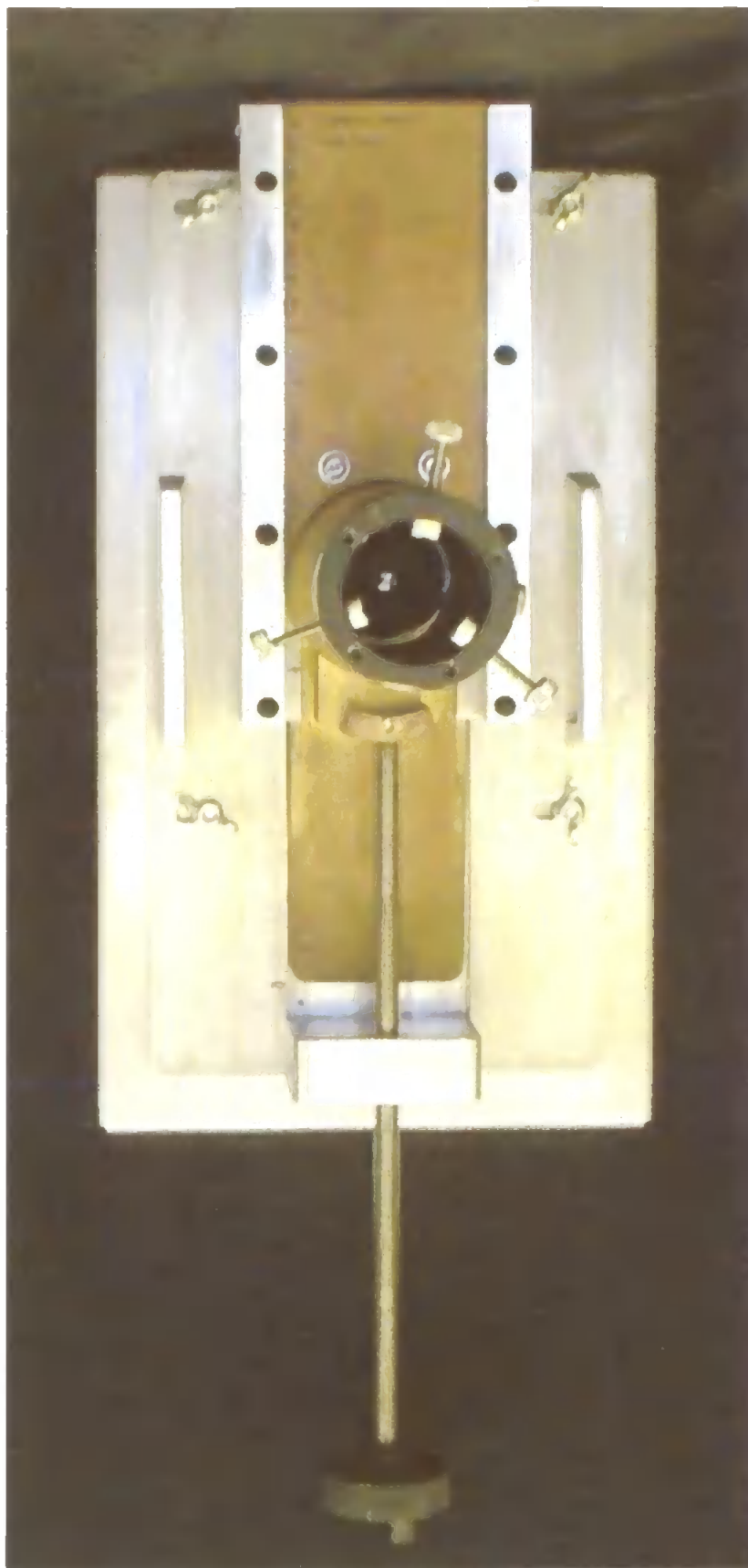
Plate 2.12: Front view of the integrated lens/door assembly for excitation

### 2.5.2.1 Integrated Lens/Door Assembly Transverse Fluorescence Experiments

The experiments outlined in Section 2.3.4 were repeated using both integrated lens/door assemblies especially designed for radial fluorescence experiments instead of fibre optics. Two silica bi-convex lenses were used to focus both the light emission from the lamp and the emission from the plasma. While vertical scanning of the whole plasma tailflame was possible using the newly constructed integrated lens/door assembly, for practical purposes the range was limited to 60 to 80 mm ALC as previous work had shown this to be the optimum viewing height ALC for Ba fluorescence to be observed (82, 83).

### 2.5.3    Results and Discussion: Preliminary Transverse Excitation Fluorescence Experiments

The purpose of carrying out the transverse fluorescence experiments was to adopt a 'back-to-basics' approach. Previous experiments had failed to show whether the axial excitation approach was to blame for the failure to observe any fluorescence signal or whether it was due to problems with equipment used in these experiments. There was no fluorescence signal observed in any of the transverse fluorescence experiments.

It is commonly known that the ordinary HCL is, under normal running conditions, too weak for AFS and needs to be square wave modulated or pulsed (10, 22). However, the asymmetric square wave-based modulation frequency of 37 Hz (8 ms square wave pulse, 19 ms dead time) appeared to be insufficient to allow the lock-in amplifier to distinguish the fluorescence signal from the background emission. It was considered that the use of a rotating chopper operated at a higher modulation frequency (*e.g.* 667 Hz), with the Ba BDHCL operated at constantly higher currents in an attempt to compensate for the loss of intensity, should have resulted in a fluorescence signal being

observed. However, one possibility for the lack of fluorescence was that the chopped intensity of the light source had been reduced to such an extent that it became insufficiently intense for fluorescence to occur. These experiments suggested that the intensity of the excitation source was still proving to be problematic as no fluorescence was observed.

## 2.6    Summary

An Optima 3000 ICP-AES instrument was modified and the equipment necessary to carry out axial excitation atomic fluorescence was designed and constructed. Two axial excitation assemblies were made, one utilised fibre optics and the other a mirror and lens system, resulting in a series of modules that could be fitted retrospectively to an Optima 3000 ICP. These modules included: an axial alignment frame; an inter-linking water cooled condenser system; an optical beam probe; a demountable X and Y-axis translation plate for collection of the atomic fluorescence signal and for horizontal and vertical scanning of the elongated plasma tailflame; and a vertically and horizontally adjustable mirror, set at a 45° angle to either a focusing or a collimating lens. Both assemblies used a novel argon gas coolant flow to reduce the excessive thermal environment above the plasma and a detection system comprising optical filters, a PMT and a lock-in amplifier.

The equipment used for the excitation and detection systems was checked before any preliminary fluorescence experiments were performed. The cold vapour mercury cell and the emission mode experiments proved that the optical and electronic detection systems were working correctly.

The ICP was calibrated between 750 – 1500 W and plasma conditions used for preliminary fluorescence experiments were consistent with those described in the

literature. The required elongated tailflame was visually observed and verified by the required plasma structure.

The preliminary axial and transverse excitation fluorescence experiments were not successful despite all the individual pieces of equipment being proven to work. However, two important factors emerged. First, a very high intensity axial excitation beam is required for fluorescence. Second, the power range available to the instrument needs to be increased to cover 900 W down to 750 W. Also, in general the plasma conditions available required greater flexibility.

## 3.0    EVALUATION AND OPTIMISATION OF INSTRUMENTATION

### 3.1    Introduction

The intensity of an analyte line in ICP-AFS is a complex function of several different factors, and while some analyses can be performed under standard conditions, the determination of optimum conditions is essential to attain the required analytical performance in any analyses. The variable factors that are of principal concern to the conventional ICP source are the forward power coupled to the plasma, the nebuliser gas flow rates for the ICP torch, and the observation height. Other parameters such as plasma (or coolant) and auxiliary gas flow rates are considered to have an effect although are not considered to be as critical (82).

In order to create conditions where fluorescence will occur the parameters need to be altered in a systematic way and the effects on the plasma monitored. Interpreting emission intensities directly gives no indication of the excitation and ionisation processes that may be occurring within the plasma. However, the values and the ratio of emission intensity of an ion line, $I_i$, to emission intensity of an atom line, $I_a$, has been previously used to measure and examine the energy characteristics of the ICP discharge (84, 85). Using ion/atom ratios, a model could be created which may help to determine the conditions where efficient fluorescence will occur.

The production of a fluorescence signal critically relies on the use of an efficient, intense external excitation source. The way in which the source is modulated, for a given 'type' of source, e.g. HCL/BDHCL or LED must be considered important as this affects its intensity and the efficiency of coupling to the analyte of interest within the atom cell. However, to date, there have been no investigations into the combined effect of modulation frequency and duty cycle of the excitation source on the production of a

fluorescence signal. The modulation frequency of a lamp is the number of cycles performed in one second. For example, a modulation frequency of 167 Hz corresponds to 167 cycles per second, each cycle lasting 5988 μs. The duty cycle is how hard the lamp is driven during one cycle. A duty cycle of 10 % corresponds to the lamp being 'on' for 10 % and 'off' for 90 % of the time during one cycle. Therefore, the lamp will have to be 'driven' at 150 mA to effectively average a primary current of 15 mA over the cycle. One focus of this investigation was to optimise the emission output from a HCL in an attempt to obtain optimal excitation conditions for the production of fluorescence. This study may then help to improve our understanding of the excitation source requirements for the production of fluorescence.

The characteristics of a HCL are not, however, defined by a single line intensity measurement. The conditions under which it is driven gives rise to a range of differing energy states for the analyte contained within the lamp. A Boltzmann Distribution measurement, from this excitation source, can be used as a physical marker to enable direct comparisons to be made and help analyse subsequent variations between a HCL operated under various modulation frequencies and duty cycles. This study may also serve as a preliminary investigation to those involving a plasma acting as an atom cell in later experiments.

The effect of the inductively coupled plasma operating parameters, *e.g.* the flexibility required with respect to forward power and nebuliser gas flows, can be studied to determine the conditions required for maximum absorbance by an analyte to occur. The absorbance of a primary line in an atom cell is indicative of the presence of ground state atoms. If ground state atoms are present and the area within the plasma where maximum absorbance is occurring can be determined, then the optimum conditions for atomic fluorescence should have also been determined.

## 3.2 Experimental: Instrumentation Designed, Constructed and used for the Modulation Studies

Most, if not all, modern AASs employ modulation of the excitation source (HCL), in order to be able to take advantage of the benefits conferred by so doing. The main advantage is the ability to employ an alternating current (AC) coupled amplifier which can be locked into the frequency of modulation, which results in a reduction in the noise component. In addition, due to advances in digital signal processing, other parameters may be encoded into the signal, such as blank subtraction. This results in a complex signal shape which is decoded by the instrumental software. The frequency of operation and the mark-space ratio of the modulation are fixed in all commercial AASs. Whilst this type of modulation is acceptable for commercial AAS instruments, it was found to be extremely limiting for the work programme to be undertaken. In addition, the use of boosted hollow cathode lamps was required, and this made the situation more difficult, as the commercially available current boosting systems employ the high voltage pulses generated by the AASs. A further requirement of the electronics system is that it be capable of providing high current, short duration pulses, since the intensity output from both hollow cathode sources and high power LEDs could be dramatically increased. Since detection relied upon photomultiplier tubes, which are capable of high speed operation feeding a lock-in amplifier, short duration high output pulses were preferred. It was therefore decided to construct a purpose built modulation system.

Since the mark-space ratio needed to be accurately varied over a very wide range, a time-base generator was designed which allowed the accurate setting of both the mark and space from 1 microsecond to 1 second. The design, illustrated in Figure 3.1, employed a quartz crystal oscillator to provide a highly accurate clock signal, with sequential "divide by ten" integrated circuit to provide the ranges. Two banks of six ten-

87

position rotary switches provided total control of the mark and space periods, thus setting the frequency of operation. The resulting output signals were buffered by the use of operational amplifiers, in order to provide the necessary voltages required by the lamp driver unit and the lock-in amplifier.

The lamp driver system was primarily a high voltage power supply to drive a normal hollow cathode lamp, which could be modulated by the signal from the time-base generator. In addition, a 'current boost' section was incorporated to enable the use of boosted hollow cathode lamps. Monitoring of the output power of this unit was provided by a liquid crystal display (LCD) meter. The unit also provided an output for driving high power LEDs, which were modulated under the control of the time-base generator.

Modulation was achieved by high power switching of the cathode circuit, which was controlled, *via* an opto-coupler, by the signal from the time-base generator. The unit incorporated a single custom-built mains transformer, which provided both the high voltage and high current secondary windings. All power supply circuits featured high levels of regulation and stability.

Two other pieces of electronic equipment were designed and built specifically for this project. The first of these was a switched gain, AC coupled, low noise instrumentation amplifier, which was employed in various experiments to provide additional amplification of the detector system as required. The second device was a 50 Hz notch filter, which was employed to remove the "mains hum" from the signal from the photomultiplier tube circuit. Although the notch filter distorted the waveform (since such filters are primarily used in sinusoidal circuits) the resulting signal was easier to measure using the lock-in amplifier, than was the case without the filter.
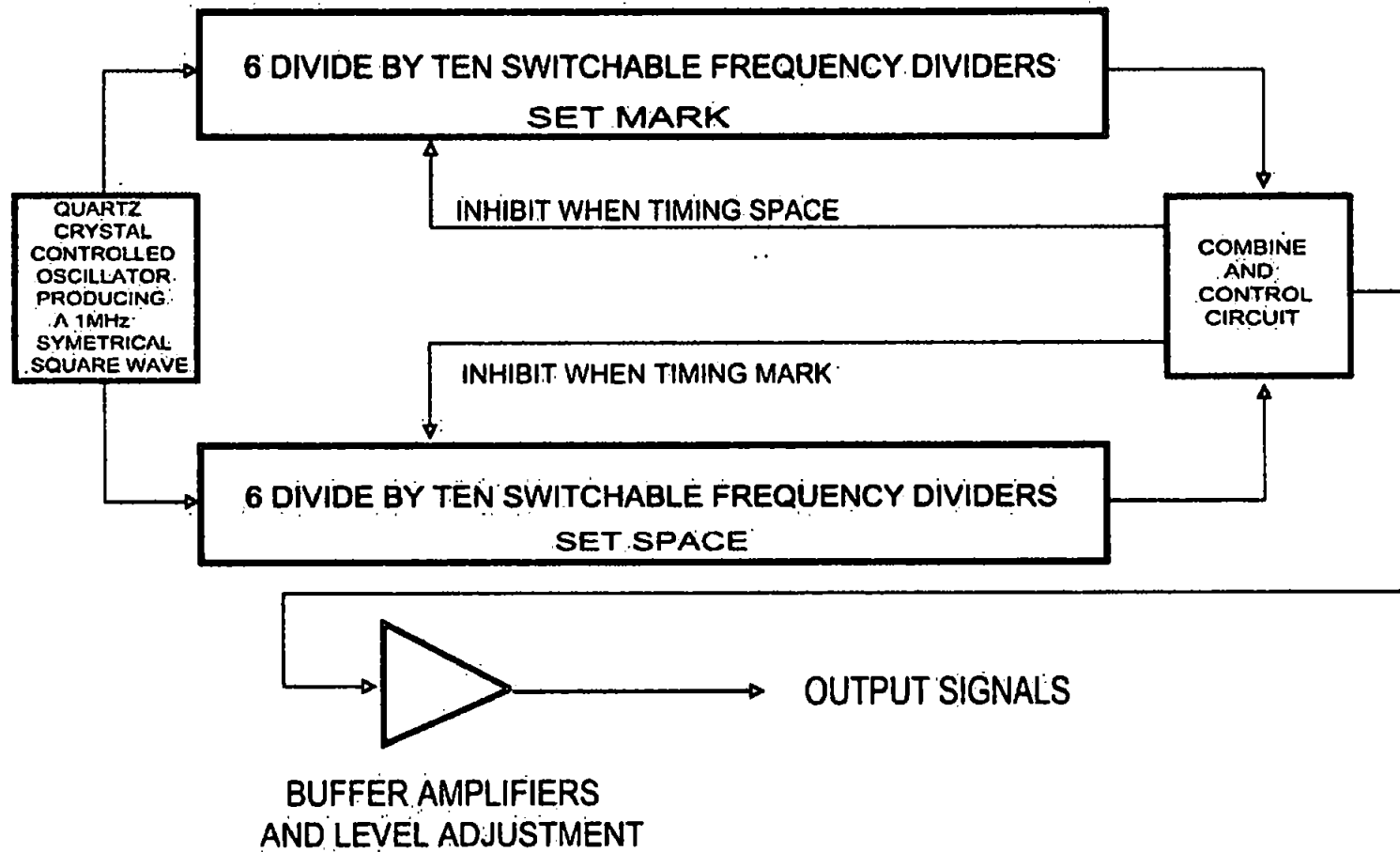
Figure 3.1: Schematic of the hollow cathode lamp and light emitting diode driver system

### 3.2.1 Modulation Studies using a Hollow Cathode Lamp

The effect of modulation frequency and duty cycle on the intensity of the 238.204 nm line emitted from a Fe HCL (Starna, Romford, Essex, UK) was investigated using the experimental arrangement illustrated in Figure 3.2. The mean primary current of the Fe HCL per unit time was kept constant at 15 mA while the lamp driver system described in Section 3.2 was used to vary the modulation frequency and duty cycle to the lamp. The modulation frequencies and duty cycles investigated are summarised in Table 3.1. A filter (1" diameter; 20 nm bandpass; $\lambda_{max}$ 240 nm; Model No. 5325; L.O.T. Oriel, Leatherhead, Surrey, UK) and photomultiplier tube (IP 28; Hamamatsu Photonics UK Ltd., Enfield, Middlesex, UK) operated by a high voltage power supply (Model 456; EG & G Ortec, Oakridge, USA) completed the assembly. A computer operated oscilloscope was used (PicoScope, Pico Technology Limited, St. Neots, UK) to record the trigger signal from the modulation supply and the signal produced by the PMT. Use of specialist software (PicoScope) enabled the trigger signal and the signal produced by the PMT to be compared.
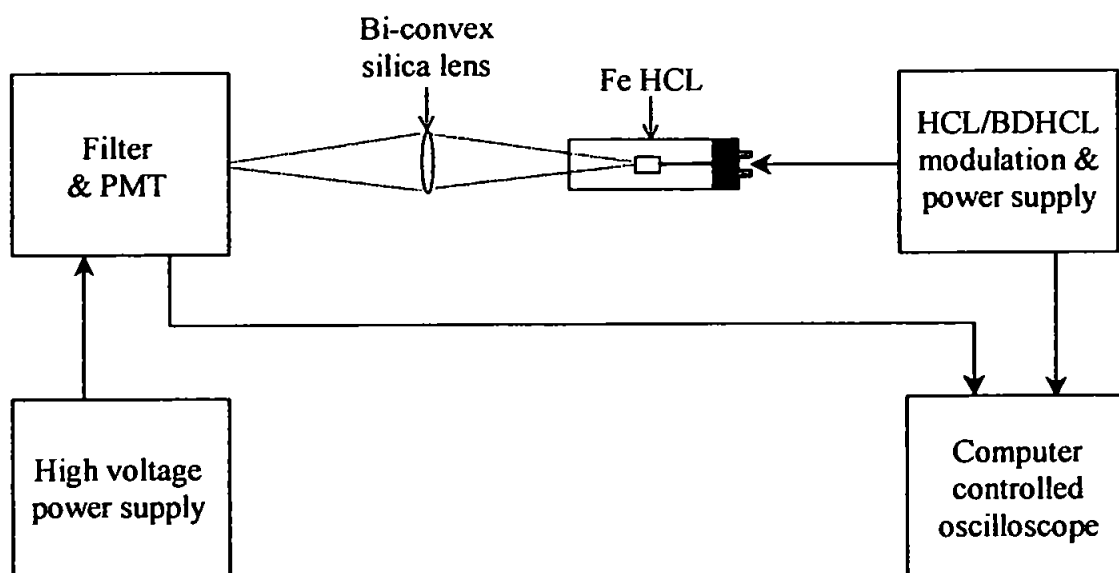
**Figure 3.2: Schematic of the experimental arrangement used to study the effect of modulation frequency and duty cycle on Fe HCL emission at 238.204 nm**

**Table 3.1: Modulation frequencies and duty cycles investigated**

| Modulation frequency (Hz) | Duty cycle (%) | Mark:space periods | |
|---|---|---|---|
| | | Mark (µs) | Space (µs) |
| 167 | 10 | 599 | 5389 |
| 167 | 20 | 1198 | 4790 |
| 167 | 30 | 1796 | 4192 |
| 167 | 40 | 2395 | 3593 |
| 167 | 50 | 2994 | 2994 |
| 292 | 10 | 342 | 3082 |
| 292 | 20 | 685 | 2740 |
| 292 | 30 | 1027 | 2397 |
| 292 | 40 | 1370 | 2055 |
| 292 | 50 | 1712 | 1712 |
| 417 | 10 | 240 | 2158 |
| 417 | 20 | 480 | 1918 |
| 417 | 30 | 719 | 1679 |
| 417 | 40 | 959 | 1439 |
| 417 | 50 | 1199 | 1199 |
| 542 | 10 | 185 | 1661 |
| 542 | 20 | 369 | 1476 |
| 542 | 30 | 554 | 1292 |
| 542 | 40 | 738 | 1107 |
| 542 | 50 | 923 | 923 |
| 667 | 10 | 150 | 1349 |
| 667 | 20 | 300 | 1199 |
| 667 | 30 | 450 | 1049 |
| 667 | 40 | 600 | 900 |
| 667 | 50 | 750 | 750 |
| 792 | 10 | 126 | 1136 |
| 792 | 20 | 253 | 1010 |
| 792 | 30 | 379 | 884 |
| 792 | 40 | 505 | 758 |
| 792 | 50 | 631 | 631 |
| 917 | 10 | 109 | 981 |
| 917 | 20 | 218 | 872 |
| 917 | 30 | 327 | 763 |
| 917 | 40 | 436 | 654 |
| 917 | 50 | 545 | 545 |
| 1042 | 10 | 96 | 864 |
| 1042 | 20 | 192 | 768 |
| 1042 | 30 | 288 | 672 |
| 1042 | 40 | 384 | 576 |
| 1042 | 50 | 480 | 480 |

### 3.2.2 Results and Discussion: Modulation Studies using a Hollow Cathode Lamp

The operation of an HCL described in Chapter 1 (Section 1.5.7) states that when a potential is applied between the electrodes, the inert filler gas becomes charged at the anode, and the ions produced are attracted to the cathode. The bombardment of these ions on the inner surface of the cathode causes metal atoms to sputter out of the cathode cup. Further collisions excite these metal atoms and a simple, intense characteristic spectrum of the metal is produced (18). Modern HCLs normally require a very short warm up period to build up the 'plasma' discharge when operated in both continuous and pulsed modes of operation, however, the effects of varying the modulation frequency and duty cycle on an HCL have not yet been extensively studied.

The effect of modulation frequency and duty cycle on the emission signal of a Fe HCL at 238.204 nm is illustrated in Figures 3.3 – 3.10. Figures 3.3 – 3.10 show that the lamp has a trigger time and a rise time, *i.e.* a time before the maximum intensity is produced, and using these figures an estimate of both can be made. Table 3.1 gives the 'on' times (Mark periods) of 185 and 150 µs for the lamp when operated at 10 % duty cycle for modulation frequencies of 542 and 667 Hz, respectively. Figure 3.6a shows that the lamp does respond and trigger during the 'Mark' period although the maximum lamp intensity is not reached due to the 'Space' period of the cycle being introduced where no power is supplied to the lamp. However, Figure 3.7a shows that the lamp does not respond at all. This suggests that the trigger (reactance) time of the lamp must be somewhere between 185 and 150 µs. The rise time of the lamp is the time taken for the full 'plasma' discharge or maximum lamp intensity to build up. This is reached when a plateau is observed on the emission traces. Figure 3.3 shows that at the lowest modulation frequency a plateau is reached in all cases irrespective of the duty cycle. The time taken for the lamp to build up to its full 'plasma' discharge can be estimated

from Figure 3.3a. The picoscope trace from the lamp signal is just beginning to plateau before the lamp is switched off again. If the 'Mark' period for a modulation frequency of 167 Hz operated with a 10 % duty cycle is 599 µs (taken from Table 3.1) and the trigger time of the lamp is between 150 - 185 µs, the rise time must be between 414 - 449 µs.

As the modulation frequency is increased the rise time does not fall within the estimated 414 - 449 µs and a 'plateau' is reached in fewer and fewer instances. In particular, at 667 Hz a plateau is not observed at all, even when operated with at 50 % duty cycle. At higher modulation frequencies and shorter duty cycles the plasma discharge is 'clipped' to such an extent that either the lamp does not have time to trigger at all or, if it does trigger then the maximum lamp intensity is not reached. This has major implications for the production of a fluorescence signal. It was expected that since fluorescence is proportional to the source lamp intensity then the higher the modulation frequency used to pulse the lamp, the higher the emission intensity and an increase in fluorescence signal would be observed. Fluorescence systems described in the literature have used modulation frequencies of 500 Hz and 997 Hz (29 – 32, 42 – 53, 66) but Figures 3.3 – 3.10 indicate an optimum modulation frequency based on lamp performance of somewhere between these two values or possibly even lower.

The duty cycle also appears to have significant implications for fluorescence. The lamp was kept at a mean primary current of 15 mA per unit time throughout the experiments, so for a 10, 20, 30, 40 and 50 % duty cycle the effective primary current for the time the lamp was switched on would have been 150, 75, 50, 37.5 and 30 mA, respectively. Therefore, an increase in fluorescence signal would be expected for a lamp operated with a 10 % duty cycle as opposed to one operated with a 50 % duty cycle because of the increased emission intensity. However, Figures 3.3 – 3.10 show that as the duty

cycle increases from 10 % to 50 % the response of the lamp changes significantly from an almost triangular shape to that of a square wave. If a square wave lock-in amplifier were used to detect the fluorescence signal then the lamp response must be or approach that of a square wave otherwise the amplifier would be unable to efficiently lock into the fluorescence signal. This indicates that a lamp operated with a higher duty cycle may provide the best conditions for the production and hence detection of fluorescence.

One other important factor must be considered. When a HCL is driven increasingly harder self absorption effects can also be present. As the concentration of excited atoms increases so can the concentration of ground state species. This would cause a broadening of the emission line and in extreme cases result in a self reversal profile of the line. The effect limits the intensity output of the line of interest, and hence the height of the 'platonic' profile. The shape of the profile before the plateau region would be dependent on the 'reactance' of the HCL system but in severe cases 'clipping' (where the lamp is driven hardest, *i.e.* at shorter duty cycles) may be a combination of both effects.
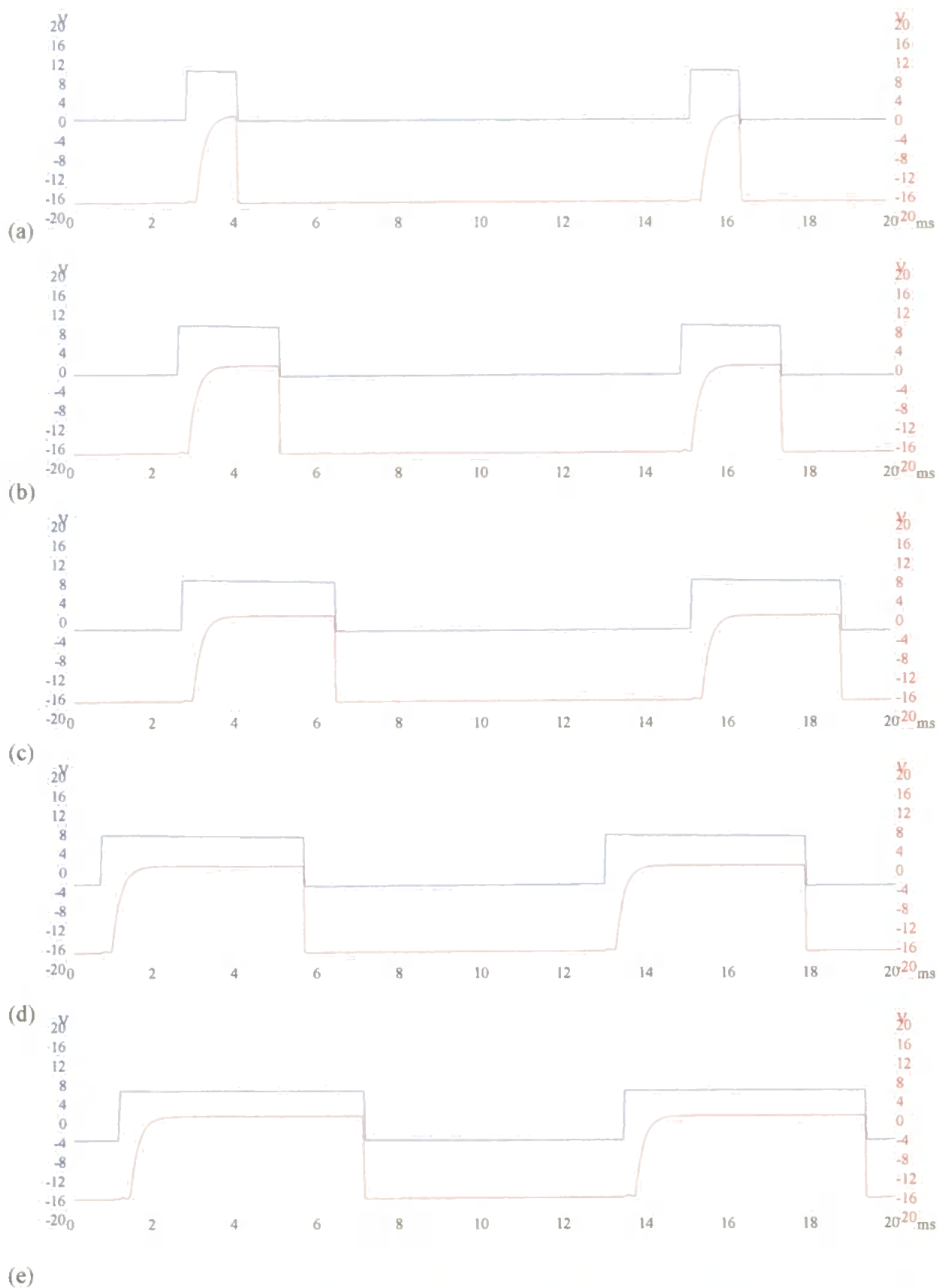
Figure 3.3: Picoscope traces for a Fe HCL operated at 167 Hz and a duty cycle of (a) 10 %, (b) 20 %, (c) 30 %, (d) 40 % and (e) 50% (— trigger signal — lamp signal)
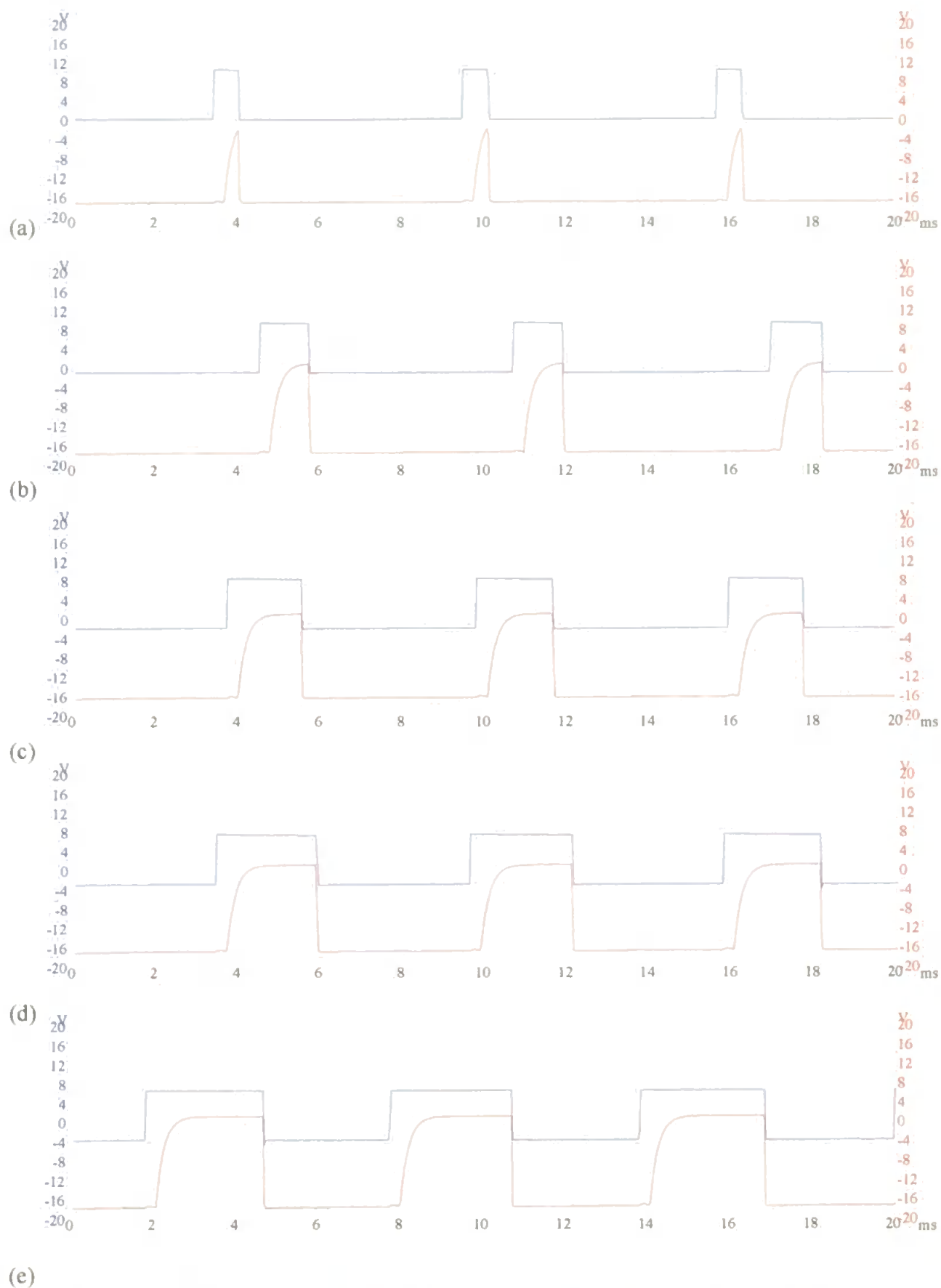
Figure 3.4: Picoscope traces for a Fe HCL operated at 292 Hz and a duty cycle of

(a) 10 %, (b) 20 %, (c) 30 %, (d) 40 % and (e) 50% (—— trigger signal —— lamp signal)
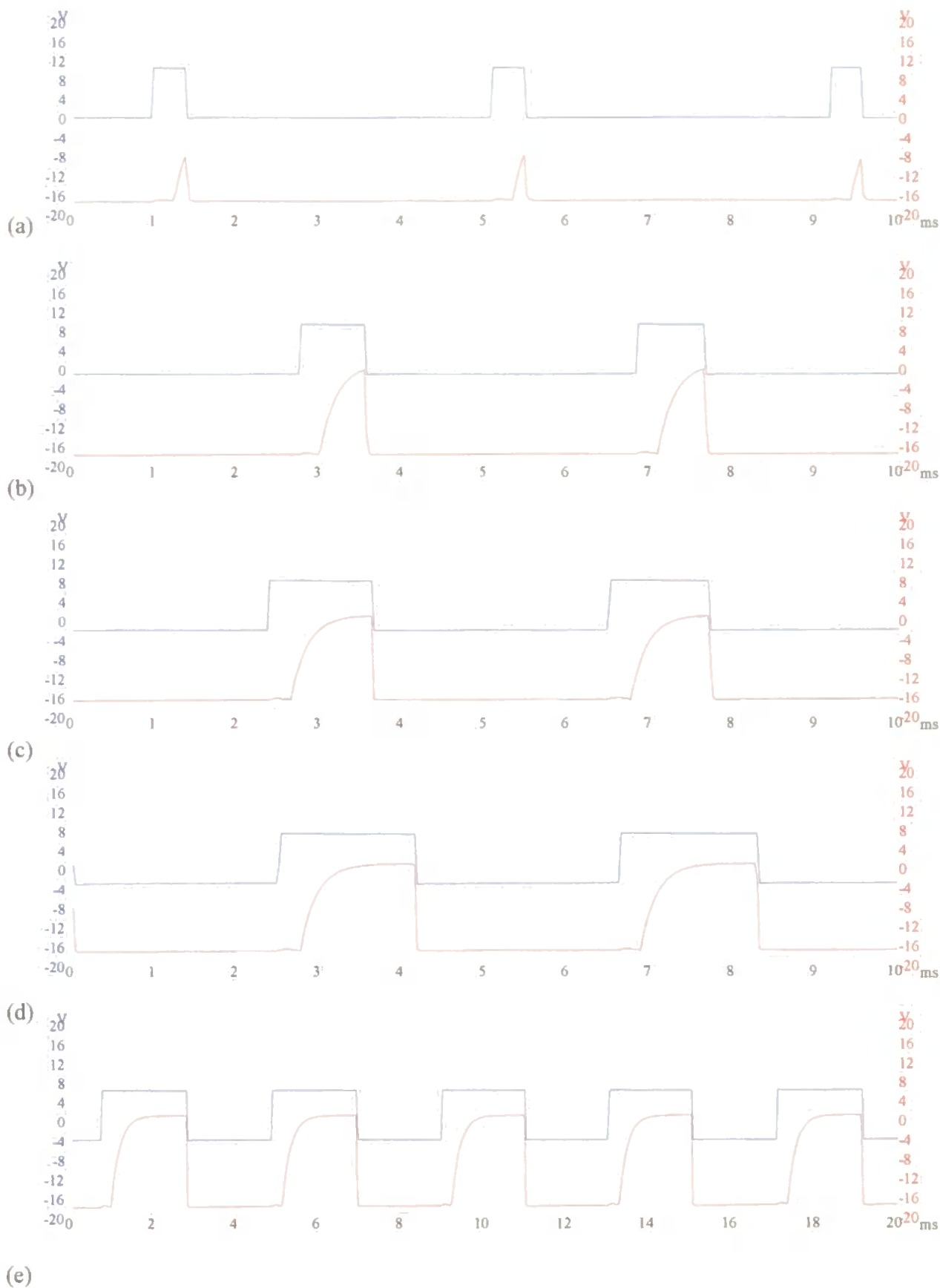
**Figure 3.5: Picoscope traces for a Fe HCL operated at 417 Hz and a duty cycle of (a) 10 %, (b) 20 %, (c) 30 %, (d) 40 % and (e) 50% (---- trigger signal ―― lamp signal)**
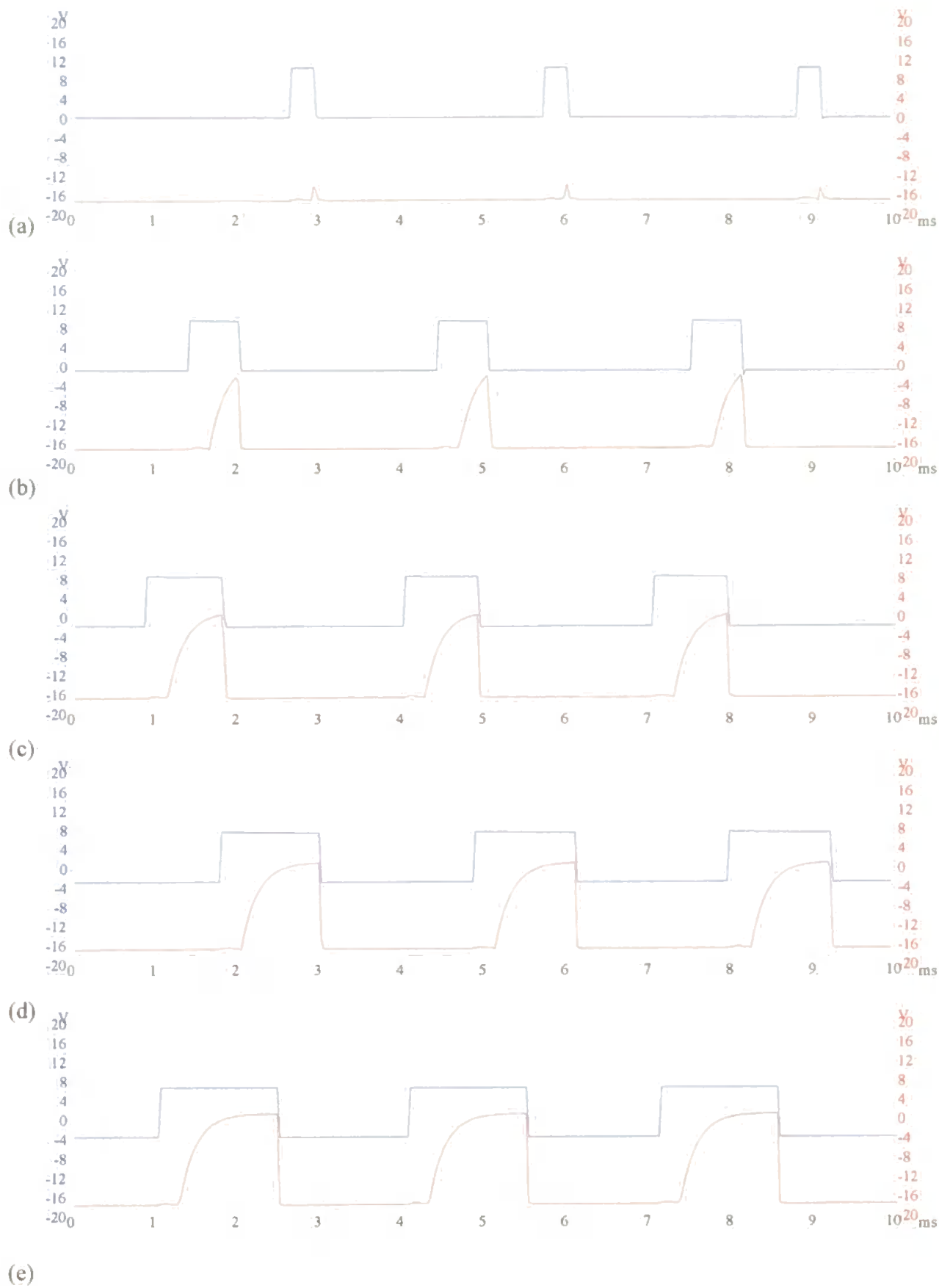
**Figure 3.6: Picoscope traces for a Fe HCL operated at 542 Hz and a duty cycle of**

**(a) 10 %, (b) 20 %, (c) 30 %, (d) 40 % and (e)   50% (——— trigger signal ——— lamp signal)**

(a)

(b)

(c)

(d)

(e)
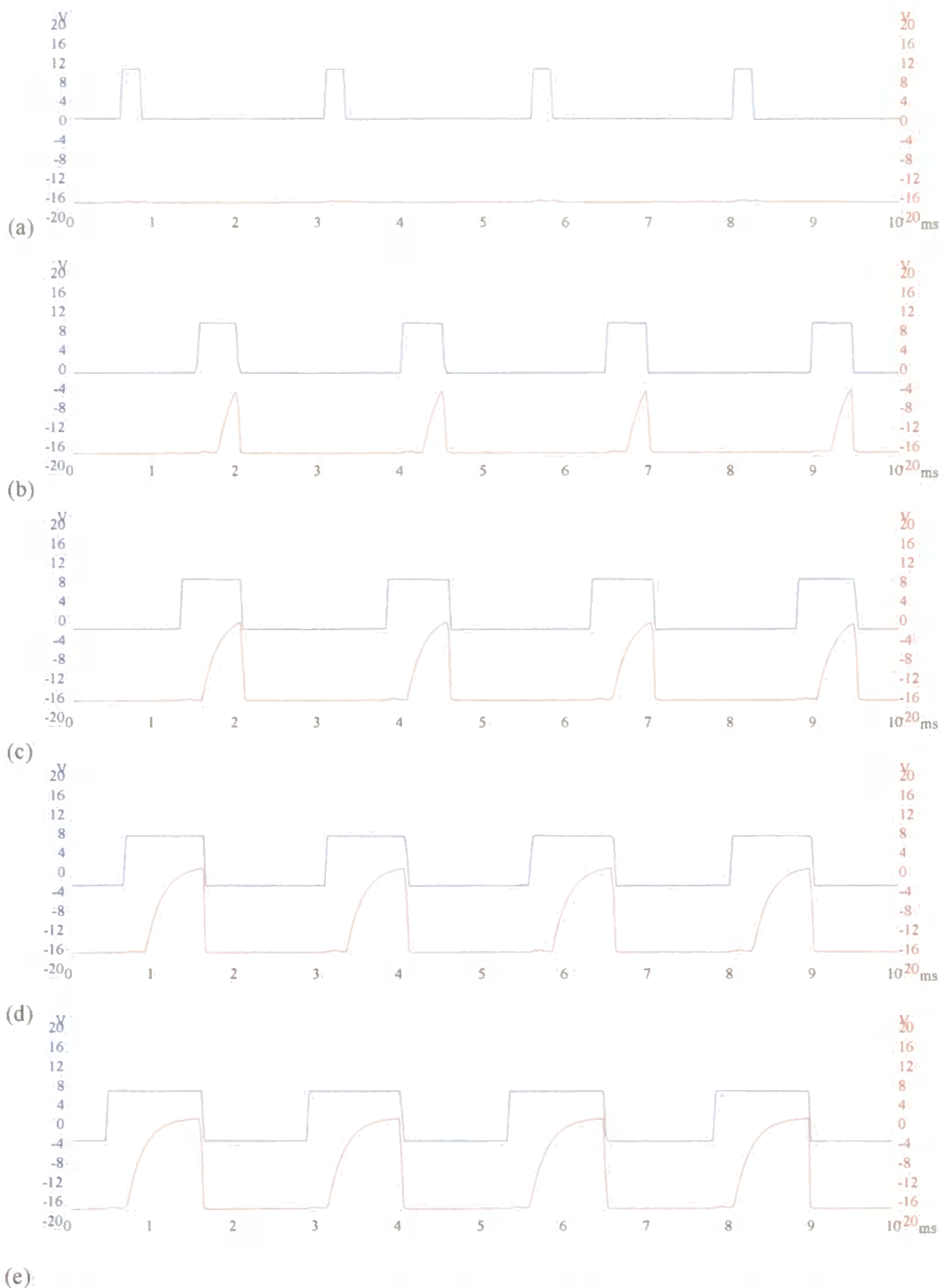
Figure 3.7: Picoscope traces for a Fe HCL operated at 667 Hz and a duty cycle of

(a) 10 %, (b) 20 %, (c) 30 %, (d) 40 % and (e) 50% (—— trigger signal —— lamp signal)

100

(a)

(b)

(c)

(d)

(e)
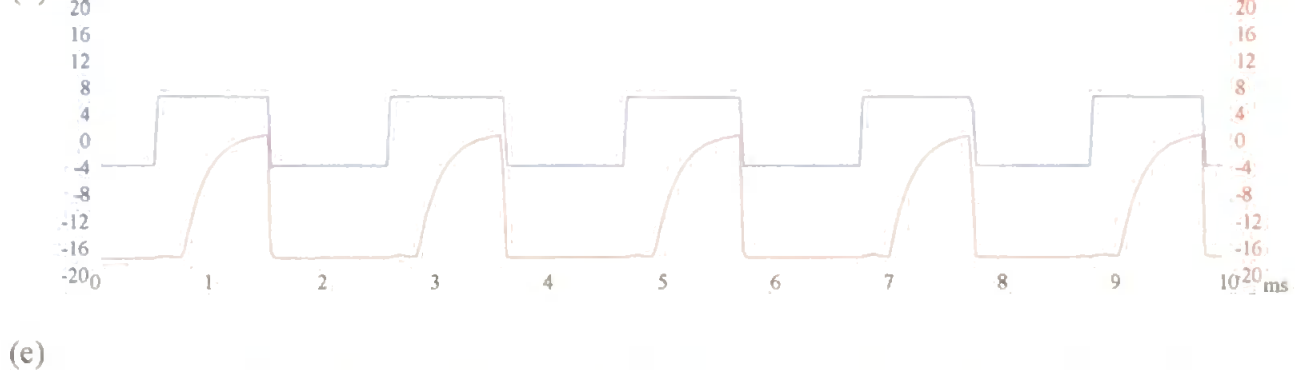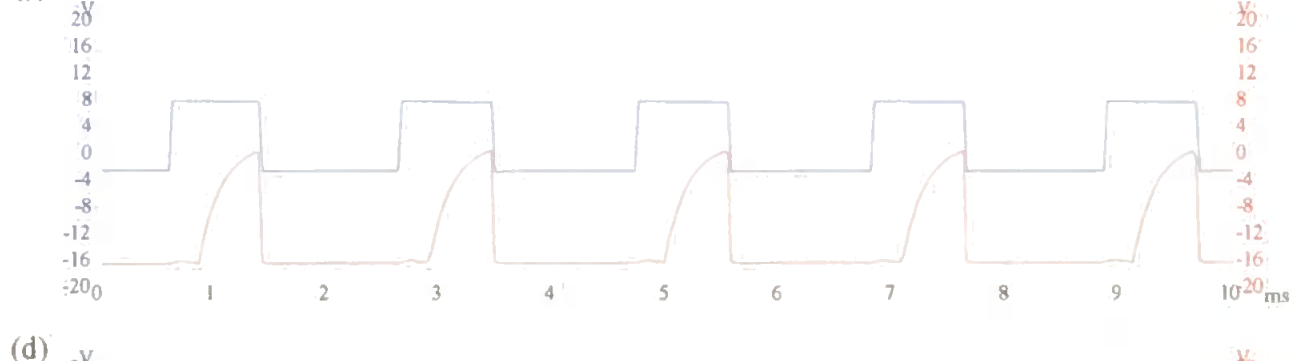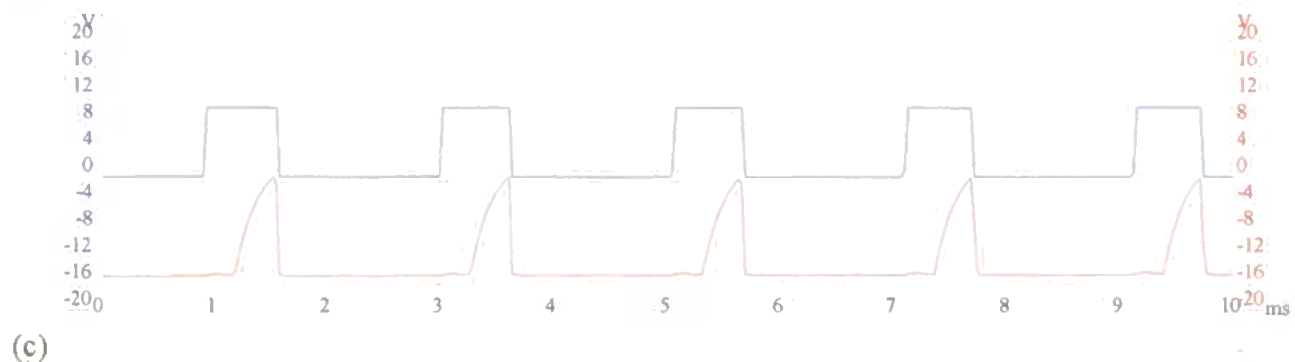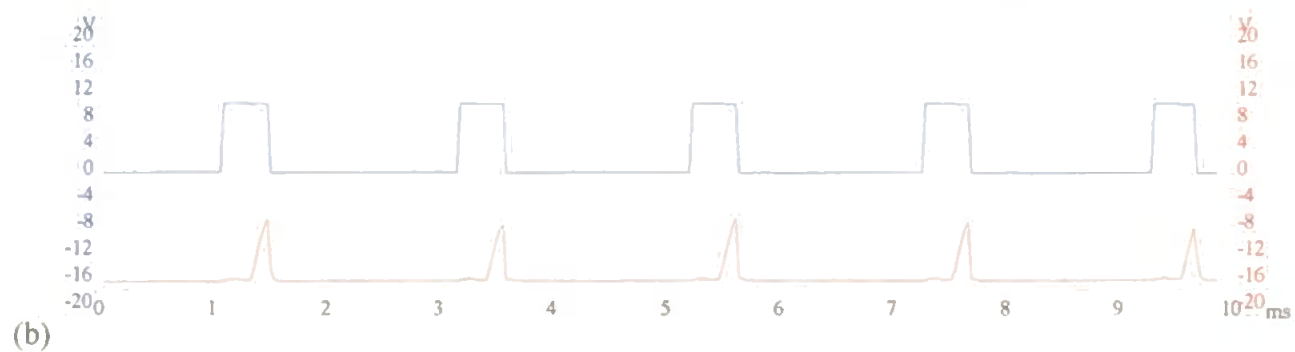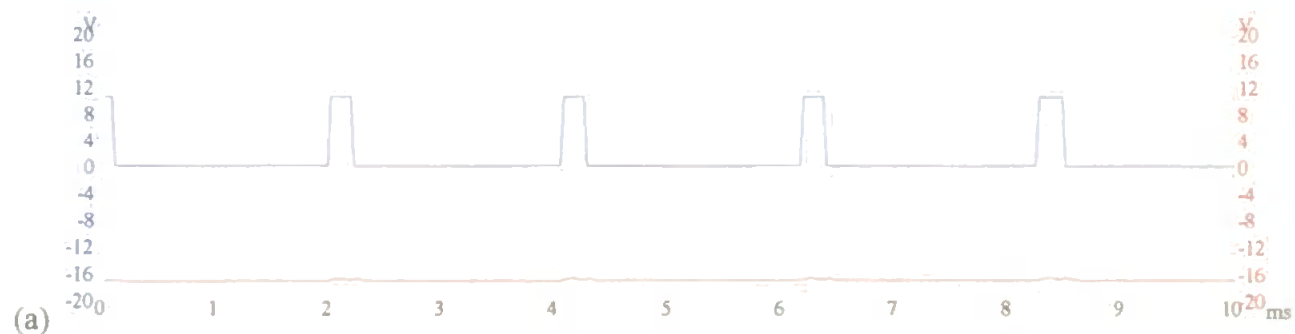
Figure 3.8: Picoscope traces for a Fe HCL operated at 792 Hz and a duty cycle of

(a) 10 %, (b) 20 %, (c) 30 %, (d) 40 % and (e)   50% (---- trigger signal —— lamp signal)

(a)

(b)

(c)

(d)

(e)
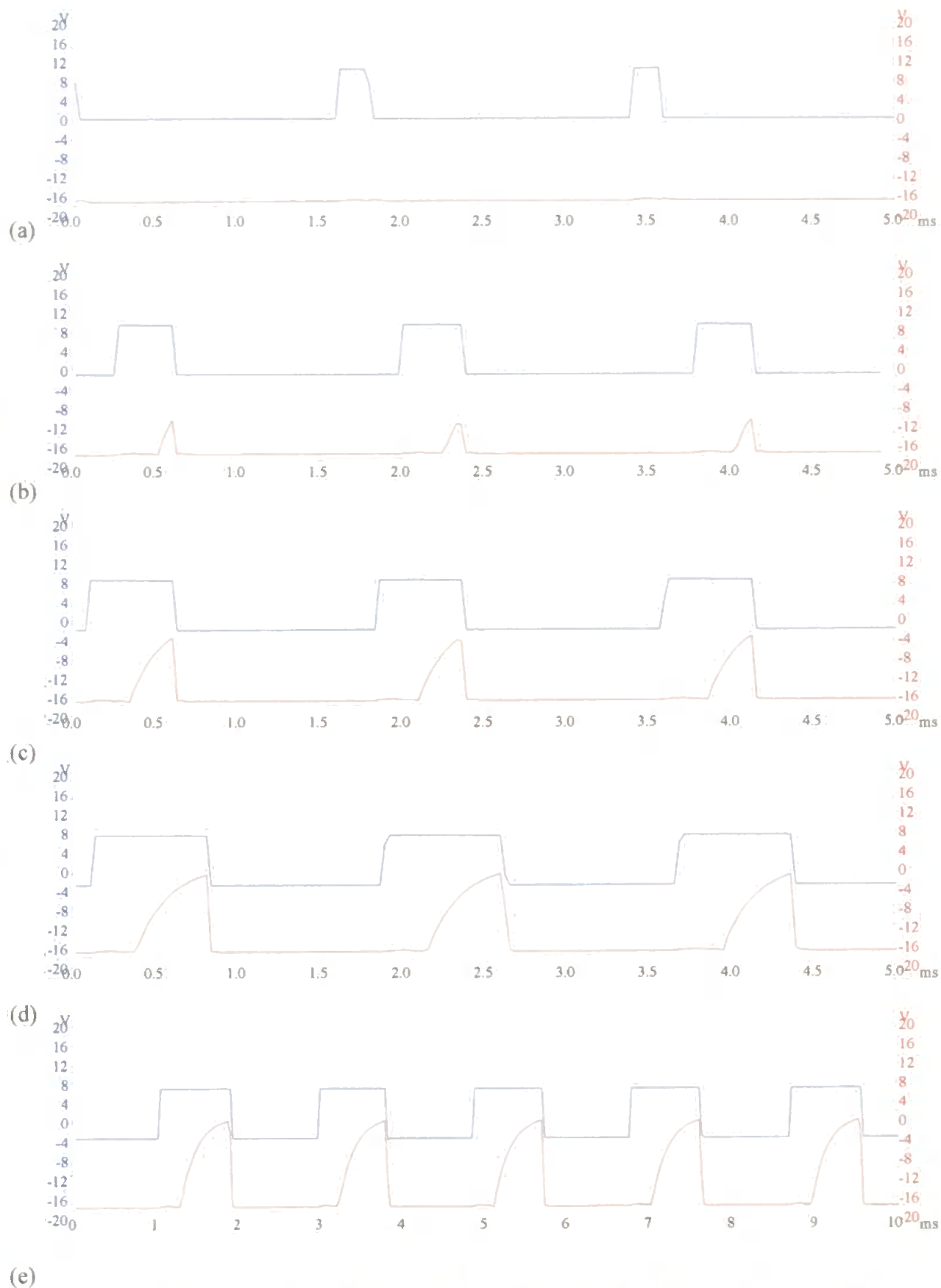
Figure 3.9: Picoscope traces for a Fe HCL operated at 917 Hz and a duty cycle of

(a) 10 %, (b) 20 %, (c) 30 %, (d) 40 % and (e) 50% (—— trigger signal —— lamp signal)

102
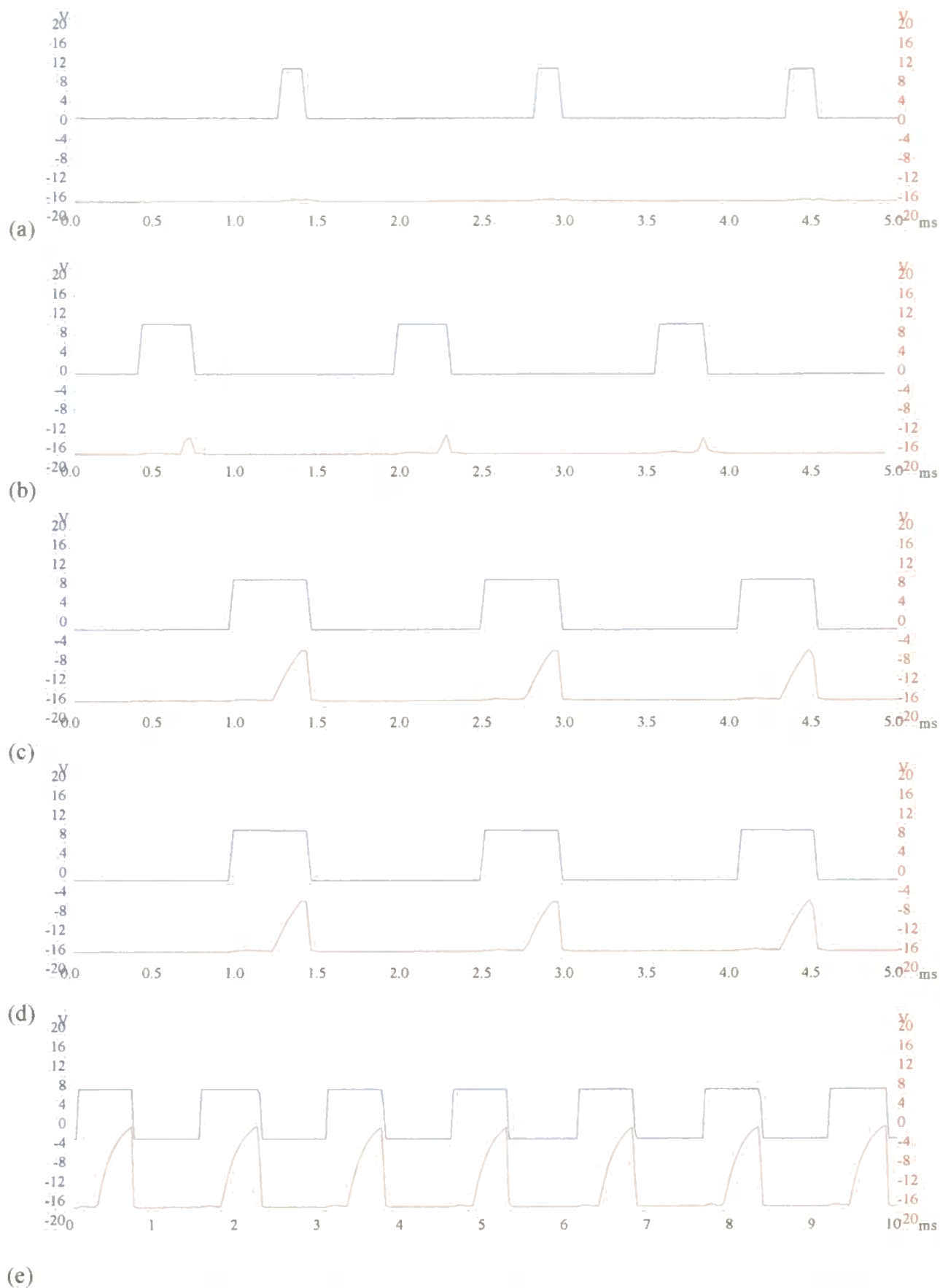
Figure 3.10: Picoscope traces for a Fe HCL operated at 1042 Hz and a duty cycle of

(a) 10 %, (b) 20 %, (c) 30 %, (d) 40 % and (e) 50% (⸻ trigger signal ⸻ lamp signal)

## 3.3 The Determination of the Characteristics of a Hollow Cathode Lamp using the Boltzmann Distribution

### 3.3.1 Introduction to Excitation Temperature

For a system in thermal equilibrium, at temperature T, the 'excitation' temperature can be deduced from the absolute intensity of an emission line through the Boltzmann equilibrium (Equation 3.1) (18).

$$I = \left(\frac{hc}{4\pi\lambda}\right) g_k A \left(\frac{n_e}{Q(T_{exc})}\right) \exp\left(\frac{-E_k}{kT_{exc}}\right) \qquad (3.1)$$

where, I is the intensity of an emitting species, h is Planck's constant ($6.63 \times 10^{-34}$ J s), c is the speed of light in a vacuum ($2.998 \times 10^8$ m s$^{-1}$), $\lambda$ is the wavelength of the emitting radiation in nm, $g_k$ is the statistical weight of the excited energy level, A is the transition probability for spontaneous emission, $n_e$ is the electron population, Q is the internal partition function, $E_k$ is the energy state in wavenumbers, (cm$^{-1}$) and k is the Boltzmann constant.

If Equation 3.1 is rearranged and logs are taken, it can be shown that log (I $\lambda$/gA) is a linear function of the excitation energy, $E_{exc}$. It is also possible to use the oscillator strength, f, whereby $E_{exc}$ is proportional to log($I\lambda^3$/gf). A graph of log (I $\lambda$/gA) or log($I\lambda^3$/gf) against $E_{exc}$ should produce a straight line if several emission lines of the same element were to be measured under LTE conditions. The slope is related to excitation temperature and is equal to $-0.625/T_{exc}$ (19).

Practically, excitation temperatures are determined using solutions of analytes nebulised into the plasma. The most commonly used element is neutral iron (86 – 103) because the atomic lines exhibit a wide range of energy and are located at closely spaced

wavelengths. In addition, many Fe I lines (Fe atom lines) are present in the 350 – 400 nm range and relatively reliable transition probabilities are available (104).

If two emission lines originating from an atom in the same ionisation state are measured, $T_{exc}$ (the 'common' excitation temperature) can be derived by the Line Pair Intensity Ratio Method (LPIRM; Equation 3.2):

$$T_{exc} = \frac{0.625(E_1 - E_2)}{\log\frac{g_1 A_1 \lambda_2}{g_2 A_2 \lambda_1} - \log\frac{I_1}{I_2}} \qquad (3.2)$$

The line pair method is less accurate than the Boltzmann Distribution but is very useful to follow the relative variation of the excitation temperature when one or several parameters of the excitation source are modified. In order for the equation to be used to produce 'relatively valid' temperature measurements, it is important that the lines measured have wavelengths existing in close proximity and have a suitably large energy difference on the Grotrian diagram of the corresponding element. Transition probabilities must be known to a relatively high (±15%) degree of accuracy for more precise temperature measurements to be made and an uncertainty of at least 20 % must be allowed for. Several test elements have been used including: titanium with Ti I 390.48/392.45 nm (105), Ti II 310.62/313.08 nm and 333.21/334.034 nm (106), Ti II 322.28/322.42 nm (88, 107, 108) iron with Fe I 391.67/391.72 nm (109), Fe I 381.58/382.44 nm (91), Fe I 382.59/382.44 nm (110), Fe I 382.043/385.991 nm (111, 112), zinc with Zn I 307.59/328.23 nm (94), strontium with Sr II 407.77/430.54 nm (113) and calcium with Ca II 393.36/373.69 nm (114, 115).

## 3.4 Experimental: Use of the Boltzmann Distribution as a Diagnostic Test to Determine the Characteristics of a Fe HCL

This experiment was completed to study the effect of modulation/duty cycle on the emission characteristics of various lines from a Fe HCL (Starna). The Boltzmann Distribution was used to determine the excitation temperature ($T_{exc}$) of a Fe HCL when operated at various modulation frequencies and duty cycles. The experimental arrangement used to determine $T_{exc}$ is shown in Figure 3.11. The mean primary current of the hollow cathode lamp was kept constant at 15 mA per unit time and lamp emission was focused onto the slit of a monochromator using a bi-convex silica lens (50 mm diameter; 50 mm focal length; L.O.T. Oriel) in a 2f:2f arrangement. Entrance and exit slit widths of the monochromator (1700 Series; SPEX Industries INC., Metochen, N.J. 08840) were fixed at 25 μm. The modulation frequencies and duty cycles investigated are summarised in Table 3.1.

The emission intensities of Fe I lines in the region 360 – 400 nm (Table 3.2) were recorded using a Datascan 2 (ISA Instruments S.A. (U.K.) Ltd., Middlesex, U.K) interfaced with a Current/Phase Stepper Drive and a monochromator (1700 Series, SPEX Industries INC.). An IEEE488 communications port provided standardised electronic protocols to receive commands and send data to a host computer. All readings were automated by constructing a program within the instrument software (SpectRad Version 2 for Windows; ISA Instruments S.A. (U.K.) Ltd.)).
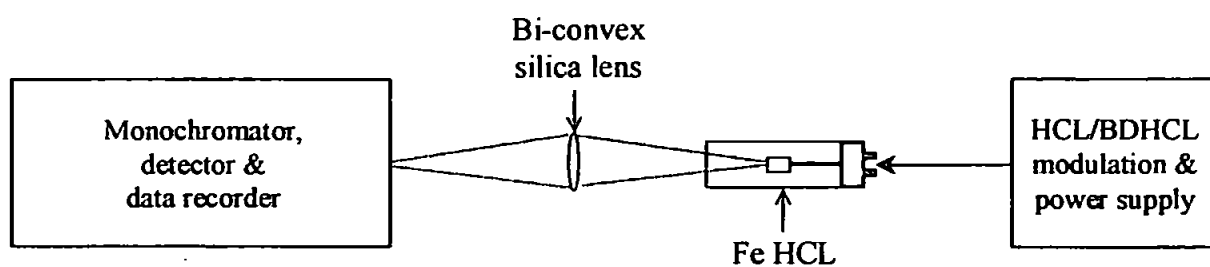
**Figure 3.11: Experimental arrangement employed to determine $T_{exc}$ of a Fe HCL using the Line Pair Intensity Ratio and the Boltzmann Distribution Methods**

:

**Table 3.2: Physical constants used to calculate $T_{exc}$ using the Boltzmann Distribution (116, 117)**

| $\lambda$ (nm) | Energy ($E_k$) (cm$^{-1}$) | $g_k$ | $A_{ik}$ ($10^8$ s$^{-1}$) |
|---|---|---|---|
| 360.886 | 35856 | 5 | 0.814 |
| 361.876 | 35612 | 7 | 0.730 |
| 362.200 | 49851 | 7 | 0.510 |
| 363.147 | 35257 | 9 | 0.517 |
| 364.040 | 49461 | 11 | 0.380 |
| 364.785 | 34782 | 11 | 0.292 |
| 367.991 | 27167 | 9 | 0.014 |
| 368.412 | 49135 | 7 | 0.340 |
| 368.600 | 50833 | 11 | 0.260 |
| 369.401 | 51570 | 7 | 0.680 |
| 370.109 | 51192 | 9 | 0.480 |
| 370.557 | 27395 | 7 | 0.032 |
| 370.925 | 34329 | 7 | 0.156 |
| 371.994 | 26875 | 11 | 0.162 |
| 372.256 | 27560 | 5 | 0.050 |
| 372.762 | 34547 | 5 | 0.225 |
| 373.332 | 27666 | 3 | 0.062 |
| 373.487 | 33695 | 11 | 0.902 |
| 374.336 | 34692 | 3 | 0.260 |
| 374.556 | 27395 | 7 | 0.115 |
| 374.590 | 27666 | 3 | 0.073 |
| 374.827 | 27560 | 5 | 0.092 |
| 376.379 | 34547 | 5 | 0.544 |
| 376.554 | 52655 | 15 | 0.980 |
| 376.719 | 34692 | 3 | 0.640 |
| 378.788 | 34547 | 5 | 0.129 |
| 379.851 | 33695 | 11 | 0.032 |
| 379.955 | 34040 | 9 | 0.073 |
| 380.670 | 52613 | 11 | 0.540 |
| 381.584 | 38175 | 7 | 1.300 |
| 382.043 | 33096 | 9 | 0.668 |
| 382.588 | 33507 | 7 | 0.598 |
| 382.782 | 38678 | 5 | 1.050 |
| 383.422 | 33802 | 5 | 0.453 |
| 384.044 | 34017 | 3 | 0.470 |
| 384.997 | 34122 | 1 | 0.606 |
| 385.637 | 26340 | 5 | 0.046 |
| 385.991 | 25900 | 9 | 0.097 |
| 386.553 | 34017 | 3 | 0.155 |
| 387.250 | 33802 | 5 | 0.105 |
| 387.803 | 33507 | 7 | 0.077 |

**Table 3.2 continued: Physical constants used to calculate $T_{exc}$ using the Boltzmann Distribution (116, 117)**

| $\lambda$ (nm) | Energy ($E_k$) (cm$^{-1}$) | $g_k$ | $A_{lk}$ ($10^8$ s$^{-1}$) |
|---|---|---|---|
| 387.857 | 26479 | 3 | 0.066 |
| 388.882 | 38678 | 3 | 0.270 |
| 389.566 | 26550 | 1 | 0.094 |
| 389.971 | 26340 | 5 | 0.026 |
| 390.295 | 38175 | 7 | 0.214 |
| 390.648 | 26479 | 3 | 0.008 |
| 392.291 | 25900 | 9 | 0.011 |
| 392.793 | 26340 | 5 | 0.022 |

### 3.4.1 Results and Discussion: Excitation Temperature and the Potential Effects on Fluorescence Signal

'Excitation' temperatures were calculated for the Fe HCL using Equation 3.1 and the physical parameters given in Table 3.2. An example of the Boltzmann Distribution plot derived from one set of experimental conditions (542 Hz at 40 % duty cycle) is given in Figure 3.12. The gradient of the curve is related to the excitation temperature and is equal to $-0.625/T_{exc}$ (19). The results of all the experimental conditions are presented in Figure 3.13 and show that $T_{exc}$ mainly varies between 5200 and 6500 K. Figure 3.13 shows that as the modulation frequency increased (from 167 to 1042 Hz) the excitation temperature, $T_{exc}$, of the lamps emission showed a small increase. It would be expected that the lamp operated with a lower percentage duty cycle would operate at a higher temperature because a 10, 20, 30, 40 and 50 % duty cycle corresponds to a primary current of 150, 75, 50, 37.5 and 30 mA, respectively. However, the results in Figure 3.13 only partly support this hypothesis. $T_{exc}$ decreased with the following duty cycles: 30 % > 40 % > 50 % > 20 % > 10 %. This was seemingly at odds with the expected result. However, this effect may be a reflection of what was shown to be occurring in Figures 3.3 – 3.10. As the duty cycle was decreased (from 50 % to 10 %), in lower duty cycle cases the lamp did not have sufficient time to react and reach the effect expected of the maximum primary current applied, *i.e.* the build up of the hollow cathode 'plasma' for a given energy input. Hence, the 'reactance' of the lamp becomes significant and the measured temperature would be lower than expected. This appeared to be the case for duty cycles of 10 and 20 %.
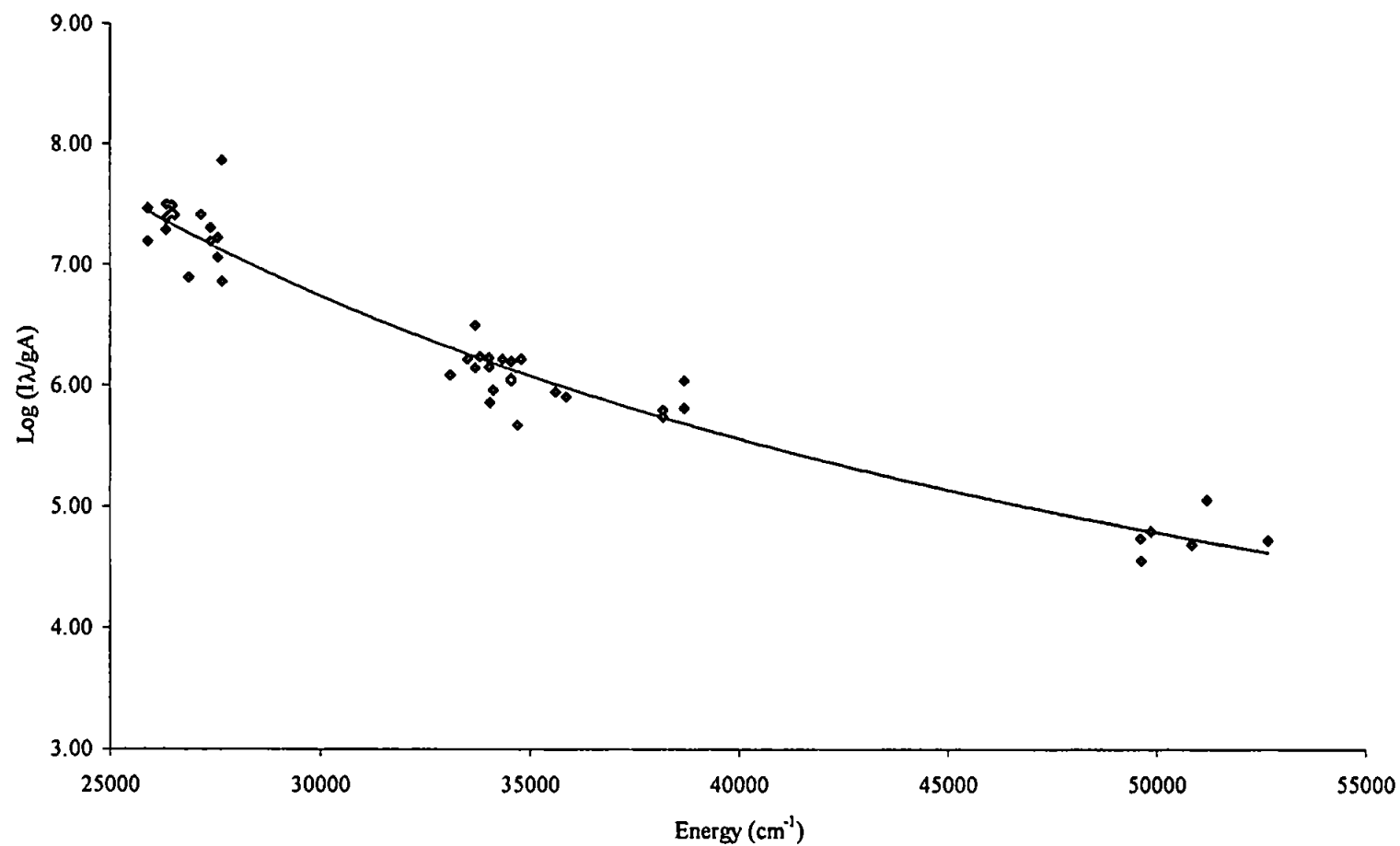
**Figure 3.12: Plot of the Boltzmann Distribution measured for a Fe HCL (primary current 15 mA; modulation frequency 542 Hz; duty cycle 40 %; n = 3, RSDs < 5 %)**
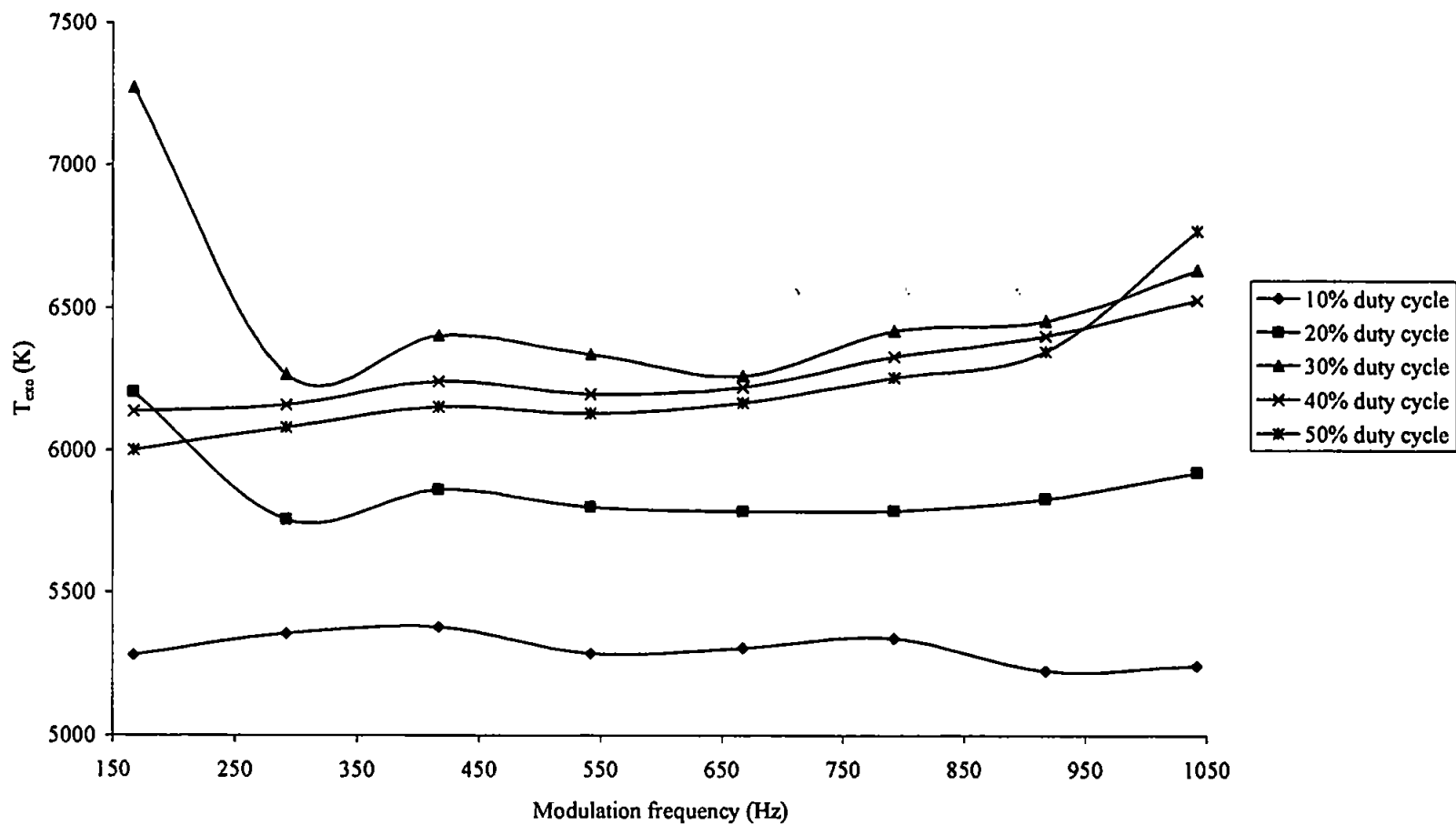
**Figure 3.13: Variation of $T_{exc}$ calculated using the Boltzmann Distribution with modulation frequency and duty cycle for a Fe HCL (primary lamp current 15 mA; n = 3, RSDs < 5 %)**

It may be noted that the Boltzmann Distribution (Figure 3.12) is not a straight line but a curve. A range of 'temperatures' may therefore be calculated from the slope under any one set of driving conditions. To illustrate this point, $T_{exc}$ was calculated in two different ways using Equation 3.1 and the physical parameters given in Table 3.2. First, using Fe I lines with excitation energies less than 35000 cm$^{-1}$ and secondly, using Fe I lines with excitation energies greater than 35000 cm$^{-1}$. The results are presented in Table 3.3 (all excitation temperatures have been rounded to the nearest 10 K and from hereon). The excitation temperatures obtained were very different from one another, typically 3700 K (range 3580 – 3880 K) and 13500 K (range 11000 – 17300 K) when calculated using excitation energies less than and greater than 35000 cm$^{-1}$, respectively. Table 3.3. shows that when the Boltzmann Distribution is calculated using Fe I lines with excitation energies of less than 35000 cm$^{-1}$ there is a negligible difference in 'temperature' values (< 10 %). However, when the Boltzmann Distribution is calculated using Fe I lines with excitation energies of greater than 35000 cm$^{-1}$ there is a significant difference in 'temperatures' which cannot be attributed to the uncertainties within the method, *i.e.* gA values. A plot of the full Boltzmann Distribution at various duty cycles when operated with a modulation frequency of 167 Hz compared with a straight line (drawn to illustrate LTE conditions) may provide the answer (Figure 3.14). Figure 3.14 illustrates that when the Fe HCL is operated at the lower duty cycles the Boltzmann Distribution is more curved, *i.e.* deviates further from LTE. This may be expected because a 'plasma' (contained at low pressure) produced from a HCL emits light and is, therefore, not near LTE. As the HCL is driven harder, the emission intensity increases, and if it is optically thin, deviates further from LTE.

Irrespective of the way in which $T_{exc}$ was calculated, the 'temperatures' calculated using the full Boltzmann Distribution are much higher than expected compared to literature values. However, in AF, the HCL is driven very much harder than its normal mode for

atomic absorption. Normally the frequency used for AA is less than 150 Hz, *e.g.* 37 Hz, with a duty cycle of 30 to 50 % and lamp primary current of typically less than 7 mA. The plasma formed in the HCL for emission in these two modes, *i.e.* for AA and AF, would therefore show different 'temperature' characteristics. Such extreme conditions may drive the plasma further from LTE and elevate its $T_{exc}$ temperature compared with those expected in the AA mode.

As previously stated in Section 3.2.2, when a HCL is driven increasingly harder self absorption effects can also be present. No evidence of self absorption was found when emission profiles of the Fe I lines produced by the HCL were examined. Therefore, the interpretation of the extreme duty cycle values in terms of intensity and $T_{exc}$ from line emissions was deemed to be accurate and could be accepted with confidence.

**Table 3.3: Excitation temperatures from a Fe HCL driven at different modulation frequencies and duty cycles calculated using the Boltzmann Distribution when Fe I lines are used with excitation energies (a) < 35 000 cm⁻¹ and (b) > 35 000 cm⁻¹**

(a)

| Frequency (Hz) | 167 | 292 | 417 | 542 | 667 | 792 | 917 | 1042 |
|---|---|---|---|---|---|---|---|---|
| Duty cycle (%) | | | | | | | | |
| 10 | 3820 | 3830 | 3800 | 3810 | 3800 | 3800 | 3810 | 3800 |
| 20 | 3850 | 3580 | 3620 | 3600 | 3580 | 3590 | 3630 | 3670 |
| 30 | 3790 | 3610 | 3600 | 3610 | 3580 | 3600 | 3610 | 3670 |
| 40 | 3670 | 3620 | 3610 | 3610 | 3630 | 3680 | 3660 | 3650 |
| 50 | 3610 | 3620 | 3580 | 3610 | 3600 | 3630 | 3630 | 3880 |

(b)

| Frequency (Hz) | 167 | 292 | 417 | 542 | 667 | 792 | 917 | 1042 |
|---|---|---|---|---|---|---|---|---|
| Duty cycle (%) | | | | | | | | |
| 10 | 16800 | 17300 | 17170 | 16800 | 17020 | 17020 | 16710 | 16620 |
| 20 | 16390 | 12290 | 12890 | 12680 | 11970 | 12560 | 13470 | 14620 |
| 30 | 15840 | 12010 | 12120 | 12100 | 11820 | 12910 | 13190 | 14210 |
| 40 | 11350 | 11580 | 11960 | 11620 | 11810 | 12680 | 13130 | 14020 |
| 50 | 11010 | 11340 | 11560 | 11210 | 11610 | 12230 | 13050 | 14470 |
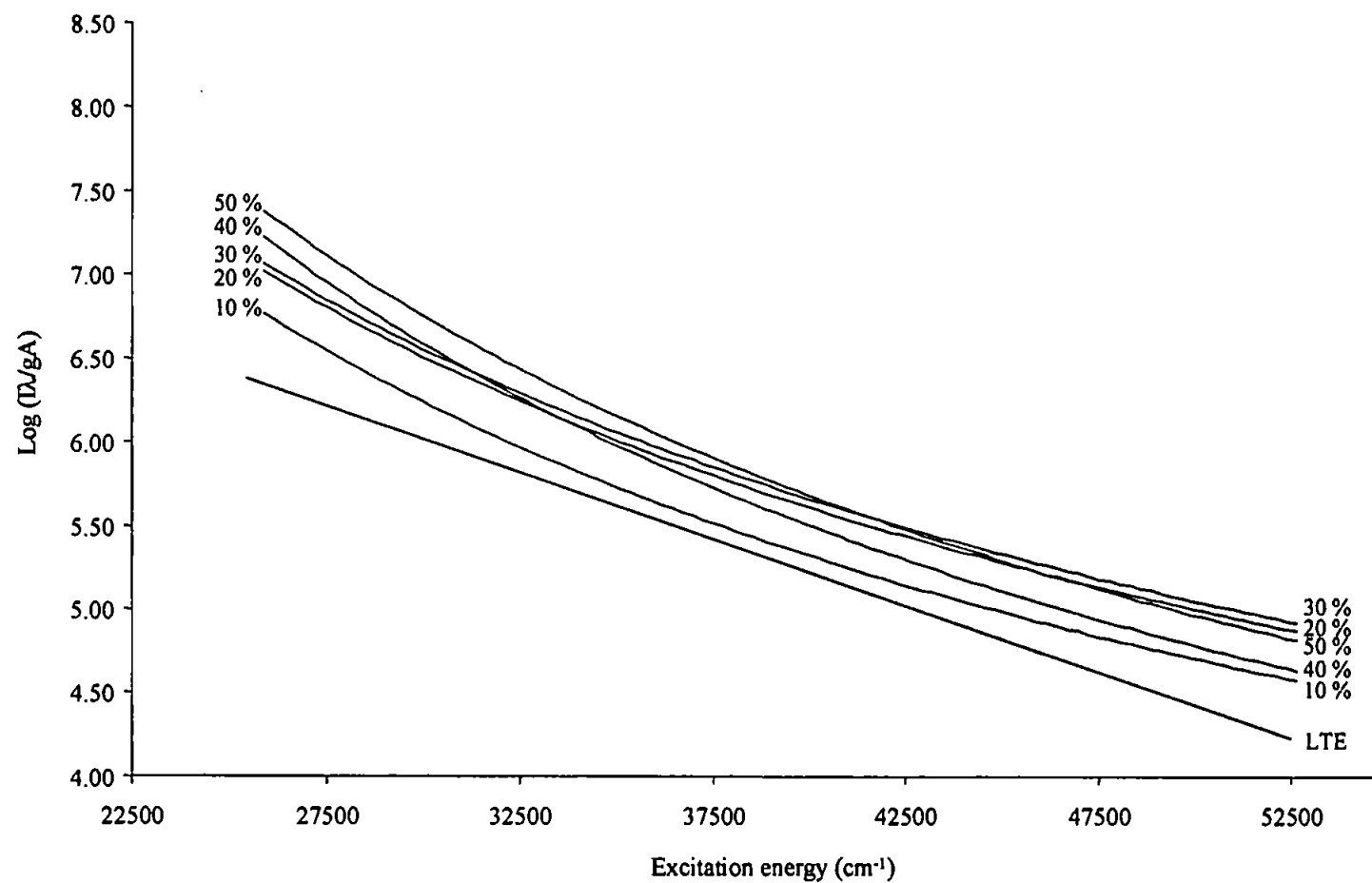
**Figure 3.14: Variation of Boltzmann Distribution plots with duty cycle for a Fe HCL (primary lamp current 15 mA; modulation frequency 167 Hz; n = 3, RSD < 5 %)**

Excitation temperatures were also calculated using the LPIRM. Equation 3.2 was used with the physical parameters listed in Table 3.2 for Fe I 382.043 and 385.991 nm. The results are presented in Figure 3.15 and show that $T_{exc}$ varies mainly between 2000 and 4500 K. A comparison of Figures 3.13 and 3.15 showed that different trends were evident with respect to modulation frequency. Figure 3.15 showed that as the modulation frequency increased, $T_{exc}$ decreased, whereas $T_{exc}$ showed a small increase with modulation frequency in Figure 3.13. In Figure 3.15, as the duty cycle increased from 10 to 50 % $T_{exc}$ increased. Once again, this was different to the trend observed in Figure 3.13.

Figure 3.12 shows three 'clusters' of data points. The LPIRM uses one data point from two of the 'clusters' and this could be the reason why the results are different to those determined by the Boltzmann Distribution. Each Fe I line may respond differently to the effect of changing the modulation frequency and duty cycle. An explanation of this difference may be obtained from the examination of a simplified version of the Grotrian diagram for Fe I illustrated in Figure 3.16. The Grotrian diagram shows that while both the 385.991 and 382.043 nm emission lines are derived from an excited 4p orbital (*i.e.* $^5D$ state) the effective ground state for both is different. While the 385.991 nm line is the equivalent of a $3d^64s^14p^1$ to $3d^64s^2$ transition, i.e. $^5D_4$ (0 eV), that of the 382.043 nm line is the equivalent of a $3d^74p^1$ to $3d^74s^1$ (*i.e.* $^5F_5$ state) transition. The latter is approximately 0.8 eV above ground state $^5D^0$ and no transition to $^5D^0$ is allowed. Hence, the two lines are independent and can be expected to display differences (111).

Attempts were made to try and determine the $T_{exc}$ using two lines from the same 'cluster'. Unfortunately, no reliable results were obtained. This was attributed to the fact that, although the wavelength difference between the two lines was small, the difference in energy level was too small to be of use. Therefore, the results determined by the

Boltzmann Distribution method allowed for effects of modulation frequency and duty cycle on a large number of lines so more confidence could be placed in the integrity of these results.

:
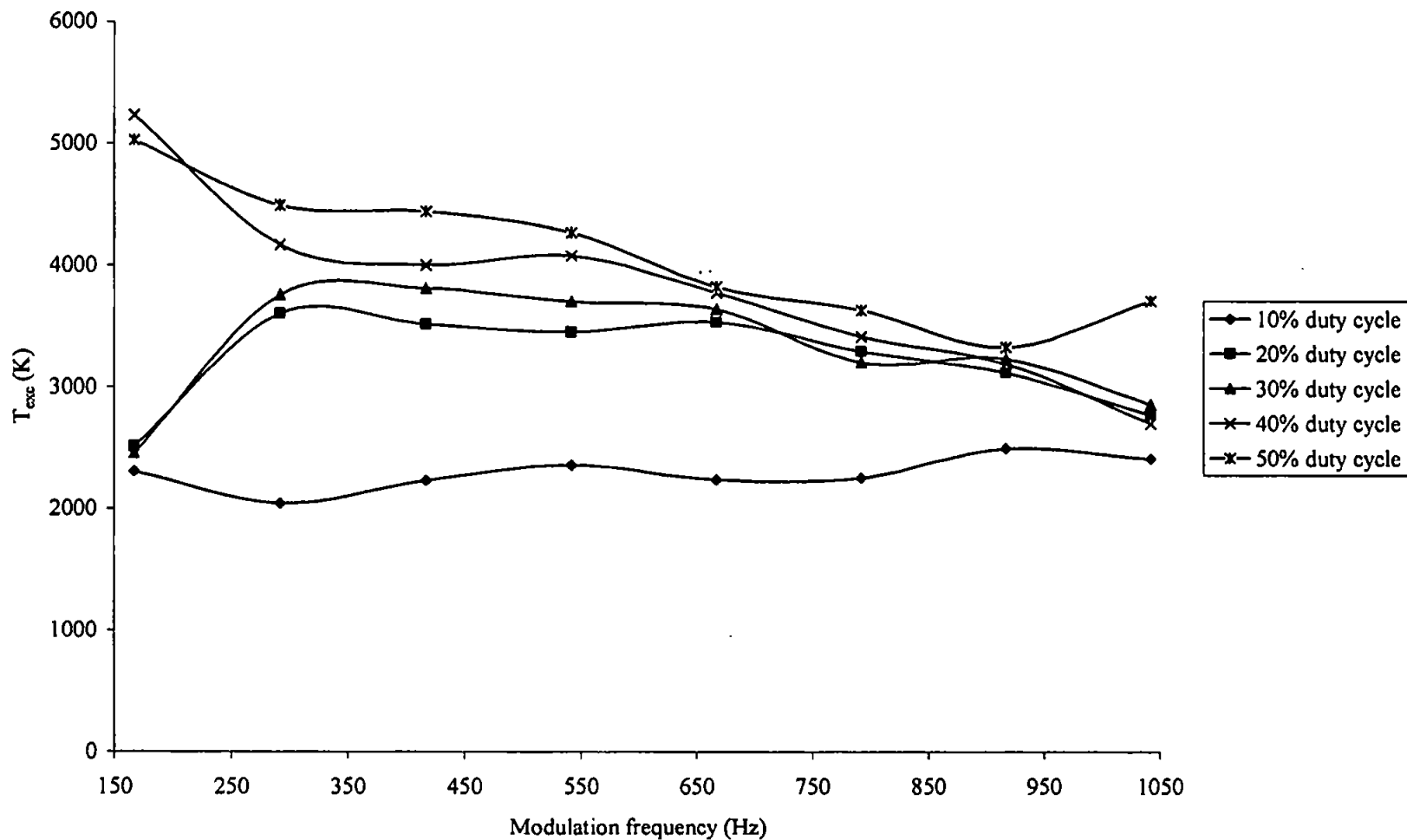
Figure 3.15: Variation of $T_{exc}$ calculated using the Line Pair Intensity Ratio Method with modulation frequency and duty cycle for a Fe HCL

(primary lamp current 15 mA; n = 3, RSDs < 5 %)
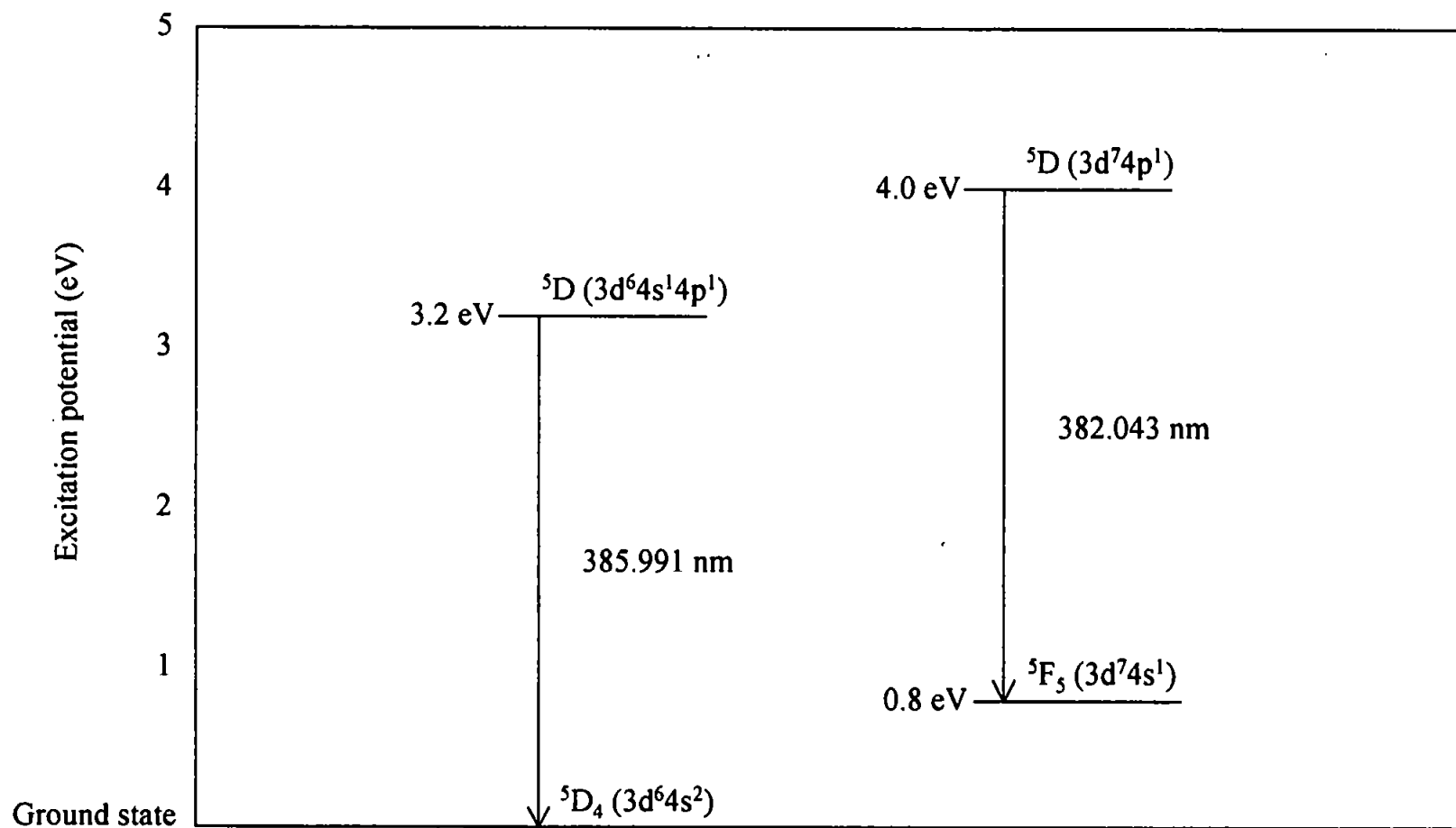
Figure 3.16: Simplified Grotrian diagram of Fe I

## 3.5 Introduction to the Optimisation of Inductively Coupled Plasma Conditions using Mg I 285.213 nm Absorbance Measurements

Atomic absorption occurring through the body of the IC plasma gives useful information for plasma studies. Assuming that the Beer-Lambert law is satisfied, AA spectrometry can provide the relative population of chemical species in the plasma (118, 119). Plasma evaluation by AAS offers several advantages: relatively remote measurement that has little perturbation of the plasma itself; straightforward knowledge obtained as to the relative densities of various species in the plasma; and simple instrumentation is employed (120).

Atomic absorption measurements were carried out in order to determine the relative number of ground state magnesium atoms (rather than excited species) in an inductively coupled plasma operated under various conditions (*i.e.* low forward powers and high nebuliser gas flow rates). Absorbance changes, as a function of forward power and nebuliser gas flow rate, were investigated at several viewing heights. As an atom must be in the GS to absorb before emitting resonance fluorescence this should provide the conditions suitable for resonance fluorescence to occur (assuming quenching effects are negated and certain molecular species are absent or avoided).

Absorbance was calculated using Equation 3.3 (18):

$$A = \log\left(\frac{I_o}{I_1}\right) = k_v l \log e \qquad (3.3)$$

where, A is absorbance, $I_o$ is the incident light intensity for a given wavelength, $I_1$ is the transmitted light intensity, $k_v$ is the absorption coefficient and $l$ is the path length.

Magnesium was chosen as the species of interest because it has often been used with the line selection Mg I 285.213 nm and Mg II 280.270 nm (or Mg II 279.553 nm) for various other studies (86, 88 – 90, 92, 94, 113, 121, 122). One advantage of this selection is the closeness of the excitation energies of the atomic and ionic lines, 35 051 and 35 669 cm$^{-1}$, respectively. The accuracy of the gA values is also acceptable (122).

## 3.6 Experimental: Attempts to Produce Conditions Suitable for Fluorescence, and Plasma Absorbance Measurements of Mg I 285.213 nm

### 3.6.1 Software

A suitable software programme ('Diagnostics'; The Perkin-Elmer Corporation, CT, USA) was obtained that allowed the forward power, as well as the plasma, auxiliary and nebuliser gas flow rates, to be controlled outside of the set instrumental (Optima 3000 ICP, The Perkin-Elmer Corporation) default values. This was imperative to provide and investigate those conditions necessary for the production of fluorescence.

### 3.6.2 Effect of Nebuliser Gas Flow Rate on Preliminary Fluorescence Experiments

The experiments described in Chapter 2 (Section 2.3.4) were repeated after an external argon supply with a high pressure regulator head was assembled. This was necessary so that the nebuliser gas flow rate could be varied in the range 0 - 3 L min$^{-1}$. Using the existing on-board pressure regulator system the back-pressure was so large that the nebuliser gas flow rate could not be altered above 1.5 L min$^{-1}$. For efficient resonance fluorescence to occur, atoms must be in the ground state (GS). A high nebuliser gas flow is necessary so that the energy exchange processes from the plasma body to the

central channel carrying the analyte of interest are modified and hence, a greater population of GS atoms are produced. The residence time of atom species is also decreased compared with conventional nebuliser gas flow rates.

The auxiliary gas flow rate was lowered to 0.1 L min$^{-1}$ as it is considered unnecessary for fluorescence experiments. Often, the nebuliser gas flow rate is so high that this alone prevents the top of the auxiliary tube from melting. The top of the demountable injector was adjusted to a position approximately 1 - 2 mm above the top of the auxiliary tube as this has previously been reported to increase the stability of the plasma under fluorescence conditions (29 – 32, 66).

### 3.6.3 Plasma Absorbance Measurements of Mg I 285.213 nm

All absorbance measurements were made using the plasma from an Optima 3000 ICP-AE spectrometer (The Perkin-Elmer Corporation) as an atomiser. The detection system comprised a fibre optic (1000 μm core diameter HPSUV1000P; Oxford Electronics Ltd., Four Marks, Hampshire, UK) held in position by the X and Y-axis translation plate described previously in Chapter 2 (Section 2.2.1.2). The X and Y-axis translation plate was originally designed for the collection of fluorescence so that the fibre optic could be positioned at right angles to the excitation source. The dimensions of the torch box were such that the lamp could not be positioned opposite the fibre optic and therefore a modification to the plate was necessary for absorbance measurements. An L-shaped aluminium bracket was made which connected to the movable arm of the plate and held the fibre optic directly opposite to the excitation source on the other side of the plasma. A filter ($\lambda_{max}$ 280 nm; Model No. 5325; L.O.T. Oriel), a photomultiplier tube (I.L. R 955; Hamamatsu Photonics UK Ltd.) operated by a high voltage power supply (Model 456; EG & G Ortec), and a lock-in amplifier (Model 9503; EG & G Brookdeal,

Bracknell, Berkshire, UK) completed the assembly. Operating conditions are listed in Table 3.4. The experimental arrangement used to complete the absorbance measurements is shown in Figure 3.17.

Optimum conditions were determined by measuring a 1000 $\mu$g ml$^{-1}$ aqueous standard of magnesium and a blank at a range of viewing heights (60 – 120 mm ALC in 10 mm increments). The magnesium concentration was so high to enable it to be observed and measured above background levels these greater heights ALC. The variable parameters to be optimised were the nebuliser gas flow rate, sample uptake rate, lamp primary current, modulation frequency and duty cycle (Table 3.4).

### 3.6.4   Chemicals and Reagents

All reagents used (Mg) were of 'AnalaR' reagent grade (Merck, Poole, Dorset, UK) and all solutions were prepared using doubly deionised water (Milli-Q, Millipore, Middlesex, UK).

Calibration standards were prepared by serial dilution of commercially available stock standard solutions (10000 $\mu$g ml$^{-1}$).

**Table 3.4: Operating conditions for Mg I 285.213 nm absorption measurements for an ICP operated at low powers and with high nebuliser gas flow rates**

| Excitation system | |
|---|---|
| Hollow cathode lamp | Mg HCL ($\lambda$ = Mg I 285.213 nm) |
| **Nebuliser gas flow and sample uptake rate absorbance experiments** | |
| Primary current | 3 mA |
| Modulation frequency | 167 Hz |
| Duty cycle | 50 % |
| **Primary current, modulation frequency and duty cycle absorbance experiments** | |
| Primary current | 3 - 15 mA (1 mA increments) |
| Modulation frequency | 542, 667 & 792 Hz |
| Duty cycle | 10 - 50 % (10 % increments) |
| **Atomiser** | |
| **RF Generator** | |
| Frequency | 40.68 MHz, free running |
| **ICP-AFS conditions** | |
| Power | 700, 800 & 900 W |
| **Sample Introduction System** | |
| Nebuliser | Ebdon V-Groove, high solids |
| Torch | Demountable, custom built with 60 mm extended coolant tube (from auxiliary) and a 1.5 mm i.d. alumina injector |
| Spray Chamber | PE Scott Double Pass |
| Peristaltic Pump | Gilson Minipuls 3, computer controlled |
| **Argon Flow Rate** | |
| Plasma | 12 L min$^{-1}$ |
| Auxiliary | 0.1 L min$^{-1}$ |
| **Nebuliser gas flow and sample uptake rate absorbance experiments** | |
| Nebuliser | 1.50 - 3.00 L min$^{-1}$ (0.50 L min$^{-1}$ increments) |
| Sample uptake rate | 1.00 – 2.00 ml min$^{-1}$ (0.25 ml min$^{-1}$ increments) |
| **Primary current, modulation frequency and duty cycle absorbance experiments** | |
| Nebuliser | 2.00 L min$^{-1}$ |
| Sample uptake rate | 2.00 ml min$^{-1}$ |
| **External detection system** | |
| Filter | $\lambda_{max}$ 280 nm |
| PMT voltage | 1000 V |

**Figure 3.17: Schematic of the experimental arrangement used for Mg I 285.213 nm absorption measurements**

### 3.6.5 Results and Discussion: Plasma Absorbance Measurements of Mg I 285.213 nm

### 3.6.5.1 Effect of Nebuliser Gas Flow and Sample Uptake Rate on Mg I 285.213 nm Absorbance Signal

Figures 3.18 – 3.20 show the effect of nebuliser gas flow and sample uptake rate on absorbance signal for a plasma operated with a forward power of 700 W at viewing heights of 100, 110 and 120 mm ALC. At lower viewing heights (60 – 90 mm ALC) the absorbance signal observed did not vary with respect to nebuliser gas flow rate and sample uptake rate so these have not been shown. However, a maximum absorbance signal was observed at a viewing height of 60 mm ALC. From 100 mm ALC upwards the nebuliser gas flow had an effect on the absorbance signal. As the nebuliser gas flow increased from 1.50 to 3.00 L min$^{-1}$ the absorbance signal decreased, whereas the sample uptake rate had no noticeable effect on absorbance signal.

Absorbance is a ratio of $I_o$, the incident light intensity, and, $I_1$, the transmitted light intensity. Therefore, the calculated absorbance may not be a true reflection of an increasing proportion of GS atoms. If $I_o$, remains fairly constant throughout the measurements then any increases/decreases in absorbance are likely to be due to the increasing/decreasing proportion of Mg GS atoms. However, if the background level rises ($I_o$,) then a false maxima/minima may be given. Examination of the raw data shows that the background level is fairly constant throughout the absorbance measurements. Therefore, confidence can be placed with the high absorbance values suggesting areas in the plasma with higher populations of GS atoms.

The maximum absorbance signal was obtained at 60 mm ALC so all other parameters were optimised using a viewing height of 60 mm ALC. This shows good agreement with the values found in the literature (42 – 53, 56).
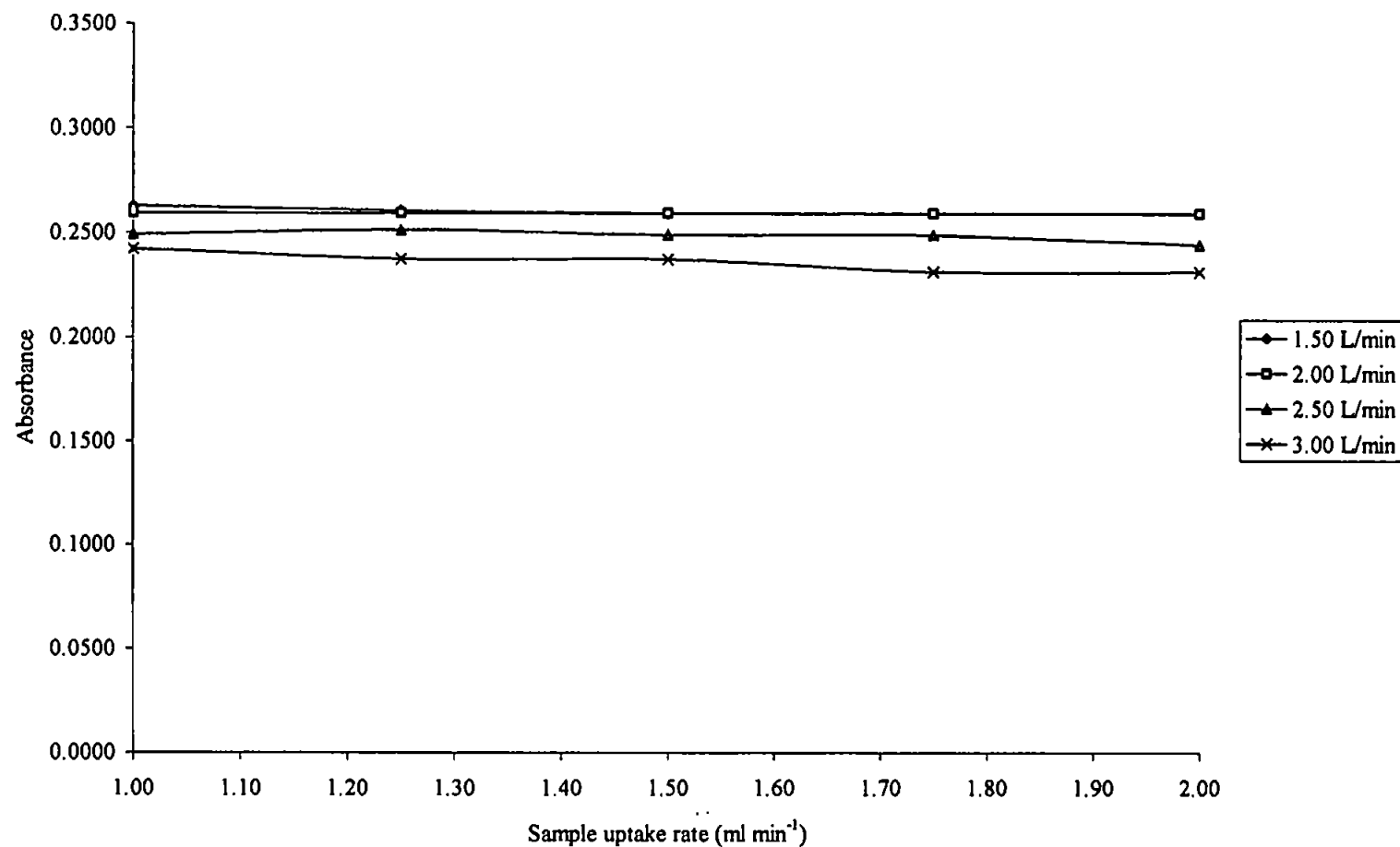
**Figure 3.18: Effect of nebuliser gas flow and sample uptake rate on Mg I 285.213 nm absorbance signal for a plasma operated under fluorescence-like conditions (forward power 700 W) at a viewing height of 100 mm ALC (n=3, RSDs <5 %)**
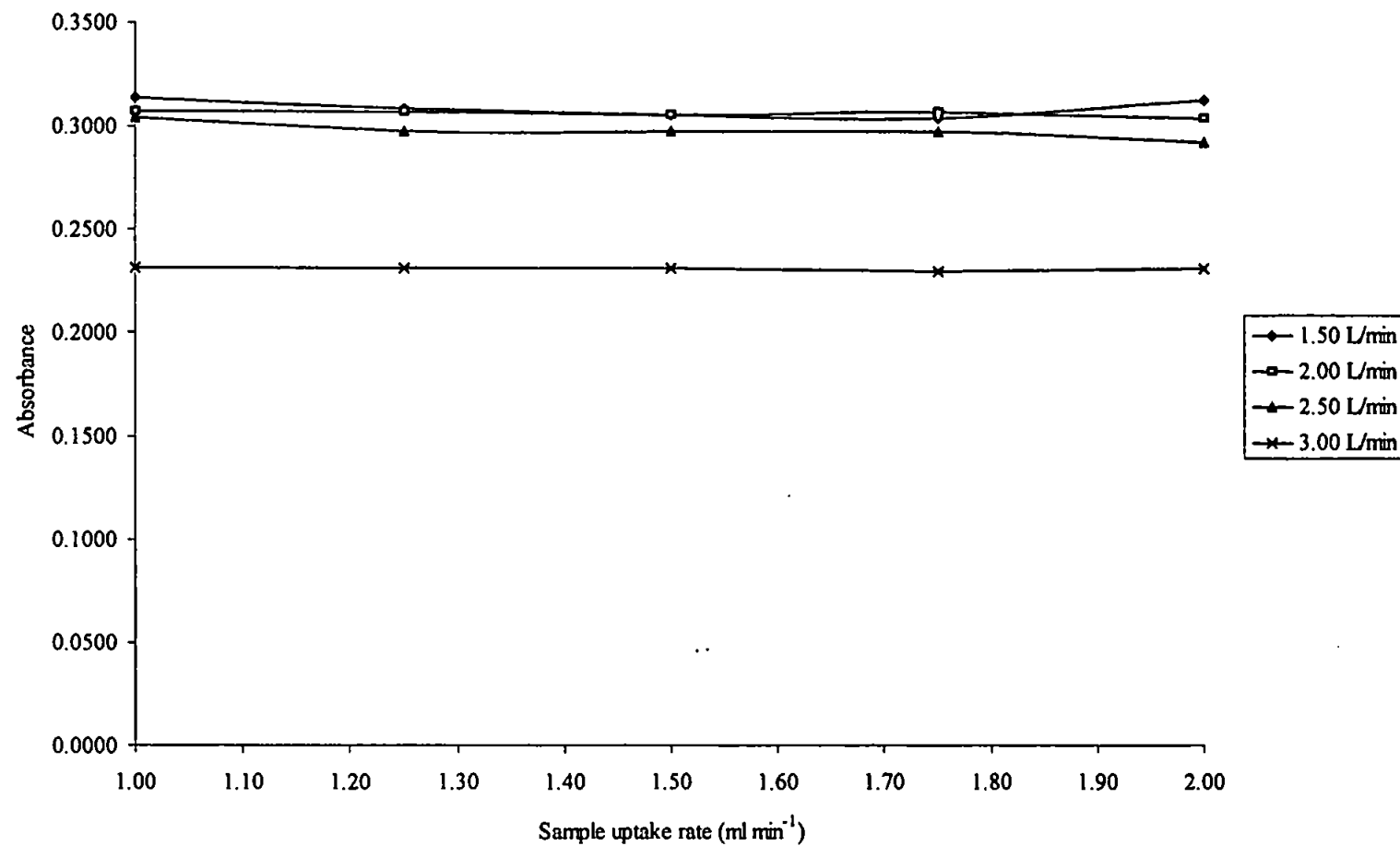
Figure 3.19: Effect of nebuliser gas flow and sample uptake rate on Mg I 285.213 nm absorbance signal for a plasma operated under

fluorescence-like conditions (forward power 700 W) at a viewing height of 110 mm ALC (n=3, RSDs <5 %)
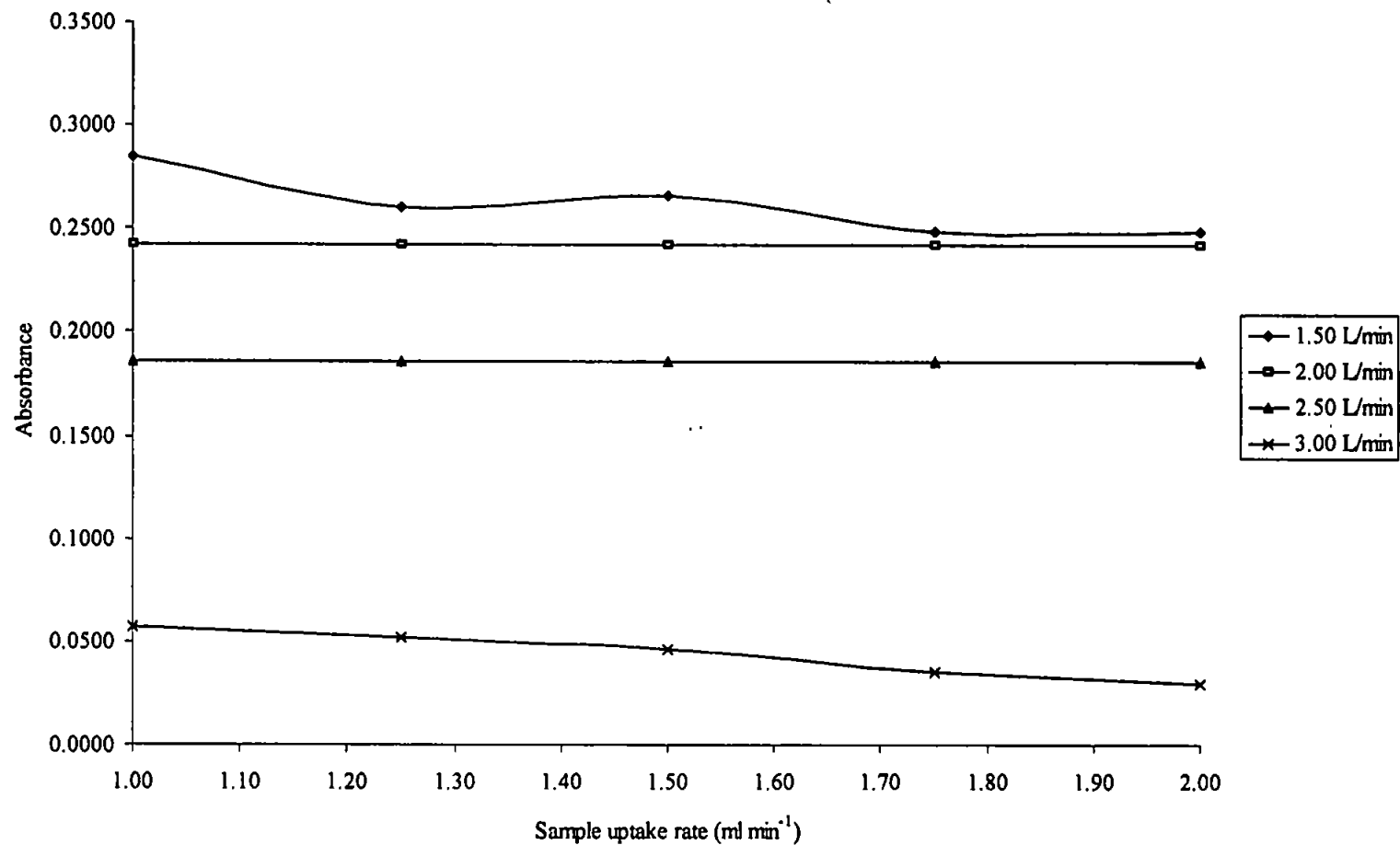
Figure 3.20: Effect of nebuliser gas flow and sample uptake rate on Mg I 285.213 nm absorbance signal for a plasma operated under fluorescence-like conditions (forward power 700 W) at a viewing height of 120 mm ALC (n=3, RSDs <5 %)

### 3.6.5.2 Effect of Primary Lamp Current on Mg I 285.213 nm Absorbance Signal

Figure 3.21 shows the effect of increasing the primary current of the lamp on the absorbance signal of Mg I 285.213 nm for a plasma operated with a forward power of 700 W. The working range of the lamp was stated to be between 3 – 7.5 mA. Figure 3.21 shows that within the working range there was a proportional relationship between primary current and absorbance signal. When the maximum advisable lamp operating current was exceeded, the absorbance decreased as the primary lamp current increased. The optimum condition (*i.e.* greatest absorbance) was obtained with a primary lamp current of 6 mA. This value was used for all further optimisation experiments.

### 3.6.5.3 Effect of Modulation Frequency and Duty Cycle on Mg I 285.213 nm Absorbance Signal

Figures 3.22 – 3.24 show the effect of varying the duty cycle and modulation frequency on the absorbance signal of Mg I 285.213 nm for a plasma operated with a forward power of 700 W. Figures 3.22 – 3.24 show, irrespective of the modulation frequency used, that the maximum absorbance is obtained when a duty cycle of 50 % is used and the absorbance decreased with the following duty cycles: 50 % > 40 % > 30 % > 20 % > 10 %.

Due to time constraints only three modulation frequencies were investigated as this was deemed sufficient to give a 'guide' to the effect of varying the modulation frequency on Mg I absorbance measurements. Figures 3.22 – 3.24 show that there was little difference between the absorbance values obtained for modulation frequencies of 667 and 792 Hz for equivalent experiments. Comparison of the lamp profiles (Figures 3.7 and 3.8 for modulation frequencies of 667 and 792 Hz, respectively) show less

'clipping' at the lower modulation frequency. Therefore, a modulation frequency of 667

Hz was used for all future experiments.

:

.

.
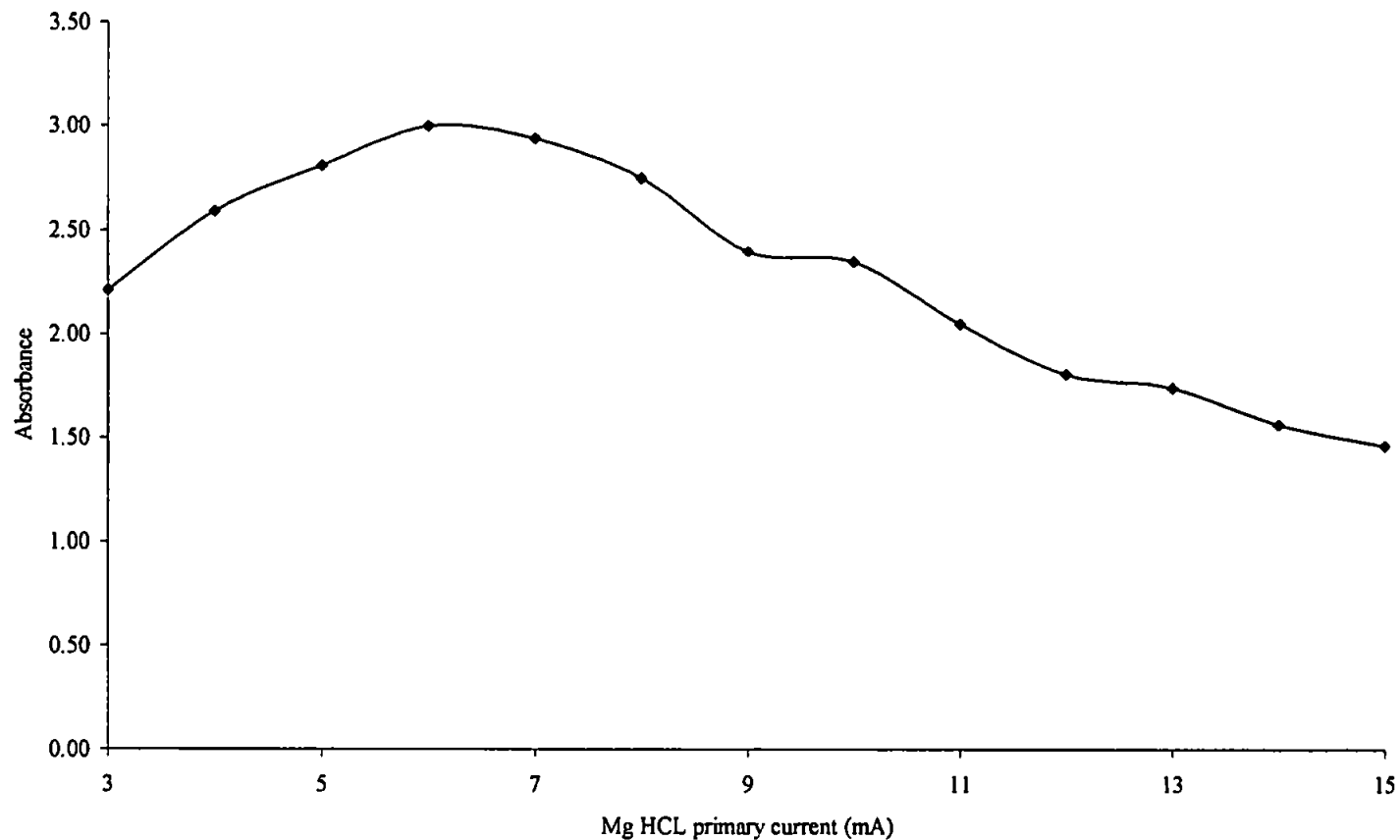
**Figure 3.21: Effect of lamp primary current on Mg I 285.213 nm absorbance signal for a plasma operated under fluorescence-like conditions (lamp modulation frequency 542 Hz; lamp duty cycle 50 %; forward power 700 W; nebuliser gas flow rate 2.00 L min$^{-1}$; viewing height 60 mm ALC; n = 3, RSDs < 5 %)**
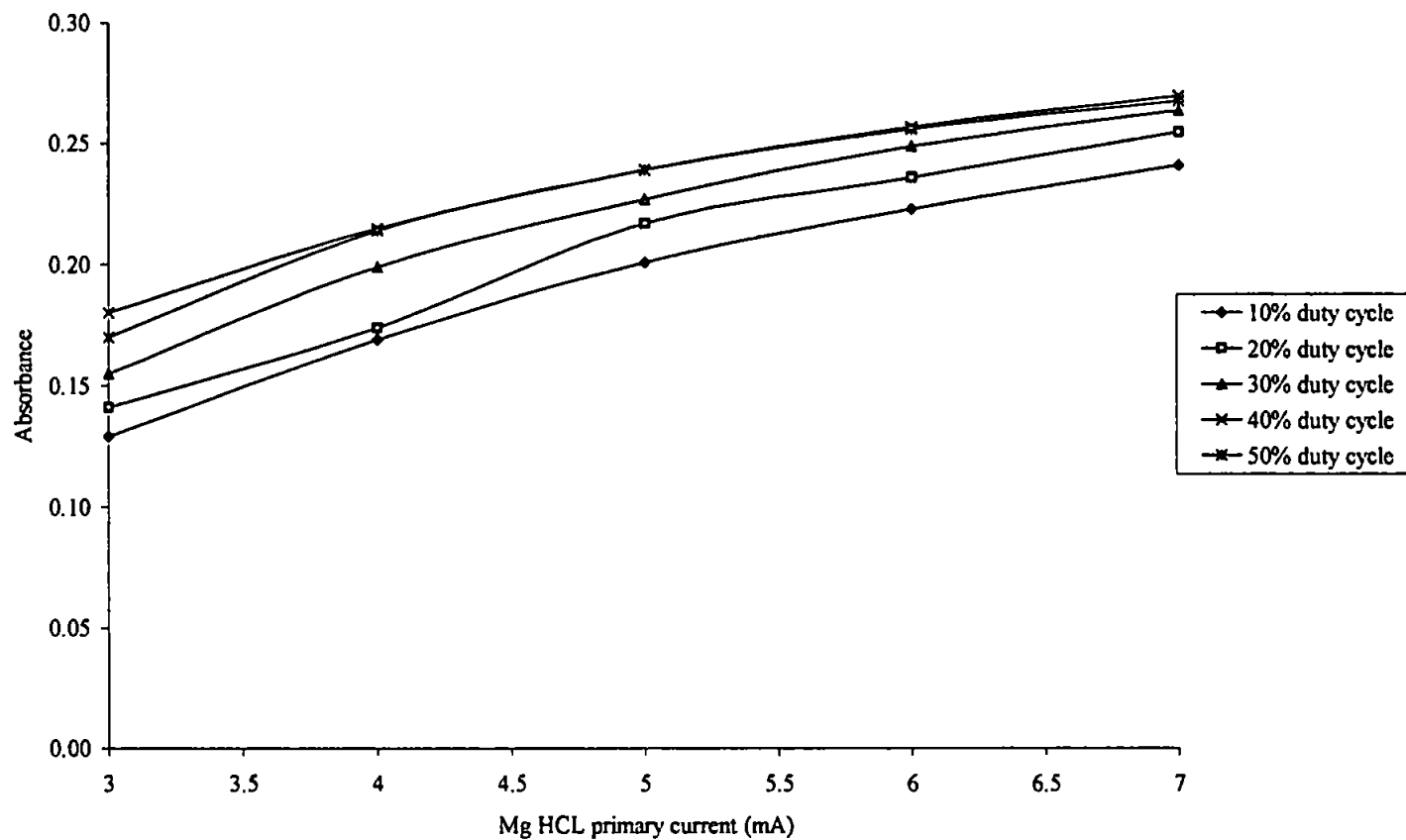
**Figure 3.22: Effect of duty cycle and lamp primary current on Mg I 285.213 nm absorbance signal for a plasma operated under fluorescence-like conditions (forward power 700 W; nebuliser gas flow rate 2.00 L min$^{-1}$; viewing height 60 mm ALC; lamp modulation frequency 542 Hz; n = 3, RSDs < 5 %)**
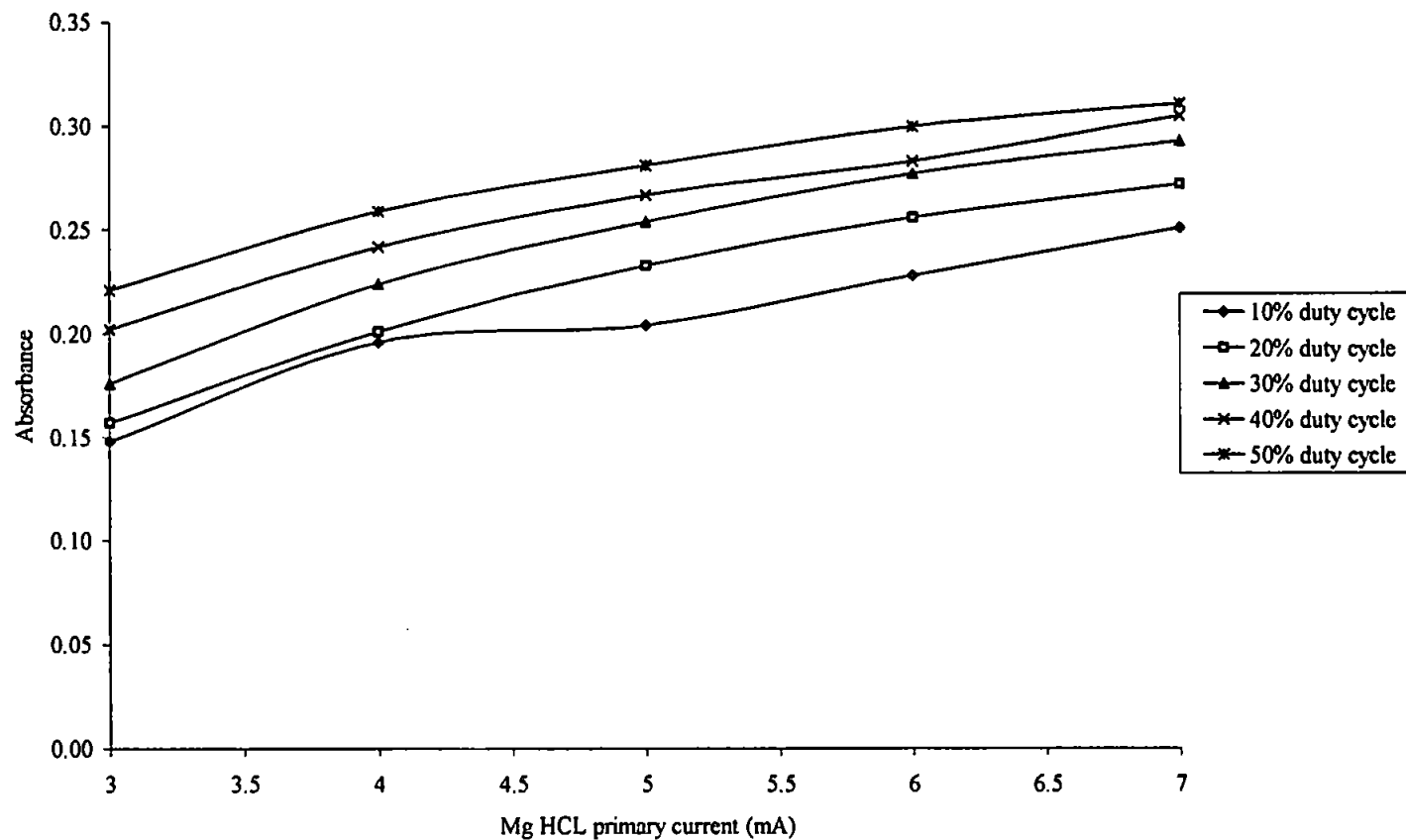
**Figure 3.23: Effect of duty cycle and lamp primary current on Mg I 285.213 nm absorbance signal for a plasma operated under fluorescence-like conditions (forward power 700 W; nebuliser gas flow rate 2.00 L min⁻¹; viewing height 60 mm ALC; lamp modulation frequency 667 Hz;**

**n = 3, RSDs < 5 %)**
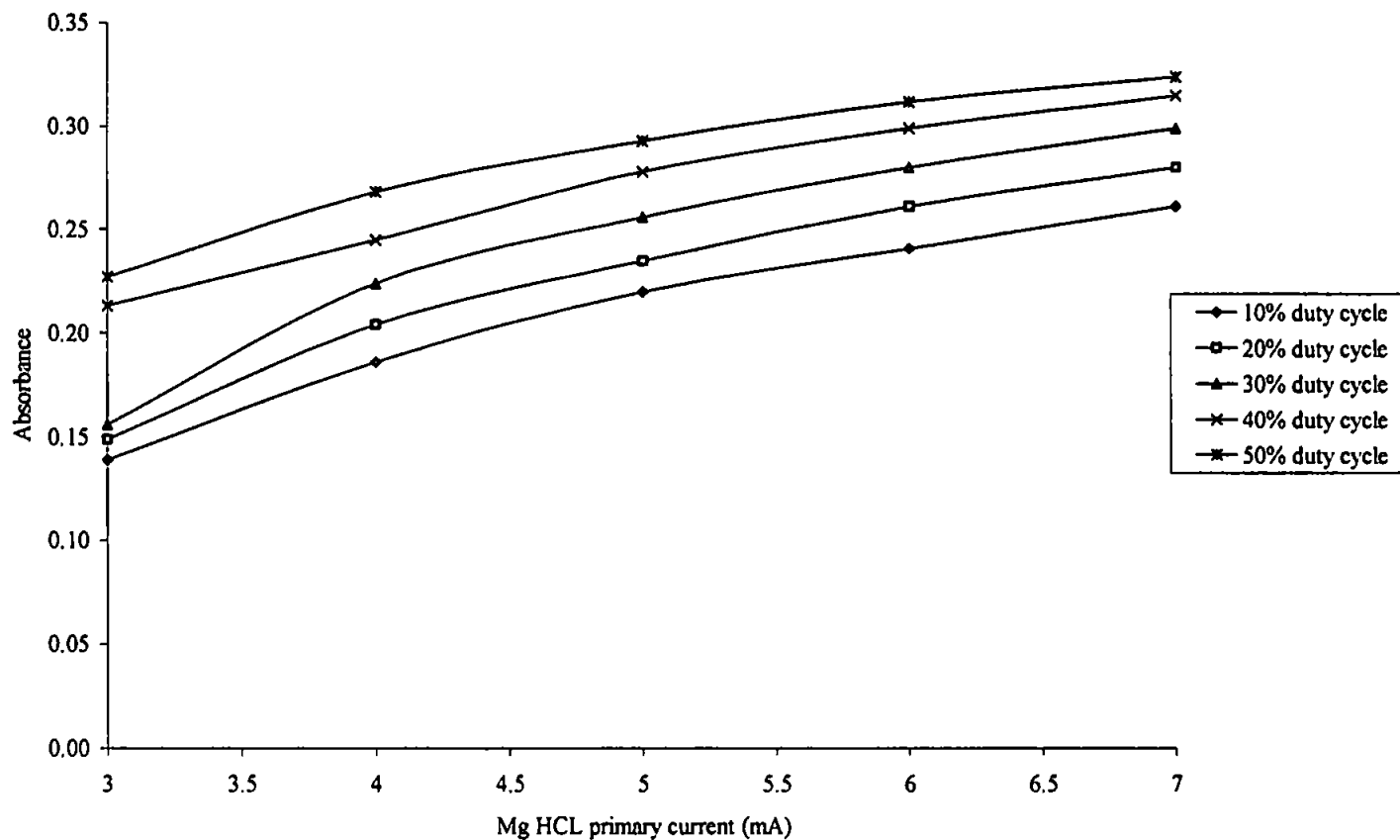
**Figure 3.24: Effect of duty cycle and lamp primary current on Mg I 285.213 nm absorbance signal for a plasma operated under fluorescence-like conditions (forward power 700 W; nebuliser gas flow rate 2.00 L min⁻¹; viewing height 60 mm ALC; lamp modulation frequency 792 Hz; n = 3, RSDs < 5 %)**

## 3.7 Introduction to Ion-Atom Line Intensity Ratios

Experimentally measured ion/atom emission intensity ratios are an important indicator of how a system may change without recourse to calculating absolute values of temperature and electron number densities. Comparing $I_i/I_a$ for the same analyte in two systems can reveal discrete differences between the behaviour of the plasma if various parameters are changed systematically. If $I_i/I_a$ from a plasma operated under a particular set of conditions is compared with $I_i/I_a$ from a plasma operated under different conditions, any variation between the two must arise through differences between excitation and/or ionisation and/or atomisation processes.

Using the Saha equation where $T_e$ is involved, and the line intensity relationship where $T_{exc}$ is involved via the Boltzmann function (19), the ionic to atomic line ratio $I_i/I_a$ can be deduced and is shown in Equation 3.4 (122):

$$\frac{I_i}{I_a} = \left(\frac{4.83x10^{21}}{n_e}\right)\left(\frac{g_iA_i\lambda_a}{g_aA_a\lambda_i}\right)T_e^{3/2}\exp\left(\frac{-E_{ion}}{kT_e}\right)\exp\left[-\left(\frac{E'_{exc} - E^*_{exc}}{kT_{exc}}\right)\right] \tag{3.4}$$

where, $n_e$ is the electron number density, g the statistical weight and A the transition probability, $E_{exc}$ the excitation energy, $\lambda$ the wavelength, $E_{ion}$ the ionisation energy and k the Boltzmann constant. For this equation $n_e$ must be expressed in $m^{-3}$. When electron number density is determined using a method independent of LTE, a corresponding $T_e$ value can then be deduced from Equation 3.4. The $T_e$ and $n_e$ values can be substituted into Equation 3.4 together with the gA values for Mg. Equation 3.4 becomes (122):

$$\frac{I_i}{I_a} = \left(\frac{1.58x10^{21}}{n_e}\right)T^{3/2}\exp\left(\frac{-88732}{T}\right) \tag{3.5}$$

A theoretical $I_i/I_a$ ratio can be deduced as a function of $n_e$. Under the LTE assumption, the values of the ratio vary between 4 and 14 over the temperature range 2000 – 10000 K (122).

In this chapter (Section 3.4) lamp characteristics and a range of conditions were established to produce suitable excitation of the atom cell for use in fluorescence experiments. It was shown (Section 3.6) that although GS atoms were present under low forward power conditions and a peak absorbance at a viewing height of 60 mm ALC was obtained, no fluorescence was observed. Under low forward power conditions (700 – 900 W) and using other fluorescence-like parameters, *e.g.* nebuliser gas flow and sample uptake rate, a preliminary 'diagnostics' investigation (using ion-atom ratios) will be performed of the plasma itself when operated in emission mode to try and understand more about the plasma production system. At viewing heights of 0 – 30 mm ALC (close to the plasma body where energy exchange processes are occurring) the type of emission present from a plasma operated under low forward power, high nebuliser gas and sample uptake rates, may help to explain what is occurring at greater viewing heights ALC. From this a 'profile' of the atom cell characteristics may be obtained (which may be added to the absorbance study).

### 3.7.1 Detector Efficiency Correction

For these experiments the instrument used was the Optima 3000 ICP (The Perkin-Elmer Corporation). The on-board spectrometer utilises an echelle grating which is used over many orders at a set blaze angle, where peak diffraction efficiency should occur. Any difference in optimum blaze angle with diffraction order of the wavelength in question will result in low optical throughput (123).

To minimise the errors due to grating efficiency and to allow adjustments to be made when directly comparing emission line intensities arising from the set blaze angle, the blaze angle for the particular wavelength can be calculated using Equation 3.6:

$$\theta = \sin^{-1}\left(\frac{N\lambda}{2d\cos\phi}\right) \qquad (3.6)$$

where, $\theta$ is the blaze angle, N is the grating order number, $\lambda$ is the wavelength, d is the groove spacing and $\phi$ is the half angle in the horizontal plane between the incident and diffracted ray from the echelle grating. The blaze angle is then substituted into a polynomial expression to calculate the grating efficiency (124).

## 3.8    Experimental: The Determination of Mg Ion-Atom Line Intensity Ratios

The emission intensities of the Mg I 285.213, Mg II 279.553 and 280.270 nm lines, were obtained using an Optima 3000 ICP spectrometer (The Perkin-Elmer Corporation) with a segmented charge-coupled device detector (SCD). The design and characteristics of the echelle grating optical system and solid state detector have been discussed in the literature (123, 124). The low forward power plasma operating conditions used are given in Table 3.5. Ion-atom ratios were determined by aspirating a 50 $\mu$g ml$^{-1}$ aqueous standard of magnesium into the ICP and by taking measurements at 2 mm increments from 0 – 30 mm ALC. The signal to noise ratio was used as the criterion of merit. The position of the optical mirror was altered using the computer controlled stepper motor in the spectrometer. In this way each viewing height ALC where emission readings were taken could be changed and would be reproducible. A custom written program within the instrument software was used to automate the analysis.

**Table 3.5: Operating conditions of the Optima 3000 ICP for measurement of ion and atom line intensity ratios**

| RF Generator | |
|---|---|
| Frequency | 40.68 MHz, free running |
| **ICP-AFS conditions** | |
| Power | 700, 800 & 900 W |
| **Sample Introduction System** | |
| Nebuliser | Ebdon V-Groove high solid |
| Torch | Demountable, custom built with 60 mm extended coolant tube (from auxiliary) and a 1.5 mm i.d. alumina injector |
| Spray Chamber | PE Scott Double Pass |
| Peristaltic Pump | Gilson Minipuls 3, computer controlled |
| Sample Uptake Rate | 2.0 ml min$^{-1}$ |
| **Argon Flow Rate** | |
| Plasma | 12 L min$^{-1}$ |
| Auxiliary | 0.1 L min$^{-1}$ |
| Nebuliser | 1.50, 2.00, 2.50 & 3.00 L min$^{-1}$ |
| **Spectrometer** | |
| Resolution | High resolution setting (31 x 250 μm) |
| Viewing height ALC | 0 – 30 mm (in 2 mm increments) |
| Mg wavelengths | Mg II 279.553 nm |
| | Mg II 280.270 nm |
| | Mg I 285.213 nm |

### 3.8.1 Results and Discussion: Ion-Atom Line Intensity Ratios

The emission intensities of the Mg I 285.213, Mg II 279.553 and 280.270 nm lines were corrected for detector efficiency and ion-atom ratios were calculated. Figures 3.25 – 3.27 show the effect of power and nebuliser gas flow rate on the $I_i/I_a$ ratio of Mg II 279.553/Mg I 285.213 nm measured at 0 – 30 mm ALC using the Optima 3000 ICP with a segmented charge-coupled detector. The values obtained remained below those calculated under LTE but it has been observed that closeness to LTE occurs at low nebuliser gas flow rates ($< 0.5$ l min$^{-1}$) and high powers (121, 125, 126). It was expected that the experimental $I_i/I_a$ ratios obtained for plasmas operated under fluorescence-type conditions (low forward power and high nebuliser gas flow rates) would be significantly different to theoretical $I_i/I_a$ ratios. The question was, how far would it deviate from LTE?

When a nebuliser gas flow of 1.00 L min$^{-1}$ was used it can be seen that the Mg II / Mg I ratio values increased with increasing power, but remained below the values calculated under LTE. However, when an increasing nebuliser gas flow rate was used, the Mg II / Mg I ratio increased at greater viewing heights ALC. Figures 3.24 – 3.26 suggest that as the nebuliser gas flow rate increases the ICP moves further towards LTE. If the results with a nebuliser gas flow rate of 1.00 L min$^{-1}$ are ignored, at the viewing heights used, the highest Mg II / Mg I ratio was obtained using a forward power of 700 W and a nebuliser gas flow rate of 2.50 L min$^{-1}$. This suggests that at a viewing height of 30 mm ALC, experimental conditions most closely match those of LTE. However, it must be remembered that ion-atom ratios are only a guide to the distribution of excited atoms within the ICP. The individual emission data must be examined to ascertain that an increase in the ion-atom ratio is truly representative of an increase in the distribution of ionic species or a decrease in the distribution of excited state atoms or both. Figures

3.28 and 3.29 show the emission intensities of the Mg II 279.553 and Mg I 285.213 nm lines and demonstrate that, changing the nebuliser gas flow rate from 1.00 to 1.50 L min$^{-1}$ produces a marked change in emission profile for each of the low forward powers studied. As the nebuliser gas flow rate increases from 1.50 to 3.00 L min$^{-1}$ both the atom and ion emission intensities decrease in order. Although this study was limited (in terms of viewing height) and gives no indication of what is occurring higher up in the plasma it suggest that at the greater viewing heights ALC there may be a loss of higher energy state atoms/ions and more unexcited species may be present.

Ion-atom ratios of Mg II 280.270/Mg I 285.213 nm were calculated but were consistently approximately twice the value of the ion-atom ratios calculated using Mg II 279.553/Mg I 285.213 nm. This phenomena has been observed previously (122) and is to be expected. The most likely explanation for this behaviour is that Mg II 279.553 and 280.270 nm lines have almost the same A values and excitation energy, and differ only in the g values, 4 and 2 for Mg II 279.553 nm and Mg II 280.270 nm, respectively.
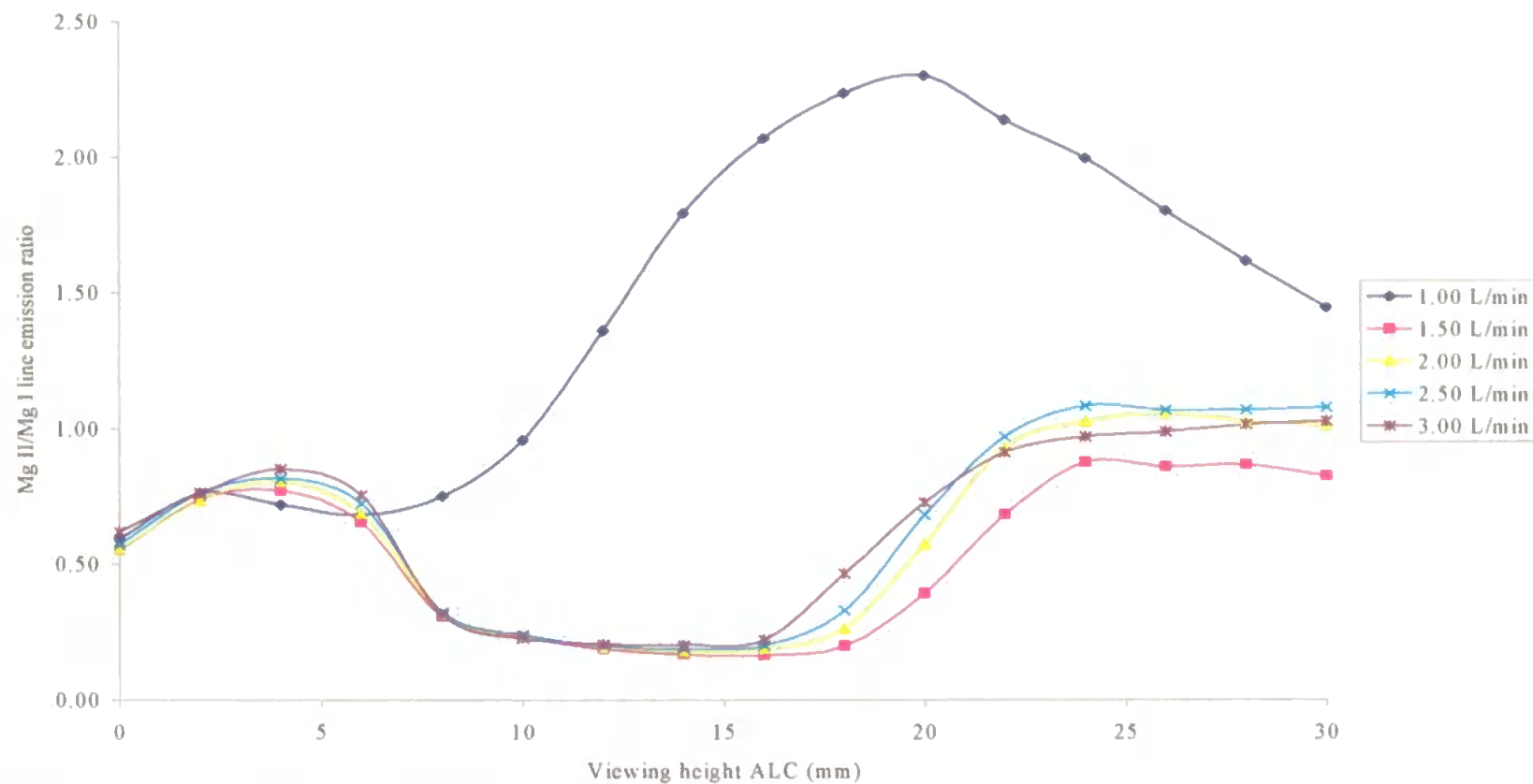
**Figure 3.25: Effect of nebuliser gas flow rate and viewing height ALC on Mg II 279.553 nm/Mg I 285.213 nm ratio for a plasma operated under fluorescence-like conditions (forward power 700 W; n = 3, RSDs < 2 %)**
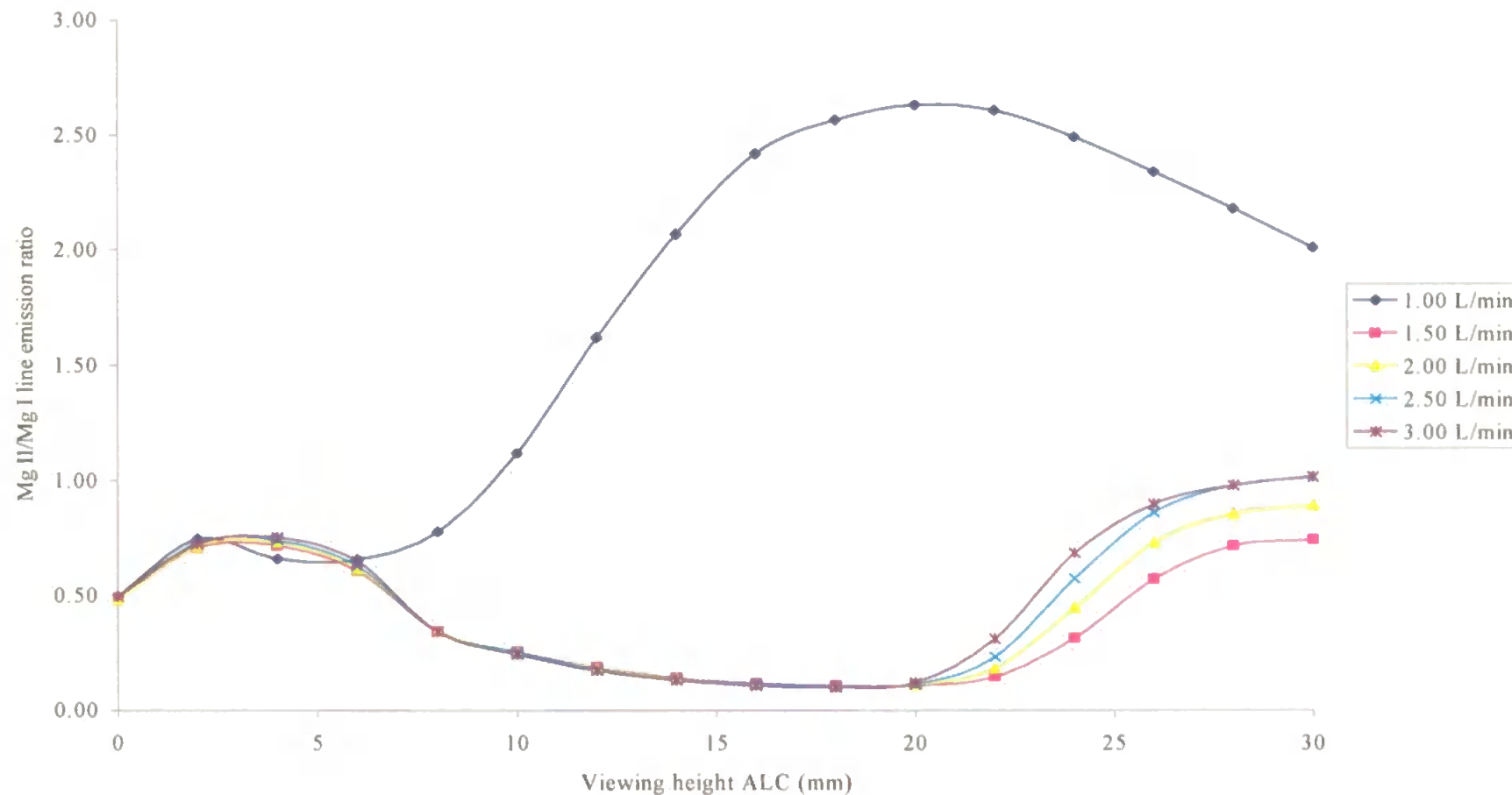
**Figure 3.26: Effect of nebuliser gas flow rate and viewing height ALC on Mg II 279.553 nm/Mg I 285.213 nm ratio for a plasma operated under fluorescence-like conditions (forward power 800 W; n = 3, RSDs < 2 %)**
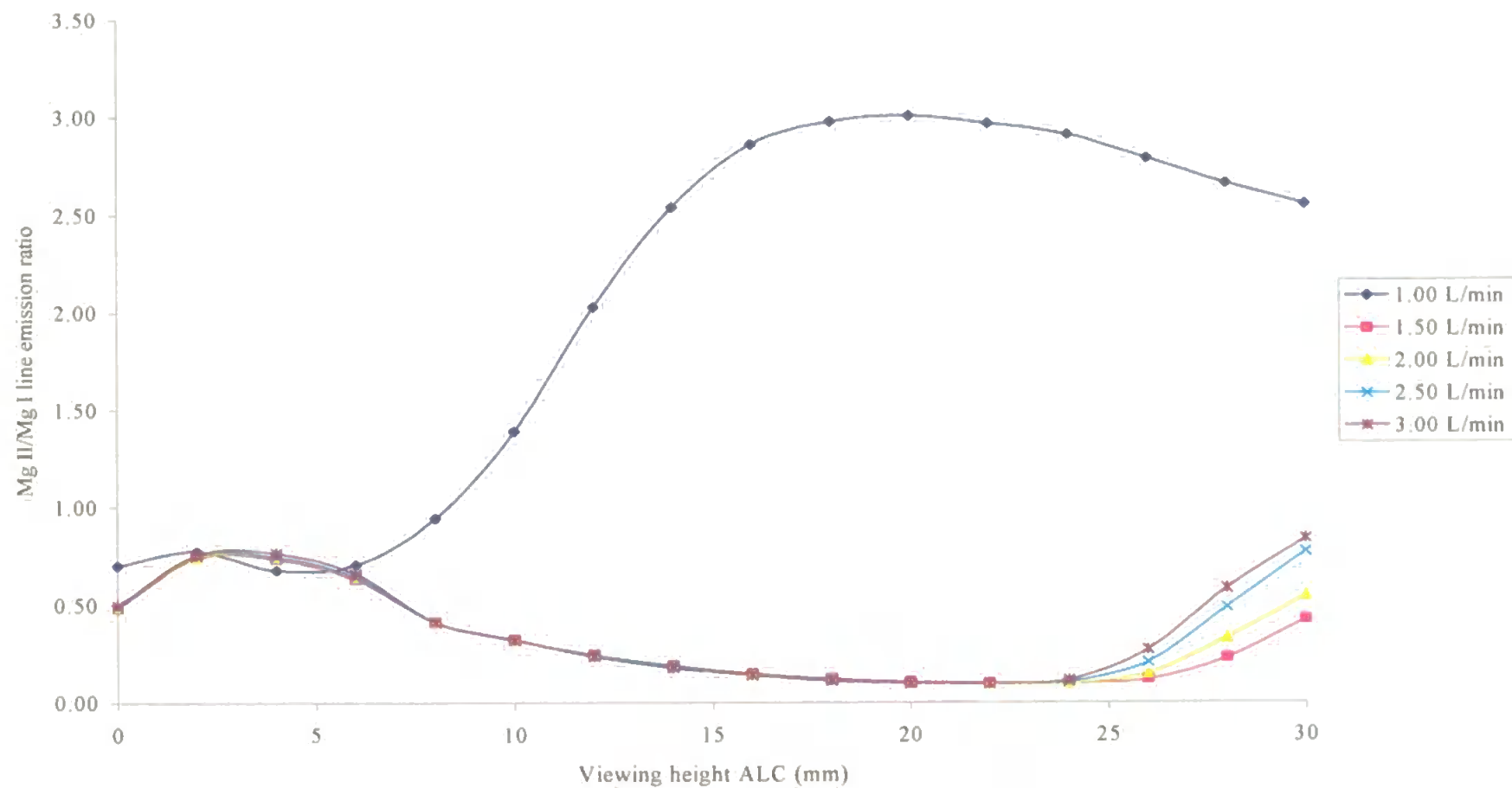
**Figure 3.27: Effect of nebuliser gas flow rate and viewing height ALC on Mg II 279.553 nm/Mg I 285.213 nm ratio for a plasma operated under fluorescence-like conditions (forward power 900 W; n = 3, RSDs < 2 %)**
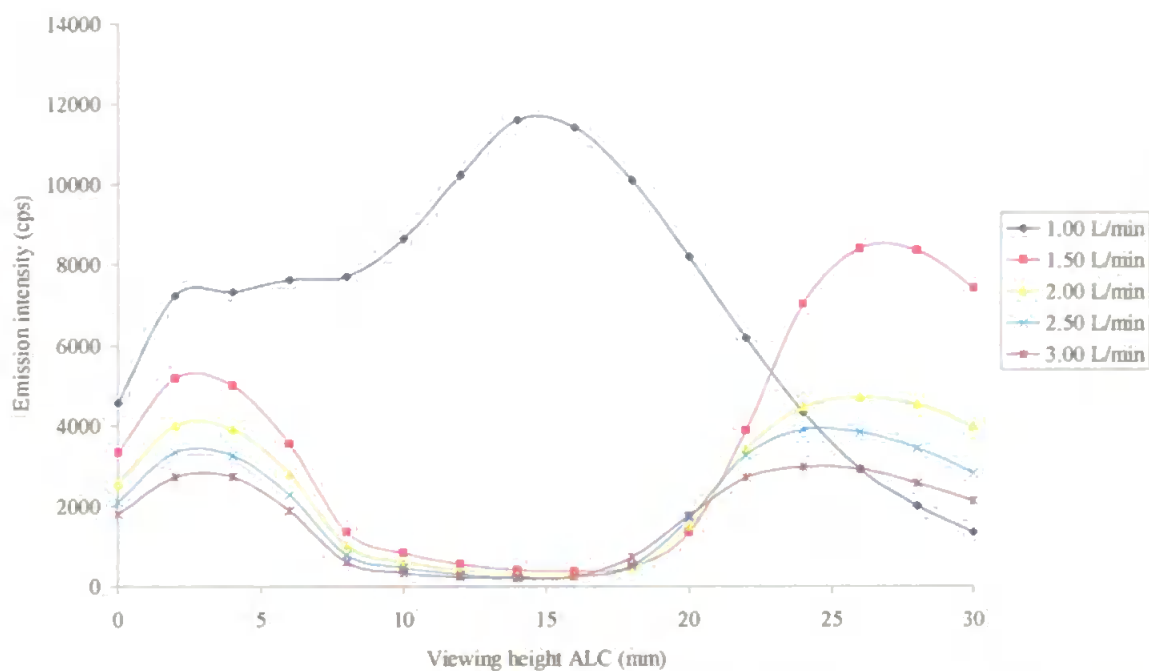
**Figure 3.28: Effect of nebuliser gas flow rate on Mg II 279.553 nm line emission intensity for a plasma operated under fluorescence-like conditions (forward power 700 W; n = 3, RSDs < 2 %)**
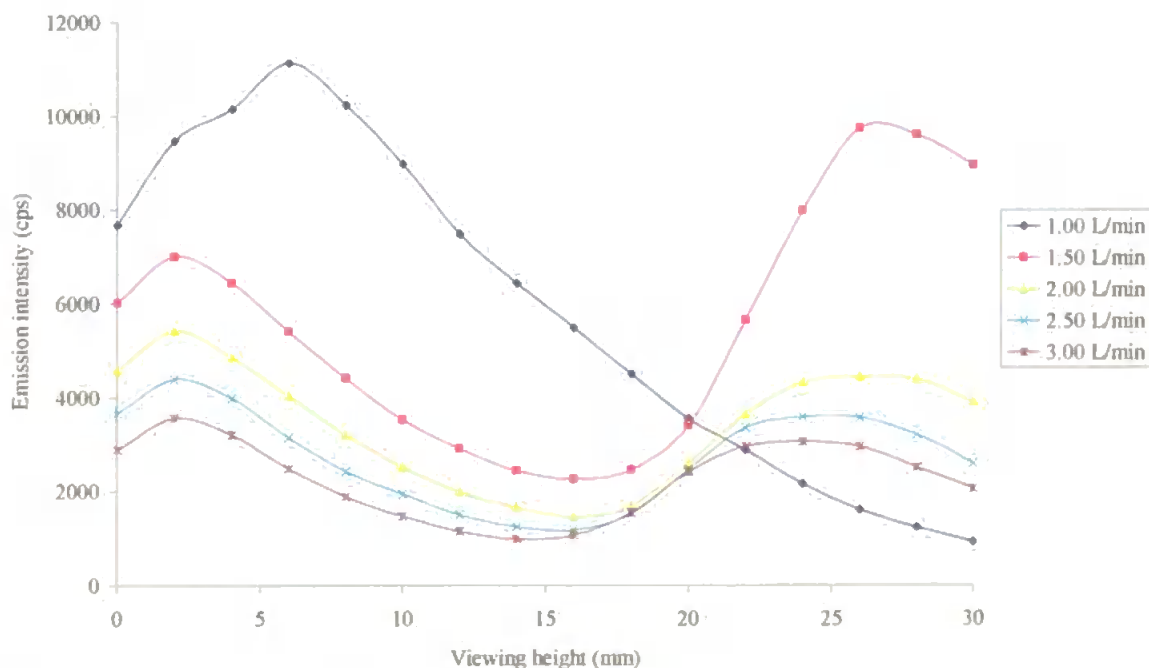


**Figure 3.29: Effect of nebuliser gas flow rate on Mg I 285.213 nm line emission intensity for a plasma operated under fluorescence-like conditions (forward power 700 W; n = 3, RSDs < 2 %)**

## 3.9    Experimental: Transverse Fluorescence Experiments

The preliminary fluorescence experiments described in Chapter 2 (Section 2.3.4) were repeated using the optimum conditions determined from the magnesium absorbance experiments (viewing height 60 mm ALC; lamp primary current 6 mA; modulation frequency 667 Hz; duty cycle 50 %). The operating parameters are given in Table 3.6 and a schematic of the experimental arrangement used is illustrated in Figure 3.30.

### 3.9.1    Results and Discussion: Transverse Fluorescence Experiments

The optimised conditions were used to perform transverse fluorescence experiments. Despite using the optimised conditions and despite all the components used in the transverse fluorescence experiments having been shown to work individually, no fluorescence was observed.

:

**Table 3.6: Operating conditions for transverse fluorescence experiments**

| Excitation system | |
|---|---|
| Lamp | Mg HCL ($\lambda = 285.213$ nm) |
| Primary current | 6 mA |
| Modulation frequency | 867 Hz |
| Duty cycle | 50 % |
| **Atomiser** | |
| **RF Generator** | |
| Frequency | 40.68 MHz, free running |
| **ICP-AFS conditions** | |
| Power | 700, 800 & 900 W |
| **Sample Introduction System** | |
| Nebuliser | Ebdon V-Groove, high solids |
| Torch | Demountable, custom built with 60 mm extended coolant tube (from auxiliary) and a 1.5 mm i.d. alumina injector |
| Spray Chamber | PE Scott Double Pass |
| Peristaltic Pump | Gilson Minipuls 3, computer controlled |
| **Argon Flow Rate** | |
| Plasma | 12 L min$^{-1}$ |
| Auxiliary | 0.1 L min$^{-1}$ |
| Nebuliser | 1.50 - 3.00 L min$^{-1}$ (0.50 L min$^{-1}$ increments) |
| Sample uptake rate | 1.00 – 2.00 ml min$^{-1}$ (0.25 ml min$^{-1}$ increments) |
| **Detection system** | |
| V/H ALC | 60 mm |
| Filter | $\lambda_{max}$ 280 nm |
| PMT voltage | 1000 V |
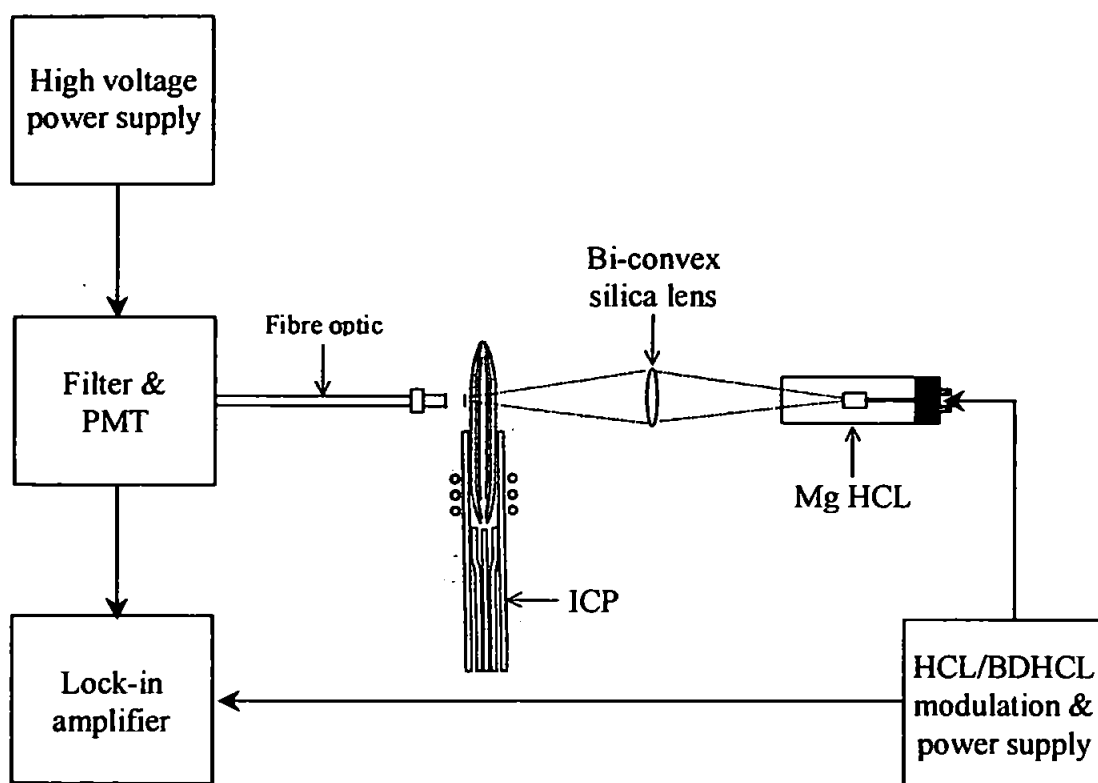
**Figure 3.30: Schematic of the experimental arrangement used for transverse**

**fluorescence experiments with Mg in the low power ICP**

## 3.10 Summary

A new modulation supply has been designed and constructed and the effect of modulation frequency and duty cycle on the emission signal of a Fe HCL illustrated. Oscilloscope traces comparing the reference signal and the emission signal from the lamp allowed an estimate of the time taken for the lamp to 'trigger' and reach its maximum intensity (full 'plasma' discharge) to be made. The lamp 'trigger' time was shown to be in the region of 150 - 185 $\mu$s and the time taken for the lamp to reach maximum intensity was in the region of 414 - 449 $\mu$s. The oscilloscope traces showed that at higher modulation frequencies and shorter duty cycles the plasma discharge was 'clipped' to such an extent that the lamp did not have time to trigger at all, or if it did trigger then the maximum lamp intensity was not reached. This suggests that a lamp operated with a lower modulation frequency and higher duty cycle may provide the best conditions for the production of fluorescence.

Excitation temperatures were calculated for the Fe HCL using the Boltzmann Distribution and showed that $T_{exc}$ mainly varied between 5200 and 6500 K. As the modulation frequency increased (from 167 to 1042 Hz) the excitation temperature of the lamp showed a small increase. $T_{exc}$ decreased with the following duty cycles: 30 % > 40 % > 50 % > 20 % > 10 %. Excitation temperatures were also calculated using the Line Pair Intensity Ratio Method. $T_{exc}$ varied mainly between 2000 and 4500 K and showed slightly different trends to those determined by the Boltzmann Distribution (50 % > 40 % > 30 % > 20 % > 10 % for middle range modulation frequency). An explanation of the differences may be obtained from examination of a simplified version of the Grotrian diagram for Fe I and from using a limited line system.

Another software programme was obtained and used to enable greater flexibility with the IC plasma conditions. Theoretically and practically, the range of conditions that could be

obtained from the Optima 3000 ICP matched those described in the literature for the production of fluorescence.

The effect of nebuliser gas flow and sample uptake rate on absorbance signal as the viewing height ALC increased was determined. At viewing heights 60 – 90 mm ALC there was no difference observed in absorbance signal for any of the parameters varied but a maximum absorbance signal was obtained at a viewing height of 60 mm ALC. From 100 mm ALC upwards, as the nebuliser gas flow increased from 1.50 to 3.00 L min$^{-1}$ the absorbance signal decreased. The sample uptake rate had no noticeable effect on absorbance signal.

The effect of increasing primary current of the lamp on the absorbance signal was investigated. Within the working range of the lamp (3 – 7.5 mA) there was a proportional relationship between primary current and absorbance signal. When the maximum advisable lamp operating current was exceeded, the absorbance decreased as the primary lamp current increased. The optimum condition (*i.e.* greatest absorbance) was obtained with a primary lamp current of 6 mA.

The effect of duty cycle on the absorbance signal of Mg I at 285.213 nm using a modulation frequency of 542, 667 and 792 Hz, respectively was studied. Absorbance signal increased as the modulation frequency and duty cycle increased with the optimum signal observed with operating conditions of 667 Hz with a 50 % duty cycle.

The effect of forward power and nebuliser gas flow rate on the Mg $I_i/I_a$ ratio was measured at 0 – 30 mm ALC using the Optima 3000 ICP with a segmented charge-coupled detector. The highest Mg II / Mg I ratios were obtained when low forward powers and high nebuliser gas flow rates were used suggesting that these conditions 'tend' towards LTE.

The optimised conditions were used to perform transverse fluorescence experiments. Despite using the optimised conditions and that individually components were shown to work satisfactorily for the production of transverse fluorescence, no fluorescence was observed. This suggests that further investigation/s of the plasma behaviour were necessary. Plasma diagnostics were required to try and gain a deeper understanding of the plasma itself when operated under low forward powers and high nebuliser gas flow rates and possibly explain why fluorescence had not been observed.

## 4.0 PLASMA DIAGNOSTICS ON AN ICP OPERATED UNDER BOTH FLUORESCENCE-LIKE AND CONVENTIONAL EMISSION CONDITIONS

### 4.1 Introduction

The fundamental properties of an inductively coupled plasma are of importance for the characterisation of plasmas and for their efficient use for analytical purposes. These parameters are well known and include plasma 'temperatures', electron number densities, atom and ion emission intensities, and spectral line widths. It has been stated by Raejmakers *et al.* (127) that "In an atmospheric discharge in local thermal equilibrium (LTE), the spatially resolved measurement of only one parameter, *e.g.* the electron density ($n_e$) or the electron temperature ($T_e$) is necessary and sufficient to characterise the discharge....". As the ICP is an inhomogeneous plasma, the spatial distributions or differences of fundamental properties should be examined to characterise the physical and spectral features of the ICP (1).

Plasma diagnostics were used to try and obtain a greater understanding of how the plasma functions under low power (*i.e.* 'fluorescence-like') conditions and why fluorescence had not been observed despite all the components being proven to work individually (Chapter 2). The purpose of the 'diagnostic' measurements was to compare a plasma operated under fluorescence-like conditions with those from a plasma operated under conventional emission conditions in order to, and if possible, identify the plasma conditions suitable for fluorescence. Some of the reported values for various plasma temperatures along with the measurement methods and species examined are presented in Tables 4.1 to 4.5.

This chapter describes the measurement of excitation and rotational temperatures and electron number densities for an ICP operated under as near to fluorescence conditions (*e.g.* low forward power and high nebuliser gas flows) as could be achieved with the instrument available. These values (termed fluorescence-like) will be compared with those obtained from a plasma operated under conventional emission conditions to try and understand in what way they differ.

### 4.1.1 The Abel Inversion

Studies of spatial distributions of various plasma parameters document that the inductively coupled plasma is not homogeneous and that it has a spatial structure (84, 93, 94, 128 - 130). Spectroscopic information, when observed with side-on projection, is obtained as the integrated intensity of the entire depth of the light source. The procedure to transform the side-on data, i.e. lateral profile, into the radial profile is called the Abel inversion. The technique has been described as a mathematical 'stripping' process (131) where the plasma is divided into equidistant sections along the radius of the discharge. The section at the outer edge of the discharge is subtracted from the next radial section to give a 'corrected' intensity value. These values are then fitted to a polynomial function and the first derivative integrated using Equation 4.1 (131). The Abel inversion assumes circular symmetry and may be carried out for laterally viewed data measured by profiling the plasma in the horizontal plane.

$$i(r) = -\frac{1}{\pi} \int_r^R \frac{dI(x)/dx}{(x^2 - r^2)^{1/2}}.dx \qquad (4.1)$$

where, R is the radius of the plasma torch, I is the experimental intensity measured along the chord of distance x from the centre and r is the radial position along the radius R (131). The procedure and programme used in this work are detailed in Appendix 1.

**Table 4.1: Literature values for excitation temperatures (K) in the ICP**

| Element | Measurement method | | | Frequency (MHz) | Power (kW) | Viewing height ALC (mm) | Excitation temperature (K) | Reference |
|---|---|---|---|---|---|---|---|---|
| | Absolute | Absorption | Slope | | | | | |
| Ar, Fe | | | y | 27 | 1.0 | 15 | 5200 - 5600 | (89) |
| Ar, Fe, Ti, V | | | y | 40 | 1.3 | 2.0 | 4800 | (90) |
| Ar, Ca, Mg | | y | | 50 | 0.50 | 3.8 - 30 | 2300 - 4000 | (91) |
| Ar | | | y | 5.4 | 6.0 | 0 - 12 | 5000 - 7000 | (128) |
| Ar | | | y | 50 | 0.3 | 0.50 | 4380 | (129) |
| Ar, Cd, Fe, Ti | | | y | 40 | 1.5 | 5.0 | 4500 - 5100 | (130) |
| Ar, H | | | y | 40 | 1.5 | 2.0 | 5900 - 7000 | (131) |
| Fe | | | y | 31 | 2.5 | 15 | 6200 | (109) |
| Ar, Zn | | | y | 50 | 2.0 | 6.0 | 4000 - 4700 | (132) |
| Ar, Fe, Ti, V | | | y | 5.4 | 6.0 | 0 - 10 | 6200 - 6300 | (88) |
| Fe | | | y | 27 | 1.0 - 1.2 | 15 | 5700 - 6400 | (4) |
| H | | | y | 9 | 12 | 10 | 6313 - 14 723 | (133) |
| Fe | | | y | 50 | 0.4 - 0.7 | 20 | 4900 - 5400 | (134) |
| Ar, Ti | | | y | 144 | 0.05 | | 5000 - 7000 | (135) |
| Ar, Fe, Ti, V | | | y | 40 | 1.8 | | 4800 - 5000 | (136) |
| Mg | | | y | 50 | 0.53 | 7.5 | 3800 | (137) |
| Ar, Fe, Ti, V | | | y | 40 | 0.50 - 4.0 | | 4500 - 5100 | (138) |
| Fe | | | y | | 1.2 | 10 – 30 | 6900 - 8500 | (92) |
| Ar | y | | | 26.5 | 0.75 | -7 – 12 | 7500 - 8300 | (139) |
| Ar | y | | | 26.5 | 0.50 - 0.75 | -7 – 12 | 6200 - 8500 | (140) |
| Fe | | | y | 27 | 1.3 | 0 – 35 | 5600 - 6700 | (93) |
| Ar | | | y | 27 | 1.5 | 15 | 7000 | (141) |

156

**Table 4.1 continued: Literature values for excitation temperatures (K) in the ICP**

| Element | Measurement method | | | Frequency (MHz) | Power (kW) | Viewing height ALC (mm) | Excitation temperature (K) | Reference |
|---------|----------|------------|-------|-----------------|------------|-------------------------|----------------------------|-----------|
|         | Absolute | Absorption | Slope |                 |            |                         |                            |           |
| Fe      |          |            | y     | 27              | 1.3        | 14                      | 4500                       | (110)     |
| Fe      |          |            | y     | 8 - 56          | 1.1 - 1.5  |                         | 4000 - 6700                | (94)      |
| Fe      |          |            | y     | 27              | 1.3        | 10 - 25                 | 3500 - 3800                | (142)     |
| Fe      |          |            | y     | 27              | 1.8        | 0 - 20                  | 4300 - 5200                | (84)      |
| Fe      |          |            | y     |                 |            | 20                      | 4700 - 9000                | (143)     |
| Fe      |          |            | y     | 40              | 1.6        |                         | 4800                       | (86)      |
| Sr      |          |            | y     | 9.1             | 9.0        | 4.0                     | 5900                       | (113)     |
| Ar      |          |            | y     | 27              | 1.5        | 15                      | 7000                       | (144)     |
| H       |          |            | y     |                 | 1.5        |                         | 12 670                     | (145)     |
| Co, Fe, Ni, V |    |            | y     | 27              | 1.1        |                         | 4400 - 5200                | (146)     |
| Fe      |          |            | y     |                 | 1.3        | 15                      | 5800                       | (96)      |

**Table 4.2: Literature values for ionisation temperatures (K) in the ICP**

| Element | Measurement method | | Frequency (MHz) | Power (kW) | Viewing height ALC (mm) | Ionisation temperature (K) | Reference |
|---|---|---|---|---|---|---|---|
| | Saha | Mass spectrometric | | | | | |
| Ar, Mg, V | y | | 40 | 1.3 | 2 | 6700 – 7400 | (90) |
| Mg | y | | 50 | 0.50 | 7.5 | 5300 | (91) |
| Ba, Sr, Cd/I | | y | 27 | 1.0 | | 7400 – 8200 | (147) |
| Cd/I | | y | 27 | 1.2 | | 8000 | (148) |
| Ti | y | | 144 | 0.05 | | 3500 | (135) |
| Ar, Mg, V | y | | 40 | 1.8 | | 7350 | (136) |
| Mg | y | | 50 | 0.53 | 7.5 | 6200 | (137) |
| Ba, Ca, Cd, Fe, Mg, Ti, Zn | y | | | 1.2 | 10 - 30 | 7700 – 8400 | (92) |
| Ar, Mg, V | y | | 27 | 1.5 | 15.0 | 9000 | (144) |

**Table 4.3: Literature values for rotational temperatures (K) in the ICP**

| Measurement band | | | | | Frequency (MHz) | Power (kW) | Viewing height ALC (mm) | Excitation temperature (K) | Reference |
|-----|-----|-----|-----|-----|-----|-----|-----|-----|-----|
| BO | $C_2$ | CN | $N_2^+$ | OH | | | | | |
| | | | | y | 50 | 0.50 | 12 | 1600 | (91) |
| | y | | | | 5.4 | 6.0 | 0 - 3.0 | 6100 | (128) |
| | | y | | | 50 | 0.27 | 0.50 | 2200 | (129) |
| | y | | y | | 40 | 1.5 | 5 | 4500 - 5000 | (130) |
| | | | | y | 50 | 2.0 | 6.0 | 3000 | (132) |
| | | y | | | 40 | 0.50 - 4 | | 4500 - 5000 | (138) |
| | | | | y | 27 | 1.3 | 0 - 35 | 2800 - 4700 | (93) |
| | | y | | | 40 | 1.6 | | 4500 | (86) |
| y | | | | | 6.3 | 12.0 | | 5000 | (149) |
| | | y | | | 9.2 | | 7 - 41 | 6140 - 8290 | (150) |

**Table 4.4: Literature values for Doppler temperatures (K) in the ICP**

| Element | Frequency (MHz) | Power (kW) | Viewing height ALC (mm) | Doppler temperature (K) | Reference |
|---------|-----------------|------------|-------------------------|-------------------------|-----------|
| Ar, Ca, Sr | 27 | 1.0 | 10 - 25 | 5200 - 6900 | (151) |
| | 27 | 1.0 | 15.0 | 3300 - 7900 | (152) |
| Fe | 27 | 1.1 | 11 | 6310 | (153) |
| Ar | 50 | 0.27 | 0.50 | 2070 | (92, 154) |

**Table 4.5: Literature values for electron temperatures (K) in the ICP**

| Measurement method | | | Frequency (MHz) | Power (kW) | Viewing height ALC (mm) | Electron temperature (K) | Reference |
|---|---|---|---|---|---|---|---|
| Continuum | Electric probe | Line/continuum ratio | | | | | |
| y | | | 27 | 1.1 | 5 - 25 | 7000 - 8400 | (155) |
| y | | | 50 | 0.27 | 0.5 | 11 400 | (129) |
| | | y | 40 | 0.90 - 20 | 5 | 8000 - 10 000 | (130) |
| | | y | 40 | 1.5 | 2 | 12 000 | (131) |
| | Y | | 144 | 0.1 | | 23 000 - 52 000 | (135) |
| y | | | 27 | 1.25 | 14 - 16 | 5480 | (156) |
| | | y | 27 | 1.25 | 10 | 7700 | (157) |

## 4.2 Experimental: Determination of Excitation Temperature using Fe I Lines under Various Plasma Conditions

### 4.2.1 Instrumentation: Radial ICP Spectrometer with a Solid State Detector Operated under Fluorescence-Like Conditions

An Optima 3000 ICP spectrometer (The Perkin-Elmer Corporation, Norwalk, CT., USA) was operated in fluorescence mode to carry out spatial profile measurements. A computer controlled stepper motor in the spectrometer was used to adjust the position of a 2-axis mirror, horizontally and/or vertically, so that a discrete region in the plasma could be examined (Figure 4.1). Data was acquired using a custom written program within the WinLab and/or Diagnostics software. Operating parameters are listed in Table 4.6.

The plasma torch designed in Chapter 2 (Section 2.2.1.1) was modified and an 8 mm viewing slot, as opposed to the traditional 4 mm, cut into it. With this arrangement viewing through the quartz torch was avoided and a wider lateral profile could also be measured. The wider slot had no observable effect on plasma stability.

To avoid the contribution of emission from an adjacent position when making spatial observations it was essential that viewing zones did not overlap. Measurements could be made using either a high, medium or low resolution setting corresponding to three different slit widths. It was calculated that no overlap occurred between lateral positions (0.40 mm apart) when the high resolution slit (31 x 250 $\mu$m) was used (123, 124).
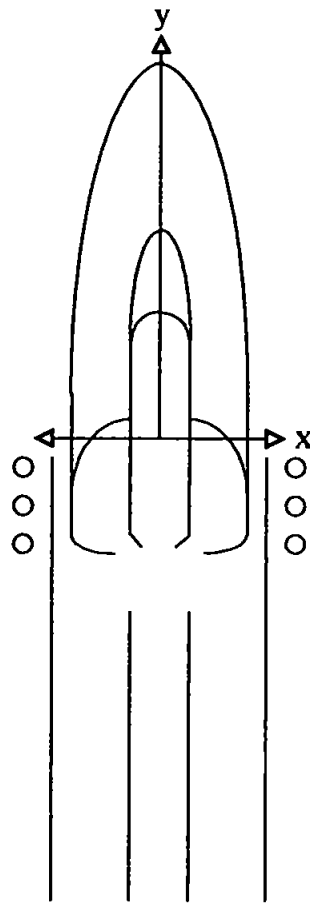
x = -2 to + 2 mm (0.4 mm increments)

y = 0 to 30 mm (2 mm increments)

**Figure 4.1: Lateral profile data acquisition range using the ICP**

**Table 4.6: Optima 3000 ICP and spectrometer operating parameters used to calculate $T_{exc}$ (K) from the LPIRM and the Boltzmann Distribution for an ICP operated under fluorescence-like and conventional emission conditions**

| RF Generator | |
|---|---|
| Frequency | 40.68 MHz, free running |
| **ICP-AFS conditions** | |
| Power | 700, 800 & 900 W |
| **Sample Introduction System** | |
| Nebuliser | Ebdon V-Groove high solids |
| Torch | Demountable, custom built with 8 mm wide observation slot and 60 mm extended coolant tube (from auxiliary) and a 1.5 mm i.d. alumina injector |
| Spray Chamber | PE Scott Double Pass |
| Peristaltic Pump | Gilson Minipuls 3, computer controlled |
| Sample Uptake Rate | 2.0 ml min$^{-1}$ |
| **Argon Flow Rate** | |
| Plasma | 12 L min$^{-1}$ |
| Auxiliary | 0.2 L min$^{-1}$ |
| Nebuliser | 1.50, 2.00, 2.50 & 3.00 L min$^{-1}$ |
| **ICP-AES conditions** | |
| Power | 1200 W |
| **Sample Introduction System** | |
| Nebuliser | Ebdon V-Groove high solids |
| Torch | Demountable, custom built with 8 mm wide observation slot and a 2.0 mm i.d. alumina injector |
| Spray Chamber | PE Scott Double Pass |
| Peristaltic Pump | Gilson Minipuls 3, computer controlled |
| Sample Uptake Rate | 1.0 ml min$^{-1}$ |
| **Argon Flow Rate** | |
| Plasma | 16 L min$^{-1}$ |
| Auxiliary | 0.8 L min$^{-1}$ |
| Nebuliser | 0.8 L min$^{-1}$ |
| **Spectrometer** | |
| Resolution | High resolution setting (31 x 250 μm) |
| Fe I wavelengths | 382.043 nm / 385.991 nm |
| Viewing height ALC | 0 – 30 mm (in 2mm increments) |
| Lateral position | -2 to + 2 mm (in 0.4 mm increments) |

**Table 4.6 continued: Optima 3000 ICP and spectrometer operating parameters used to calculate $T_{exc}$ (K) from the LPIRM and the Boltzmann Distribution for an ICP operated under fluorescence-like and conventional emission conditions**

| SPEX Monochromator | |
|---|---|
| Entrance & exit slit widths | 25 μm |
| PMT voltage | 1200 V |
| Viewing height ALC | 10 – 100 mm (in 10 mm increments) |
| Lateral position | 0.0 mm (centre of the plasma) |
| **Fe LPIRM and Boltzmann distribution measurements** | |
| Scan range | 360 - 400 nm |
| Step size | 0.1 nm |
| Scan speed | 0.1 nm s$^{-1}$ |

For LPIR measurements, the emission intensities of the Fe 382.043 and 385.991 nm atom lines were monitored by accessing the Eu 381.967 and U 385.958 nm sub-arrays on the visible segmented charge coupled detector of the instrument. The Abel inversion technique was then used to transform the lateral profiles obtained and this information was used to determine the excitation 'temperatures' of the ICP at various spatial positions. For Boltzmann Distribution measurements, the emission intensities of the Fe 361.016, 369.401, 382.043, 385.991, 393.030 and 396.926 nm atom lines were monitored by accessing the Cd 195, Yb 219, Eu 381.967, U 385.958, Eu 230 and Ca 224/237 nm sub-arrays on the visible SCD of the instrument.

The experiment was repeated with a plasma operated using conventional emission conditions so that a 'temperature' comparison could be made those temperatures determined from a plasma operated under fluorescence-like conditions and also with data found in the literature. Operating parameters are listed in Table 4.6.

### 4.2.2 Instrumentation: The Radial ICP using a SPEX Monochromator Operated under Fluorescence-Like Conditions

Excitation temperature measurements were obtained at greater viewing heights ALC using the Optima 3000 ICP spectrometer (The Perkin-Elmer Corporation) fitted with a demountable X and Y-axis translation plate (described in Chapter 2, Section 2.2.1.2). The plate held a fibre optic (1000 $\mu$m core diameter HPSUV1000P; Oxford Electronics Ltd., Four Marks, Hampshire, UK) and, as described in Chapter 2 (Section 2.2.1.2), was capable of both horizontal and vertical translation of the tailflame in 0.1 mm increments.

Measurements were taken using a Datascan 2 (ISA Instruments S.A. (U.K.) Ltd., Middlesex, U.K.) interfaced with a Current/Phase Stepper Drive and a monochromator

(1700 Series; SPEX Industries INC., Metochen, N.J. 08840). An IEEE488 communications port provided standardised electronic protocols to receive commands and send data to a host computer. All readings were automated by constructing a program within the instrument software (SpectRad Version 2 for Windows (ISA Instruments S.A. (U.K.) Ltd.). Operating parameters are presented in Table 4.6.

For LPIR and Boltzmann Distribution measurements, the emission intensities of Fe I lines in the region 360 – 400 nm were recorded. Manual background correction points were used for all measurements. The Abel inversion technique was not performed as data collected in this manner may result in overlapping viewing zones (due to the relatively large diameter of the fibre optic, approximately 1 mm).

The experiment was repeated with a plasma operated using conventional emission conditions so that a 'temperature' comparison could be made between those excitation temperatures determined from a plasma operated under fluorescence-like conditions and also with data found in the literature. Operating parameters are listed in Table 4.6.

### 4.2.3   Chemicals and Reagents

All reagents (Fe) used were of 'AnalaR' reagent grade (Merck, Poole, Dorset, UK) and all solutions were prepared using doubly deionised water (Milli-Q, Millipore, Middlesex, UK).

Calibration standards were prepared by serial dilution of commercially available stock standard solutions (10000 $\mu$g ml$^{-1}$). Fe concentrations of 100 $\mu$g ml$^{-1}$ were used for temperature measurement experiments.

### 4.2.4 Results and Discussion: Determination of Excitation Temperature using Fe Atom Species

**4.2.4.1 Line Pair Intensity Ratio Method**

When the Optima 3000 with an SCD (The Perkin-Elmer Corporation) was employed for measurements the software and instrumental limitations prevented the use of a number of test elements described in Chapter 3 (Section 3.3) for the determination of excitation temperature by the LPIRM. Iron was chosen as the thermometric species of study as this element has been well characterised, studied by many workers, and fulfils the criteria to successfully perform temperature calculations (86 - 103). It has two wavelengths that are reasonably close together (Fe I 382.043 and 385.991 nm), a suitable energy difference between the upper levels (25 900 and 33 096 $cm^{-1}$) and the transition probabilities are also known to a relatively high degree of accuracy (104).

Relative line intensities for the two lines were measured simultaneously for a particular set of conditions. Excitation temperatures were calculated using Equation 3.2 (Section 3.3.1) and the physical parameters given in Table 4.7.

Figure 4.2 illustrates the effect on excitation temperature from forward power, nebuliser gas flow rate and viewing height ALC when the plasma is operated under fluorescence-like and conventional emission conditions using the Optima's own detection system. The results are as expected and show that $T_{exc}$ decreases with decreasing forward power and increasing viewing heights ALC. Temperatures ranged from 2100 K to 2700 K with a typical increase of 30 K for each 100 W increase in power. As the viewing height was varied (2 mm increments ALC) the excitation temperature decreased by approximately 20 K. Although not shown graphically, this trend was identical to that observed at other nebuliser gas flow rates (1.50, 2.50 and 3.00 L $min^{-1}$) studied. However, at each forward

power, at low viewing heights ALC there was no significant variation in $T_{exc}$ with varying nebuliser gas flow rate but it was evident higher up in the tailflame. Values ranged from 2430 K at 0 mm ALC to 2170 K at 30 mm ALC. For each forward power, a typical increase of 15 K for each 0.50 L min$^{-1}$ increase in nebuliser gas flow was observed and each 2 mm increase in viewing height corresponded to a 30 K decrease in excitation temperature. For a plasma operated under conventional conditions, the values determined by the LPIRM were lower than those observed in the literature (86 – 103) However, the values obtained were consistent with those obtained from a previous study using the same instrument and method of calculation (111).

**Table 4.7: Physical constants used in the LPIRM to calculate $T_{exc}$ (K) from Fe I**

**(116)**

| Fe I emission line (nm) | Energy (eV) | Energy (cm$^{-1}$) | gA (x 10$^8$ sec$^{-1}$) | % error in gA values |
|---|---|---|---|---|
| 382.043 | 4.10 | 33 096 | 0.668 | ± 10% |
| 385.991 | 3.21 | 25 900 | 0.097 | ± 15% |
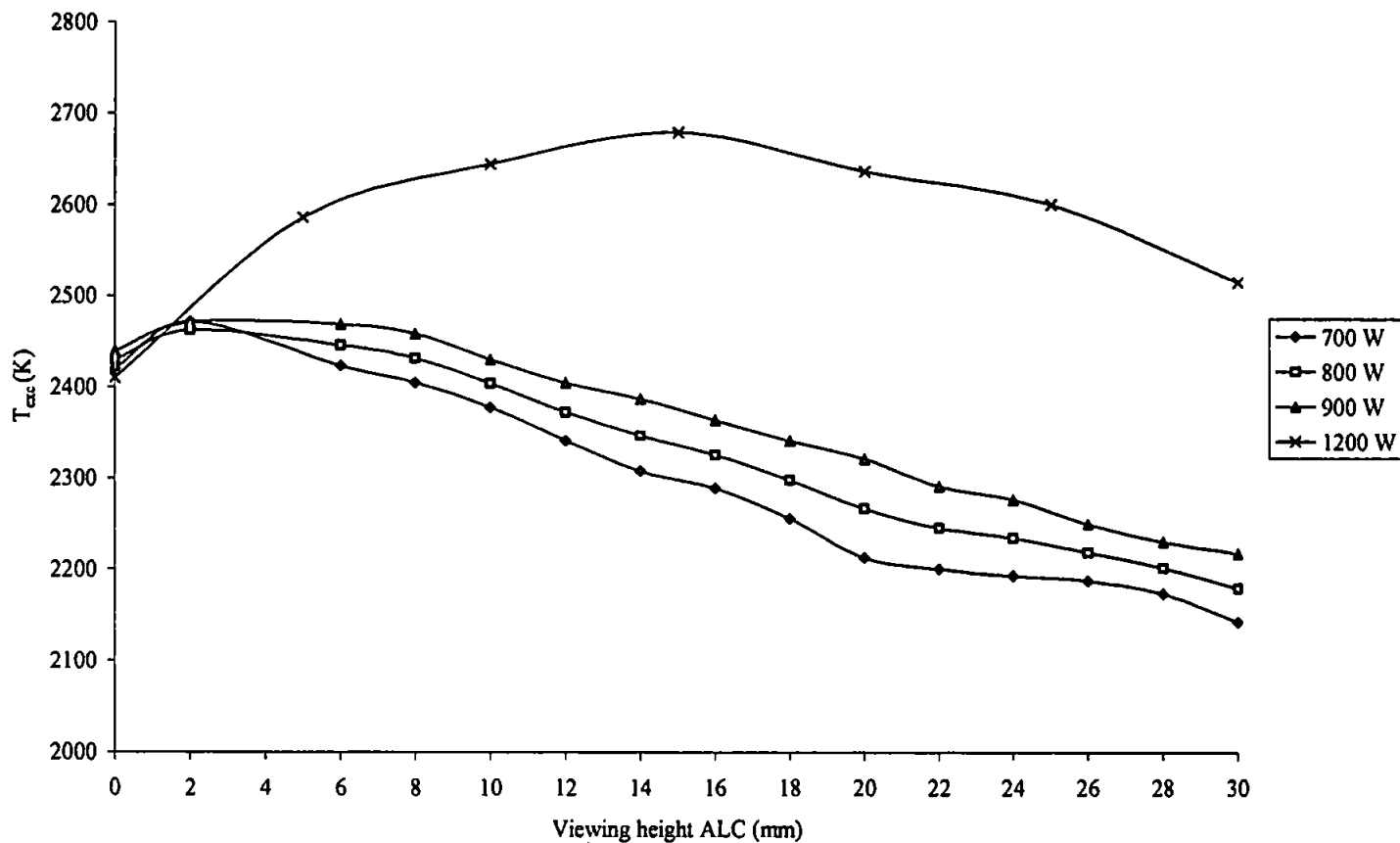
**Figure 4.2: Comparison of $T_{exc}$ (K) calculated by the LPIRM with power and viewing height ALC for a plasma operated under fluorescence-like (forward powers 700 – 900 W; nebuliser gas flow rate 2.00 L min$^{-1}$) and conventional emission (forward power 1200 W; nebuliser gas flow rate 0.80 L min$^{-1}$) conditions (n = 3, RSDs < 2 %)**

Radial excitation temperatures were calculated for a plasma operated under fluorescence-like conditions using the Optima's own detection system using Equations 3.2 (Section 3.3.1) and 4.1 (Section 4.1.1). The results are presented in Figure 4.3.

Figure 4.3 shows the radial profile for $T_{exc}$ at a viewing height of 15 mm ALC from the central position of the plasma out to 3.2 mm for forward powers of 700, 800 and 900 W. Values ranged from 2270 K at 0 mm up to 2360 K at 3.2 mm and for any given lateral position, $T_{exc}$ increases with increasing forward power. The profiles obtained show some structure and the edge of the 'atom emission channel' can be visualised. As the forward power increases, the edge of this emission channel 'moves' slightly closer towards the centre of the plasma. This might be expected to occur, for as the forward power is increased there is a contraction of this central channel due to the increased resistance of the plasma body to being punched.
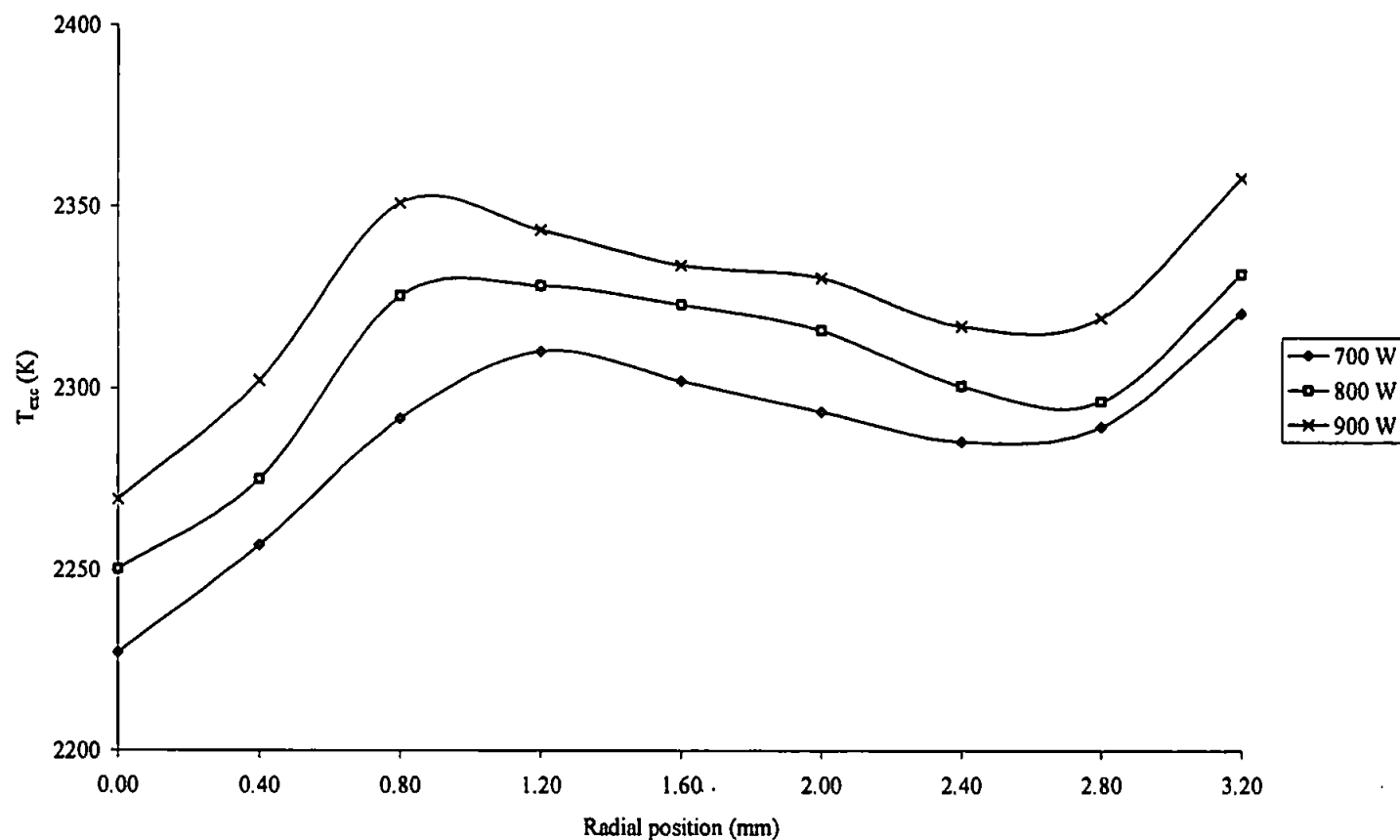
Figure 4.3: Variation of $T_{exc}$ (K) calculated by the LPIRM and abel corrected for radial position with forward power for a plasma operated

under fluorescence-like conditions (forward powers 700 – 900 W; nebuliser gas flow rate 2.00 L min$^{-1}$) at a viewing height of 15 mm ALC

(n = 3, RSDs < 2%)

Excitation temperatures using the LPIRM were also determined using a fibre optic and the SPEX monochromator as a detector. The results are presented in Tables 4.8 and 4.9 for a plasma operated under fluorescence-like and conventional emission conditions, respectively.

The excitation temperatures obtained using the SPEX monochromator as a detector showed greater variation compared with those determined using the Optima detection system. As the excitation temperature was determined by a ratio method the size of the viewing window should make little difference to the determination of $T_{exc}$. However, the area of the plasma observed using the Optima's own detection system was smaller than that using the fibre optic and SPEX monochromator. When using the fibre optic to transmit light to the monochromator, the area observed in the plasma represented the central zone plus the sum of the emitting species at various other points in the plasma and no correction could be made for this. Excitation temperatures ranged from 1770 – 3060 K but the trends were the same as those determined using the Optima's own detector.

Comparison of the excitation temperatures obtained with a plasma operated under fluorescence-like conditions with those under conventional emission conditions show $T_{exc}$ to be higher when the plasma is operated under conventional emission conditions. However, irrespective of the experimental procedure used, excitation temperatures calculated using the LPIRM show good consistency for each set of plasma conditions. For a plasma operated under fluorescence-like conditions, $T_{exc}$ is in the range 2000 – 2500 K. For a plasma operated under conventional emission conditions, $T_{exc}$ is in the range 2000 – 3000 K.

**Table 4.8: Variation of $T_{exc}$ (K) calculated using the LPIRM for a plasma operated under fluorescence-like conditions (forward powers 700 – 900 W; nebuliser gas flow rates 1.50 – 3.00 L min$^{-1}$; viewing heights 10 – 100 mm ALC) using a fibre optic and SPEX monochromator as a detection system**

| Nebuliser gas flow rate (L min$^{-1}$) | *$T_{exc}$ (K) | | | | | | | | | | | |
| | 1.50 | | | 2.00 | | | 2.50 | | | 3.00 | | |
| Power (W) | 700 | 800 | 900 | 700 | 800 | 900 | 700 | 800 | 900 | 700 | 800 | 900 |
| V/H ALC (mm) | | | | | | | | | | | | |
|---|---|---|---|---|---|---|---|---|---|---|---|---|
| 10 | 2440 | 2490 | 2930 | 2180 | 2170 | 2940 | 2200 | 2330 | 3060 | n/d | 2250 | 2800 |
| 20 | 2210 | 2220 | 2620 | 1770 | 2170 | 2420 | 2090 | 2310 | 3040 | n/d | 2200 | 2770 |
| 30 | 2040 | 2200 | 2440 | 1760 | 2100 | 2220 | 1990 | 2370 | 2750 | n/d | 2060 | 2500 |
| 40 | 1920 | 2110 | 2390 | 1940 | 2160 | 2460 | 1930 | 2410 | 2880 | n/d | 1960 | 2300 |
| 50 | 1890 | 2100 | 2330 | 1960 | 2160 | 2330 | 1820 | 2560 | 2910 | n/d | 1780 | 2130 |
| 60 | 1880 | 2100 | 2360 | 1860 | 2180 | 2320 | 1760 | 2700 | 2760 | n/d | 1550 | 2080 |
| 70 | 1900 | 2170 | 2440 | 1950 | 2310 | 2320 | 1920 | 2330 | 3000 | n/d | 2470 | 3180 |
| 80 | 1940 | 2250 | 2650 | 1910 | 2370 | 2420 | 2040 | 2970 | 2830 | n/d | 3010 | 2880 |
| 90 | 2070 | 2340 | 2520 | 2290 | 2840 | 2260 | 2260 | 3200 | 3350 | n/d | 3630 | 3800 |
| 100 | 2180 | 2680 | 3130 | 3370 | 2780 | 2660 | 1960 | 2940 | 3110 | n/d | 2400 | 3740 |

*n = 3, RSDs are less than 5 % for all positions; n/d = not detected

**Table 4.9: Variation of $T_{exc}$ (K) calculated using the LPIRM with viewing height for a plasma operated under conventional emission conditions (forward power 1200 W; nebuliser gas flow rate 0.80 L min$^{-1}$) using a fibre optic and SPEX monochromator as a detection system**

| Viewing height ALC (mm) | *$T_{exc}$ (K) | | | | | | | | | |
| | 10 | 20 | 30 | 40 | 50 | 60 | 70 | 80 | 90 | 100 |
|---|---|---|---|---|---|---|---|---|---|---|
| $T_{exc}$ (K) | 3070 | 2500 | 2150 | 1960 | 1900 | 2070 | 1940 | n/d | n/d | n/d |

*n = 3, RSDs are less than 5 % for all positions; n/d = not detected

It was noted that some of the lowest temperatures are seen at 700 W at a nebuliser gas flow rate of 2.0 to 2.5 L min$^{-1}$ and at 50 to 60 mm ALC. These are the conditions, determined previously from this study and from literature, for an ICP to be used for the observation of fluorescence. These lower temperatures would suggest that, having passed through the efficient atomisation region of the plasma, this higher region ALC (60 ± 10 mm) would contain the greater fraction of ground state atoms suitable for external source excitation and hence fluorescence.

### 4.2.4.2 Boltzmann Distribution Method

When the Optima 3000 ICP was used as a detector the software system limited the number of Fe I lines that could be used for the determination of excitation temperature by the Boltzmann Distribution Method. Relative line intensities for six Fe I lines (Fe I 361.016, 369.401, 382.043, 385.991, 393.030 and 396.926 nm) were measured simultaneously for a particular set of conditions. The emission intensities were corrected for detector efficiency using Equation 3.6 (Section 3.7.1) and excitation temperatures calculated using Equation 3.1 (Section 3.3.1) and the physical parameters listed in Table 3.2 (Section 3.4). However, the excitation temperatures obtained using the Boltzmann Distribution method and the Optima as a detector yielded little useful information. The plotted graphs (not shown) showed that calculated values of $T_{exc}$ were variable and no obvious trends could be established, in contrast to the use of the LPIR method. This poor correlation was attributed to the very low intensities obtained for three (361.016, 369.401 and 396.926 nm) of the six Fe I emission lines used to plot the Boltzmann Distribution. More concentrated solutions were used to increase the emission intensity of the lines but this saturated the detector for the more intense Fe I lines.

Excitation temperatures using the Boltzmann Distribution Method were also determined using the SPEX monochromator as a detector. Instrumental parameters are given in Table 4.6, except that the nebuliser gas flow rate was set at 2.00 L min$^{-1}$. The emission intensities of 50 Fe I lines in the region 360 – 400 nm were recorded. Manual background correction points were used for all measurements. A typical spectral scan is shown in Figure 4.4. Excitation temperatures were calculated using Equation 3.1 (Section 3.3.1) and the physical parameters given in Table 3.2 (Section 3.4). A plot of the Boltzmann Distribution is shown in Figure 4.5 and the results are presented in Tables 4.10 and 4.11, for a plasma operated under fluorescence-like and conventional emission conditions, respectively.
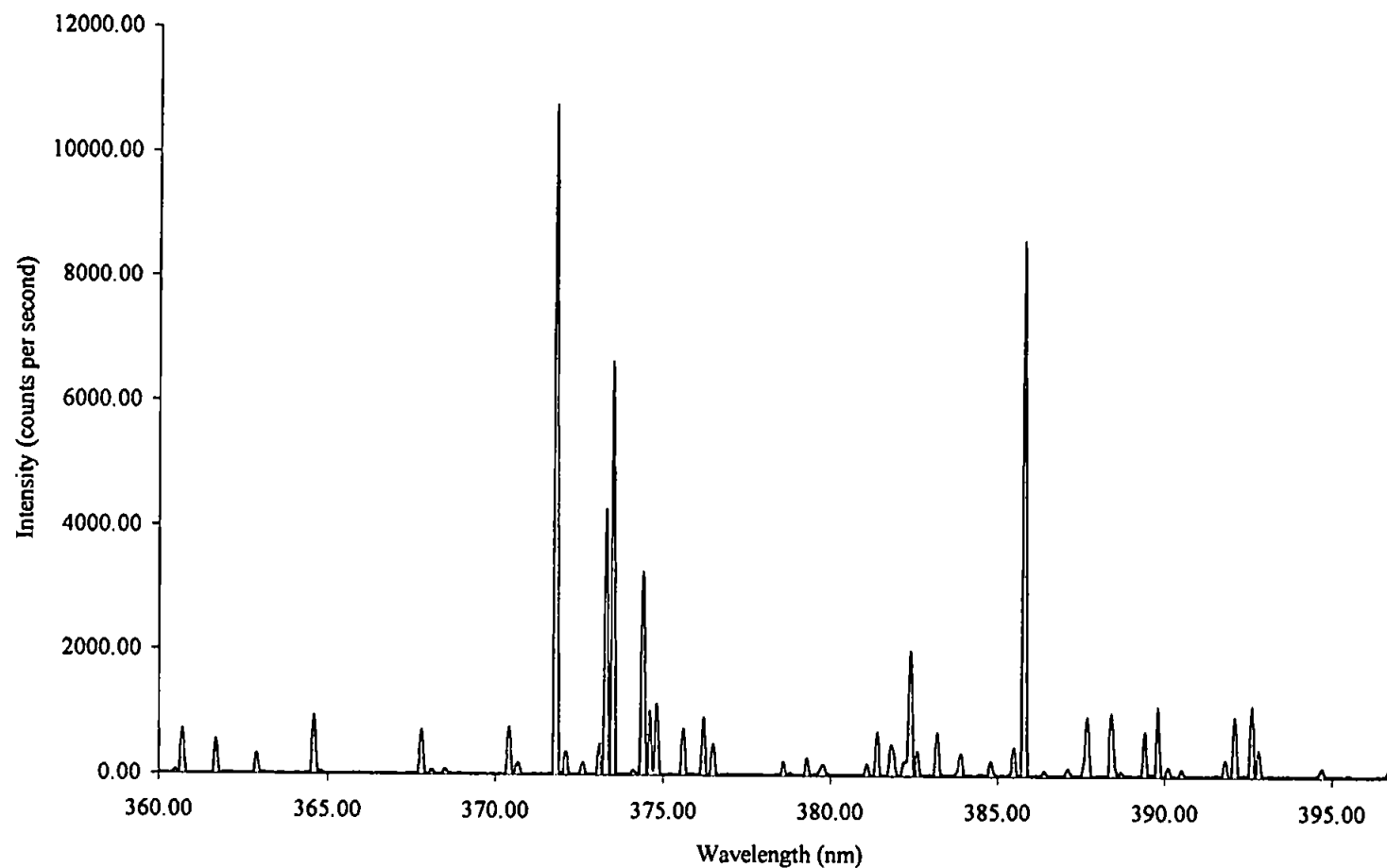
Figure 4.4: Typical spectral scan of Fe I wavelengths using the SPEX monochromator for the determination of $T_{exc}$ using the Boltzmann Distribution method for a plasma operated under fluorescence-like conditions (forward power 900 W; nebuliser gas flow rate 2.00 L min$^{-1}$; viewing height 10 mm ALC)
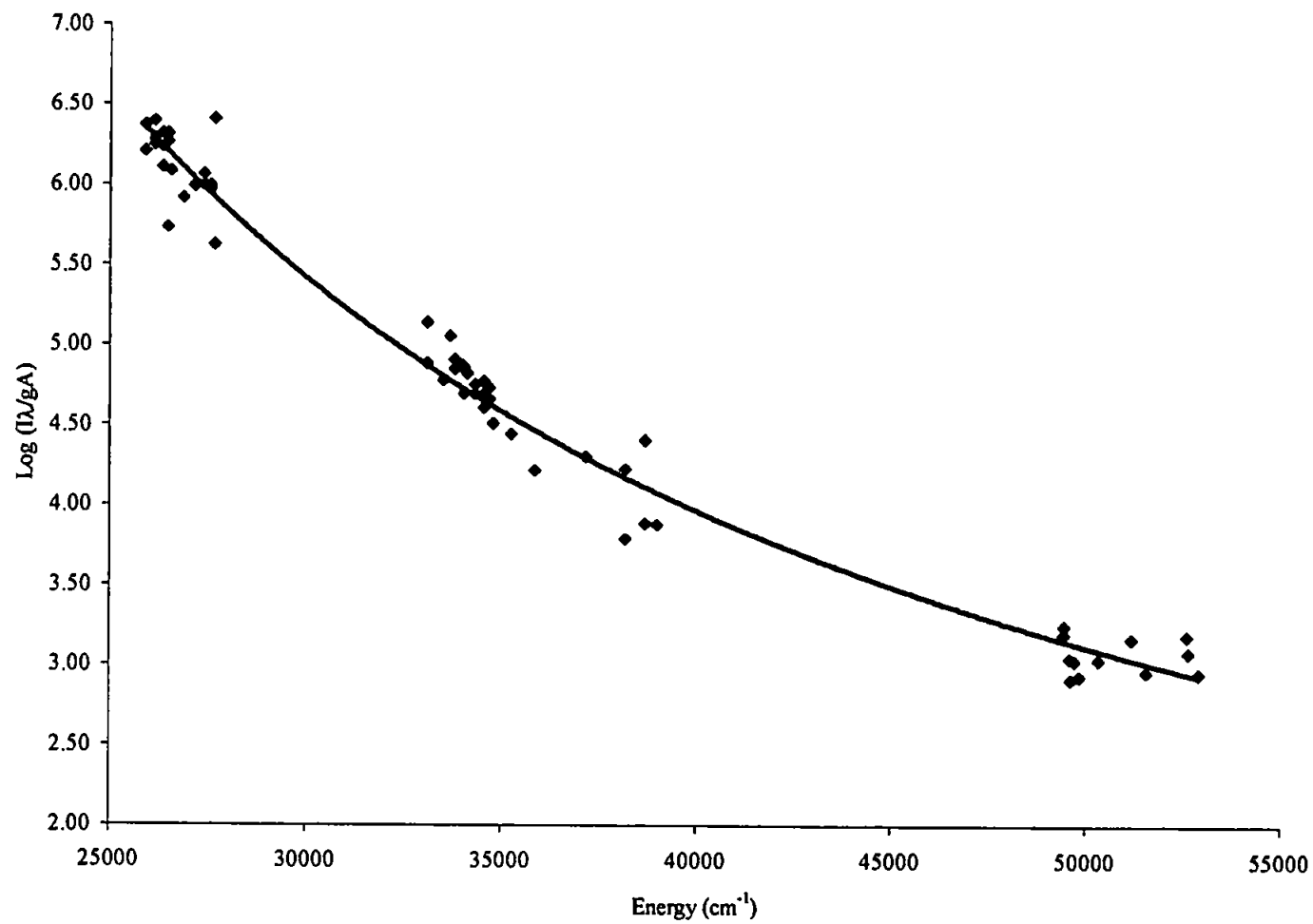
Figure 4.5: Plot of the Boltzmann Distribution measured at 10 mm viewing height ALC for a plasma operated under fluorescence-like conditions (forward power 900 W; nebuliser gas flow rate 2.00 L min$^{-1}$; n= 3, RSDs < 5%)

**Table 4.10: Variation of $T_{exc}$ (K) calculated using the Boltzmann Distribution for a plasma operated under fluorescence-like conditions (forward powers 700 - 900W; nebuliser gas flow rate 2.00 L min$^{-1}$; viewing heights of 10 - 100 mm ALC)**

| Viewing height ALC (mm) | *$T_{exc}$ (K) | | | | | | | | | |
|---|---|---|---|---|---|---|---|---|---|---|
| | 10 | 20 | 30 | 40 | 50 | 60 | 70 | 80 | 90 | 100 |
| Power (W) | | | | | | | | | | |
| 700 | 3130 | 3030 | 3510 | 3170 | 3140 | 3080 | 3100 | 3260 | 3180 | 3600 |
| 800 | 3250 | 3250 | 3600 | 3510 | 3510 | 3560 | 3600 | 3540 | 3520 | 3440 |
| 900 | 3610 | 3430 | 3870 | 3910 | 3590 | 3590 | 3700 | 3630 | 3780 | 4470 |

*n = 3, RSDs are less than 5 % at all spatial positions

**Table 4.11: Variation of $T_{exc}$ (K) calculated using the Boltzmann Distribution for a plasma operated under conventional ICP conditions (forward power 1200W; nebuliser gas flow rate 0.80 L min$^{-1}$) at viewing heights of 10 - 100 mm ALC**

| V/H ALC (mm) | *$T_{exc}$ (K) | | | | | | | | | |
|---|---|---|---|---|---|---|---|---|---|---|
| | 10 | 20 | 30 | 40 | 50 | 60 | 70 | 80 | 90 | 100 |
| $T_{exc}$ (K) | 5540 | 5370 | 4940 | 4680 | 4980 | 4890 | 5470 | n/d | n/d | n/d |

*n = 3, RSDs are less than 5 % at all spatial positions; n/d = not detected

Figure 4.5 shows that the Boltzmann plot is curved and is not a straight line. This effect was previously illustrated in Figure 3.12 (Section 3.4.1) but Figure 4.5 shows a greater degree of curvature. As previously suggested in Chapter 3 (Section 3.4.1), the 'degree' of curvature may indicate whether the plasma conditions are closer to or deviating further from LTE. Figures 4.6 and 4.7 attempt to illustrate this point. Figure 4.6 shows that the Boltzmann Distribution is more curved at 10 mm ALC than at 100 mm ALC and that there is little difference between the curves obtained for forward powers of 800 and 900 W. At both viewing heights observed (10 and 100 mm ALC) the Boltzmann Distribution is less curved for forward powers of 700 W than 800 and 900W. Figure 4.7 illustrates the degree of curvature of the Boltzmann Distribution for a 900 W plasma observed at different viewing heights ALC. Similarly to Figure 4.6, the degree of curvature lessens as the viewing height ALC increases. Figures 4.6 and 4.7 suggest that the plasma is closer to LTE at lower forward powers and higher viewing heights ALC.

Curvature of the Boltzmann Distribution has previously been described in the literature for plasmas operated under high power and low nebuliser gas flows but not for a low power plasma (92, 98). All of the Fe I excitation temperatures indicated an increasing trend with upper energy level. It could be stated that either the high levels are overpopulated with respect to the low levels at a low electron temperature, or that the low levels are over-populated with respect to the high levels at a higher electron temperature (92). Alder *et al.* (92) concluded that this phenomenon could be due to the existence of non-homogeneous emitting regions in the plasma. The view that Fe atoms are not distributed according to the Boltzmann population was considered revolutionary, but was based on the use of twenty to twenty two Fe I lines, few upper levels between 26875 – 55754 cm$^{-1}$, and the determination of the transition probabilities using only the arc method. Nakamura investigated this phenomenon further using sixty nine Fe I lines with upper energy levels of 25900 – 55754 cm$^{-1}$ and contradicted the findings of those

180

who argued that the Fe atoms in the plasma are not distributed according to the Boltzmann Distribution (117). He concluded that Fe atoms were generated in a small area at the top of the inner part of the load coil, under thermal equilibrium conditions and are distributed according to the Boltzmann population. Under non-LTE conditions then Fe atoms were not distributed according to the Boltzmann Distribution and the use of high-energy excitation levels (greater than 35 000 cm$^{-1}$) were not recommended because of possible curvatures of the Boltzmann plot.

The excitation temperatures presented in Tables 4.10 and 4.11 show a decrease in $T_{exc}$ with decreasing power. It should be emphasised that even a difference of $\pm$ 10 % in relative transition probabilities can lead to significant errors in temperature measurements. Using the LPIRM as an example, a line pair whose upper energy levels differ by 1000 cm$^{-1}$ in a 3000 K plasma may result in an error of 100 K being obtained. Obviously, larger differences in transition probabilities will result in larger temperature differences. However, we are looking at relative not absolute temperature values in this study and any trends that can be observed.
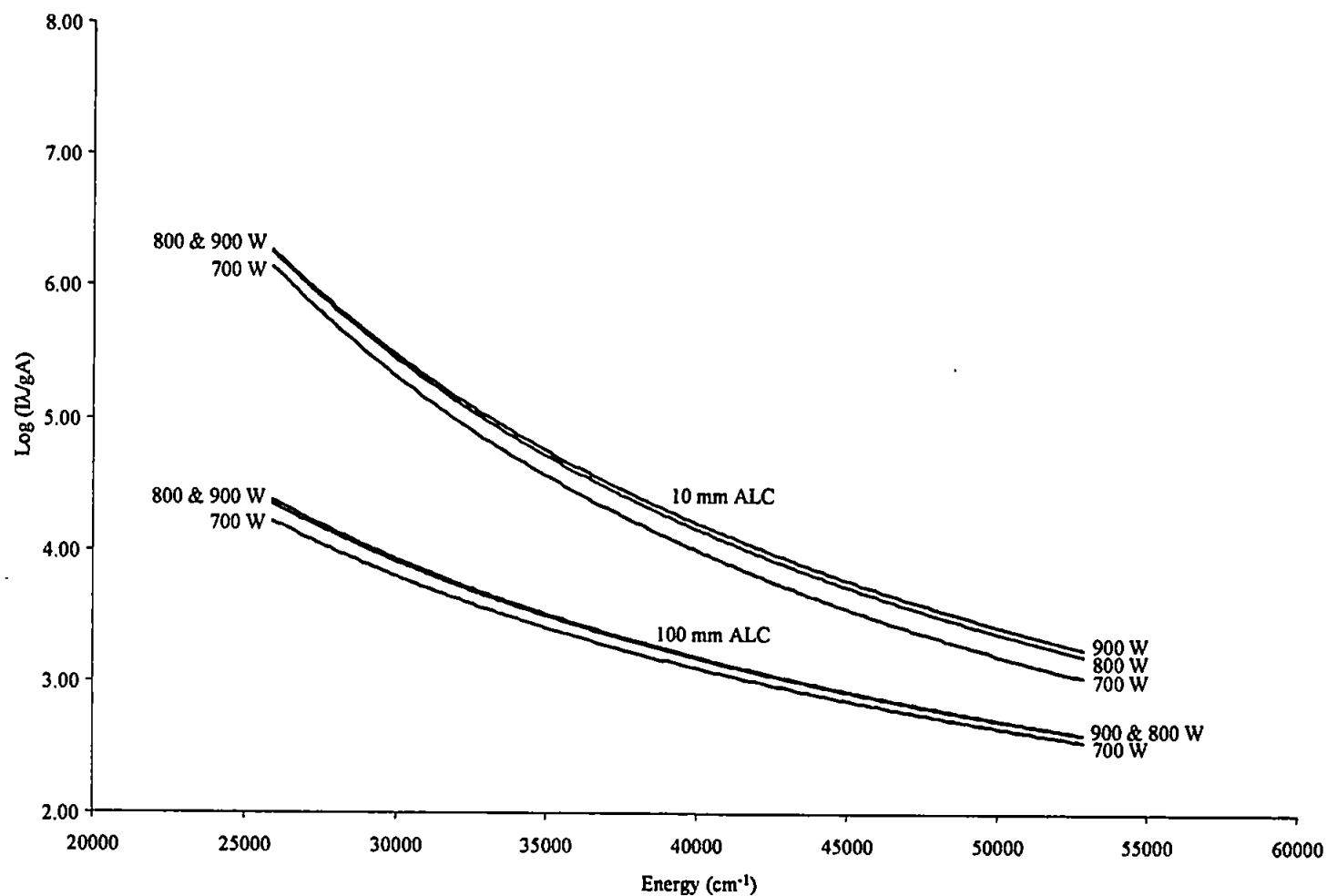
**Figure 4.6: Plot of the Boltzmann Distribution measured for a plasma operated under fluorescence-like conditions (forward power 700 – 900W; nebuliser gas flow rate 2.00 L min⁻¹; viewing heights 10 and 100 mm ALC; n = 3, RSDs < 5 %)**
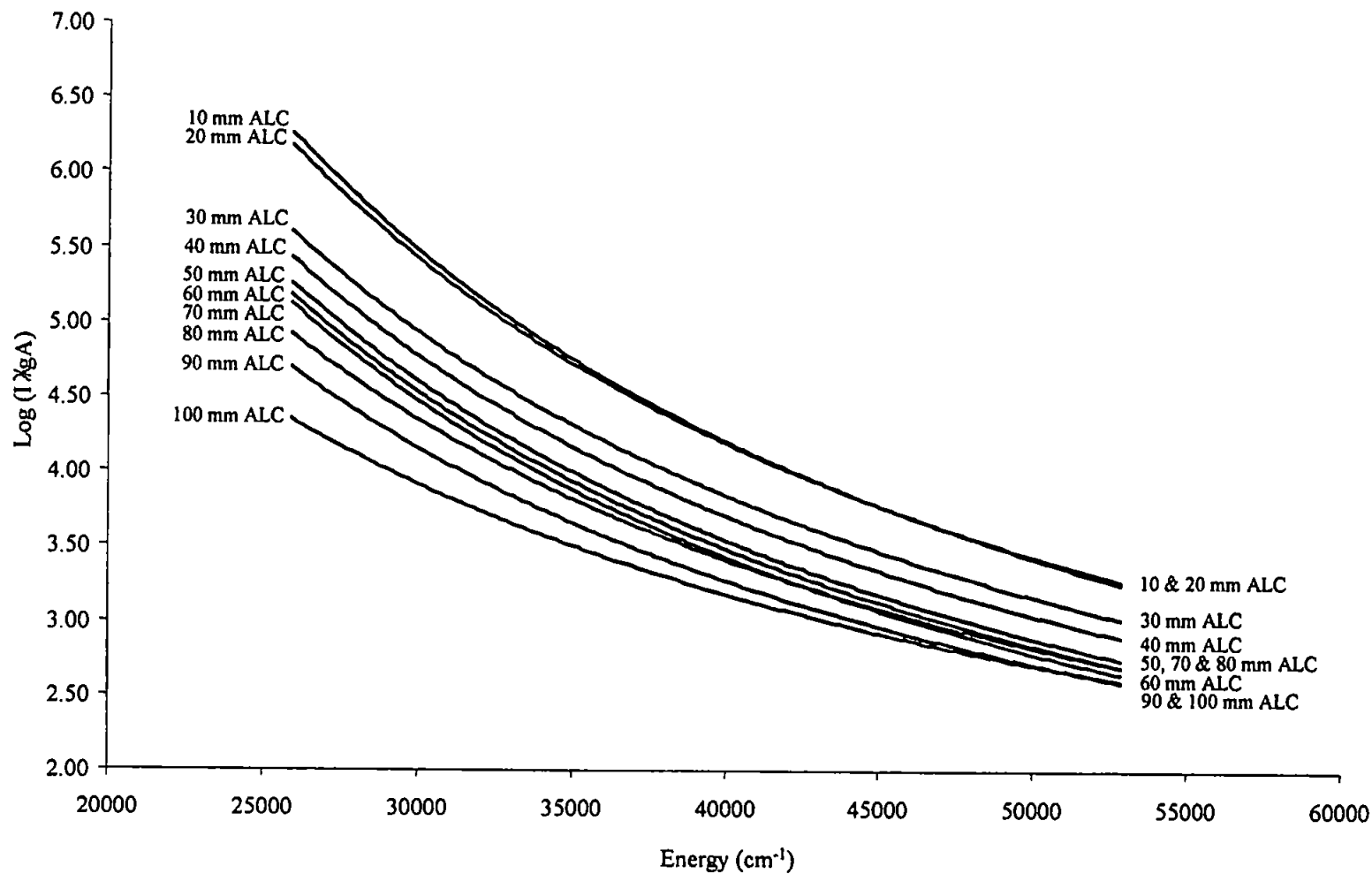
Figure 4.7: Plot of the Boltzmann Distribution measured for a plasma operated under fluorescence-like conditions (forward power 900 W; nebuliser gas flow rate 2.00 L min$^{-1}$; viewing heights 10 – 100 mm ALC; n = 3, RSDs < 5 %)

183

In the literature, excitation temperatures have been determined using a number of different elements (Table 4.1, Section 4.1). For a plasma operated under low forward power (< 1.0 kW) conditions, the following excitation temperatures have been calculated: 2300 – 4000 K for a 500 W plasma (91); 4380 K for a 300 W plasma (129), 4900 – 5400 K for a 400 to 700 W plasma (134); 3800 K for a 530 W plasma (137); 7500 – 8300 K for a 750 W plasma (139) and 6200 – 6700 K for a 500 to 750 W plasma (140). The excitation temperatures determined for a plasma operated under fluorescence-like conditions (*i.e.* low forward power and high nebuliser gas flow rates) in this section have all been in the region of 2000 to 2500 K. These values are somewhat lower than those previously described in the literature where other elements were chosen as their species for study (*e.g.* Ar, Ca, Mg, Ti) and not Fe as used in the current study. However, the operating conditions used in the current study (high nebuliser gas flow and sample uptake rates) were different to those used in the literature.

Table 4.1 (Section 4.1) shows that the typical $T_{exc}$ values obtained for a plasma operated under conventional emission conditions (*i.e.* forward power of 1200 W) are generally higher than those obtained from a plasma operated under fluorescence-like conditions. Excitation temperatures in the region of 5400 – 5700 K were obtained for a 1200 W plasma (92). $T_{exc}$ obtained from the Boltzmann Distribution show good agreement with literature values, however, $T_{exc}$ values obtained from the LPIRM appear to be lower. A possible reason for the difference in calculated temperature from the Boltzmann Distribution and the LPIRM has already been discussed in Chapter 3, Section 3.4.1.

## 4.3    Introduction to Rotational Temperature

The rotational fine structure of electronic bands can be used to determine the rotational temperature. Several species have been used for this purpose with the most common being the molecular ion of nitrogen ($N_2^+$) (86, 138, 158) and the hydroxyl radical (86, 137).

For a transition J'- J", the intensity of a rotational line can be expressed as a function of either the oscillator strength, $S_J$ (Equation 4.2), or the probability transition, $A_J$ (Equation 4.3) (19):

$$I = DS_J v^4 \exp\left(\frac{-B_v hc J'(J'+1)}{kT_{rot}}\right) \qquad (4.2)$$

$$I = DA_J v^4 \exp\left(\frac{-B_v hc J'(J'+1)}{kT_{rot}}\right) \qquad (4.3)$$

where, $v$ is the wavenumber of the line, and $B_v$ is the rotational constant belonging to the vibrational quantum number $v$. The oscillator strength, $S_J$, is given in Equation 4.4:

$$S_J = K'+K''+1 \qquad (4.4)$$

In the case of $N_2^+$, two branches (P and R) can be used for temperature measurements. It is possible to determine the rotational temperature by plotting a slope of the curve log[I/(K'+K''+1)] versus K'(K''+1) (19). The slope of the curve can be calculated using Equation 4.5:

$$\frac{-Bhc}{kT_{rot}} = \frac{-2.983}{T_{rot}} \qquad (4.5)$$

If a decadic logarithm is used then the value of the slope becomes −1.296/T. Assignments of the available rotational lines as a functions of K" for the P and R

branches are presented in Table 4.12 (159, 160). It should be noted that because of the even-odd alternation, line intensities with odd K" must be multiplied by 2 (161).

It is similarly possible to determine the rotational temperature using OH bands, however, because of a $A^2\Sigma^+ \rightarrow X^2\Pi$ transition, it is more complex. Five main branches (O, P, Q, R, and S) can be observed with a total of 12 branches ($O_{12}$, $P_1$, $P_2$, $P_{12}$, $Q_1$, $Q_{21}$, $Q_2$, $Q_{12}$, $R_1$, $R_2$, $R_2$, and $S_{21}$) (34). Practically, the $Q_1$ and $R_2$ branches of the most intense (0-0) vibrational band are used (86, 87, 154, 162, 163). Line assignments, wavelengths, energies (161) and transition probabilities are presented in Table 4.13. The intensity measurements are inserted in Equation 4.3 and the temperature is obtained from a plot of log (I $\lambda$/gA) versus energy (E). The slope is related to rotational temperature and is equal to $-0.625/T_{rot}$. Other molecular species can be used to determine $T_{rot}$, such as CN (129), BO (149) and $C_2$ (154, 164).

**Table 4.12: Wavelengths and K'(K"+1) values for the (0-0) band of the first negative system of $N_2^+$ (19)**

| K" | P branch | | R branch | |
|---|---|---|---|---|
| | λ (nm) | $S_J = K''(K''-1)$ | λ (nm) | $S_J = (K''+1)(K''+2)$ |
| 6 | | | 390.490 | 56 |
| 7 | | | 390.400 | 72 |
| 8 | | | 390.290 | 90 |
| 9 | | | 390.190 | 110 |
| 10 | | | 390.080 | 132 |
| 11 | | | 389.970 | 156 |
| 12 | | | 389.850 | 182 |
| 13 | | | 389.730 | 210 |
| 16 | | | 389.330 | 306 |
| 18 | 391.350 | 306 | 389.040 | 380 |
| 20 | 391.300 | 380 | 388.740 | 462 |
| 21 | 391.290 | 420 | 388.580 | 506 |
| 22 | 391.250 | 462 | | |
| 23 | 391.200 | 506 | | |
| 24 | 391.150 | 552 | | |
| 25 | 391.100 | 600 | | |
| 26 | 391.040 | 650 | | |
| 27 | 390.970 | 702 | | |
| 28 | 390.910 | 756 | | |
| 29 | 390.840 | 812 | | |
| 30 | 390.760 | 870 | | |
| 31 | 390.680 | 930 | | |
| 32 | 390.600 | 992 | | |
| 33 | 390.510 | 1056 | | |
| 34 | 390.410 | 1122 | | |
| 35 | 390.310 | 1190 | | |

**Table 4.13: Assignment, wavelength, energies, and A values for the $Q_1$ and $R_2$ branch lines of the OH (0–0) band (116)**

| K | $\lambda$ (nm) | E (cm$^{-1}$) | A ($10^8$ s$^{-1}$) |
|---|---|---|---|
| **$Q_1$ branch** | | | |
| 1 | 307.844 | 32,475 | 0.0 |
| 2 | 307.995 | 32,543 | 17.0 |
| 4 | 308.328 | 32,779 | 33.7 |
| 5 | 308.520 | 32,948 | 42.2 |
| 6 | 308.734 | 33,150 | 50.6 |
| 8 | 309.239 | 33,652 | 67.5 |
| 9 | 309.534 | 33,952 | 75.8 |
| 10 | 309.859 | 34,283 | 84.1 |
| 13 | 311.022 | 35,462 | 100.6 |
| 14 | 311.477 | 35,915 | 108.8 |
| 15 | 311.967 | 36,397 | 125.2 |
| 16 | 312.493 | 36,906 | 133.3 |
| 17 | 313.057 | 37,444 | 141.5 |
| 18 | 313.689 | 38,008 | 149.6 |
| 19 | 314.301 | 38,598 | 157.7 |
| **$R_2$ branch** | | | |
| 1 | 308.405 | 32,542 | 2.7 |
| 2 | 308.023 | 32,643 | 5.7 |
| 3 | 307.703 | 32,778 | 8.9 |
| 4 | 307.437 | 32,947 | 12.8 |
| 7 | 306.918 | 33,650 | 24.8 |
| 13 | 309.967 | 35,912 | 49.1 |
| 14 | 307.114 | 36,393 | 53.2 |
| 15 | 307.303 | 36,903 | 57.2 |
| 16 | 307.553 | 37,440 | 61.3 |
| 17 | 307.807 | 38,004 | 65.3 |
| 18 | 308.125 | 38,594 | 69.3 |
| 19 | 308.489 | 39,209 | 73.4 |
| 20 | 308.901 | 39,847 | 77.4 |

## 4.4    Experimental: Rotational Temperature Measurements

Rotational temperature measurements were obtained using the same instrumentation as that described in Section 4.2.2. An Optima 3000 ICP spectrometer (The Perkin-Elmer Corporation) fitted with a demountable X and Y-axis translation plate held a fibre optic (1000 μm core diameter HPSUV1000P; Oxford Electronics Ltd) that was capable of both horizontal and vertical translation of the tailflame in 0.1 mm increments. Measurements were taken using a Datascan 2 (ISA Instruments S.A. (U.K.) Ltd.) interfaced with a Current/Phase Stepper Drive and a monochromator (1700 Series, SPEX Industries INC.). An IEEE488 communications port provided standardised electronic protocols to receive commands and send data to a host computer. All readings were automated by constructing a program within the instrument software (SpectRad Version 2 for Windows; ISA Instruments S.A. (U.K.) Ltd.).   For OH rotational temperature measurements, the OH band spectra were recorded between 306.5 – 310.0. Other operating conditions are specified in Table 4.14. Spectra were recorded at various forward powers (700, 800 and 900W), nebuliser gas flow rates (1.50, 2.00, 2.50 and 3.00 L min$^{-1}$), and viewing heights ALC (10 – 100 mm in 10 mm increments). Pure water aerosols were produced for measurement at a constant flow rate of 2.00 ml min$^{-1}$.

For $N_2^+$ rotational temperature measurements, the $N_2^+$ band spectra were recorded between 388.5 – 391.5 nm using the ICP spectrometer and monochromator described above. Other operating conditions are specified in Table 4.14. Spectra were recorded at various forward powers (700, 800 and 900W), nebuliser gas flow rates (1.50, 2.00, 2.50 and 3.00 L min$^{-1}$), and viewing heights ALC (10 – 100 mm in 10 mm increments). Nitrogen (10 %) was introduced to the nebuliser gas flow (Series 850 gas blender, Signal, Camberley, Surrey, U.K.).

Both OH and $N_2^+$ rotational temperature experiments were repeated using conventional emission conditions so that comparisons between the two systems could be made. Operating parameters are listed in Table 4.14.

**Table 4.14: Optima 3000 ICP operating parameters for OH and $N_2^+$ rotational 'temperature' measurements for a plasma operated under fluorescence-like and conventional emission conditions**

| | |
|---|---|
| **RF Generator** | |
| Frequency | 40.68 MHz, free running |
| **ICP-AFS conditions** | |
| Power | 700, 800 and 900 W |
| **Sample Introduction System** | |
| Nebuliser | Ebdon V-Groove high solid |
| Torch | Demountable, custom built with 8 mm wide observation slot And 60 mm extended coolant tube (from auxiliary) and a 1.5 mm i.d. alumina injector |
| Spray Chamber | PE Scott Double Pass |
| Peristaltic Pump | Gilson Minipuls 3, computer controlled |
| Sample Uptake Rate | 2.0 ml min$^{-1}$ |
| **Argon Flow Rate** | |
| Plasma | 12 L min$^{-1}$ |
| Auxiliary | 0.2 L min$^{-1}$ |
| Nebuliser | 1.50, 2.00, 2.50 and 3.00 L min$^{-1}$ |
| **ICP-AES conditions** | |
| Power | 1200 W |
| **Sample Introduction System** | |
| Nebuliser | Ebdon V-Groove high solid |
| Torch | Demountable, custom built with 8 mm wide observation slot and a 2.0 mm i.d. alumina injector |
| Spray Chamber | PE Scott Double Pass |
| Peristaltic Pump | Gilson Minipuls 3, computer controlled |
| Sample Uptake Rate | 1.0 ml min$^{-1}$ |
| **Argon Flow Rate** | |
| Plasma | 16 L min$^{-1}$ |
| Auxiliary | 0.8 L min$^{-1}$ |
| Nebuliser | 0.8 L min$^{-1}$ |

**Table 4.14 continued: SPEX monochromator operating parameters for OH and N$_2^+$ rotational 'temperature' measurements for a plasma operated under fluorescence-like and conventional emission conditions**

| SPEX Monochromator | |
|---|---|
| Entrance and exit slit widths | 25 μm |
| PMT voltage | 1200 V |
| Viewing height ALC | 10 – 100 mm (in 10 mm increments) |
| Lateral position | 0.0 mm (centre of the plasma) |
| **OH molecular species** | |
| Scan range | 306.5 - 310.0 nm |
| Step size | 0.01 nm |
| Scan speed | 0.01 nm s$^{-1}$ |
| **N$_2$+ molecular species** | |
| Scan range | 388.5 - 391.5 nm |
| Step size | 0.01 nm |
| Scan speed | 0.01 nm s$^{-1}$ |

## 4.4.1 Results and Discussion: Rotational Temperature Measurements

### 4.4.1.1 OH Rotational Temperature Measurements

The relative intensities of the assigned $Q_1$ (and $R_2$) branch lines were measured using the fibre optic and monochromator and the rotational temperature ($T_{rot}$, K) was determined from a plot of log ($I \lambda/gA$) versus E, energy. The slope is related to rotational temperature and is equal to $-0.625/T_{rot}$. A spectral scan of the (0-0) band emission from OH showing Q and R branch lines is shown in Figure 4.8 and typical plots of $Q_1$ and $R_2$ branch line emission intensities against energy level from the OH (0-0) band are shown in Figures 4.9 and 4.10, respectively. The effects of forward power, nebuliser gas flow rate and viewing height ALC, with respect to rotational temperature (calculated using $R_2$ branch lines), are shown in Table 4.15. Results from a plasma operated under conventional emission conditions are presented in Table 4.16. Rotational temperatures were also calculated using $Q_1$ branch lines for a plasma operated under fluorescence-like and conventional emission conditions, respectively. The rotational temperature values obtained were similar to those calculated using $R_2$ branch lines so have not been shown.

The rotational temperature values are affected by forward power, nebuliser gas flow rate and viewing height ALC. The values cover the range 2700 - 3600 K for a plasma operated under fluorescence conditions and show an increase in $T_{rot}$ with increasing power and nebuliser gas flow rate and a decrease in $T_{rot}$ with increasing viewing height.

For a plasma operated under conventional emission conditions the values cover the range 2300 – 3030 K. The values obtained for $T_{rot}$ under conventional emission conditions are of the same order of magnitude as those found by a number of other workers. Fleitz and Seliskar (165) found a range of values between 3700 - 4500 K while

193

Hasegawa and Winefordner (166) found a value of 2000 K for $T_{rot}$ from the OH radical from water vapour.

Figures 4.9 and 4.10 suggest that the $Q_1$ and $R_2$ branch plots are not simple Boltzmann distributions but may be a combination of at least two separate Boltzmann-like distributions. For $Q_1$, this deviation is mentioned in the literature (165) and for subsequent calculations to determine $T_{rot}$, all branch plots were drawn with no weight from the first two points $Q_1^2$ and $Q_1^3$. Similarly for $R_2$, all branch plots were drawn with no weight from the first three points $R_2^1$, $R_2^2$ and $R_2^3$. Extrapolation of the plots showed the deviation to be constant in both cases and could possibly be attributed to the value of the relative transition probability being used. For the $Q_1$ branch, the transition probability (for $Q_1^2$) was calculated from the extrapolated line and determined to be 22.5 x $10^8$ $s^{-1}$ (n = 10). This compares with an original value of 17.0 x $10^8$ $s^{-1}$ (161). The rotational transition probabilities have been tabulated for the $Q_1$ series using two different coupling constants with the majority of workers using a coupling constant of – 7.55 for the $^2\Sigma \rightarrow ^2\Pi$ transition. Closer scrutiny of the decoupled system suggests a coupling constant of 0 and shows the $Q_1^2$ transition probability to be approximately 22.3 x $10^8$ $s^{-1}$ (161). The close agreement between the literature value and the experimental value of the $Q_1^2$ transition probability suggests that, at low $Q_1$ transitions, deviation from the Boltzmann distribution may be due to a change in the degree of coupling within the rotronic system (167).
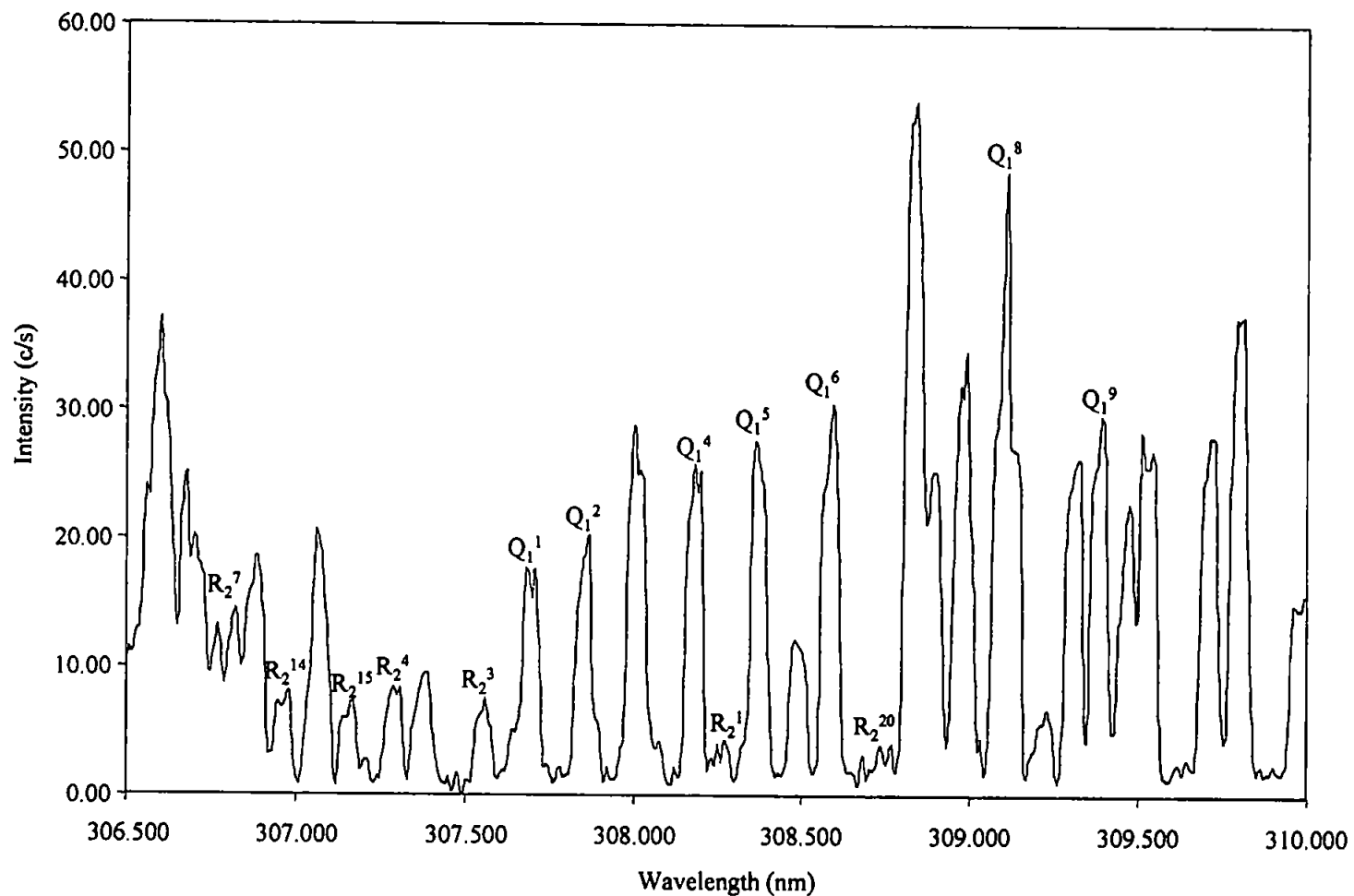
Figure 4.8: Spectral scan of the (0-0) band emission from OH showing Q and R branches from a plasma operated under fluorescence-like conditions (forward power 900 W; nebuliser gas flow rate 2.00 L min$^{-1}$; viewing height 50 mm ALC; n = 3, RSDs < 5 %)
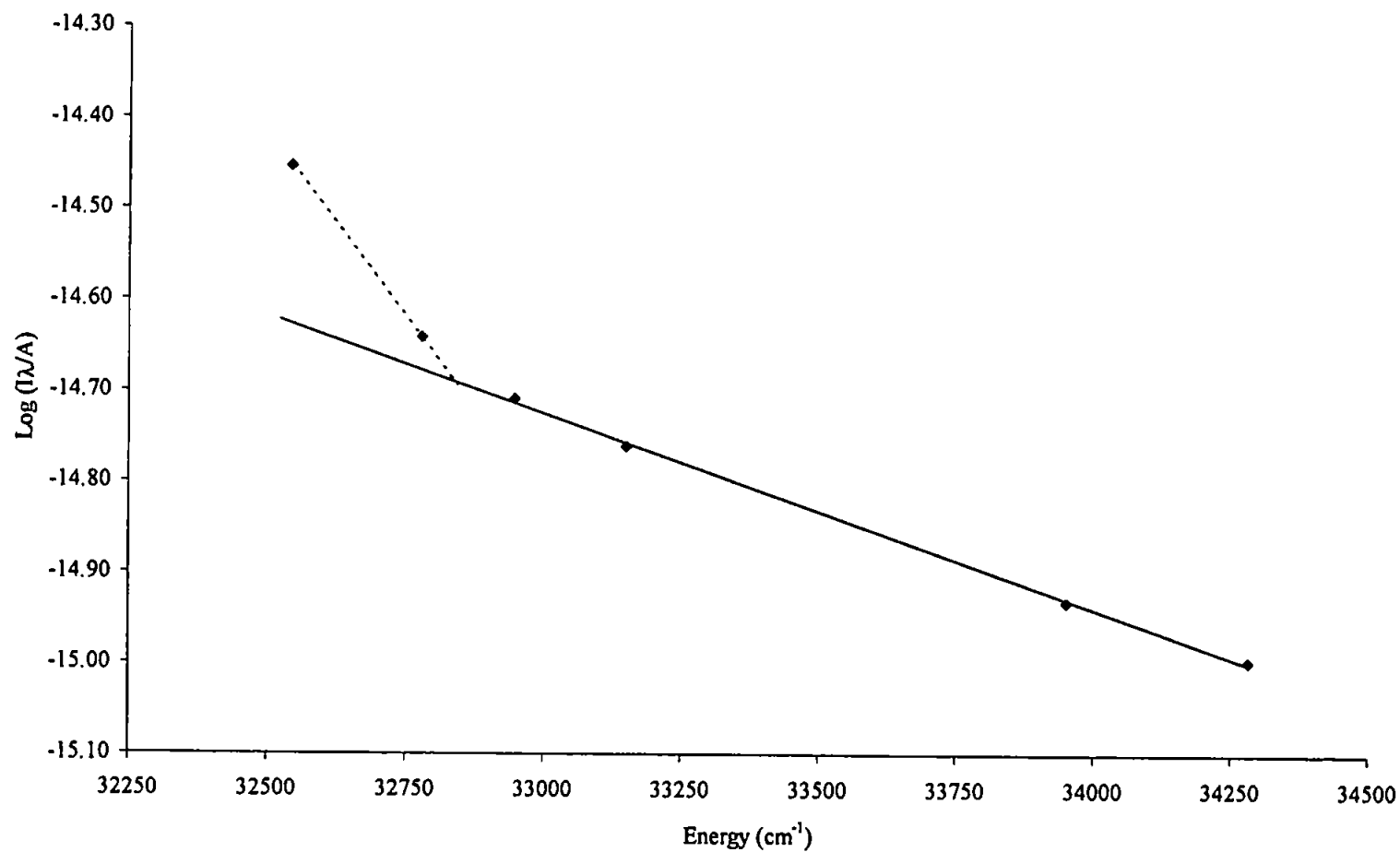
Figure 4.9: Plot of $Q_1$ branch line emission intensities against energy level from the OH (0-0) band measured from a plasma operated under fluorescence-like conditions (forward power 900 W; nebuliser gas flow rate 2.00 L min$^{-1}$; viewing height 50 mm ALC; n = 3, RSDs < 5 %)
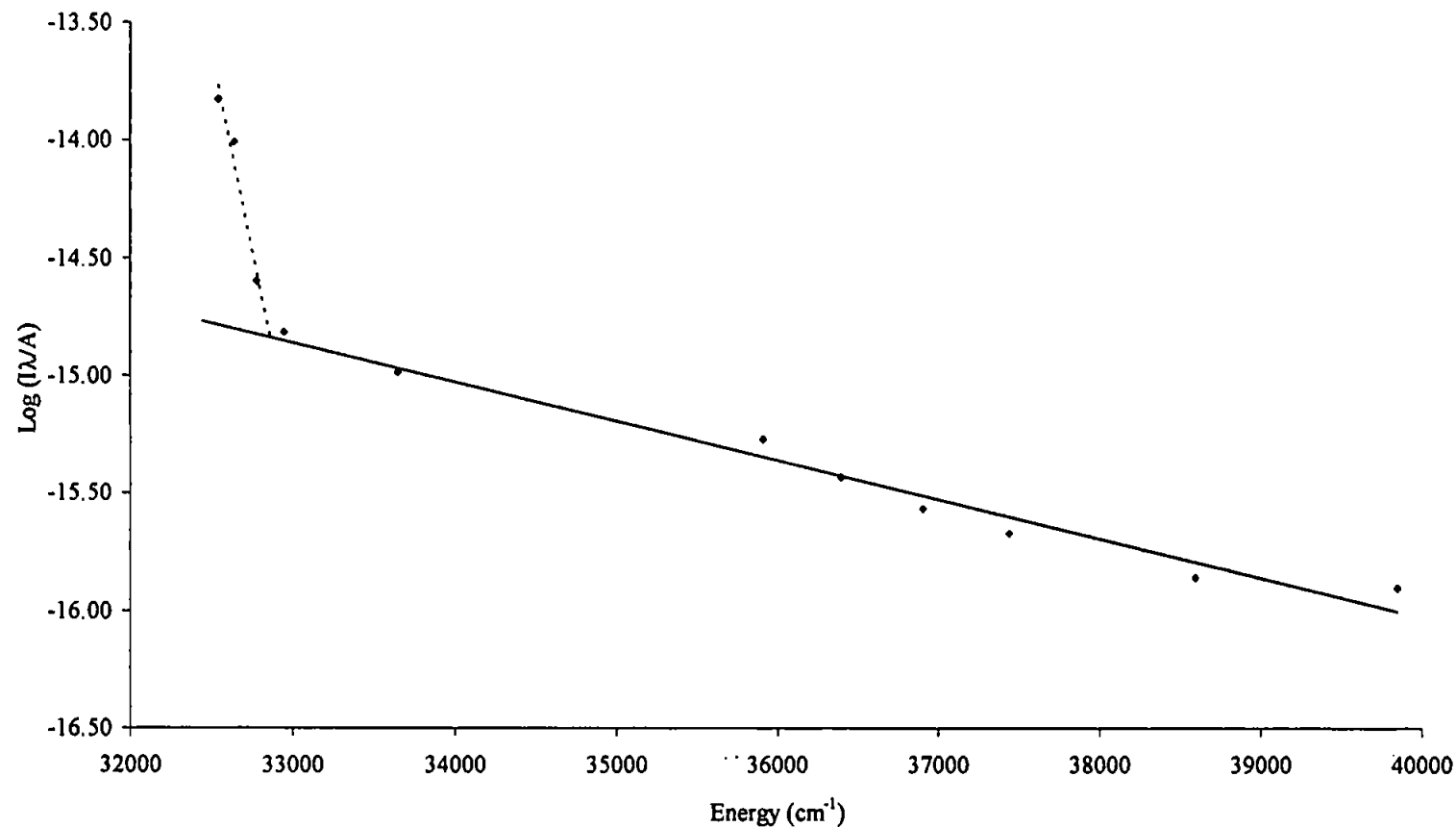
**Figure 4.10: Plot of R$_2$ branch line emission intensities against energy level from the OH (0-0) band measured from a plasma operated under fluorescence-like conditions (forward power 900 W; nebuliser gas flow rate 2.00 L min$^{-1}$; viewing height 50 mm ALC; n = 3, RSDs < 5 %)**

**Table 4.15: Variation of $T_{rot}$ (K) calculated using $R_2$ branch lines for a plasma operated under fluorescence-like conditions (forward powers 700 – 900 W; nebuliser gas flow rates 1.50 – 3.00 L min$^{-1}$; viewing heights 10 – 80 mm ALC)**

| | \*$T_{rot}$ (K) | | | | | | | |
|---|---|---|---|---|---|---|---|---|
| **Nebuliser gas flow (L min$^{-1}$) = 1.50** | | | | | | | | |
| **V/H ALC (mm)** | **10** | **20** | **30** | **40** | **50** | **60** | **70** | **80** |
| **Power (W)** | | | | | | | | |
| 700 | 2700 | 2700 | 2880 | 2820 | 2890 | 2680 | 2450 | 2300 |
| 800 | 3050 | 3040 | 2990 | 2850 | 2790 | 2730 | 2720 | 2320 |
| 900 | 3300 | 3140 | 3090 | 2880 | 3120 | 2940 | 2930 | 3010 |
| **Nebuliser gas flow (L min$^{-1}$) = 2.00** | | | | | | | | |
| 700 | 3050 | 2710 | 2670 | 2540 | 2630 | n/d | n/d | n/d |
| 800 | 3450 | 3040 | 2750 | 2970 | 3170 | n/d | n/d | n/d |
| 900 | 3410 | 3270 | 2970 | 2930 | 2710 | 2830 | 2240 | 2440 |
| **Nebuliser gas flow (L min$^{-1}$) = 2.50** | | | | | | | | |
| 700 | 3150 | 2870 | 2580 | 2490 | 2320 | n/d | n/d | n/d |
| 800 | 3490 | 3300 | 3290 | 2690 | 2510 | n/d | n/d | n/d |
| 900 | 3600 | 3340 | 3460 | 2870 | 2940 | n/d | n/d | n/d |
| **Nebuliser gas flow (L min$^{-1}$) = 3.00** | | | | | | | | |
| 700 | n/d | n/d | n/d | n/d | n/d | n/d | n/d | n/d |
| 800 | n/d | n/d | n/d | n/d | n/d | n/d | n/d | n/d |
| 900 | 3560 | 3340 | 3300 | 2980 | 3230 | n/d | n/d | n/d |

\*n = 3, RSDs are less than 5 % at all spatial positions; n/d = not detected

**Table 4.16: Variation of $T_{rot}$ (K) calculated using $R_2$ branch lines for a plasma operated under conventional emission conditions (forward power 1200 W; nebuliser gas flow rate 0.80 L min$^{-1}$) at viewing heights of 10 – 80 mm ALC**

| Viewing height ALC (mm) | 10 | 20 | 30 | 40 | 50 | 60 | 70 | 80 | 90 | 100 |
|---|---|---|---|---|---|---|---|---|---|---|
| $T_{rot}$ (K)\* | 2330 | 3030 | 2870 | 3020 | 2930 | 2520 | 2310 | n/d | n/d | n/d |

\*n = 3, RSDs are less than 5 % at all spatial positions; n/d = not detected

## 4.4.1.2 $N_2^+$ Rotational Temperature Measurements

$N_2^+$ band spectra were recorded between 388.5 – 391.5 nm and the rotational temperature ($T_{rot}$, K) determined from a plot of log $[I/(K'+K''+1)]$ against $K'(K'+1)$. The slope is related to the rotational temperature and is equal to $-1.296/T_{rot}$ when a decadic logarithm is used or $-2.983/T_{rot}$ if natural logarithms are used. A spectral scan of the (0-0) band emission from $N_2^+$ showing P and R branches is shown in Figure 4.11 and a typical plot from the $N_2^+$ (0-0) band is shown in Figure 4.12. Attempts were made to study the effects of forward power, nebuliser gas flow and viewing height ALC with respect to rotational temperature but, in the majority of cases, the emission intensities obtained were close to background levels even when a concentration of nitrogen of 15 % was introduced through the nebuliser gas flow. Further attempts to complete the measurements by adding a nitrogen-containing compound to the plasma were not successful. Therefore only rotational temperatures where the emission intensity was greater than the mean plus three standard deviations of the blank were calculated. To aid with peak assignment, $N_2^+$ rotational temperatures were determined with a plasma operated under conventional ICP conditions (Table 4.12, Section 4.3).

Rotational temperatures were calculated and found to be 1670 and 1390 K for a 1200 W plasma operated under conventional emission conditions viewed at 10 and 20 mm ALC respectively. This compares with 1230 K for a 900 W plasma operated under fluorescence-like conditions viewed at 10 mm ALC.

The values obtained in this study were of the same order of magnitude as those found by a number of other workers. Values of 1600 - 1700 K and 1650 - 1850 K have been reported for the $N_2$ rotational spectra and $N_2^+$ rotational spectra, respectively (168). Hasegawa and Winefordner (166) found values of 3200 - 4000 K from the $N_2$ rotational spectra and 4500 - 5000 K from the $N_2^+$ rotational spectra.
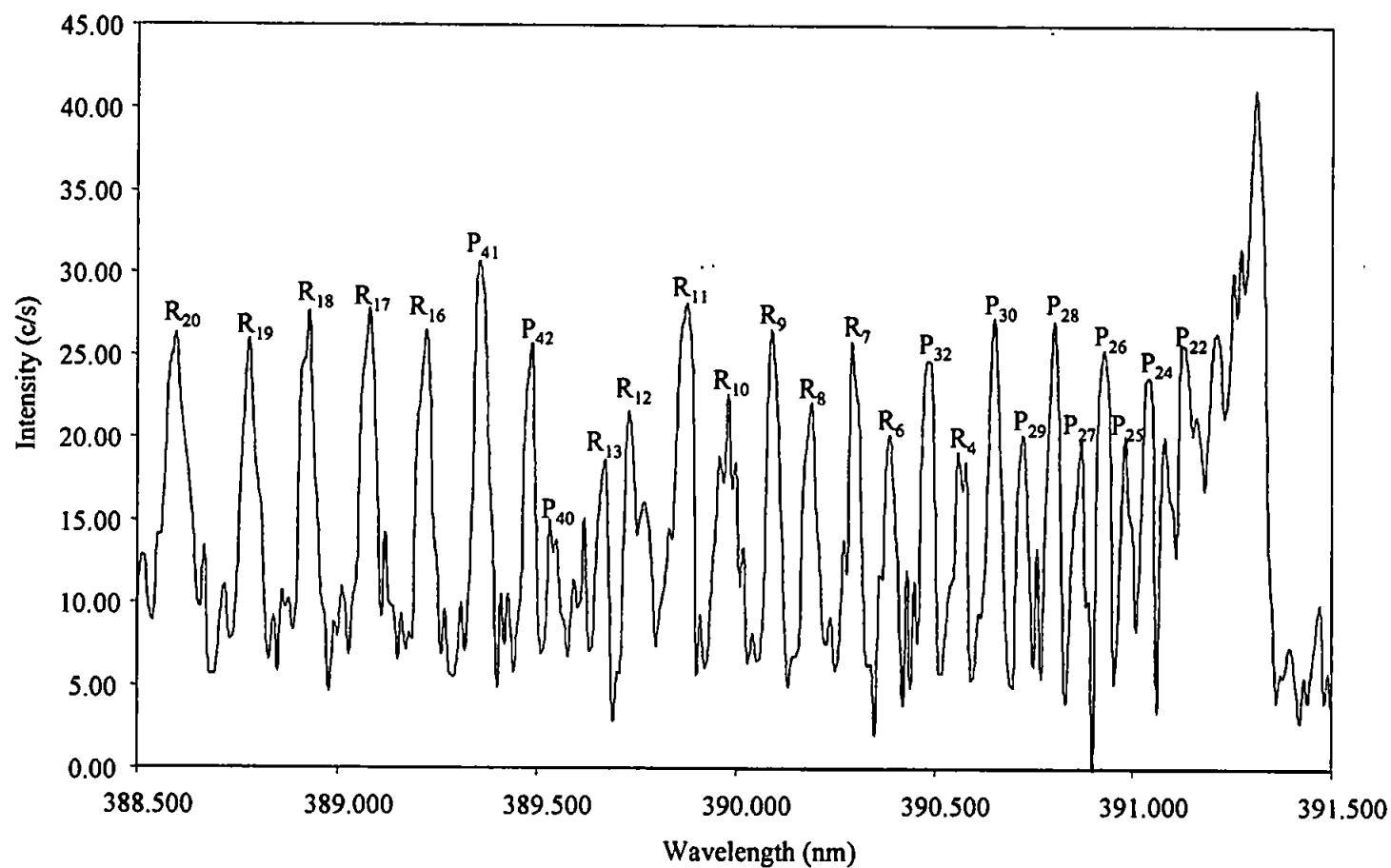
Figure 4.11: Spectral scan of (0-0) band of $N_2^+$ with bandhead at 391.4 nm showing P and R branches for an ICP operated under fluorescence-like conditions (forward power 900 W; nebuliser gas flow rate 2.00 L min$^{-1}$; viewing height 10 mm ALC; n = 3, RSDs < 5 %)
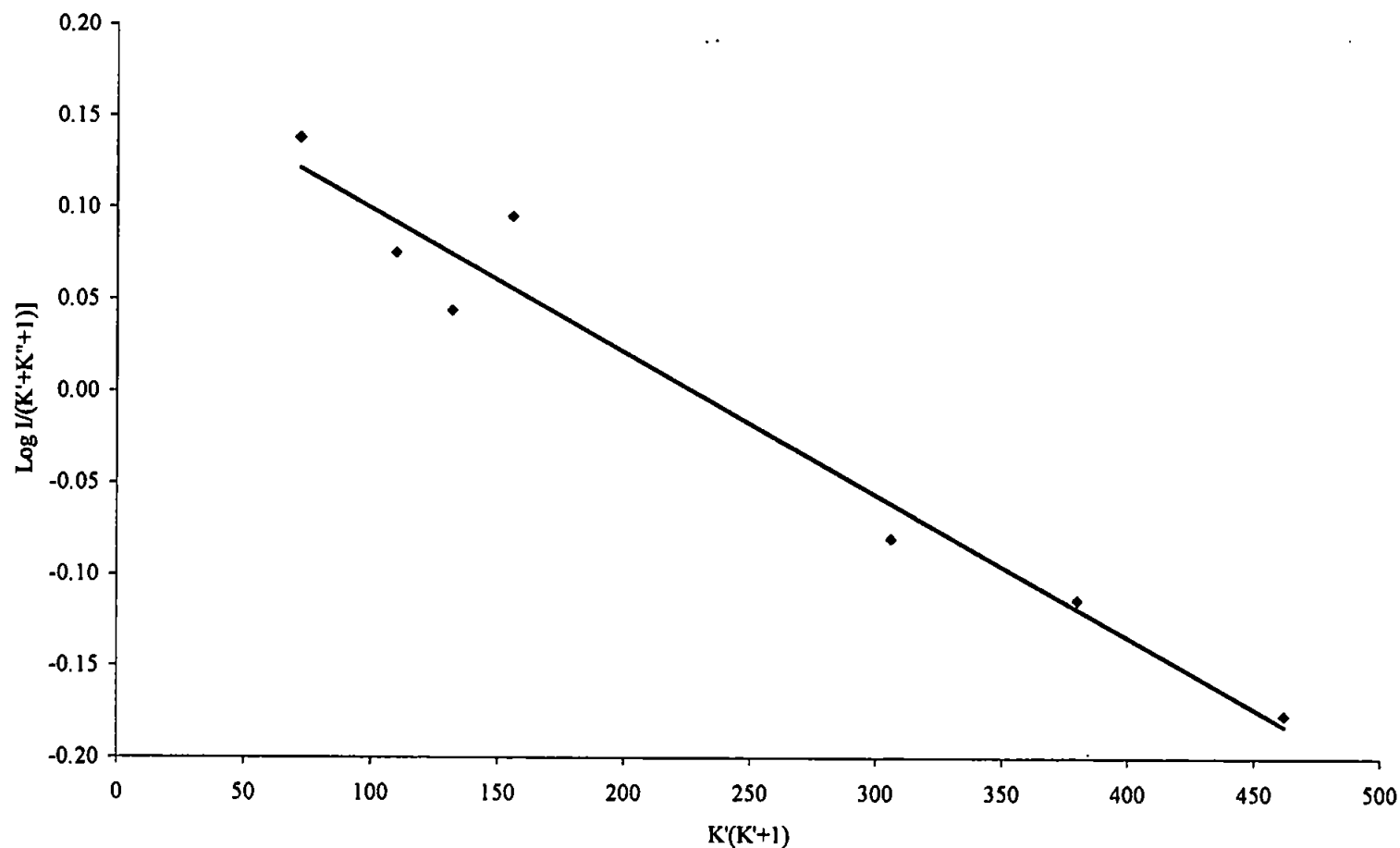
**Figure 4.12:** Plot of K'(K'+1) versus. log[I/(K'+K''+1)] from the $N_2^+$ (0-0) band measured from plasma operated under fluorescence-like conditions (forward power 900 W; nebuliser gas flow rate 2.00 L $min^{-1}$; viewing height 10 mm ALC; n = 3, RSDs < 5 %)

Rotational temperatures have been calculated using OH and $N_2^+$ species for a plasma operated under fluorescence-like and conventional ICP conditions. For a plasma operated under fluorescence-like conditions $T_{rot}$ was calculated to be in the range 2700 – 3400 K and 1229 K for measurements using OH and $N_2^+$ species, respectively. This compares with 2300 – 3030 K and 1390 – 1665 K for measurements by OH and $N_2^+$ species respectively for a plasma operated under conventional emission conditions.

$T_{rot}$ measurements calculated using $N_2^+$ species are consistently lower than those obtained using OH species. This is to be expected as the $N_2$ gas addition modifies the central channel of the plasma. The addition of 15 % of a molecular gas, such as $N_2$, causes the plasma to change because molecular gases like $N_2$ absorb energy and redistribute the energy transfer processes (*e.g.* $N_2$ → $N_2^+$, $N_2^*$, $N^. + N^.$). This high percentage of nitrogen addition may cause a 'cooling' of the plasma, hence, the lower $T_{rot}$ values observed. Unfortunately, while this may be favourable for providing ground state atoms, $N_2$ is a quenching gas and would disrupt the fluorescence process.

## 4.5 Introduction to Electron Number Density

Electron number density measurements have been discussed in the literature in depth (89 – 92, 97, 114, 129, 141, 158) and can be calculated using a number of different methods. These methods include: Stark effect on hydrogen or argon lines, continuum intensity, or the Inglis-Teller method. The strong Stark effect on the Balmer series of lines of H mean that these lines are commonly used to determine the electron number density, particularly the H$\beta$ 486.1 nm line. Stark broadening is caused by the interaction of the electric field generated by the electrons and ions created by the plasma and the emitting ions (19). The relationship between the Stark effect, $\Delta\lambda_S$, the full-width-half-

maximum (FWHM; nm), and the electron number density ($m^{-3}$) is shown in Equation 4.6 (169):

$$n_e = C(n_e, T_e)\Delta\lambda_s^{3/2}10^{13} \qquad (4.6)$$

As C is a function of $n_e$, interpolation between values of the electron number densities is quite difficult. An equation based on Griems' results has been proposed that avoids the interpolation (Equation 4.7) (170):

$$n_e = (C_0 + C_1 \log \Delta\lambda)\Delta\lambda^{3/2}10^{13} \qquad (4.7)$$

where, $C_0$ is equal to 36.57, $C_1$ to $-1.72$ and $\lambda$ is expressed in Angstroms. Greig *et al.* proposed a more sophisticated formula with four derived parameters (Equation 4.8) (171):

$$n_e = [C_0 + C_1 \ln \Delta\lambda + C_2(\ln \Delta\lambda)^2 + C_3(\ln \Delta\lambda)^3]\Delta\lambda^{3/2}10^{13} \qquad (4.8)$$

where, $C_0 = 36.84$, $C_1 = -1.30$, $C_2 = -0.133$ and $C_3 = 0.0089$. A more recent formula has been proposed that includes the variation of T (K) with $\Delta\lambda$ (nm; Equation 4.9) (172):

$$n_e = C_0 + C_1 \log \Delta\lambda + C_2(\log \Delta\lambda)^2 + C_3 \log T \qquad (4.9)$$

## 4.6    Experimental: Electron Number Density Measurements

Electron number density measurements were obtained using the same instrumentation as that described in Section 4.2.2. Fluorescence-like plasma and monochromator operating parameters are given in Tables 4.14 and 4.17, respectively.

The emission intensity of the 486.1 nm Hβ line was recorded at various viewing heights ALC (10, 20 and 30 mm) and forward powers (700, 800 and 900 W). Viewing heights

greater than 30 mm ALC could not be measured due to the low intensity of the H$\beta$ 486.1 nm line at these viewing heights. Doppler broadening and instrumental broadening were determined by measuring the Ti (I) 487.014 nm line. The experiment was repeated using conventional emission conditions listed in Tables 4.14 and 4.17 so that a comparison between the two systems could be made.

**Table 4.17: SPEX monochromator operating parameters for electron number density measurements for a plasma operated under fluorescence-like and conventional emission conditions**

| SPEX Monochromator | |
| --- | --- |
| Entrance and exit slit widths | 25 $\mu$m |
| PMT voltage | 1200 V |
| Viewing height ALC | 10 – 100 mm (in 10 mm increments) |
| Lateral position | 0.0 mm (centre of the plasma) |
| **Electron number density measurements** | |
| Scan range | 485.0 - 488.0 nm |
| Step size | 0.01 nm |
| Scan speed | 0.01 nm s$^{-1}$ |

### 4.6.1 Results and Discussion: Electron Number Density Measurements

The electron density, $n_e$, was determined by measuring the Stark FWHM, $\Delta\lambda_S$, of the broadened $H_\beta$ line at 486.133 nm. Doppler broadening and instrumental broadening were determined by measuring the Ti I 487.014 nm line. The Doppler component was calculated using Equation 4.10 (9):

$$\Delta\lambda_D = 7.16x10^{-7}\left(\frac{T}{M}\right)^{1/2}\lambda \qquad (4.10)$$

where, $\Delta\lambda_D$ is the Doppler half-width, T is the temperature (K), M is the relative atomic mass of the species used (Ti = 47.9) and $\lambda$ (nm) is the spectral wavelength of the species studied. As the Doppler half-width is temperature dependent, values were calculated from 2000 – 10000 K in 100 K increments.

The instrumental broadening was calculated using Equation 4.11:

$$\Delta\lambda_{ins} = [(\Delta\lambda_{1/2}(Ti(I)487.014))^2) - (\Delta\lambda_D)^2]^{1/2} \qquad (4.11)$$

where, $\Delta\lambda_{1/2}$ is the FWHM of the Ti I 487.014 nm line. The variation of Doppler broadening with temperature means that the instrumental broadening also needed to be calculated for the range 2000 – 10000 K.

Values of $C(n_e,T_e)$ below 5000 K were not found in the literature and so had to be interpolated from values obtained from Griem (173). Graphs of electron number density against temperature were plotted and the gradient of the line determined. For T = 2500 K, $C(n_e,T_e)$ was calculated to be 3.86 x $10^{20}$, 3.69 x $10^{20}$ and 3.45 x $10^{20}$ when $n_e$ equalled $10^{20}$, $10^{21}$ and $10^{22}$ m$^{-3}$, respectively.

For a plasma operated under conventional emission conditions, electron number densities were calculated using Equations 4.7, 4.8 and 4.9 (Hill's, Grieg's and Czernikowski's theories, respectively) and values are plotted in Figure 4.13. Figures 4.14 – 4.16 illustrate the effect of forward power and viewing height ALC on electron number density, for a plasma operated under fluorescence-like conditions.

Figure 4.13 (conventional emission conditions) demonstrates that as the viewing height ALC increases the electron number density decreases. This was to be expected and has been described in the literature (89 – 92, 97, 114, 129, 141, 158). Calculated electron number densities were similar, irrespective of which theory was used to calculate the values. There was typically less than 1 % variation in values between Hill's and Greig's method but this variation increased to 20 % when Czernikowski's method was considered. It is known that Czernikowski's method provides slightly higher values and these are considered by some to correspond to more accurate values (174). In the literature, electron number densities of 1.00 (169), 1.02 (175), 1.01 (171) and 0.93 (172) x $10^{21}$ m$^{-3}$ have been observed for a plasma operated under conventional conditions. These values agree closely to those calculated.

Figures 4.14 – 4.16 (fluorescence-like conditions) illustrate that, again there was less typically than 1 % variation in values between Hill's and Greig's method and this variation increased to 20 % when Czernikowski's method was considered. However, in this case, Czernikowski's method gave lower values than those calculated by the other two methods. Figures 4.14 – 4.16 show that the electron number density increases with increasing forward power and viewing height ALC. The increase in electron number density with increasing forward power was to be expected but the values calculated for increasing viewing heights ALC show a different trend to that illustrated in Figure 4.13.
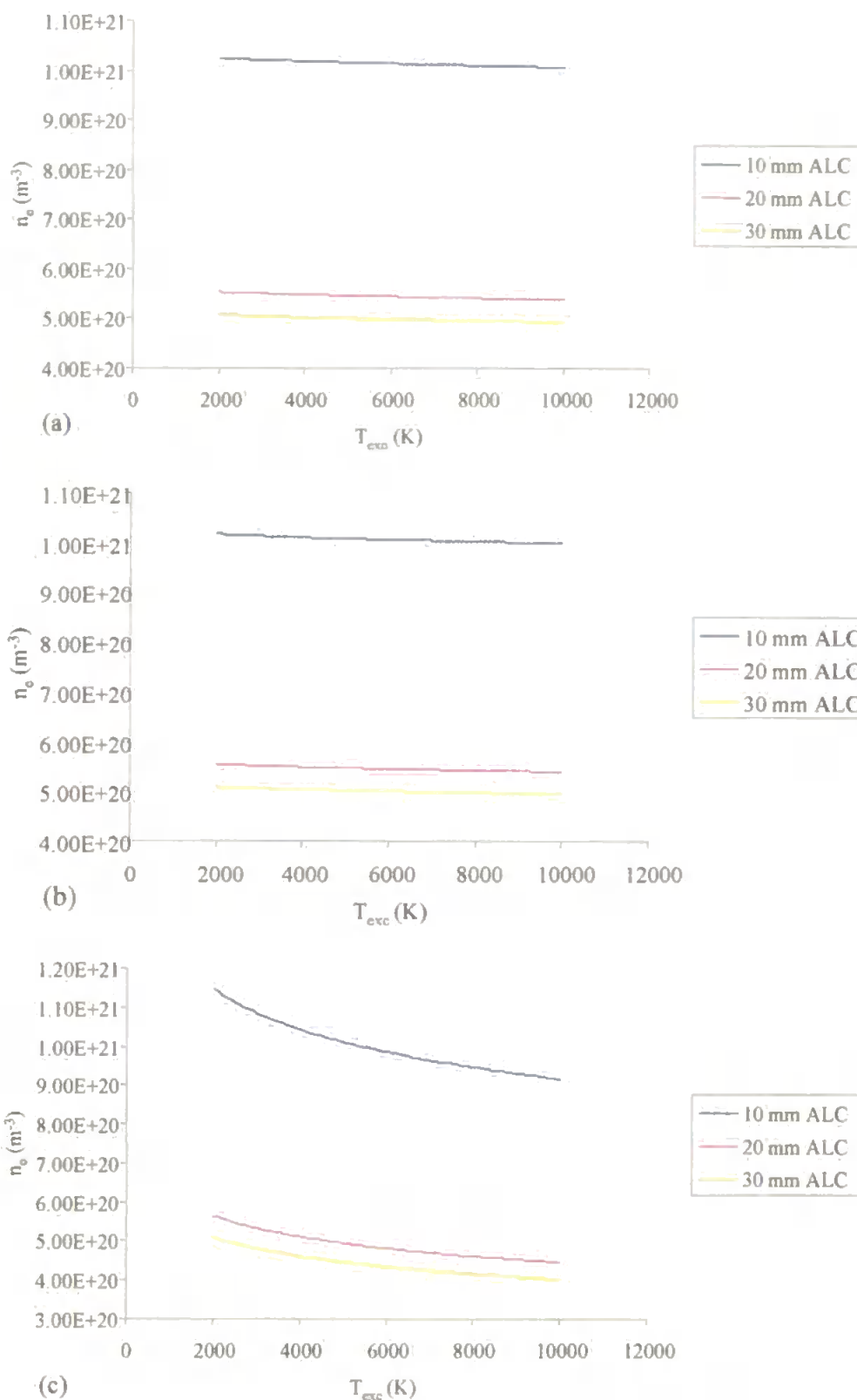
Figure 4.13: Variation of electron number density for a plasma operated under conventional emission conditions (forward power 1200 W; nebuliser gas flow rate 0.80 L min$^{-1}$; viewing heights 10 - 30 ALC) calculated using (a) Hill's, (b) Greig's and (c) Czernikowski's theories (n = 3, RSDs < 5 %)
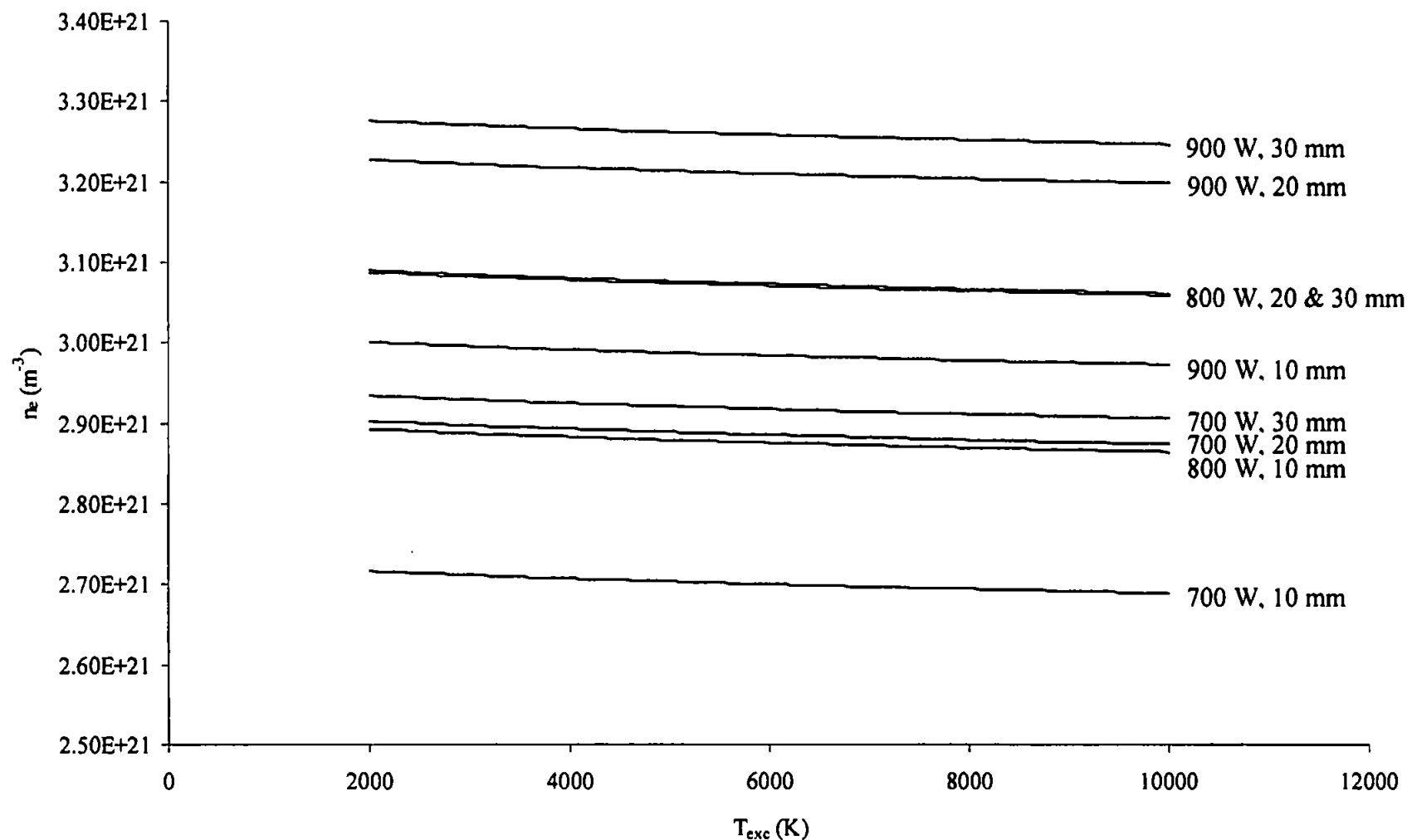
**Figure 4.14: Variation in electron number densities calculated for a plasma operated under fluorescence-like conditions (forward powers 700 – 900 W; nebuliser gas flow rate 2.00 L min⁻¹) at various viewing heights ALC calculated using Hill's theory (n = 3, RSDs < 5 %)**
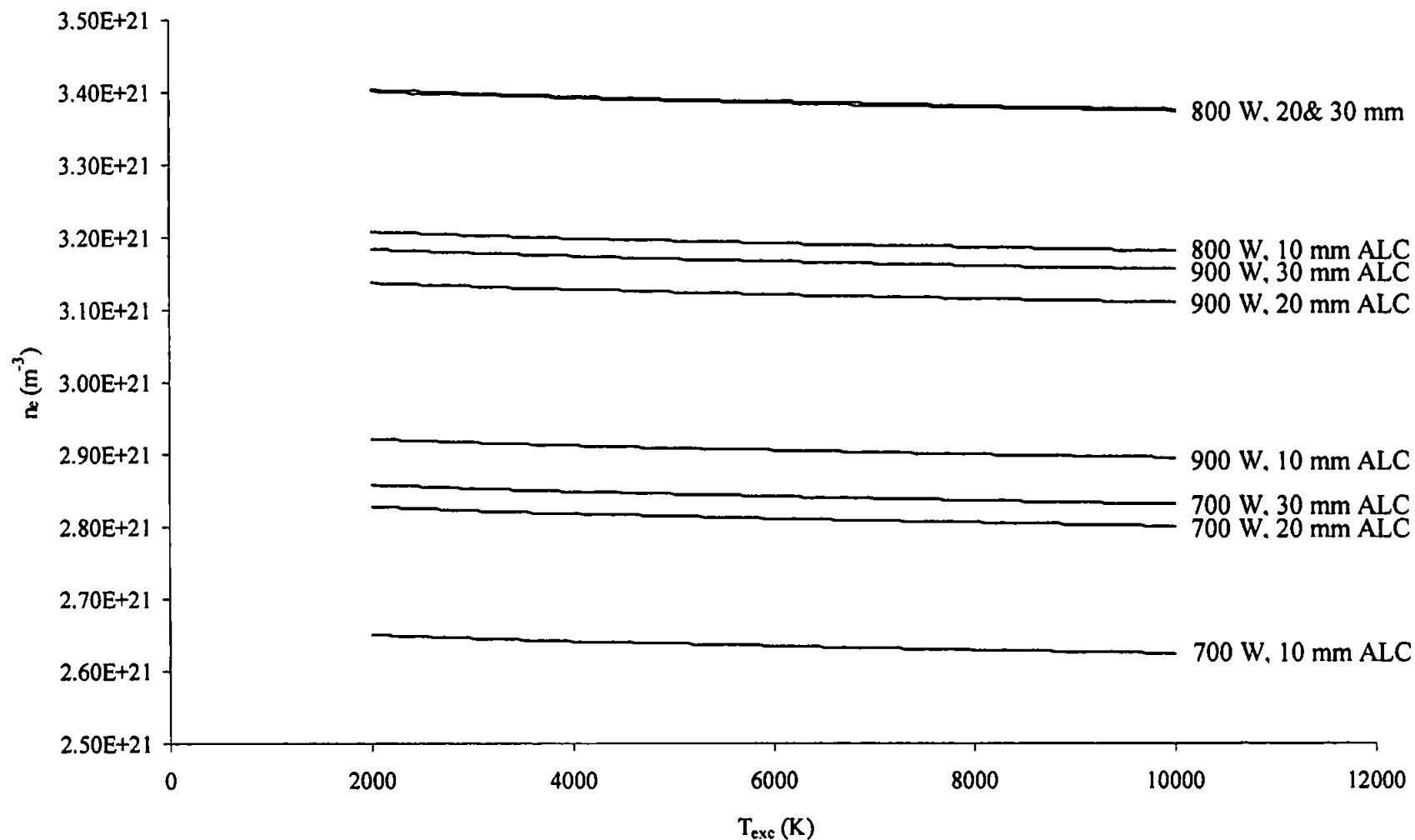
**Figure 4.15: Variation of electron numbers densities calculated for a plasma operated under fluorescence-like conditions (forward powers 700 – 900 W; nebuliser gas flow rate 2.00 L min$^{-1}$) at various viewing heights ALC calculated using Greig's theory (n = 3, RSDs < 5 %)**

The y-axis is labeled $n_e$ (m$^{-3}$) with values from 2.50E+21 to 4.30E+21.

The x-axis is labeled $T_{exc}$ (K) with values from 0 to 12000.

Curve labels (top to bottom):
900 W, 30 mm ALC
900 W, 20 mm ALC
800 W, 20 & 30 mm
900 W, 10 mm ALC
700 W, 30 mm ALC
700 W, 20 mm ALC
800 W, 10 mm ALC
700 W, 10 mm ALC
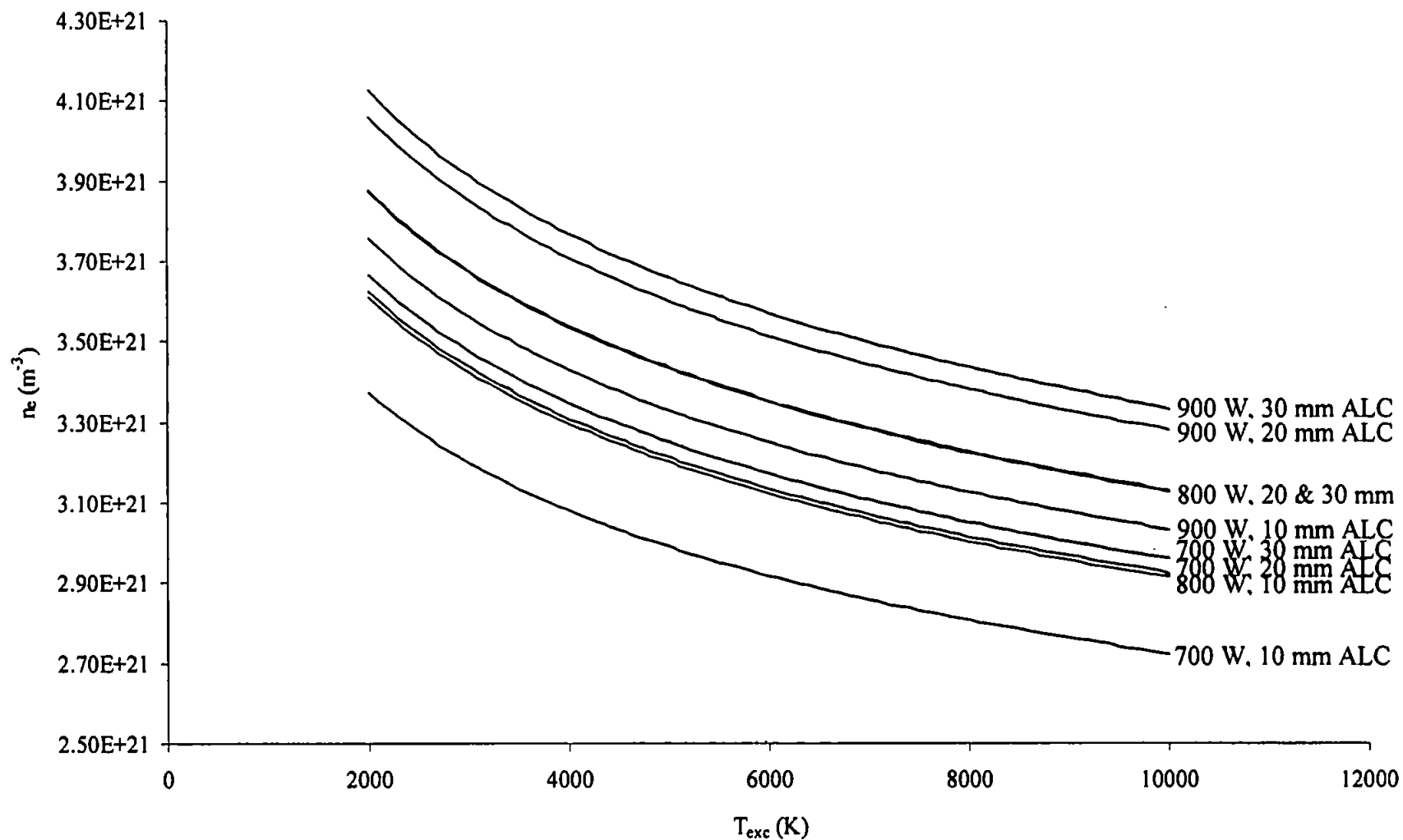
**Figure 4.16:** Variation of electron numbers densities calculated for a plasma operated under fluorescence-like conditions (forward powers 700 – 900 W; nebuliser gas flow rate 2.00 L min$^{-1}$) at various viewing heights ALC calculated using Czernikoswki's theory (n = 3, RSDs < 5 %)

The possibilities that need to be considered are: it is a real effect of the generator coupling system used to generate the plasma, there are self absorption changes for $H\beta$ 486.1 nm line with viewing height ALC, or there is a change of excitation profile with increasing viewing height ALC.

Comparison of Figures 4.14 – 4.16 show that the values for electron density obtained from a plasma operated under fluorescence-like conditions are greater than those obtained from a plasma operated under conventional emission conditions. For a plasma operated under conventional emission conditions the electron number density decreased considerably as the viewing height ALC increased, whereas there was less variation from the plasma operated under fluorescence-like conditions. This was not what was expected and could be due to any of the reasons mentioned previously. It must be noted that this effect could also be due to the different conditions under which the measurements were performed. It was not a simple case of comparing electron number densities as the power decreased. For a plasma operated under conventional emission conditions, the nebuliser gas flow rate was 0.80 L min$^{-1}$ and the sample uptake rate was 1.0 ml min$^{-1}$. When the plasma was operated under fluorescence-like conditions the nebuliser gas flow rate was 2.0 L min$^{-1}$ and the sample uptake rate was 2.0 ml min$^{-1}$. It may be that electron density measurements cannot be performed as accurately using such extreme conditions and an alternative approach would be necessary to confirm these trends.

The electron number density calculations for a plasma operated under fluorescence-like conditions suggest one possible reason why fluorescence has not been observed for this instrument. As stated in Section 4.1 by Raejmakers *et al.* (127) "...the spatially resolved measurement of only one parameter, e.g. the electron density ($n_e$) or the electron temperature ($T_e$) is necessary and sufficient to characterise the discharge...". Given this

is correct and that the trends observed are real, this suggests that the plasma is not performing as it should under this particular set of conditions. This may be why, despite all the components of the experimental arrangement being calibrated and proven to work individually, the conditions do not produce a plasma suitable for the production of fluorescence. To test this theory another plasma generator (which became available for use at a very late stage in the project) was used in an attempt to try and observe fluorescence using the same equipment and similar conditions to those used in the Optima 3000 fluorescence experiments.

## 4.7   Summary

The Line Pair Intensity Ratio Method was used to calculate the effect on excitation temperature from varying the forward power, nebuliser gas flow rate and viewing height ALC, when the plasma was operated under fluorescence-like and conventional emission conditions using the Optima's own detection system. For a plasma operated under fluorescence-like conditions (forward powers 700 – 900 W; nebuliser gas flow rates 1.50 – 3.00 L min$^{-1}$), $T_{exc}$ decreases with decreasing forward power and increasing viewing heights (0 – 30 mm ALC). Temperatures ranged from 2100 - 2700 K. For a plasma operated under conventional emission conditions (forward power 1200 W; nebuliser gas flow rate 0.80 L min$^{-1}$), $T_{exc}$ was in the range 2000 – 3000 K. Excitation temperatures (calculated by the LPIR method) were obtained using the SPEX monochromator as a detector and showed greater variation compared with those determined by the Optima detection system but the trends established were the same. Using the SPEX monochromator as a detector, excitation temperatures ranged from 1770 – 3060 K and 2530 – 2860 K for a plasma operated under fluorescence-like and conventional emission conditions, respectively.

The radial profile for $T_{exc}$ at a viewing height of 15 mm ALC from the central position of the plasma out to 3.2 mm for forward powers of 700, 800 and 900 W was calculated. Values ranged from 2270 K at the centre (0 mm) up to 2360 K at 3.2 mm and for any given lateral position, $T_{exc}$ increased with increasing forward power. The profiles obtained show some structure and the edge of the atom channel could be visualised. As the forward power was increased, the edge of the atom channel 'moved' closer towards the centre of the plasma. This was as expected, because as the forward power was increased there should have been less dispersion of the central channel as the plasma increasingly resists 'punching'.

Excitation temperatures were calculated using the Boltzmann Distribution. $T_{exc}$ ranged from 3130 – 3600 K and from 4940 – 5540 K at viewing heights of 10 – 100 mm ALC for a plasma operated under fluorescence-like (forward powers 700 – 900 W; nebuliser gas flow rate 2.00 L min$^{-1}$) and conventional emission conditions (forward powers 1200 W; nebuliser gas flow rate 0.80 L min$^{-1}$), respectively. $T_{exc}$ obtained from the Boltzmann Distribution show good agreement with literature values, however, $T_{exc}$ values obtained from the LPIRM appeared to be lower. Plots of the Boltzmann Distribution were curved and not straight lines. The 'degree' of curvature may be indicative whether the plasma conditions are closer to, or deviating further from, LTE. The Boltzmann Distribution plots were more curved at the lower viewing heights ALC and higher forward powers suggesting that the plasma operated under fluorescence-like conditions were closer to LTE at lower forward powers and higher viewing heights ALC.

Rotational temperatures have been calculated using OH and $N_2^+$ species for a plasma operated under fluorescence-like (forward powers 700 – 900 W; nebuliser gas flow rate 2.00 L min$^{-1}$) and conventional emission conditions (forward powers 1200 W; nebuliser

gas flow rate 0.80 L min$^{-1}$) at viewing heights of 10 – 80 mm ALC. For a plasma operated under fluorescence-like conditions $T_{rot}$ was calculated to be in the range 2700 to 3400 K and 1250 K for measurements by OH and $N_2^+$ species, respectively. This compares to 2300 – 3030 K and 1390 – 1665 K for measurements by OH and $N_2^+$ species, respectively for a plasma operated under conventional emission conditions.

For a plasma operated under conventional emission conditions (forward power 1200 W; nebuliser gas flow rate 0.80 L min$^{-1}$; viewing heights 0 – 30 mm ALC), calculated electron number densities typically varied by less than 1 % between Hill's and Greig's method but this variation increased to 20 % when Czernikowski's method was used. It is known that Czernikowski's method provides slightly higher values and may be considered to be more accurate. Literature values agree closely to those calculated.

Electron density values obtained from a plasma operated under fluorescence-like conditions (forward powers 700 – 900 W; nebuliser gas flow rate 2.00 L min$^{-1}$) at viewing heights of 0 – 30 mm ALC were greater than those obtained from a plasma operated under conventional emission conditions. For a plasma operated under conventional emission conditions the electron number density decreased considerably as the viewing height ALC increased whereas there was less variation from the plasma operated under fluorescence-like conditions. This was unexpected and could be due: to a real effect of the generator coupling system used to produce the plasma, self absorption changes for the Hβ 486.1 nm line with change in viewing height ALC, or change of excitation profile with increasing viewing height ALC.

The electron number density calculations for a plasma operated under fluorescence-like conditions suggest a possible reason why fluorescence has not been observed. The values obtained suggest that the plasma is not performing as one would expect under this particular set of conditions. This may be why, despite all the components of the

experimental arrangement being proven to work individually, the conditions used did not create a plasma suitable for the production of fluorescence. To test this theory another plasma generator (which became available for use at a very late stage in the project) was to be used in an attempt to try and observe fluorescence using the same equipment and similar conditions to those used in the Optima 3000 ICP fluorescence experiments.

# 5.0 A COMPARISON OF RADIAL EXCITATION WITH AXIAL EXCITATION FLUORESCENCE

## 5.1 Introduction

Previous chapters show the instrumental development and the modifications necessary to use a commercial ICP for both radial and axial excitation fluorescence experiments. The plasma conditions used were comparable to those described in the literature (29 – 32, 66) but no fluorescence was observed. Diagnostic studies were performed as described in Chapters 3 and 4 to provide a greater understanding of the plasma operated under fluorescence-like conditions through a comparison with a plasma operated under conventional emission conditions. These studies showed that $T_{exc}$, calculated using the Boltzmann Distribution ranged from 3130 – 3600 and from 4940 – 5540 K for a plasma operated under fluorescence-like (forward power 700 – 900W; nebuliser gas flow rate 2.00 L min$^{-1}$; sample uptake rate 2.00 ml min$^{-1}$) and conventional emission conditions (forward power 1200W; nebuliser gas flow rate 0.80 L min$^{-1}$; sample uptake rate 0.80 ml min$^{-1}$), respectively. Using OH species, $T_{rot}$ was calculated to be in the range 2700 – 3400 K and 2300 – 3030 K for a plasma operated under fluorescence-like and conventional emission conditions, respectively. For an Optima 3000 ICP operated under conventional emission conditions, calculated electron number densities agree closely to those calculated in the literature. Values obtained from this plasma operated under fluorescence-like conditions were greater than those obtained from the plasma operated under conventional emission conditions. This was not what was expected and could be due to: a real effect of the generator coupling system producing the ICP; self absorption changes for Hβ 486.1 nm line with viewing height ALC, or a change of Hβ excitation profile with increasing viewing height ALC.

Another generator became available for use at a very late stage in the project and when used, under the optimum conditions determined in Chapters 3 and 4, fluorescence was obtained almost immediately. This chapter describes the use of HCLs and LEDs as excitation sources and the use of an ICP as an atomiser, for both radial and axial excitation fluorescence for Ba, Mg, Li and Na atomic species. Preliminary diagnostic measurements using the emission intensities from Fe atom and OH species were also performed in an attempt to further explain the differences between the plasmas produced from the two generators used and why fluorescence was observed on one system and not the other.

## 5.2 Experimental: Preliminary Optimisation Studies using Ba, Li, Mg and Na for Radial Excitation Fluorescence Experiments

HCLs (Ba and Mg, Starna, Romford, Essex, UK) and LEDs (Li and Na, TOSBright, RS Components, Corby, Northants, UK) controlled by the 'purpose-built' Lamp/LED unit previously described in Section 3.2 were used as excitation sources for the optimisation experiments. A bi-convex silica lens (50 mm diameter, 50 mm focal length, L.O.T. Oriel, Leatherhead, Surrey, UK) was used in a 2f:2f (inverted) arrangement to focus the light emission from the HCL/LED onto the plasma tailflame.

A radially viewed plasma, produced by the torch box and generator assembly from an alternative ICP (PlasmaQuad PQ2 Thermo Elemental, Winsford, Cheshire, UK) was used as the atom cell. The instrument was equipped with an ICP-MS demountable plasma torch fitted with a glass injector (1.5 mm i.d.; Figure 5.1), a 'Scott-type' double pass spray chamber, and an Ebdon low-back pressure high solids nebuliser (P.S. Analytical, Orpington, Kent, UK). The detection system comprised a fibre optic (1000 μm core diameter HPSUV1000P; Oxford Electronics Ltd., Four Marks, Hampshire,

UK), optical filters $\lambda_{max}$ 280 (Mg I 285.213 nm), 460 (Ba II 455.403 nm), 580 (Na I 589.0 nm) and 680 (Li I 670.80 nm) nm, (Model Nos. 5325 & 5370, L.O.T. Oriel), a PMT (IP 28, Hamamatsu Photonics UK Ltd., Welwyn Garden City, Hertfordshire, UK) operated by a high voltage power supply (Model 456, EG & G Ortec, Oakridge, USA), and a lock-in amplifier (Model 9503, EG & G Brookdeal, Bracknell, Berkshire, UK). A schematic of the experimental arrangement used for the optimisation studies is shown in Figure 5.2.
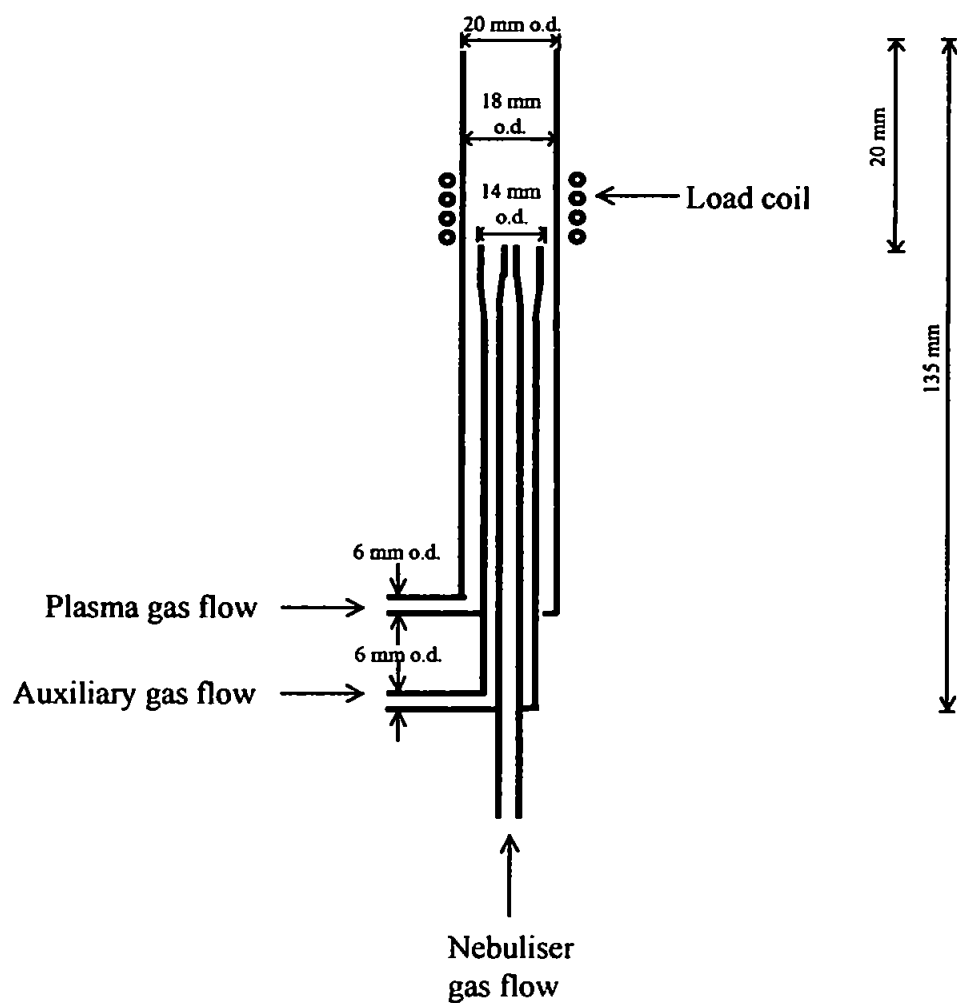
**Figure 5.1: Schematic of the plasma torch used for fluorescence experiments using the Thermo Elemental ICP system**
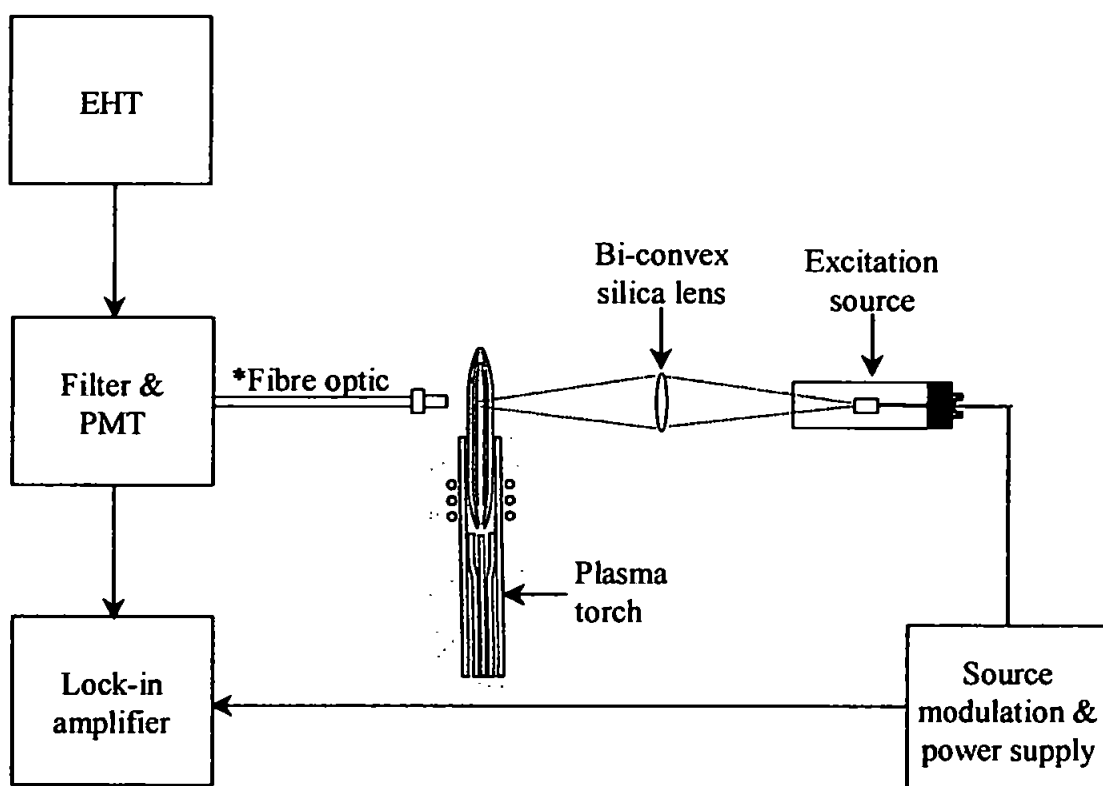
* Fibre optic is positioned at right angles to the excitation source (out of plane of paper schematic)

**Figure 5.2: Schematic of the experimental arrangement used for preliminary radial excitation fluorescence optimisation experiments utilising a Thermo Elemental ICP**

A series of univariate searches were used to ascertain the boundary conditions and help optimise plasma performance. The main parameters to be optimised were viewing height ALC, nebuliser gas flow rate and forward power as these are considered to be the most critical (2). The plasma coolant and auxiliary gas flow rates were also optimised, although, these are considered to be less critical. The range of instrumental operating conditions used is given in Table 5.1. The boundary conditions were set at 60 – 120 mm for the viewing height ALC, 1.50 – 3.00 L min$^{-1}$ for the nebuliser gas flow rate, 300 – 900 W for the forward power, 8 – 15 L min$^{-1}$ for the plasma gas flow rate and 0.0 – 1.0 L min$^{-1}$ for the auxiliary gas flow rate. The fluorescence emission lines of the analytes of interest (Ba, Li, Mg and Na) are presented in Table 5.2. Preliminary HCL and LED operating conditions are presented in Table 5.3.

Optimum conditions were evaluated by measuring the fluorescence emission intensity from the aspiration of a 100 µg ml$^{-1}$ standard of each of the analytes (Ba, Li, Mg and Na). The signal to background ratio was used as the criterion of merit for the optimisation.

## 5.2.1  Chemicals and Reagents

Reagents used in this work were of 'AnalaR' reagent grade (Merck, Poole, Dorset, UK) and all solutions were prepared using doubly deionised water (Milli-Q, Millipore, Harrow, Middlesex, UK) and stabilised with nitric acid to a concentration of 2 %.

Calibration standards were prepared by serial dilution of commercially available stock standard solutions (Ba, Li, Mg and Na, 1000 or 10000 µg ml$^{-1}$).

**Table 5.1: ICP instrument parameters used in preliminary radial excitation fluorescence optimisation studies utilising a Thermo Elemental ICP**

| RF Generator | |
|---|---|
| Frequency | 27.1 MHz, free running |
| Power | 300 - 900 W (in 25 W increments) |
| **Sample Introduction System** | |
| Nebuliser | Ebdon, low back-pressure high solids |
| Torch | Demountable with 1.5 mm i.d. silica injector |
| Spray Chamber | Scott Double Pass, water cooled |
| Peristaltic Pump | Gilson Minipuls 3, computer controlled |
| Sample Uptake Rate | 2.0 ml min$^{-1}$ |
| **Argon Flow Rate** | |
| Plasma | 8 - 15 L min$^{-1}$ (in 1.0 L min$^{-1}$ increments) |
| Auxiliary | 0.0 – 1.0 L min$^{-1}$ (in 0.10 L min$^{-1}$ increments) |
| Nebuliser | 1.50 - 3.00 L min$^{-1}$ (in 0.25 L min$^{-1}$ increments) |

**Table 5.2: Line selection for analytes of interest used in preliminary radial excitation fluorescence optimisation studies**

| Excitation source | Element | Analytical line (nm) |
|---|---|---|
| HCL | Ba | Ba II 455.403 |
| | Mg | Mg I 285.213 |
| LED | Li | Li I 670.800 |
| | Na | Na I 589.000 |

**Table 5.3: HCL and LED operating conditions used in preliminary radial excitation fluorescence optimisation studies**

| Operating parameter | |
|---|---|
| HCL primary current | 6 mA |
| LED operating current | 20 mA |
| HCL/LED modulation frequency | 667 Hz |
| Duty cycle | 50% |

### 5.2.2 Results and Discussion: Preliminary Radial Fluorescence Optimisation Studies of Ba, Li, Mg and Na using a Thermo Elemental ICP

The preliminary optimum plasma parameters derived from the univariate searches are presented in Table 5.4 for the various analyte lines. Figures 5.3 and 5.4 illustrate the effects of forward power and nebuliser gas flow rate on fluorescence signal for the Mg 283. 213 nm line. The range of conditions determined (Table 5.4) agree closely with those found in the literature (29 – 32, 66) and those used in the Optima 3000 ICP experiments.

:
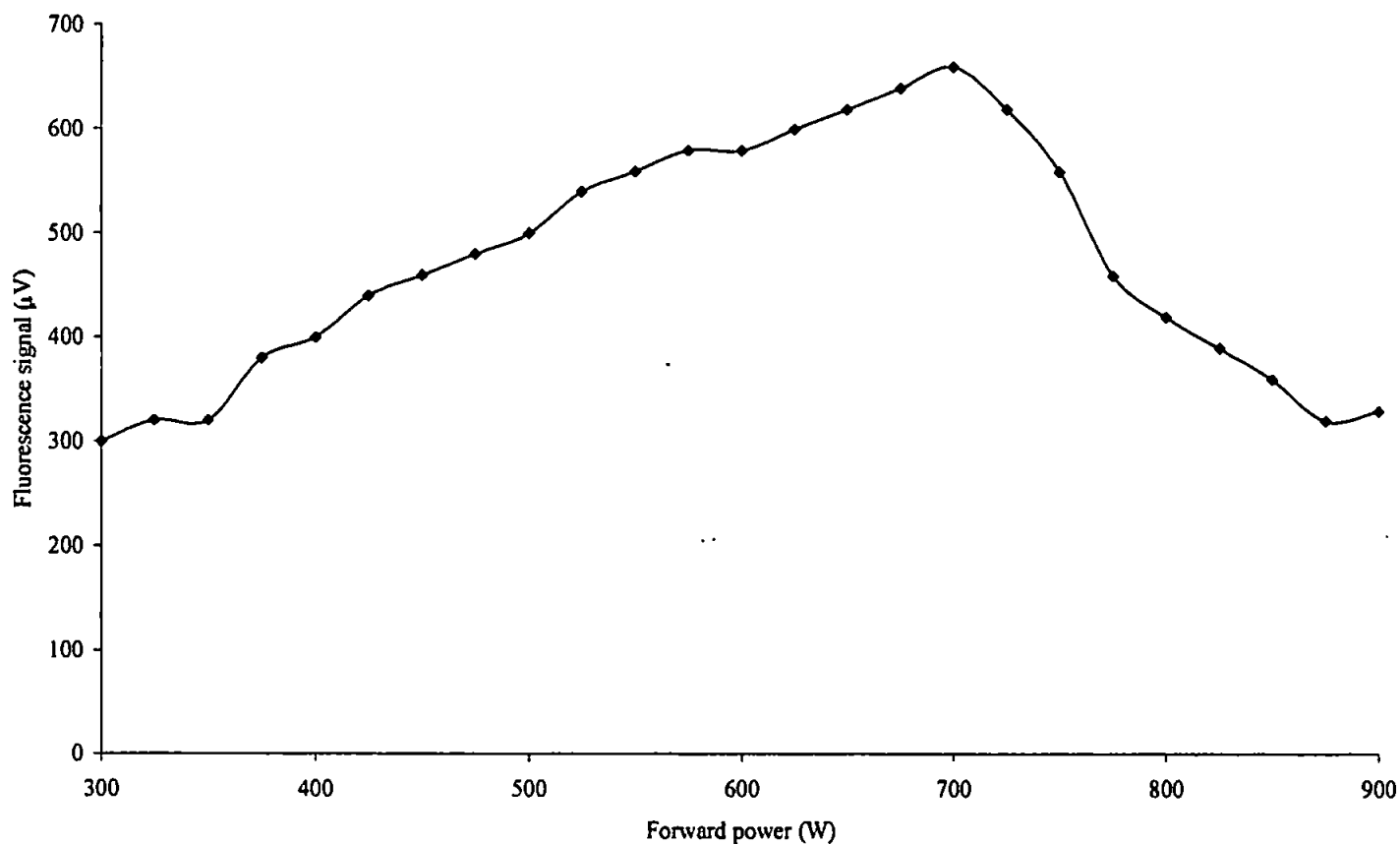
Figure 5.3: Effect of forward power on Mg I 285. 213 nm fluorescence signal in preliminary optimisation experiments utilising a Thermo Elemental ICP operated under fluorescence conditions (plasma gas flow rate 10 L min$^{-1}$; nebuliser gas flow rate 2.00 L min$^{-1}$; auxiliary gas flow rate 0.80 L min$^{-1}$; viewing height 60 mm ALC; n = 5, RSDs < 5%)
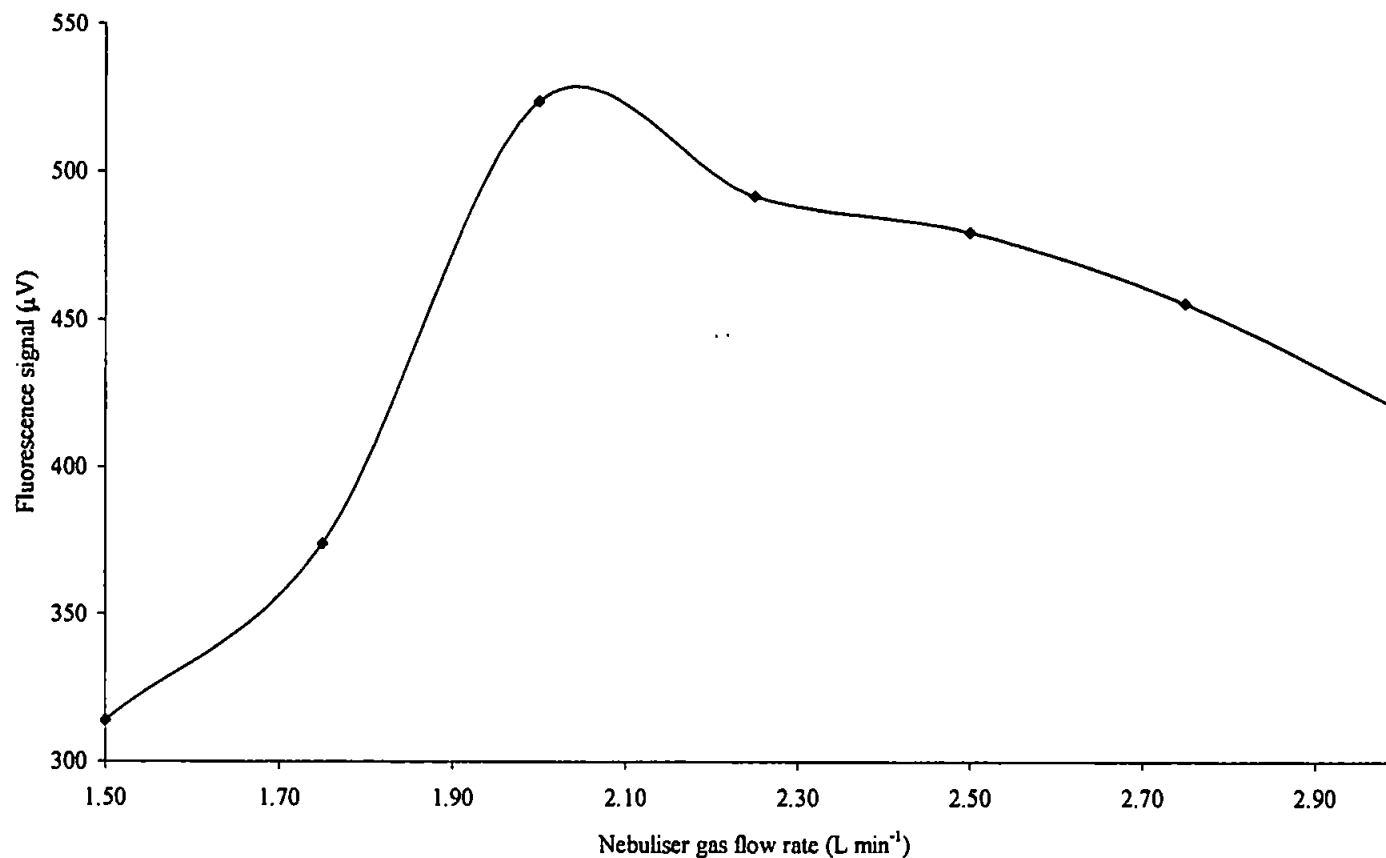
**Figure 5.4: Effect of nebuliser gas flow rate on Mg I 285. 213 nm fluorescence signal in preliminary optimisation experiments utilising a Thermo Elemental ICP operated under fluorescence conditions (forward power 700 W; plasma gas flow rate 10 L min$^{-1}$; auxiliary gas flow rate 0.80 L min$^{-1}$; viewing height 60 mm ALC; n = 5, RSDs < 5%)**

**Table 5.4: Preliminary optimum operating conditions determined from radial excitation fluorescence experiments obtained using a univariate search**

| Excitation source | Current (mA) | Element | Wavelength (nm) | Power (W) | Viewing height ALC (mm) | Gas flow rate (L min⁻¹) Nebuliser | Plasma | Auxiliary |
|---|---|---|---|---|---|---|---|---|
| HCL | 15 | Ba | 455.403 | 750 | 70 | 2.25 | 10 | 0.20 |
|  | 6 | Mg | 285.213 | 700 | 60 | 2.00 | 10 | 0.80 |
| LED | 20 | Li | 670.800 | 500 | 80 | 2.50 | 14 | 0.50 |
|  | 20 | Na | 589.000 | 475 | 80 | 2.00 | 9 | 0.20 |

:

## 5.3 Experimental: Optimisation of Modulation Frequency and Duty Cycle for HCLs

Using the preliminary optimum conditions determined for Mg presented in Table 5.4, the study was extended and the modulation frequency and duty cycle of the excitation source were optimised. A schematic of the experimental arrangement used to optimise the modulation frequency and the duty cycle is shown in Figure 5.5. The mean primary current of the Mg HCL per unit time was kept constant at 6 mA whilst the modulation frequencies and duty cycles investigated were the same as those summarised in Chapter 3 (Section 3.2.1, Table 3.1).

### 5.3.1 Results and Discussion: Optimisation of Modulation Frequency and Duty Cycle for HCLs

Using the preliminary optimum conditions determined for Mg (Table 5.4) and the optimum lamp current determined in Section 3.4.5.2, the effect of modulation frequency and duty cycle on fluorescence signal was investigated. These results are presented in Figure 5.6.

As the fluorescence signal is proportional to the source intensity it would be expected that the harder the lamp was pulsed, the greater the fluorescence signal observed. In this experiment, for any given modulation frequency, the lamp primary current would be equivalent to 150, 75, 50, 37.5 and 7.5 mA for a 10, 20, 30, 40 and 50 % duty cycle, respectively. Therefore, one would expect the maximum fluorescence signal to be observed when the lamp was driven at its hardest (*i.e.* 10 % duty cycle, 1042 Hz modulation frequency). However, Figure 5.6 showed that the maximum fluorescence signal was obtained with a modulation frequency of 542 Hz and a duty cycle of 30 %. There could be two possible explanations for this effect. Firstly, when the lamp is

operated at duty cycles of 20 % or less, it may not have had sufficient reactance time to reach the maximum lamp primary current. Secondly, when the lamp was operated at the higher modulation frequencies, the lamp was being switched on and off so rapidly that the maximum lamp primary current was not reached. A combination of these two effects could result in the maximum fluorescence signal being observed when the lamp was operated under less extreme conditions. Also, as stated previously, the possibility of self absorption effects when the lamp is driven hard at shorter duty cycles is noted.

The results presented in Figure 5.6 support the results obtained in Chapter 3 (Section 3.4.1) Figure 3.13 showed that the excitation temperature, $T_{exc}$, of the lamp was dependent upon duty cycle and to a smaller extent modulation frequency. $T_{exc}$ was found to vary with the duty cycle in the order 30 % > 40 % > 50 % > 20 % > 10%. The same trend is shown in Figure 5.6 for fluorescence signal. The optimum operating conditions, a modulation frequency of 542 Hz and duty cycle of 30 %, were used for all subsequent experiments.

LEDs were not optimised for the effects of modulation frequency and duty cycle due to time constraints. The same optimum conditions used for the HCL were used for all the LED experiments.
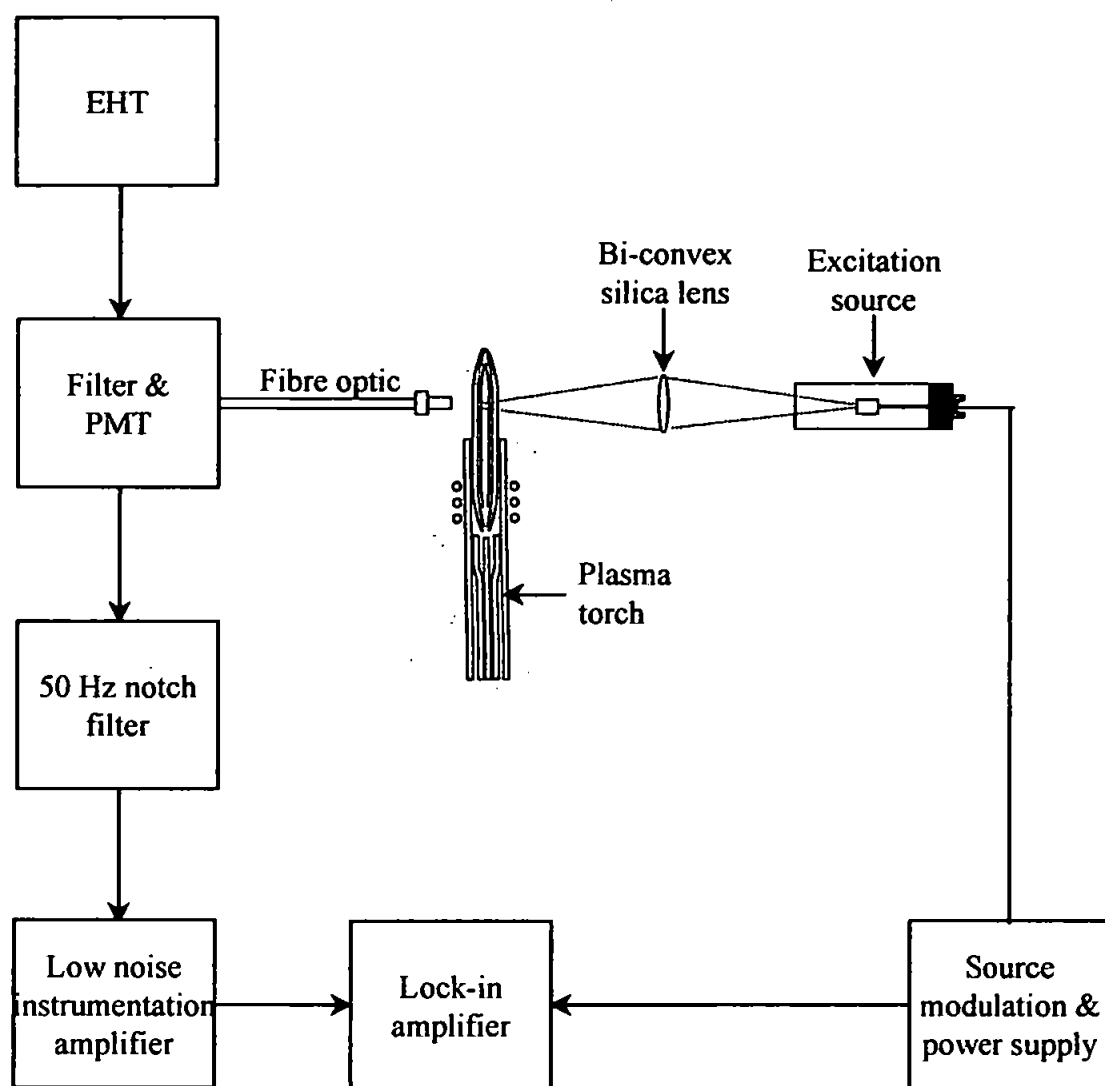
**Figure 5.5: Schematic of the experimental arrangement used to optimise HCL modulation frequency and duty cycle utilising the Thermo Elemental ICP**
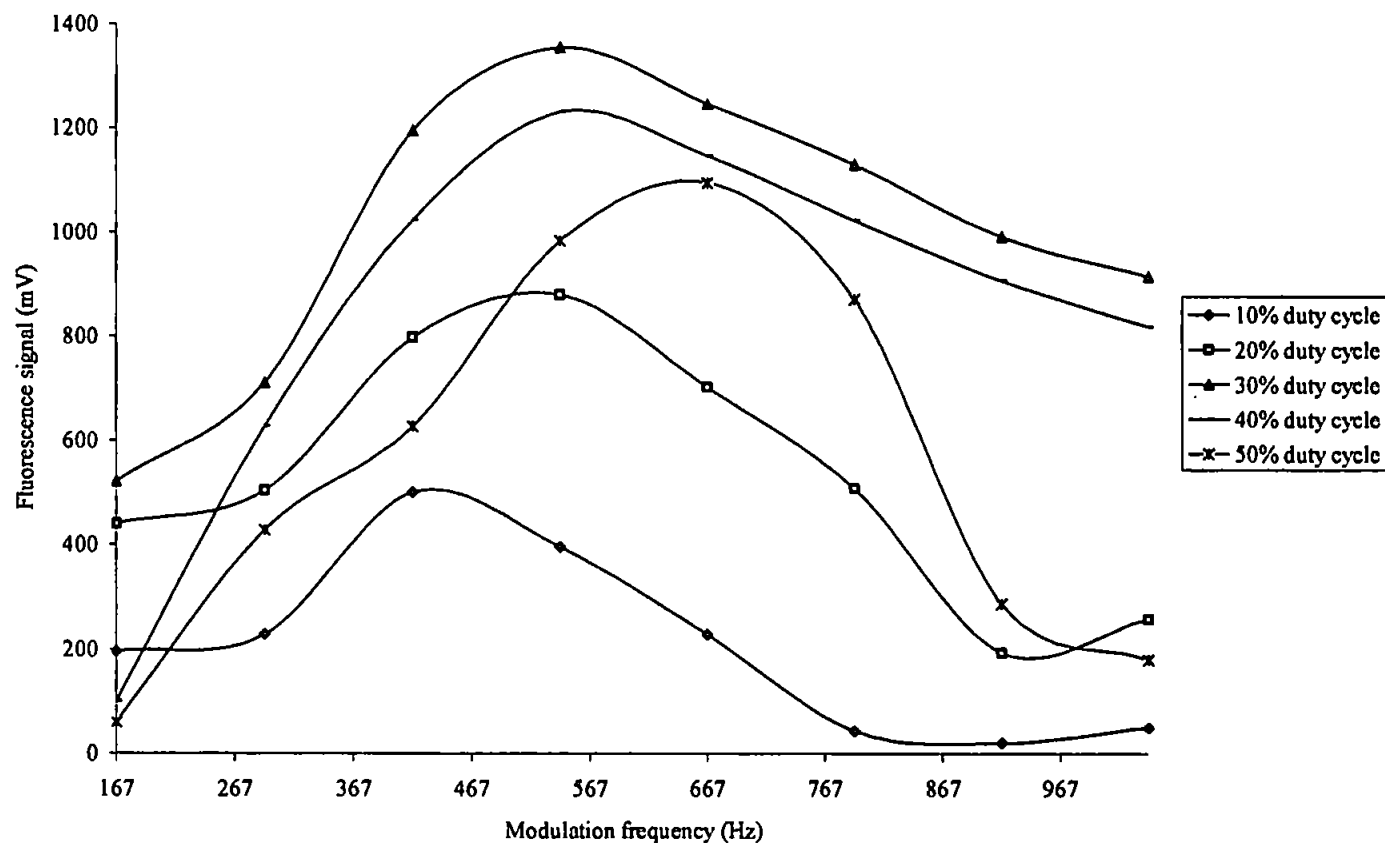
Figure 5.6: Effect of varying modulation frequency and duty cycle on Mg I 285.213 nm radial excitation fluorescence signal utilising a Thermo

Elemental ICP (forward power 700 W; plasma gas flow rate 10 L min⁻¹; nebuliser gas flow rate 2.00 L min⁻¹; auxiliary gas flow rate 0.80 L

min⁻¹; viewing height 60 mm ALC; n = 5, RSDs < 5%)

## 5.4 Experimental: Radial Excitation Fluorescence Linear Range and Limits of Detection for Ba, Li, Mg and Na

### 5.4.1 Linear Range for Ba, Li, Mg and Na

Using the optimum conditions presented in Table 5.4 and Section 5.3.1, a series of standards (0.001 - 100 μg ml$^{-1}$) of Ba, Li, Mg and Na were aspirated into the plasma in order to create a calibration curve for each analyte of interest and establish their linear ranges.

### 5.4.2 Detection Limits for Ba, Li, Mg and Na

Using the previously determined optimum conditions (Table 5.4), the LOD for each element was calculated using Equation 5.1 (3):

$$LOD = x_{bl} + 3 s_{bl} \qquad (5.1)$$

where, $x_{bl}$ is the mean blank signal and $s_{bl}$ is the standard deviation of the blank.

### 5.4.3 Results and Discussion: Linear Range and Limits of Detection

#### 5.4.3.1 Linear Range

Using the optimum parameters given in Table 5.4, calibration curves were plotted for each of the elements studied. Results are shown in Figure 5.7. The calibration showed excellent linearity over 5 orders of magnitude ($R^2$ values range from 0.99995 to 1.0000) and the precision on each data point was better than 5 %.

232
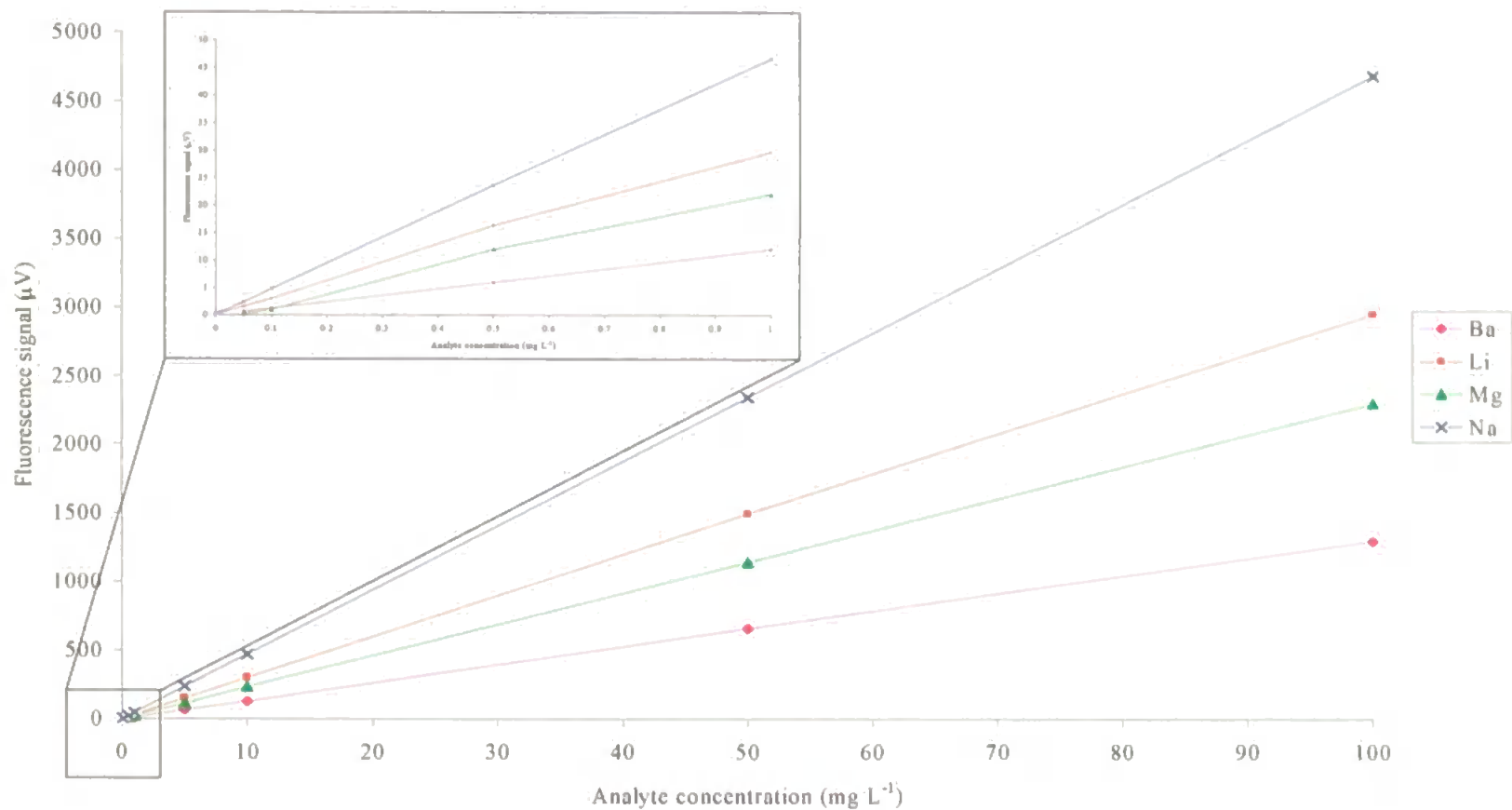
**Figure 5.7:** Radial fluorescence calibration curves for Ba, Li, Mg and Na solutions covering the concentration range 0.001 to 100 mg L$^{-1}$

utilising the Thermo Elemental ICP (n =3, RSDs < 5 %)

## 5.4.3.2 Limits of Detection

Limits of detection were calculated using Equation 5.1 and determined to be 27.6, 0.51, 0.43 and 0.20 µg L$^{-1}$ for Ba, Li, Mg and Na, respectively. These LODs are of the same order of magnitude as those obtained by HCL-ICP-AFS. A comparison of the LODs obtained for this system with the LODs listed in Tables 1.7 and 1.8 (Chapter 1, Section 1.5.6) for HCL-ICP-AFS (25, <0.1, <0.1 and <0.1 µg l$^{-1}$ for Ba, Li, Mg and Na, respectively) show that the values obtained are approaching those of a commercial system. This was despite the fact that the experimental arrangement used was still being refined and many improvements could have been made in terms of collection efficiency and optical coupling.

## 5.5 Experimental: Radial and Axial Excitation Fluorescence Profiling of the ICP

### 5.5.1 Instrumentation Required for Profiling Studies using Radial Excitation Fluorescence

The instrumentation used for radial excitation fluorescence experiments was identical to that used for the optimisation experiments described in Section 5.2.1.

The lamp emission from an HCL (6 and 15 mA primary current for Mg and Ba respectively, 667 Hz modulation frequency, 50 % duty cycle) was focused at a particular viewing height ALC and the fibre optic (1000 µm core diameter HPSUV1000P; Oxford Electronics Ltd.) used for detection aligned at a 90° angle. Using the optimum plasma conditions given in Table 5.4 vertical profiles of the plasma were obtained for Ba, Li, Mg and Na by measuring a 100 µg ml$^{-1}$ standard at different viewing heights ALC. The signal to background ratio was used as the criterion of merit.

## 5.5.2 Instrumentation Required for Profiling Studies using Axial Excitation Fluorescence

The instrumentation used for axial excitation fluorescence experiments was similar to that used in Section 5.2.1 with the exception of the experimental arrangement. A schematic of the instrumental arrangement operated in axial excitation fluorescence mode using the Thermo Elemental ICP is shown in Figure 5.8.

For the axial excitation fluorescence experiments two lens systems were investigated.

1.  A focusing lens (50 mm diameter; 50 mm focal length; L.O.T. Oriel) was used to focus the excitation source emission from a HCL/LED at a particular viewing height ALC.

2.  A collimating lens (18 mm diameter; 100 mm focal length; Speirs Robertson Ltd., Bromham, Bedford, UK) was used to illuminate the whole length of the tailflame at once.

Axial excitation fluorescence profiles of the plasma were obtained by measuring a 100 $\mu$g ml$^{-1}$ standard solution of Ba, Li, Mg and Na at viewing heights of 60 – 120 mm ALC (10 mm increments). The signal to background ratio was used as the criterion of merit. The fibre optic used for detection was aligned at a 90° angle at a range of viewing heights ALC to collect the fluorescence.

The effect of LED operating current on fluorescence signal was investigated using both a focusing and a collimating lens system. For the Li and Na LEDs, the optimum plasma conditions were used (Table 5.4) and the fibre optic (used for detection) was positioned at the viewing height ALC that gave the maximum fluorescence signal in the axial profiles (80 mm ALC for Li and Na). The light emission from the LED was either focused at this point or was collimated along the whole length of the plasma tailflame.

The fluorescence signal was measured when a 100 μg ml$^{-1}$ standard was aspirated into

the plasma. The signal to background ratio was used as the criterion of merit.
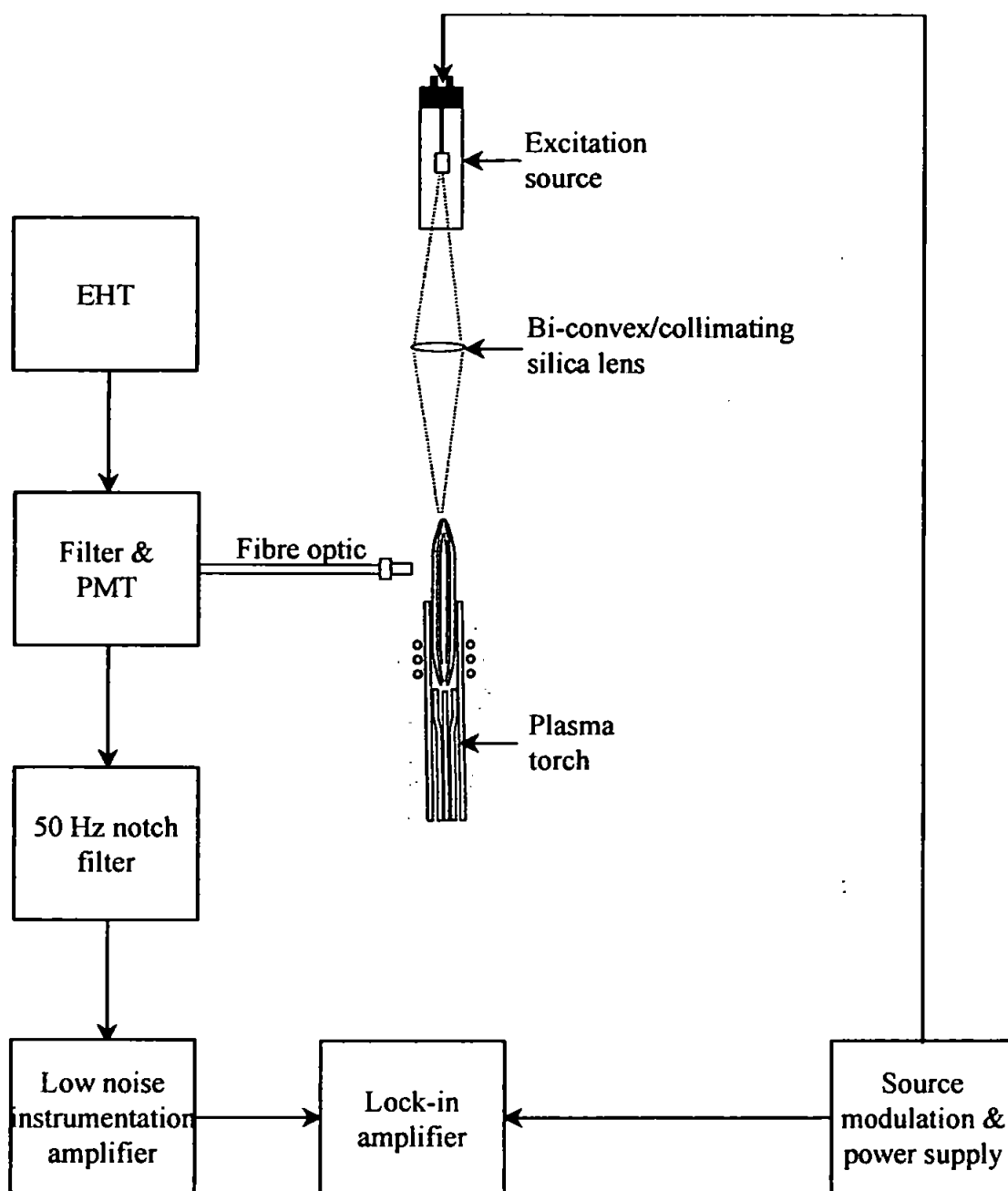
**Figure 5.8: Schematic of experimental arrangement used for axial excitation fluorescence experiments utilising a Thermo Elemental ICP**

### 5.5.3 Results and Discussion: Vertical Plasma Profile using Radial Excitation Fluorescence

The results from the profiling studies using radial excitation fluorescence are presented in Figure 5.9. Figure 5.9 shows that there is a relatively sharp optimum for viewing height ALC and that the fluorescence signal observed was much greater for Li and Na than for Ba and Mg. This has been attributed to source intensity of the LEDs being greater than that of the HCLs. Optimum viewing heights for the ASIA system have been reported as 70, 72 and 84 mm ALC for Ba, Li and Na respectively (158). These agree closely with those determined in this study.

An attempt was made to measure the fluorescence signal at viewing heights of less than 60 mm ALC. Unfortunately, coupling of the RF power to the detection system prevented a stable signal from being obtained.

:
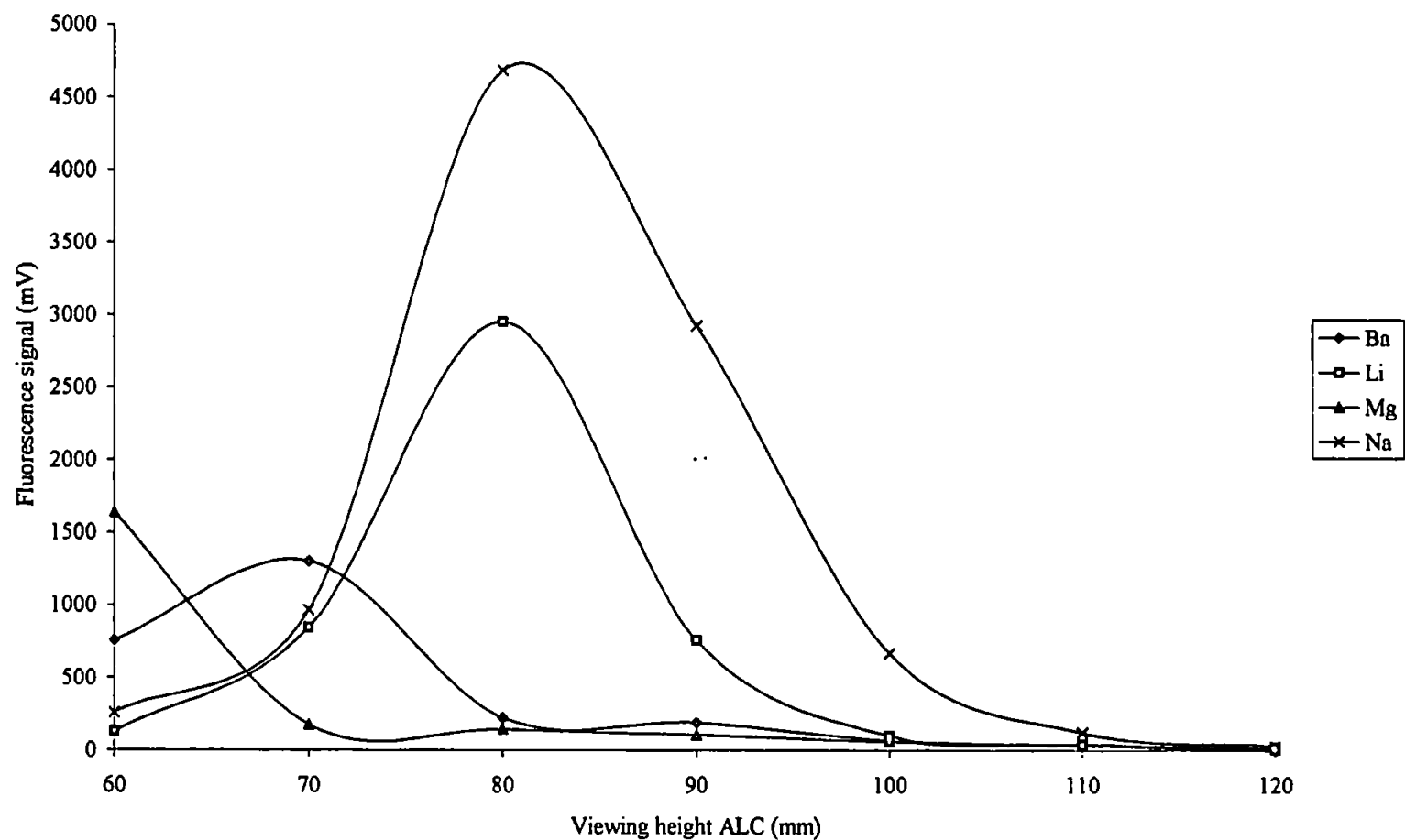
**Figure 5.9: Results from a profiling study using radial excitation fluorescence signal for Ba, Li, Mg and Na utilising a Thermo Elemental ICP**

**(n = 3, RSDs < 5 %)**

### 5.5.4 Results and Discussion: Vertical Plasma Profile using Axial Excitation Fluorescence

Axial profiles of the plasma could not be obtained for Ba and Mg as the light emission produced from the HCLs was not sufficiently intense to produce a measurable fluorescence signal. However, using the optimum conditions determined in Section 5.3.1 for Li and Na, vertical profiles of the plasma, using axial excitation, were obtained using the more intense LEDs. These results are presented in Figure 5.10.

Figure 5.10 shows that there was a relatively sharp optimum, of fluorescence signal, with respect to the viewing height ALC. The optimum viewing height ALC was identical to that determined from the vertical profiles of the plasma, using radial excitation fluorescence. It was also independent of the use of focusing or collimating lens conditions. This suggests that, irrespective of the excitation arrangement employed, only particular conditions produced in the plasma give the optimum conditions for fluorescence and that these are spatially dependent.

LEDs have a broad bandwidth of between 10 – 20 nm and will illuminate any species that has a transition in this range. Although the calibration curve for Li and Na is linear there could be an Ar atom or ion line, or another species, present that will give a constant value or a high background. For each analyte line of interest there were no Ar atom or ion lines of sufficient intensity that could potentially interfere with the primary Li or Na line. However, as background correction was employed, if an Ar interference was measured this would be removed.

Two different lens systems were investigated. Initially, a focusing lens was used to focus the light emission from the excitation source at a particular viewing height ALC
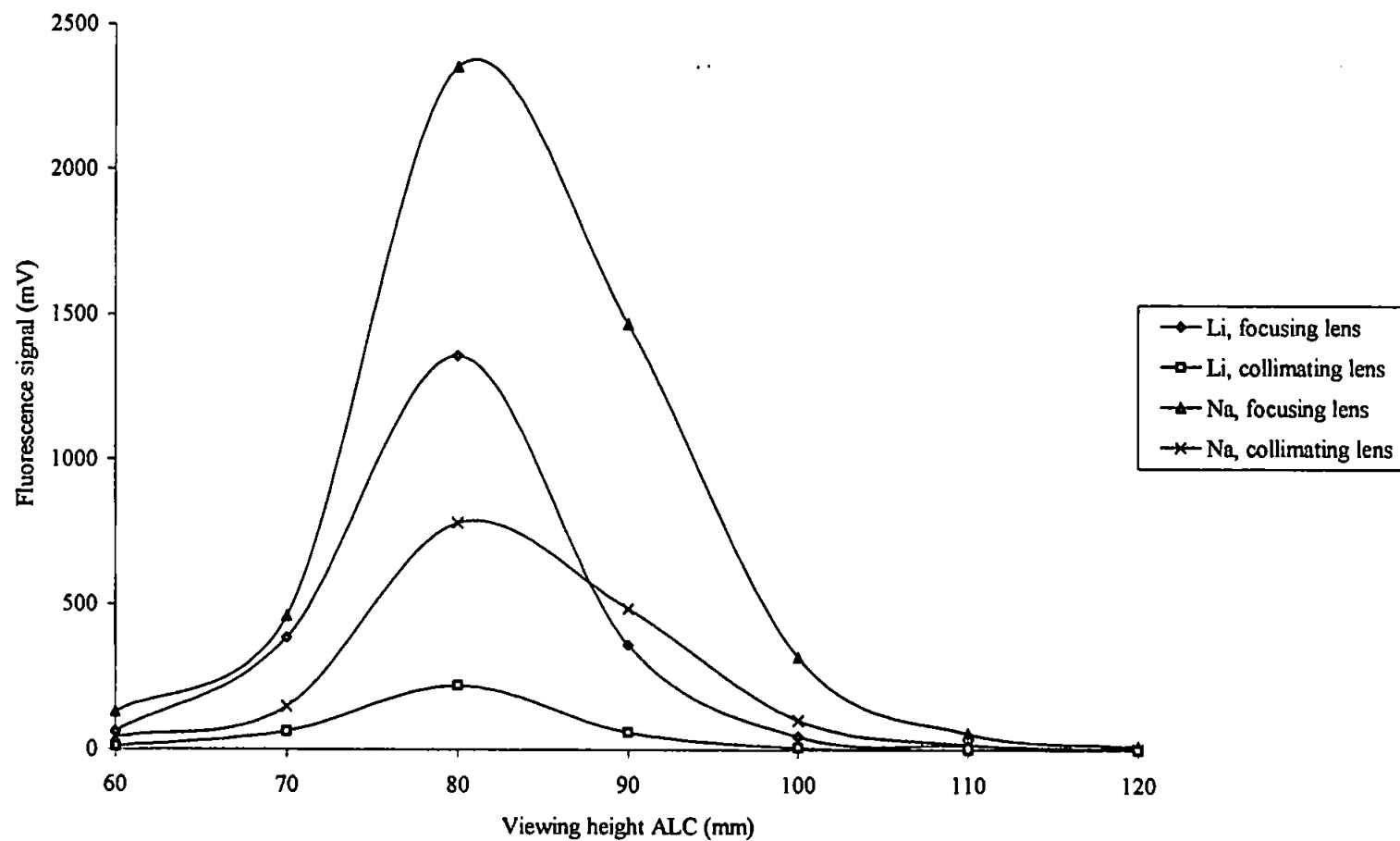
**Figure 5.10: Results from a profiling study using axial excitation fluorescence for Li and Na utilising a Thermo Elemental ICP**

**(n = 3, RSDs < 5 %)**

in the plasma tailflame and the fluorescence radiation measured. The axial profile (Figure 5.10) obtained shows that, despite an optimum fluorescence signal being observed at a particular viewing height ALC, there was a detectable fluorescence signal at other viewing heights ALC. This suggests that if the axial fluorescence radiation could be collected along and around the whole length of the tailflame at any one time then lower limits of detection could be possible. One way to achieve this broad excitation of the central channel of the tailflame was to use a collimating lens to produce a narrow beam of light of equal intensity along the length of the plasma tailflame. Using this set-up the fluorescence radiation was collected and an axial profile plotted. Unfortunately, as Figure 5.10 shows the intensity of the fluorescence signal produced was less than that produced using a focusing lens. The loss of intensity was such that even if the fluorescence signal measured along the whole length of the tailflame was summed then the signal obtained would be less than that observed at the optimum viewing height ALC using a focusing lens arrangement. This is somewhat surprising as it would be expected that the LOD would be decreased using axial excitation as opposed to radial excitation. If the whole of the excitation energy is being absorbed down the length of the tailflame then fluorescence must be produced where it is absorbed. As the cell size is increased when using axial excitation, rather than radial, decreased LODs would be expected. It would appear that, in this case, either the collimated excitation beam was being attenuated in some way or an inner filter effect was present. Another possibility is that the ground state atom cloud is sharply defined over a short distance in the plasma, in which case the fluorescence cell cannot be extended by the use of axial excitation. However, the most likely explanation is due to the experimental arrangements used for the radial and axial excitation experiments. For the radial excitation fluorescence experiments, the excitation source and the focusing lens used were very close to the plasma tailflame. For the axial excitation experiments

242

the excitation source and collimating lens were further away from the end of the plasma tailflame. As fluorescence signal is proportional to the source intensity, then the difference in intensity of the source would result in a lower fluorescence signal being observed.

These results suggested the potential for axial excitation fluorescence. If a system could be designed with focused axial excitation fluorescence in mind, and with improved collection efficiency (*e.g.* the use of an integrating sphere or a cylindrical lens system), then lower limits of detection should be possible. The use of a very high intensity axial excitation beam would be necessary for a collimated system but this could easily be achieved with the use of a tuneable laser.

The effect of the LED operating current on fluorescence signal of Li using both a focusing and a collimating lens system is shown in Figure 5.11. Using both lens systems, the relationship between current and fluorescence obtained was linear, however, using the focusing lens system resulted in a more intense fluorescence signal.

The use of the LEDs as excitation sources has much potential, as one of their major advantages is that they are considerably cheaper (£0.10 - £2.00 each) than existing excitation sources (HCLs, BDHCLs, lasers) However, there are some potential disadvantages. The LEDs currently available have a relatively large spectral bandwidth (10 – 20 nm). The use of a monochromator between the LED and the atom cell would isolate a small portion of the spectral bandwidth and should enable the LED to be used effectively as an element selective source although the intensity will be decreased. Interference from concomitant species with excitation lines in this region should be greatly reduced. This could prove to be an advantage. A series of LEDs could be used to cover the wavelength range 300 – 700 nm. If the LEDs were incorporated into commercial instruments then this is a possibility of producing a multi-element

243
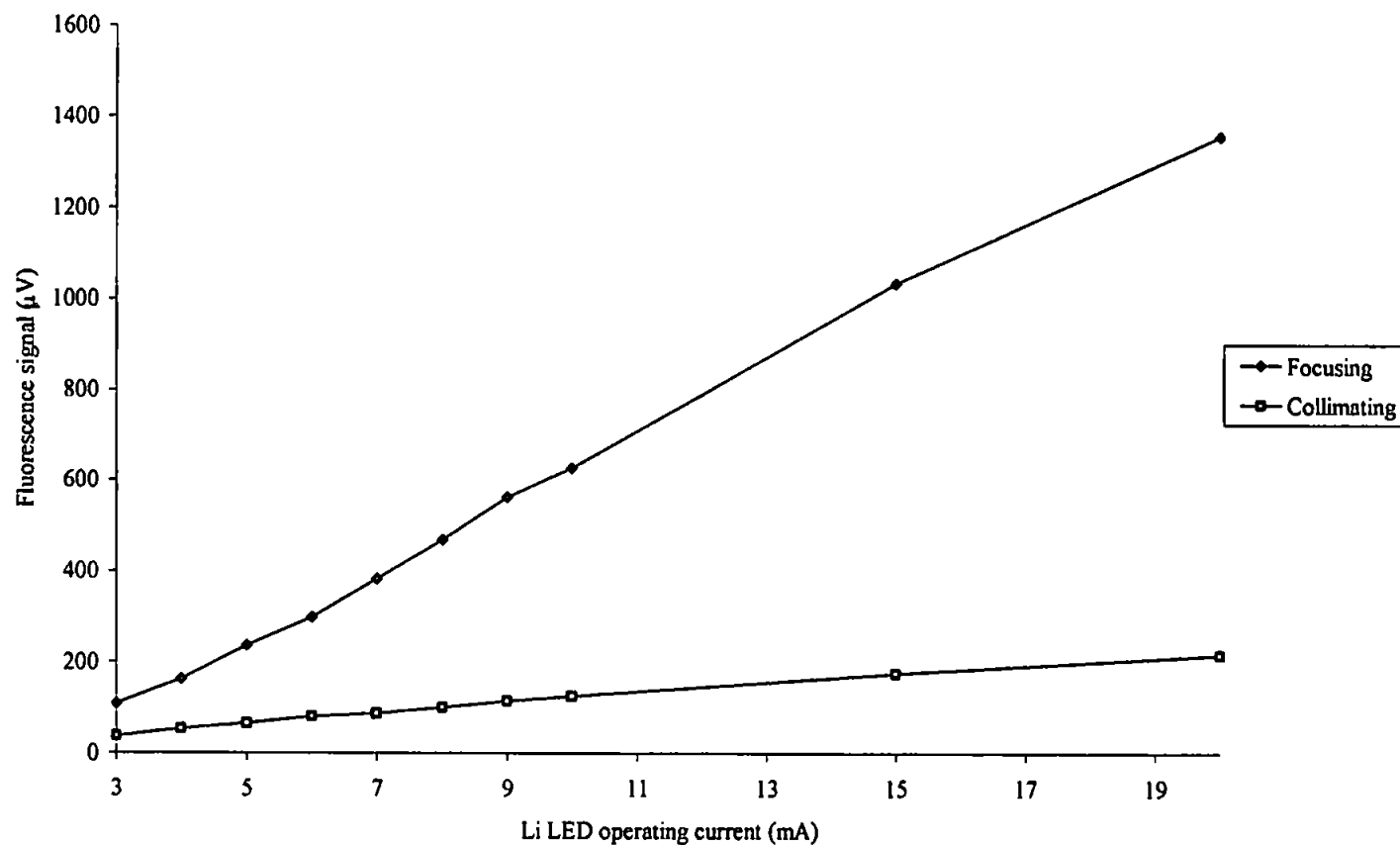
**Figure 5.11: Effect of LED operating current on fluorescence signal of Li at 100 mg l⁻¹ utilising a Thermo Elemental ICP (forward power 500 W; plasma gas flow rate 14 L min⁻¹; nebuliser gas flow rate 2.50 L min⁻¹; auxiliary gas flow rate 0.50 L min⁻¹; viewing height 75 mm ALC; n = 3, RSDs < 5%)**

capability instrument. This instrument could therefore be switched between ICP-AES or -AFS mode depending on the element to be analysed.


## 5.6    Experimental: Diagnostic Excitation and Rotational Temperature Measurements of Fe and OH Species

Temperature measurements were performed on the recently acquired Thermo Elemental ICP in the same manner as those described in Chapter 4 (Sections 4.2 – 4.4). This was undertaken in order to try and characterise any differences between the plasma produced by the Thermo Elemental ICP and that previously produced by the Optima 3000 ICP under conditions required to produce fluorescence. The experimental conditions used on the Thermo Elemental ICP are described in Table 5.5.

**Table 5.5: Experimental conditions used for excitational and rotational temperature measurements utilising a Thermo Elemental ICP**

| RF Generator | |
|---|---|
| Frequency | 27.1 MHz, crystal controlled |
| **ICP-AFS conditions** | |
| Power | 300, 500, 700 and 900 W |
| **Sample Introduction System** | |
| Nebuliser | Meinhard cross–flow |
| Torch | Demountable (illustrated in Figure 5.1) |
| Spray Chamber | Scott Double Pass, water cooled |
| Peristaltic Pump | Gilson Minipuls 3, computer controlled |
| Sample Uptake Rate | 2.0 ml min$^{-1}$ |
| **Argon Flow Rate** | |
| Plasma | 10 L min$^{-1}$ |
| Auxiliary | 0.2 L min$^{-1}$ |
| Nebuliser | 2.00 L min$^{-1}$ |
| **SPEX Monochromator** | |
| Entrance and exit slit widths | 25 $\mu$m |
| PMT voltage | 1200 V |
| Viewing height ALC | 10 – 100 mm (in 10 mm increments) |
| Lateral position | 0.0 mm (centre of the plasma) |
| **Fe LPIRM and Boltzmann distribution measurements** | |
| Scan range | 360 - 400 nm |
| Step size | 0.1 nm |
| Scan speed | 0.1 nm s$^{-1}$ |
| **OH molecular species** | |
| Scan range | 306.5 - 310.0 nm |
| Step size | 0.01 nm |
| Scan speed | 0.01 nm s$^{-1}$ |

## 5.6.1 Results and Discussion: Temperature Measurements

Excitation temperatures ($T_{exc}$, Fe I species) obtained using the Boltzmann Distribution and the Line Pair Intensity Ratio Method are presented in Tables 5.6 and 5.7. An example plot of the Boltzmann Distribution is given in Figure 5.12.

Rotational temperature measurements were determined using the OH (0-0) rotational band spectra. These results are presented in Table 5.8. The $N_2$ rotational band could not be used to determine the rotational temperature because a sufficiently intense spectrum was not observed.

Table 5.6 showed that there was a decrease in $T_{exc}$ as the viewing height ALC increased and as the power decreased. These results were as expected but there was a significant difference between the excitation temperatures obtained using the Boltzmann distribution and those determined using the LPIRM (Table 5.8). However, it is well known that the LPIRM can be (although not always) less accurate than the Boltzmann distribution and is only used to follow the relative variation of the excitation temperature when one or several parameters of the plasma are modified. The trends established in Table 5.7 are identical to those found in Table 5.6. The only difference between the two being that the values are higher when determined by the LPIRM.

A comparison of $T_{exc}$ obtained by the Boltzmann Distribution method using two different instruments but operated under supposedly 'identical conditions' gives a possible explanation into why fluorescence was observed using the Thermo Elemental ICP but not on the Optima 3000 ICP. Table 5.6 showed that at a viewing height of 20 mm ALC, $T_{exc}$ was 3740 K for a 900 W plasma. This compares with a $T_{exc}$ of 3430 K for a plasma operated under 'identical conditions' for the Optima instrument (Chapter 4, Section 4.2.4.2, Table 4.10).

**Table 5.6: T_exc (K) calculated using the Boltzmann Distribution from a Thermo Elemental ICP operated under fluorescence conditions (plasma gas flow rate 10 L min$^{-1}$; nebuliser gas flow rate 2.00 L min$^{-1}$; auxiliary gas flow rate 0.20 L min$^{-1}$; n = 3, RSDs < 5 %)**

| Power (W) | 900 | 700 | 500 | 300 |
|---|---|---|---|---|
| Viewing height ALC (mm) | | | | |
| 10 | n/d | n/d | n/d | n/d |
| 20 | 3740 | 3330 | 3220 | 3140 |
| 30 | 3210 | 3270 | 3260 | n/d |
| 40 | 3050 | 3140 | n/d | n/d |
| 50 | 3080 | n/d | n/d | n/d |
| 60 | n/d | n/d | n/d | n/d |
| 70 | n/d | n/d | n/d | n/d |
| 80 | n/d | n/d | n/d | n/d |
| 90 | n/d | n/d | n/d | n/d |
| 100 | n/d | n/d | n/d | n/d |

n/d = not detected

**Table 5.7: T_exc calculated using the LPIRM from a Thermo Elemental ICP operated under fluorescence conditions (plasma gas flow rate 10 L min$^{-1}$; nebuliser gas flow rate 2.00 L min$^{-1}$; auxiliary gas flow rate 0.20 L min$^{-1}$; n = 3, RSDs < 5 %)**

| Power (W) | 900 | 700 | 500 | 300 |
|---|---|---|---|---|
| Viewing height ALC (mm) | | | | |
| 10 | n/d | n/d | n/d | n/d |
| 20 | 4030 | 3660 | 3840 | 4640 |
| 30 | 3760 | 3680 | 4180 | n/d |
| 40 | 3750 | 3630 | n/d | n/d |
| 50 | 3650 | n/d | n/d | n/d |
| 60 | n/d | n/d | n/d | n/d |
| 70 | n/d | n/d | n/d | n/d |
| 80 | n/d | n/d | n/d | n/d |
| 90 | n/d | n/d | n/d | n/d |
| 100 | n/d | n/d | n/d | n/d |

n/d = not detected
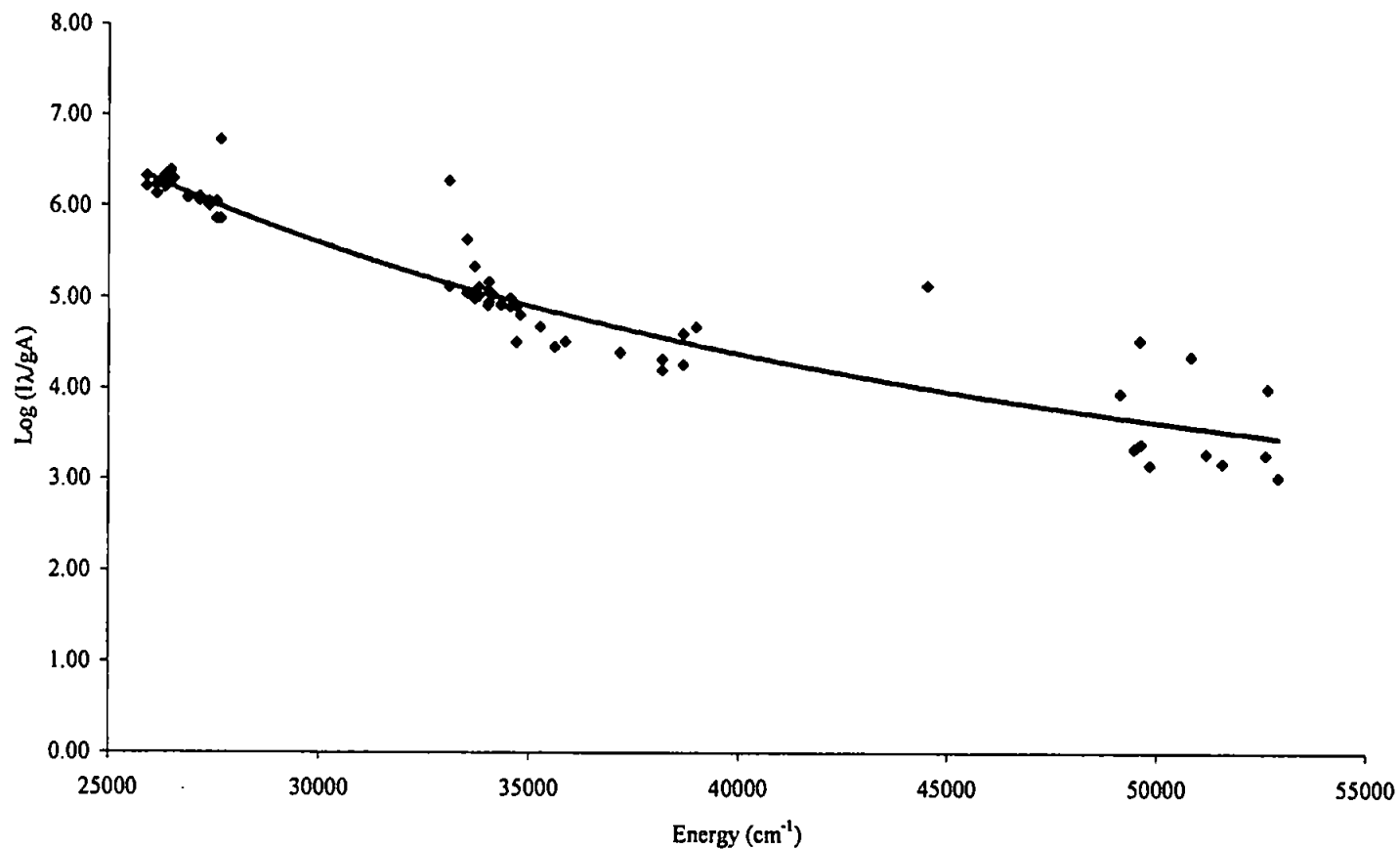
Figure 5.12: Plot of the Fe I Boltzmann Distribution for the Thermo Elemental plasma operated under fluorescence conditions (forward power 900 W; plasma gas flow rate 10 L min^{-1}; nebuliser gas flow rate 2.00 L min^{-1}; auxiliary gas flow rate 0.20 L min^{-1}; viewing height 20 mm ALC; n=3, RSDs < 5%)

**Table 5.8: $T_{rot}$ (K) calculated using OH rotational spectra from a Thermo Elemental ICP operated under fluorescence conditions (plasma gas flow rate 10 L min$^{-1}$; nebuliser gas flow rate 2.00 L min$^{-1}$; auxiliary gas flow rate 0.20 L min$^{-1}$; n = 3, RSDs < 5 %)**

| Power (W) | 900 | 700 | 500 | 300 |
|---|---|---|---|---|
| Viewing height ALC (mm) | | | | |
| 10 | n/d | n/d | n/d | n/d |
| 20 | 3200 | 3230 | 2760 | 2820 |
| 30 | 3370 | 2870 | 2680 | n/d |
| 40 | 3080 | 2860 | n/d | n/d |
| 50 | 2720 | 2670 | n/d | n/d |
| 60 | 2500 | n/d | n/d | n/d |
| 70 | n/d | n/d | n/d | n/d |
| 80 | n/d | n/d | n/d | n/d |
| 90 | n/d | n/d | n/d | n/d |
| 100 | n/d | n/d | n/d | n/d |

At this viewing height it appeared that the plasma produced by the Thermo Elemental ICP was hotter than that produced by the Optima 3000 ICP. However, if the temperatures are compared further up in the tailflame then the results are quite different. At a viewing height of 50 mm ALC, $T_{exc}$ were 3080 K and 3590 K for plasmas produced by the Thermo Elemental and Optima ICP, respectively. In this case the plasma produced from the Optima 3000 ICP was hotter than that produced by the Thermo Elemental ICP. This is of vital importance because for fluorescence to occur the majority of atoms have to be in the ground state, meaning that a relatively 'cool' plasma is required. This suggests that, although supposedly identical conditions were used on both systems, the plasma produced by the Thermo Elemental ICP was cooler than that produced by the Optima ICP.

The same observation can be made for $T_{rot}$. Table 5.8 showed that at a viewing height of 20 mm ALC, $T_{rot}$ was 3200 K for a 900 W plasma. This compares with a $T_{rot}$ of 3270 K for a plasma operated under 'identical conditions' using the Optima 3000 ICP (Chapter 4, Section 4.3.2.1, Table 4.15). At a viewing height of 50 mm ALC, $T_{rots}$ were 2500 K and 2830 K for plasmas produced from the Thermo Elemental and Optima 3000 ICPs, respectively.

Temperatures were calculated using the mean emission intensity at particular wavelengths. However, for a fluorescence signal to be distinguished over and above the background the background emission must be low. Typically, this is why it is only at the greater viewing heights ALC that fluorescence is usually observed. Therefore it would be expected that at viewing heights suitable for fluorescence to occur the emission intensity measured would be negligible. Tables 5.6 – 5.8 illustrate this point. Emission intensities from Fe I and OH species were used to calculate excitation and rotational temperatures. The intensities of the emitting species from the Thermo

251

Elemental ICP are lower than those obtained from the Optima 3000 ICP for supposedly 'identical' conditions. Therefore, as you go higher ALC in the plasma you cannot easily see them. If the excited species have lower intensities then there must be more atoms in the ground state using the Thermo Elemental ICP. As similar plasma conditions and the same concentration solutions were used in both sets of fluorescence experiments this suggests there were more ground state atoms (Fe I) would be present which are available for fluorescence. Therefore, more intense fluorescence emission is expected and observed.

## 5.7  Summary

Univariate searches were used to optimise several plasma parameters. Once the optimum conditions had been determined calibration curves were plotted for each of the elements studied. Limits of detection were determined to be 27.6, 0.51, 0.43 and 0.20 $\mu g \ l^{-1}$ for barium, lithium, magnesium and sodium respectively which are comparable to those obtained by HCL-ICP-AFS. In addition, precisions were less than 5 %.

The effect of modulation frequency and duty cycle on fluorescence signal was investigated. The maximum fluorescence signal was obtained with a modulation frequency of 542 Hz and a duty cycle of 30 %.

Vertical profiles of the plasma, using radial excitation, were obtained for Ba, Li, Mg and Na. Axial profiles of the plasma could not be obtained for Ba and Mg as the light emission produced from the HCLs was not sufficiently intense to produce a fluorescence signal. However, using the optimum conditions for Li and Na LEDs, which are more intense, vertical profiles of the plasma, using axial excitation, were obtained.

Both profiles showed that there was a relatively sharp optimum, with respect to fluorescence signal, as a function of the viewing height ALC. The optimum viewing heights ALC obtained, for both radial and axial excitation fluorescence, were identical. This suggested that, irrespective of the excitation arrangement employed, only particular conditions produced in the plasma gave the optimum conditions for fluorescence and are spatially dependent.

Comparison of $T_{exc}$ and $T_{rot}$ obtained using a Thermo Elemental and an Optima 3000 ICP operated under 'identical conditions' provides a possible explanation into why fluorescence was observed using the plasma produced by the Thermo Elemental ICP but not by the Optima 3000 ICP. Although supposedly identical conditions were used on both systems, the plasma produced by the Thermo Elemental ICP produced much lower emission intensities than those produced by the Optima 3000 ICP. If the excited species have lower intensities then there must be more atoms in the ground state from the plasma produced by the Thermo Elemental ICP. This is of vital importance, because for fluorescence to occur the majority of atoms have to be in the ground state, meaning that a relatively 'cool' plasma is required. As similar plasma conditions and the same concentration solutions were used in both sets of fluorescence experiments, this suggests there were more ground state atoms (Fe I) and other species (like OH) available for fluorescence. Therefore, more intense fluorescence emission is expected and observed.

# 6.0 CONCLUSIONS AND FUTURE WORK

## 6.1 Conclusions

An Optima 3000 ICP-AES instrument was modified and the equipment necessary to carry out axial excitation atomic fluorescence was designed and constructed. Two axial excitation assemblies were constructed, one utilised fibre optics and the other a mirror and lens system, resulting in a series of modules that could be fitted retrospectively to a, Optima 3000 ICP instrument. These modules included: an axial excitation alignment frame, an inter-linking water cooled condenser system, an optical beam probe; a demountable X and Y-axis translation plate for collection of the atomic fluorescence signal and for horizontal and vertical scanning of the elongated plasma tailflame; and a vertically and horizontally adjustable mirror, set at a 45° angle to either a focusing or a collimating lens. Both the condenser and mirror assemblies used a novel argon gas coolant flow to reduce the excessive thermal environment above the elongated plasma tailflame needed for fluorescence and a detection system comprising optical filters, a photomultiplier tube and a lock-in amplifier.

The ICP instrument was calibrated between forward powers of 750 and 1500 W and nebuliser gas flow rates of 1.50 to 3.00 L min$^{-1}$. These plasma conditions were used for preliminary fluorescence experiments, as they were consistent with those described in the literature. Visual inspection of the plasma, verified that the elongated tailflame, required for fluorescence, was present under these operating conditions.

Preliminary fluorescence experiments were not successful. This was despite all of the individual pieces of equipment being proven to work, *e.g.* by cold vapour mercury cell and emission mode experiments, and despite numerous modifications being made to the experimental arrangements. It was considered that, because fluorescence is proportional

to source intensity, the excitation source may not have been sufficiently intense to produce fluorescence. A novel excitation source-driver system was designed and built in-house to operate HCLs, BDHCLs and LEDs with variable modulation frequencies and duty cycle capabilities.

The production of a fluorescence signal critically relies on the use of an efficient, intense external excitation source. The way in which the source is modulated, for a given 'type' of source, e.g. HCL/BDHCL or LED must be considered important as this affects its intensity and the efficiency of coupling to the analyte of interest within the atom cell. In order to improve our understanding of the excitation source requirements and to optimise the emission output from a HCL for the production of fluorescence, the emission signal from an Fe HCL was measured to determine how the lamp responds to changes in modulation frequency and duty cycle. Oscilloscope traces comparing the reference signal and the emission signal from the lamp allowed an estimate of the time taken for the lamp to 'trigger' and reach its maximum intensity (full 'plasma' discharge) to be made. The lamp 'trigger' time was shown to be in the region of 150 - 185 µs and the time taken for the lamp to reach maximum intensity was in the region of 414 - 449 µs. The oscilloscope traces showed that at higher modulation frequencies (667 - 1042 Hz) and shorter duty cycles (10 – 20 %) the lamp's plasma 'discharge' was 'clipped' to such an extent that the lamp did not have time to trigger at all, or that when it did trigger the maximum lamp intensity was not reached. This indicated that a lamp operated with a lower modulation frequency range (167 – 542 Hz) and higher duty cycles (30 – 50 %) should provide the preferred intense excitation conditions for the production of fluorescence in the ICP.

The characteristics of a HCL are not defined by a single line intensity measurement. The conditions under which it is driven give rise to a range of differing energy states for

the analyte contained within the lamp. A Boltzmann Distribution and a Line Pair Intensity Ratio measurement from this excitation source can be used as a physical marker to enable direct comparisons to be made (and help analyse subsequent variations) between a HCL operated under various modulation frequencies and duty cycles. The Boltzmann Distribution method was used to calculate excitation temperatures ($T_{exc}$) in order to study the effect of modulation frequency and duty cycle on the emission characteristics of a Fe HCL. $T_{exc}$ typically varied between 5200 and 6500 K. As the modulation frequency increased (from 167 to 1042 Hz) the $T_{exc}$ of the lamp showed a small increase. However, $T_{exc}$ decreased with the following order of duty cycles: 30 % > 40 % > 50 % > 20 % > 10 %. $T_{exc}$ was also calculated using the LPIRM. Using this method, $T_{exc}$ varied mainly between 2000 and 4500 K and showed different trends to those determined by the Boltzmann Distribution. From an examination of a simplified version of the Grotrian diagram for Fe I, these differences were attributed to the effective ground state for both the 385.991 and 382.043 nm emission lines being different. Hence, as the two lines are energetically independent the deviation from thermo-equilibrium has to be considered (under the driving conditions of the lamp used), and differences in $T_{exc}$ are to be expected.

Atomic absorption measurements were carried out on an inductively coupled plasma using a HCL in order to determine the relative number of ground state magnesium atoms (rather than excited species) present under different plasma conditions. As absorbance and fluorescence are directly linked to the atomic population in a given energy state, then the optimum conditions found for absorption should also hold for fluorescence (assuming quenching effects are absent). Preliminary optimisation experiments were performed and the effect of increasing the primary current of a Mg HCL on the Mg I 285.213 nm absorbance signal was investigated. Within the working range of the lamp (3 – 7.5 mA) there was a proportional relationship between primary

current and absorbance signal. When the maximum advisable lamp operating current was exceeded, the absorbance decreased as the primary lamp current increased. The optimum condition (*i.e.* greatest absorbance) was obtained with a primary lamp current of 6 mA. The effect of duty cycle on the Mg I 285.213 nm absorbance signal using modulation frequencies of 542, 667 and 792 Hz, respectively, was determined. Absorbance signal increased as the modulation frequency and duty cycle increased, however, there was little difference with the optimum signal observed using operating conditions of 667 and 792 Hz with a 50 % duty cycle. Comparison of the lamp profiles (Figures 3.7 and 3.8 for modulation frequencies of 667 and 792 Hz, respectively) showed less 'clipping' at the lower modulation frequency. Therefore, a modulation frequency of 667 Hz was used for all future absorbance experiments.

Using the Optima 3000 ICP instrument, the maximum absorbance signal observed for the Mg I 285.213 nm line was obtained at a viewing height of 60 mm ALC. It is of note that whilst fluorescence was not observed from the plasma produced using the Optima 3000 ICP, the maximum fluorescence signal observed in later studies by the plasma produced using the Thermo Elemental ICP under identical conditions (forward power 700 W; nebuliser gas flow rate 2.00 L min$^{-1}$; sample uptake rate 2.00 ml min$^{-1}$) and using the same Mg I 285.213 nm line was at a viewing height of 60 mm ALC.

The optimised plasma and lamp-excitation conditions from the preliminary studies were used to perform a series of 'back-to-basics' transverse fluorescence experiments using the Optima 3000 instrument. Despite all the components used in the transverse fluorescence experiments having been shown to work individually, no fluorescence was observed. This suggested that the plasma produced by the Optima was not operating in a manner expected for the calibrated conditions used. Hence further investigation was necessary. Plasma diagnostics were therefore performed to gain a deeper understanding

of this plasma under the conditions used and to explain why fluorescence had not been observed. A plasma operated under fluorescence-like conditions was compared with a plasma operated under conventional emission conditions in order to, and if possible, identify the plasma conditions suitable for fluorescence.

The excitation temperature ($T_{exc}$) was used as a physical marker to establish direct comparisons and subsequent variations from varying forward powers, nebuliser gas flow rates and viewing heights of $0 - 30$ mm ALC when the plasma was operated under fluorescence-like and conventional emission conditions using the Optima's own detection system. Comparison of the excitation temperatures, calculated using the LPIR method, showed $T_{exc}$ to be higher when the plasma was operated under conventional emission conditions. For a plasma operated under fluorescence-like conditions (forward power $700 - 900$W; nebuliser gas flow rate $2.00$ L $min^{-1}$; sample uptake rate $2.00$ ml $min^{-1}$), $T_{exc}$ was in the range $2100 - 2700$ K and decreased with decreasing forward power and increasing viewing heights ALC. For a plasma operated under conventional emission conditions (forward power $1200$W; nebuliser gas flow rate $0.80$ L $min^{-1}$; sample uptake rate $0.80$ ml $min^{-1}$), $T_{exc}$ was in the range $2000 - 3000$ K. Using a SPEX monochromator, excitation temperatures could be obtained at greater viewing heights ALC ($10 - 100$ mm). $T_{exc}$ showed greater variation compared with those determined by the Optima detection system although the trends were the same as those determined using the Optima's own detector. Excitation temperatures ranged from $1765 - 3060$ K and $2530 - 2860$ K for a plasma operated under fluorescence-like and conventional emission conditions, respectively.

Excitation temperatures were also calculated using the Boltzmann Distribution. Values ranged from $3130 - 3600$ K and from $4940 - 5540$ K for a plasma operated under fluorescence-like and conventional emission conditions, respectively. $T_{exc}$ obtained

from the Boltzmann Distribution showed good agreement with literature values, however, $T_{exc}$ values obtained from the LPIRM appeared to be lower. Plots of the Boltzmann Distribution were curved and not linear. The 'degree' of curvature may help to indicate the extent of deviation of the plasma from LTE. The Boltzmann Distribution plots were more curved at the lower viewing heights ALC and higher forward powers, suggesting that the plasma operated under fluorescence-like conditions was closer to LTE at lower forward powers and higher viewing heights ALC.

Rotational temperatures ($T_{rot}$) were calculated using OH and $N_2^+$ species for a plasma operated under fluorescence-like (forward power 700 – 900W; nebuliser gas flow rate 1.50 – 3.00 L min$^{-1}$; sample uptake rate 2.00 ml min$^{-1}$) and conventional emission conditions (forward power 1200W; nebuliser gas flow rate 0.80 L min$^{-1}$; sample uptake rate 1.00 ml min$^{-1}$) using the Optima 3000 instrument. For a plasma operated under fluorescence-like conditions $T_{rot}$ was calculated to be in the range 2700 – 3400 K and 1230 K for measurements using OH and $N_2^+$ species, respectively. This compares with 2300 – 3030 K and 1390 – 1670 K for measurements using OH and $N_2^+$ species, respectively, for a plasma operated under conventional emission conditions.

For the Optima 3000 instrument operated under conventional emission conditions (forward power 1200W; nebuliser gas flow rate 0.80 L min$^{-1}$; sample uptake rate 1.00 ml min$^{-1}$), calculated electron number densities ($n_e$) agree closely to those reported in the literature. Values for $n_e$ obtained from this plasma operated under fluorescence-like conditions were greater than those obtained from the plasma operated under conventional emission conditions. For the plasma operated under conventional emission conditions, the electron number density decreased as the viewing height ALC increased. However, there was little variation from the plasma operated under fluorescence-like conditions. This was not unexpected and may have been due to: a real effect of the

generator coupling system producing the ICP, self absorption changes for Hβ 486.1 nm line with viewing height ALC, or a change of Hβ excitation profile with increasing viewing height ALC.

The electron number density calculations for a plasma operated under fluorescence-like conditions suggest one possible reason why fluorescence had not been observed using the Optima 3000 instrument. As stated by Raejmakers *et al.* (127; Section 4.1) "...the spatially resolved measurement of only one parameter, e.g. the electron density ($n_e$) or the electron temperature ($T_e$), is necessary and sufficient to characterise the discharge...". If this is correct and the observed trends are real, this suggests that the plasma was not performing as expected under the set of conditions used. This may be why, despite all the components of the experimental arrangement being calibrated and proven to work individually, the conditions did not produce a plasma suitable for the production of fluorescence. To test this theory, another plasma generator (which became available for use at a very late stage in the project) was used in an attempt to try and observe fluorescence using the same equipment and similar conditions to those used in the Optima 3000 fluorescence experiments.

When a low power plasma was produced using the Thermo Elemental PQ2 generator, and transverse excitation experiments performed, fluorescence was obtained immediately. Hence, all subsequent experiments were performed using this plasma system. Univariate searches were used to optimise several plasma parameters (forward power; viewing height ALC; plasma, nebuliser and auxiliary gas flow rates). Once the optimum conditions had been determined, calibration curves were plotted for each of the elements studied (Ba, Li, Mg and Na). The calibration showed excellent linearity over five orders of magnitude ($R^2$ values range from 0.99995 to 1.0000) and the precision on each data point was better than 5 % RSD. Limits of detection were

determined to be 27.6, 0.51, 0.43 and 0.20 µg l$^{-1}$ for Ba, Li, Mg and Na, respectively. A comparison of the LODs obtained for this system with the LODs listed in Tables 1.7 and 1.8 (Chapter 1, Section 1.5.6) for HCL-ICP-AFS (25, <0.1, <0.1 and <0.1 µg l$^{-1}$ for Ba, Li, Mg and Na, respectively) show that the values obtained were approaching those of a commercial system. This was despite the fact that the experimental arrangement used was still being refined and many improvements could have been made in terms of collection efficiency and optical coupling.

The effect of modulation frequency and duty cycle on Mg I 285.213 nm fluorescence signal was investigated. The maximum fluorescence signal was obtained with a modulation frequency of 667 Hz and a duty cycle of 30 %. The trends observed agreed with those obtained from the $T_{exc}$ investigations of a Fe HCL.

Vertical profiles of the plasma, using radial excitation, were obtained for Ba, Li, Mg and Na. Axial profiles of the plasma could not be obtained for Ba and Mg as the emission produced from the HCLs was not sufficiently intense to produce a fluorescence signal. However, using the optimum conditions for Li and Na, vertical profiles of the plasma, using axial excitation with the more intense LEDs, were obtained. Both profiles showed that there was a relatively sharp optimum, with respect to fluorescence signal, as a function of the viewing height ALC. The optimum viewing heights ALC obtained, for both radial and axial excitation fluorescence, were identical. This suggests that, irrespective of the excitation arrangement employed, only particular conditions produced in the plasma give the optimum conditions for fluorescence and that these are spatially dependent.

Comparison of $T_{exc}$ and $T_{rot}$ values obtained using Thermo Elemental and Optima 3000 instruments operated under supposedly 'identical conditions' provides one possible explanation why fluorescence was only observed using the plasma produced by the

Thermo Elemental generator. At a viewing height of 50 mm ALC, $T_{exc}$ were 3080 K and 3590 K for plasmas produced by the Thermo Elemental and Optima instruments, respectively. At a viewing height of 50 mm ALC, $T_{rot}$ were 2500 K and 2830 K for plasmas produced from the Thermo Elemental and Optima 3000, respectively. Temperatures were calculated using the mean emission intensity at particular wavelengths. However, for a fluorescence signal to be distinguished over and above the background, the background emission must be low. Typically, this is why it is only at the greater viewing heights ALC that fluorescence is usually observed. Therefore it would be expected that at viewing heights suitable for fluorescence to occur the emission intensity measured would be negligible. The intensities of the emitting species from the Thermo Elemental ICP were lower than those obtained from the Optima 3000 ICP under supposedly 'identical' fluorescence conditions. Therefore, as you go higher ALC in the plasma the emitting species are not easily seen. If the number of excited species gives rise to lower emission intensities, then there must be more atoms in the lower/ground state from the plasma produced using the Thermo Elemental generator. This is of vital importance because for fluorescence to occur the fluorescence emission intensity will be dependent on the number available in the ground state for excitation (*i.e.* a relatively 'cool' plasma is required for fluorescence to occur). As very similar plasma operating conditions and the same concentration solutions were used in the fluorescence experiments performed using both the Optima 3000 and the Thermo Elemental ICPs, the differences observed in plasma performance may be attributed to efficiency of coupling of the generators used.

## 6.2    Future Work

Further diagnostic investigations of the plasma produced by the Thermo Elemental instrument would enable a greater understanding into why fluorescence was observed

on this system and not from a plasma produced by the Optima 3000. If a more complete set of absorbance and electron density measurements were to be obtained from a plasma produced by the Thermo Elemental PQ2 generator operated using fluorescence conditions, then a more detailed comparison of the two plasma systems could be made.

The plasma produced using the Optima 3000 used a 40.68 MHz free running generator whereas the plasma produced using the Thermo Elemental ICP used a 27.1 MHz crystal controlled generator. If an experiment to determine the coupling efficiencies of the generators was completed (*i.e.* using calorific values) it might help to explain why fluorescence was observed using a plasma produced by the Thermo Elemental ICP and not using the Optima 3000 ICP.

The use of LEDs as potential excitation sources for fluorescence was encouraging and warrants further investigation. In order to optimise the emission output from a LED for the production of fluorescence, the emission signal should be measured to determine how the LED responds to changes in modulation frequency and duty cycle. LEDs have a broad bandwidth of between 10 – 20 nm and will excite any species that has a transition in this range. A monochromator could be employed to isolate a narrow wavelength to provide a more element-specific excitation source for fluorescence. A series of LEDs could be used to cover the wavelength range 300 – 700 nm. If the LEDs were incorporated into commercial instruments then there is the possibility of producing a multi-element capability instrument. The instrument could be switched between ICP-AES or -AFS mode depending on the element to be determined.

The potential for lower limits of detection for fluorescence could be realised if a different detection system was employed using axial excitation. The system used was quite basic and simple, owing to time limitations, but could easily be improved. If a system could be designed with axial excitation fluorescence in mind and with improved

collection efficiency (*e.g.* the use of an integrating sphere or a cylindrical lens system), then lower limits of detection should be possible. The use of a very high intensity axial excitation beam would be necessary but this could easily be achieved with the use of a tunable laser.

:

# REFERENCES

1. Hasegawa, T. and Haraguchi, H., in "Inductively Coupled Plasmas in Analytical Atomic Spectrometry", Montaser, A. and Golightly, D.W., (Eds), VCH, New York, 1987, Chapter 8.

2. Blades, D.W., in "Inductively Coupled Plasma – Emission Spectroscopy, Pt II: Applications and Fundamentals", Boumans, P.W.J.M., (Ed), Wiley, New York, 1987, Chapter 11.

3. Blades, M.W., and Weir, D.G., *Spectrosc.*, 1994, 9, 14.

4. Kalnicky, D.J., Kniseley, R.N. and Fassel, V.A., *Spectrochim. Acta*, 1975, **30B**, 511.

5. Reed, T.B., *J. Appl. Phys.*, 1961, **32**, 821.

6. Reed, T.B., *J. Appl. Phys.*, 1961, **32**, 2534.

7. Greenfield, S., Jones, I. Ll. W. and Berry, C.T., *Proc. Soc. Anal. Chem.*, 1963, **88**, 904.

8. Greenfield, S., Jones, I. L. and Berry, C.T., *Analyst*, 1964, **89**, 713.

9. Wendt, R.H. and Fassel,, V.A., *Anal. Chem.*, 1965, **37**, 920.

10. Greenfield, S., in "Inductively Coupled Plasmas in Analytical Atomic Spectrometry", Montaser, A. and Golightly, D.W., (Eds), VCH, New York, 1987, Chapter 4.

11. Greenfield, S. and Foulkes, M., in "Inductively Coupled Plasma Spectrometry And Its Applications", Hill, S.J., (Ed), Sheffield Academic Press, Sheffield, 1999, Chapter 1.

12. Fassel, V.A., and Dickinson, G.W., *Anal. Chem.*, 1968, **40**, 247.

13. Dickinson, G.W. and Fassel, V.A., *Anal. Chem.*, 1969, **41**, 1021.

14. Hoare, H.C. and Mostyn, R.A., *Anal. Chem.*, 1967, **39**, 1153.

15. Biancifiori, M.A. and Bordonali, C., *La Metallurgica Italiana*, 1967, **8**, 631.

16. Veillon, C. and Margoshes, M., *Spectrochim. Acta*, 1968, **23B**, 501.

17. Miller, R.C. and Ayen, R.J., *J. Appl. Phys.*, 1969, **40**, 5260.

18. Ebdon, L., Evans, E.H., Fisher, A. and Hill, S.J, "An Introduction To Analytical Atomic Spectrometry", John Wiley & Sons, Chichester, 1998.

19. Mermet, J.M., in "An Introduction to Analytical Atomic Spectroscopy", Hill, S.J. (Ed.), Sheffield Academic Press, Sheffield, 1999, Chapter 2.

20. Robin, J.P., *Prog. Anal. At. Spectrosc.*, 1982, **5**, 79.

21. De Galan, L., *Spectrochim. Acta*, 1984, **39B**, 537.

22. Mermet, J.M., *Acad. Sci.*, 1975, **Series B 281**, 273.

23. Greenfield, S., *J. Anal. At. Spectrom.*, 1994, **9**, 565.

24. Sychra, V., Svoboda, V. and Rubeska, I., "Atomic Fluorescence Spectroscopy", Van Nostrand Reinhold Company, London, 1975.

25. Hussein, Ch. A.M., & Nickless, G., paper presented at the 2$^{nd}$ ICAS, Sheffield, U.K. (1969).

26. Montaser, A., and Fassel, V. A., *Anal. Chem.*, 1976, **48**, 1490.

27. Pollard, B. D., Blackburn, M. B., Nikdel, S., Massoumi, A. and Winefordner, J. D., *Appl. Spectrosc.*, 1979, **33**, 5.

28. Epstein, M. S., Nikdel, S., Bradshaw, J. D., Kosinski, M. A., Bower, J. N. and Winefordner, J. D., *Anal. Chim. Acta*, 1980, **113**, 221.

29. Demers, D. R., and Allemand, C. D., *Anal. Chem.*, 1981, **53**, 1915.

30. Demers, D. R., and Allemand, C. D., paper No. 122 presented at the 1981 Pittsburg Conference, Atlantic City, NJ, SA.

31. Demers, D. R., and Allemand, C. D., paper No. 123 presented at the 1981 Pittsburg Conference, Atlantic City, NJ, USA.

32. Demers, D. R., Busch, D. A., and Allemand, C. D., *Am. Lab.*, 1982, **14**, 167.

33. Omenetto, N., *Analytiktreffen: Atomspektrosk, Fortschr. Anal. Annend Hauptvortr.*, Meeting held at Karl Marx University, Leipzig, Germany, 1982.

34. Kosinski, M. A., Uchida, H. and Winefordner, J. D., *Anal. Chem.*, 1983, **55**, 688.

35. Epstein, M. S., Nikdel, S., Omenetto, N., Reeves, R., Bradshaw, J., and Winefordner, J. D., *Anal. Chem.*, 1979, **51**, 2071.

36. Greenfield, S., *Anal. Proc.*, 1984, **21**, 61.

37. Omenetto, N., Human, H. G. C., Cavalli, P. and Rossi. G., *Spectrochim. Acta*, 1984, **39B**, 115.

38. Winge, R. K., Peterson, V. J. and Fassel, V. A., *Appl. Spectrosc.*, 1979, **33**, 206.

39. P. W. J. M.. Boumans, Line Coincidence Tables for Inductively Coupled Plasma Atomic Emission Spectrometry, Pergamon Press, Oxford (1980).

40. Omenetto, N. and Human, H. G. C., *Spectrochim. Acta*, 1984, **39B**, 1333.

41. Human, H. G. C., Omenetto, N., Cavalli, P. and Rossi. G., *Spectrochim. Acta*, 1984, **39B**, 1345.

42. Greenfield, S. and Thomsen, M., *Spectrochim. Acta*, 1985, **40B**, 1369.

43. Greenfield, S., Malcolm, F. M. and Thomsen, M., *J. Anal. At. Spectrom.*, 1987, **2**, 711.

44. Greenfield, S. and Thomsen, M., *European Spectroscopy News*, 1986, **68**, 8.

45. Greenfield, S. and Thomsen, M., *Spectrochim. Acta*, 1986, **41B**, 677.

46. Greenfield, S. and Thomsen, M., *Anal. Proc.*, 1987, **24**, 22.

47. Greenfield, S., Salman, M. S. and Tyson, J. F., *Spectrochim. Acta*, 1988, **43B**, 1087.

48. Greenfield, S., Salman, M. S., Thomsen, M. and Tyson, J. F., *J. Anal. At. Spectrom.*, 1989, **4**, 55.

49. Greenfield, S., *ICP Inf. Newsl.*, 1988, **13**, 655.

50. Greenfield, S., Salman, M. S., Thomsen, M. and Tyson, J. F., *Anal. Proc.*, 1988, **25**, 79.

51. Greenfield, S., Durrani, T. M., Kaya, S. and Tyson, J. F., *Anal. Proc.*, 1989, **26**, 382.

52. Greenfield, S., Durrani, T. M., Kaya, S. and Tyson, J. F., *Analyst*, 1990, **115**, 531.

53. Greenfield, S., Durrani, T. M., and Tyson, J. F., *ICP Inf. Newsl.*, 1990, **16**, 159.

54. Demers, D. R., *Am. Lab.*, 1987, **19**, 30.

55. Greenfield, S., Durrani, T. M., Tyson, J. F. and Watson, C. A., *Spectrochim. Acta*, 1990, **45B**, 341.

56. Demers, D.R. and Montaser, A., in "Inductively Coupled Plasmas in Analytical Atomic Spectrometry", Montaser, A. and Golightly, D.W., (Eds), 2$^{nd}$ Edition, VCH, New York, 1992, Chapter 11.

57. Cavalli, P., Rossi, G. and Omenetto, N., *Analyst*, 1983, **108**, 297.

58. Greenfield, S., Personnel Communication, July 1997.

59. Montaser, A., *Spectrosc. Lett.*, 1979, **12**, 725.

60. Omenetto, N., Nikdel, S., Bradshaw, J. D., Epstein, M. S., Reeves, R. and Winefordner, J. D., *Anal. Chem.*, 1979, **51**, 1521.

61. Epstein, M. S., Omenetto, N., Nikdel, S., Bradshaw, J., and Winefordner, J. D., *Anal. Chem.*, 1980, **52**, 284.

62. Lancione, R. L. and Drew, D. M., *Ind. Res. & Devel.*, 1983, **25**, 100.

63. Long, G. L. and Winefordner, J. D., *Appl. Spectrosc.*, 1984, **38**, 563.

64. Lancione, R. L. and Drew, D. M., *Metal Finish.*, 1984, **82**, 17.

65. Lancione, R. L. and Drew, D. M., *J. Test. and Eval.*, 1984, **12**, 203.

66. Demers, D. R., *Spectrochim. Acta*, 1985, **40B**, 93.

67. Lancione, R. L. and Drew, D. M., *Spectrochim. Acta*, 1985, **40B**, 107.

68. Jansen, E. B. M. and Demers, D. R., *Analyst*, 1985, **110**, 541.

69. Sanzolone, R. F., *J. of Anal. At. Spectrom.*, 1986, **1**, 343.

70. Sanzolone, R. F. and Meier, A. L., *Analyst*, 1986, **11**, 645.

71. Yeah, K. S., Masamba, W. and Winefordner, J. D., *Anal. Sci.*, 1987, **3**, 245.

72. Zhu, S. F., Wang, H. and Keliher, P. N., *Microchem. J.*, 1988, **38**, 264.

73. Sansoni, B., Brunner, W., Wolff, G., Ruppert, H. and Dittrich, R., *Fresenius' Z. Anal. Chem.*, 1988, **2**, 154.

74. Caughlin, B. L., *J. Geochem. Explor.*, 1989, **34**, 245.

75. Liu, X. R. and Horlick, G., *Spectrochim. Acta*, 1994, **50B**, 537.

76. Greenfield, S., *J. of Anal. At. Spectrom.*, 1995, **10**, 183.

77. Krupa, R.J., Long, G.L. and Winefordner, J.D., *Spectrochim. Acta*, 1985, **40B**, 1485.

78. Krupa, R.J. and Winefordner, J.D., *Spectrochim. Acta*, 1986, **41B**, 1015.

79. Taobi, A-A.,H., PhD Thesis, University of Manchester, 1993.

80. Demers, D. R., Busch, D.A. and Allemand, C.D., *Int. Lab.*, 1987, **14**, 40.

81. Greenfield, S., Personnel Communication, October 1997.

82. Greenfield, S., Personnel Communication, January 1998.

83. Greenfield, S., Personnel Communication, July 1998.

84. Furuta, N. and Horlick, G., *Spectrochim. Acta*, 1982, **37B**, 53.

85. Boumans, P.W.J.M. and de Boer, F.J., *Spectrochim. Acta*, 1977, **32B**, 365.

86. Abdallah, M.H. and Mermet, J.M., *Spectrochim. Acta*, 1982, **37B**, 391.

87. Novotny, I., Farinas, J.C., Wan Jia-Liang, Poussel, E. and Mermet, J.M., *Spectrochim. Acta*, 1996, **51B**, 1517.

88. Mermet, J.M., *Spectrochim. Acta*, 1975, **30B**, 383.

89. Kalnicky, D.J., Kniseley, R.N. and Fassel, V.A., *Appl. Spectrosc.*, 1977, **31**, 137.

90. Jarosz, J., Mermet, J.M. and Robin, J., *Spectrochim. Acta*, 1978, **33B**, 55.

91. Kornblum, G.R. and De Galan, L., *Spectrochim. Acta*, 1977, **32B**, 71.

92. Alder, J.F., Bombelka, R.M. and Kirkbright, G.F., *Spectrochim. Acta*, 1980, **35B**, 163.

93. Kawaguchi, H., Ito, T. and Mizuike, A., *Spectrochim. Acta*, 1981, **36B**, 615.

94. Capelle, B., Mermet, J.M. and Robin, J.P., *Appl. Spectrosc.*, 1982, **36**, 102.

95. Faires, L.M. , Palmer, B.A., Engleman, Jr, R. and Niemczyk, T.M., *Spectrochim. Acta*, 1984, **39B**, 819.

96. Furuta, N., *Spectrochim. Acta*, 1985, **40B**, 1013.

97. Blades, M.W. and Caughlin, B.L., *Spectrochim. Acta*, 1985, **40B**, 579.

98. Walker, Z. and Blades, M.W., *Spectrochim. Acta*, 1986, **41B**, 761.

99. Ishii, I., Golightly, D.W. and Montaser, A., *J. Anal. At. Spectrom.*, 1988, **3**, 965.

100. Murillo, M. and Mermet, J.M., *Spectrochim. Acta*, 1989, **44B**, 359.

101. Nixon, D.E., *J. Anal. At. Spectrom.*, 1990, **5**, 531.

102. Montaser, A., Ishii, I., Palmer, B.A. and Layman, L.R., *Spectrochim. Acta*, 1990, **45B**, 603.

103. Kitagawa, K. and Horlick, G., *J. Anal. At. Spectrom.*, 1992, **7**, 1207.

104. Fuhr, J.R., Martin, G.A. and Wiese, W.L., *J. Phys. Chem. Ref. Data*, 1988, **17**, suppl. 4.

105. Besombes-Vailhe, *J. Chim. Phys. Chim. Biol.*, 1976, **64**, 370.

106. Triche, H., Saadate, A., Talayrach, B. and Besombes-Vailhe, *Analusis*, 1972, **1**, 413.

107. Mermet, J.M., Jarosz, J. and Robin, J., *Preprints 17<sup>th</sup> Coll. Spectrosc. Intern.*, Florence, 1973, **1**, p. 101.

108. Ripson, P.A.M., de Galan, L. and de Ruiter, J.W., *Spectrochim. Acta Part B*, 1982, **37**, 733.

109. Barnett, W.B., Fassel, V.A. and Kniseley, R.N., *Spectrochim. Acta Part B*, 1970, **25**, 139.

110. Rybarczyk, J.P., Jester, C.P., Yates, D.A. and Koirtyohann, S.R., *Anal. Chem.*, 1982, **54**, 2162.

111. O'Hanlon, K.L., Slurry, solution and speciation analysis by inductively coupled plasma atomic emission spectrometry, PhD Thesis, University of Plymouth, 1996, chapter 6.

112. Boumans, P.W.J.M., Wagenaar, H. and de Boer, F.J., *Preprints 17$^{th}$ Coll. Spectrosc. Intern.*, Florence, 1973, 1, p. 114.

113. Gunter, W.H., Visser, K. and Zeeman, P.B., *Spectrochim. Acta*, 1982, **37B**, 571.

114. Gunter, W.H., Visser, K. and Zeeman, P.B., *Spectrochim. Acta*, 1983, **38B**, 949.

115. Gunter, W.H., Visser, K. and Zeeman, P.B., *Spectrochim. Acta*, 1985, **40B**, 617.

116. National Institute of Standards and Technology, 'DAS' database, available from http://physics.nist.gov/asd.

117. Nakamura, S., *J. Anal. At. Spectrom.*, 1995, **10**, 467.

118. Rayson, G.D. and Shen, D.Y., *Spectrochim. Acta*, 1991, **46B**, 1237.

119. Hensman, C.E., Mihalic, J.F. and Rayson, G.D., *Anal. Comm.*, 1997, **43**, 355.

120. Wagatsuma, K. and Hirokawa, K., *Anal. Chim. Acta*, 1993, **283**, 351.

121. Olesik, J.W. and Den, S.-J., *Spectrochim. Acta*, 1990, **45B**, 731.

122. Mermet, J.M., *Anal. Chim. Acta*, 1991, **250**, 85.

123. Barnard, T.W., Crockett, M.I., Ivaldi, J.C., Lundberg, P.L., Yates, D.A., Levine, P.A. and Saver, D.J., *Anal. Chem.*, 1993, **65**, 1231.

124. Barnard, T.W., Crockett, M.I., Ivaldi, J.C. and Lundberg, P.L., *Anal. Chem.*, 1993, **65**, 1225.

125. Nowak, S., Van der Mullen, J.A.M. and Schram, D.C., *Spectrochim. Acta*, 1988, **43B**, 1235.

126. Cicerone, M.T. and Farnsworth, P.B., *Spectrochim. Acta*, 1989, **44B**, 897.

127. Raejmaker, I.J.M.M., Boumans, P.W.J.M., Van der Sijde, B. and Schram, D.C., *Spectrochim. Acta*, 1983, **38B**, 697.

128. Alder, J.F. and Mermet, J.M., *Spectrochim. Acta*, 1973, **28B**, 421.

129. Kleinmann, I. and Cajko, J., *Spectrochim. Acta Part B.*, 1970, **25B**, 657.

130. Batal, A., Jarosz, J. and Mermet, J.M, *Spectrochim. Acta*, 1982, **37B**, 983.

131. Batal, A., Jarosz, J. and Mermet, J.M, *Spectrochim. Acta*, 1982, **37B**, 511.

132. Kornblum, G.R. and De Galan, L., *Spectrochim. Acta*, 1974, **29B**, 249.

133. Visser, K., Hamm, F.M. and Zeeman, P.B., *Appl. Spectrosc.*, 1976, **30**, 34.

134. Boumans, P.W.J.M. and de Boer, F.J., *Spectrochim. Acta*, 1976, **31B**, 355.

135. Walters, P.E., Chester, T.L. and Winefordner, J.D., *Appl. Spectrosc.*, 1977, **31**, 1.

136. Mermet, J.M. and Trassy, T.C., *Rev. Phys. Appl.*, 1977, **12**, 1219.

137. Kornblum, G.R. and de Galan, L., *Spectrochim. Acta*, 1977, **32B**, 455.

138. Abdallah, M.H. and Mermet, J.M., *J. Quant. Spectrosc. Radiat. Transfer*, 1978, **19**, 83.

139. Barnes, R.M. and Schleicher, R.G., *Spectrochim. Acta*, 1981, **36B**, 81.

140. Barnes, R.M. and Genna, J.L., *Spectrochim. Acta*, 1981, **36B**, 299.

141. Uchida, H., Tanabe, K., Nojiri, Y., Haraguchi, H. and Fuwa, K., *Spectrochim. Acta*, 1981, **36B**, 711.

142. Roederer, J.E., Bastiaans, G.J., Fernandez, M.A. and Fredeen, K.J., *Appl. Spectrosc.*, 1982, **36**, 383.

143. Kornblum, G.R. and Smeyers-Verbeke, J., *Spectrochim. Acta*, 1982, **37B**, 83.

144. Nojiri, Y., Tanabe, K., Uchida, U., Haraguchi, H., Fuwa, K. and Winefordner, J.D., *Spectrochim. Acta*, 1983, **36B**, 61.

145. Carr, J.W. and Blades, M.W., *Spectrochim. Acta*, 1984, **39B**, 567.

146. Faires, L.M., Palmer, B.A., Engleman, Jr., R. and Niemczyk, T.M., *Spectrochim. Acta*, 1984, **39B**, 819.

147. Houk, R.S., Svec, H.V. and Fassel, V.A., *Appl. Spectrosc.*, 1981, **35**, 380.

148. Houk, R.S., Montaser, A. and Fassel, V.A., *Appl. Spectrosc.*, 1983, **37**, 425.

149. Talayrach, B., Besombes-Vailhe, J. and Triche, H., *Analysis*, 1972, **1**, 135.

150. Zeeman, P.B., Terblanche, S.P., Visser, K. and Hamm, F.H., *Appl. Spectrosc.*, 1978, **32**, 572.

151. Human, H.G.C. and Scott, R.H., *Spectrochim. Acta*, 1976, **31B**, 459.

152. Hasegawa, T. and Haraguchi, H., *Spectrochim. Acta*, 1985, **40B**, 123.

153. Faires, L.M., Palmer, B.A. and Brault, J.M., *Spectrochim. Acta*, 1985, **40B**, 135.

154. Ishii, I. and Montaser, A., *Spectrochim. Acta*, 1991, **46B**, 1197.

155. Hasegawa, T. and Haraguchi, H., *Spectrochim. Acta*, 1985, **40B**, 1505.

156. Trassy, D.H. and Myers, S.A., *Spectrochim. Acta*, 1982, **37B**, 1055.

157. Goldfarh, V.M. and Goldfarh, H.V., *Spectrochim. Acta*, 1985, **40B**, 177.

158. Eckert, H.U., Kelly, F.L. and Olsen, H.N., *J. Appl. Phys.*, 1968, **39**, 1846.

159. Childs, W.H.J., *Proc. R. Soc. London Ser. A*, 1932, **137**, 641.

160. Coster, D. and Brons, F., *Z Physik*, 1932, **73**, 747.

161. Dieke, G.H. and Crosswhite, H.M., *J. Quant. Spectrosc. Radiat. Transfer*, 1962, **2**, 97.

162. Raeymaekers, B., Broekaert, J.A.C. and Leis, F., *Spectro. Chim. Acta Part B*, 1988, **43**, 941.

163. Abila, P.A. and Trassy, C., *Mikrochim. Acta*, 1989, **3**, 159.

164. Mermet, J.M. and Robin, J., *Rev. Intern Htes Temp. Refract.*, 1973, **10**, 133.

165. Fleitz, P.A. and Seliskar, C.J., *Appl. Spectrosc.*, 1987, **41**, 679.

166. Hasegawa, T. and Winefordner, J.D., *Spectro. Chim. Acta Part B*, 1987, **42**, 637.

167. Ebdon, L. and Foulkes, M.E., *Anal. Chem.*, 1990, **35**, 17.

168. Seliskar, C.J., Miller, D.C. and Fleitz, P.A., *Appl. Spectrosc.*, 1987, **41**, 658.

169. Kepple, P. and Griem, H.R., *Phys. Rev.*, 1968, **173**, 317.

170. Hill, R.A, *J. Quant. Spectrosc. Radiat. Transfer*, 1964, **4**, 857.

171. Greig, J.R., Lim, C.P., Moo-Yourig, A., Palumpo, G and Griem, H.R., *Phys. Rev.*, 1968, **172**, 148.

172.   Czernikowski, A. and Chapelle, J., *Acta Phys. Pol.*, 1983, **63A**, 67.

173.   Preston, R.C., *J. Phys. B: Atom Mol. Phys.*, 1977, **10**, 1377.

174.   Griem, H.R., "Plasma Spectroscopy", McGraw Hill, New York, 1964.

175.   Hill, R.A., *J. Quant. Spectrosc. Radiat. Transfer*, 1967, **7**, 401.

176.   Greenfield, S., Personnel Communication, July 2001.

**Papers Published as a Result of This Study**

"A Preliminary Comparison of Radial and Axial Excitation Fluorescence in the ICP", Young, A., Pitts, L., Greenfield, S. and Foulkes, M.E., J. Anal. At. Spectrom., 2002 (submitted).

# Meetings and Conferences Attended

AD Research and Development Topics, University of Durham, UK, April 1998.

Ninth Biennial National Atomic Spectroscopy Symposium (BNASS), University of Bath, UK, July 1998.

AD Research and Development Topics, University of Greenwich, UK, April 1999.

European Winter Conference, Pau, France, January 1999.

SAC 99, University of Dublin, Republic of Ireland, July 1999.

AD Research and Development Topics, University of Manchester, UK, April 2000.

Tenth BNASS, University of Sheffield, UK, July 2000.

Also attended, during the course of the study from 1997 – 2002, were invited Royal Society of Chemistry Lectures and invited postgraduate lectures in analytical and environmental chemistry.

## Presentations

Departmental research lecture, University of Plymouth, UK, March 1998.

Poster presentation, AD Research and Development Topics, University of Durham, UK, April 1998.

Poster presentation, Ninth BNASS, University of Bath, UK, July 1998.

Poster presentation, AD Research and Development Topics, University of Greenwich, UK, April 1999.

Poster presentation, European Winter Conference, Pau, France, January 1999.

Departmental research lecture, University of Plymouth, UK, March 1999.

Poster presentation, SAC 99, University of Dublin, Republic of Ireland, July 1999.

Poster presentation, AD Research and Development Topics, University of Manchester, UK, April 2000.

Departmental research lecture, University of Plymouth, UK, June 2000.

Poster presentation, Tenth BNASS, University of Sheffield, UK, July 2000.

Poster presentation, Eleventh BNASS, University of Loughborough, UK, July 2002.

## Appendix 1

## Abel Inversion Programme to calculate radial profiles from lateral data

Written by Dr. Izumi Ishii, The George Washington University, USA, October 1987

```
10 REM ***** RADIAL DISTRIBUTION FOR TEMPERATURE *****
30 REM WRITEN BY IZUMI ISHII  *****  OCT 1987
70 REM PART-1: By using the NESTOR-OLSON ABEL INVERSION method the
lateral data
80 REM are spatially resolved.see refs. 2 & 3.
90 REM PART-2: By using the SLOPE METHOD, the EXCITATION
TEMPERATURE at
100 REM different radius is calculated. For SLOPE-METHOD.
140 DIM QA(10,10), BS(10), JC(10), IR(10), JO(10), VY(10), AA(10), BB(10),
CC(10), DD(10), EE(10), FF(10), GG(10)
150 DIM XI(51), A(51,51), B(51,51), TRI(51), T(51), J(10,51), xs(10,10)
160 DIM G(10), RTP(10), W(10), E(10), Y(10)
170 DIM SX#(12), SY#(12), SY(12), VA(10), DX(51), DY(51), VARIANCE(10)
180 DIM XX(200), YY(200), XP(200)
200 INPUT "The number of lines :",ELINE
1900 REM       EXCITATION TEMPERATURE MEASUREMENT (SLOPE
METHOD)
1920 nN=ELINE
1930 FOR ELINE=1 TO nN
    PRINT "SPECTRAL LINE #",ELINE
    INPUT "INPUT DATAFILE :",FILE$
    OPEN "I",1,FILE$
    INPUT#1,NPTS
    NR=NPTS
    FOR I=1 TO NPTS
    INPUT#1,XX(I), YY(I):J(ELINE,I)=YY(I):NEXT I:CLOSE#1
1940 INPUT "DEXCITATION ENERGY (eV)<Ha=1.89,Hb=2.55>  ";W(ELINE)
1950 INPUT "EXCITATION ENERGY  (eV)<Ha=12.09,Hb=12.75>";E(ELINE)
1960 INPUT "gf VALUES <Ha=0.696,Hb=0.122>";RTP(ELINE) print "  "
1970 NEXT ELINE
1980 REM
1990 REM CALCULATE LOG(G.RTP.W^3/J(line,radius))
2000 REM assuming G is RTP already includes G factor
    REM calculate log(rtp*W^3/j(line,radius))
2010 FOR RADIUS=1 TO nr
2020 FOR ELINE= 1 TO nN if j(eline,radius)=0. then y(eline)=0.:goto 2040
2030 Y(ELINE)=RTP(ELINE)*w(eline)^3/J(ELINE,RADIUS)
2040 NEXT ELINE
2050 REM
2060 REM CALCULATE SLOPE FOR LOG(G.RTP.V/J(LINE<RADIUS)) VERSUS
E
2070 REM USING LINEAR LEAST SQUARE FIT, Y=M*X+B (log(y)=M*e+B
M=1/(8.614e-5*T(K))
2080 REM
        REM if nn>2 then goto 2090
```

```
        REM if y(1)<=0 then yy(radius)=0:goto 2250
        REM if y(2)<=0 then yy(radius)=0:goto 2250
        REM m=(log(y(2))-log(y(1)))/(e(2)-e(1))
        REM goto 2245
2090 XYSUM=0:XSUM=0:YSUM=0:X2SUM=0: Y2SUM=O :n=0
2100 FOR J=1 TO eline
        if y(j)<=0 then goto 2160
        n=n+1
        y(j)=log(y(j))
2110 XYSUM=XYSUM+(E(J)*Y(J))
2120 XSUM=XSUM+E(J)
2130 YSUM=YSUM+Y(J)
2140 X2SUM=X2SUM+(E(J)^2)
2150 Y2SUM=Y2SUM+(Y(J)^2)
2160 NEXT J if n<=1 then yy(radius)=0:goto 2250
2170 M=(N*XYSUM-XSUM*YSUM)/(N*X2SUM-XSUM^2)
2180 REM B=YSUM/N-M*XSUM/N
2190 REM CC=(N*XYSUM-XSUM*YSUM)/SQR((N*X2SUM-
XSUM^2)*(N*Y2SUM-YSUM^2))
        REM if cc=0 then xp(radius)=0 else cc=1/cc/8.614e-5:xp(radius)=cc
2230 REM PRINT "CORRELATION COEFICIENT";CC
2240 REM PRINT "RADIUS";RADIUS;"EXCITATION TEMP.";T(RADIUS)
2245 yy(radius)=1/m:yy(radius)=yy(radius)/8.614e-5
2250 PRINT radius;yy(radius):NEXT RADIUS
        gosub 3000
        INPUT "OUTPUT FILENAME(T)=",FILE$
        OPEN "O",3,FILE$
        PRINT#3, NR
        FOR I=1 TO NR
        PRINT#3,XX(I),YY(I):NEXT I:CLOSE#3
2260 END
2270 RETURN
2280 REM
********************************************************************
2290 PRINT" SIMULTANEOUS LINEAR EQUATIONS(SLE)
2300 FL%=0
2310 DT=1:MZ%=N: IF FL%>=0 THEN MZ%=N+1
2320 EP=1E-12
2330 FOR K=1 TO N
2340 PV#=0
2350 FOR I=1 TO N
2360 FOR J=1 TO N
2370 IF K=1 THEN 2430
2380 FOR IS=1 TO K-1
2390 FOR JS=1 TO K-1
2400 IF I=IR(IS) THEN 2450
2410 IF J=JC(JS) THEN 2450
2420 NEXT JS,IS
2430 IF ABS(QA(I,J)) <=ABS(PV#) THEN 2450
2440 PV#=QA(I,J):IR(K)=I:JC(K)=J
2450 NEXT J,I
2460 IF ABS(PV#) <EP THEN DT=0:PRINT "DETERMINANT ZERO":RETURN
```

```
2470 DT=DT*PV#
2480 FOR J=1 TO MZ%:QA(IR(K),J)=QA(IR(K),J)/PV#:NEXT J
2490 QA(IR(K),JC(K))=1/PV#
2500 FOR I=1 TO N
2510 QA=QA(I,JC(K))
2520 IF I=IR(K) THEN 2570
2530 QA(I,JC(K))=-QA/PV#
2540 FOR J=1 TO MZ%
2550 IF J<>JC(K) THEN QA(I,J)=QA(I,J)-QA*QA(IR(K),J)
2560 NEXT J
2570 NEXT I,K
2580 FOR I=1 TO N: JO(IR(I))=JC(I)
2590 IF FL%=>0 THEN BS(JC(I))=QA(IR(I),MZ%)
2600 NEXT I
2610 IN=0
2620 FOR I=1 TO N-1
2630 FOR J=I+1 TO N
2640 IF JO(J)>=JO(I) THEN 2660
2650 JT=JO(J):JO(J)=JO(I):JO(I)=JT:IN=IN+1
2660 NEXT J,I
2670 IF 2*INT(IN/2)<>IN THEN DT=-DT
2680 IF FL%>0 THEN RETURN
2690 FOR J=1 TO N
2700 FOR I= 1 TO N
2710 VY(JC(I))=QA(IR(I),J)
2720 NEXT I
2730 FOR I= 1 TO N
2740 QA(I,J)=VY(I):NEXT I
2750 NEXT J
2760 FOR I= 1 TO N
2770 FOR J= 1 TO N
2780 VY(IR(J))=QA(I,JC(J)):NEXT J
2790 FOR J= 1 TO N
2800 QA(I,J)=VY(J):NEXT J
2810 NEXT I
2820 RETURN
2830 REM ref.1: Physical Chemistry On A Microcomputer by Joseph H.Noggle,
Univ. of Delaware, 1985, chapter 4.
2840 REM ref.2: C.J.Cremers and R.C.Birkebak, Appl. Optics,5,1057(1966)
2850 REM ref.3: Theor. & Exper. Invest. of Ar ICP as a Spectrochemical Source ,Ph.D.
Thesis by R.G.Schleicher,U. of Mass., 1979, see P288-290,317-319.
3000 REM subroutine plot
3010 REM find ymin and ymax
3020 YMIN=YY(1):YMAX=YY(1)
3030 FOR N=1 TO NPTS
3040 IF YY(N)>YMAX THEN YMAX=YY(N)
3050 IF YY(N)<YMIN THEN YMIN=YY(N)
3060 NEXT N
3070 XMIN=XX(1):XMAX=XX(NPTS)
3080 REM plot
3090 SCREEN 2,0,0
3100 LINE(10,10)-(630,10)
```

280

```
3110 LINE(630,10)-(630,180)
3120 LINE(630,180)-(10,180)
3130 LINE(10,180)-(10,10)
3140 CX=600/(XMAX-XMIN)
3150 CY=160/(YMAX-YMIN)
3160 X0=20
3170 Y0=175
3180 FOR N=1 TO NPTS
3190 XL=(XX(N)-XMIN)*CX
3200 XL=XL+X0
3210 YL=(YY(N)-ymin)*CY
3220 YL=Y0-YL
3230 PSET(XL,YL)
3240 NEXT N
3315 locate 1,35:print "Temperature Profile"
3340 LOCATE 1,1
3350 INPUT X$
3360 SCREEN 0,0:RETURN
```

# Procedure for Abel inversion of data

1. From Excel:

   Save each line of lateral data as follows:

   ```
   10
   0.0    0001
   0.4    0002
   0.8    0003
   3.6    0010
   ```

   where the first column is the lateral position and the second is the emission intensity.

2. Save these files as .prn files (space delimited files).

3. Exit Windows.

4. Start DOS.

5. Run qbasic.

6. Run sabel.bas program.

7. Type in number of lines, *e.g.* 10.

8. Type in file name, *e.g.* 382a.prn.

9. Press enter when prompted.

10. Save output as a space delimited file, *e.g.* 382a1.prn.

11. Repeat Abel inversion for other data files.

12. Exit qbasic.

13. Restart Windows.

14. Run Excel and open .prn files.